AFRL-RB-WP-TR-2010-3068,V1

AIR VEHICLE INTEGRATION AND TECHNOLOGY RESEARCH (AVIATR)

Task Order 0015: Predictive Capability for Hypersonic Structural Response and Life Prediction: Phase 1-Identification of Knowledge Gaps, Volume 1–Nonproprietary Version

George Tzong, Richard Jacobs, and Salvatore Liguore

The Boeing Company

SEPTEMBER 2010
Final Report

AIR FORCE RESEARCH LABORATORY
AIR VEHICLES DIRECTORATE
WRIGHT-PATTERSON AIR FORCE BASE, OH 45433-7542
AIR FORCE MATERIEL COMMAND
UNITED STATES AIR FORCE

NOTICE AND SIGNATURE PAGE

Using Government drawings, specifications, or other data included in this document for any purpose other than Government procurement does not in any way obligate the U.S. Government. The fact that the Government formulated or supplied the drawings, specifications, or other data does not license the holder or any other person or corporation; or convey any rights or permission to manufacture, use, or sell any patented invention that may relate to them.

This report was cleared for public release by the USAF 88th Air Base Wing (88 ABW) Public Affairs Office (PAO) and is available to the general public, including foreign nationals. Copies may be obtained from the Defense Technical Information Center (DTIC) (http://www.dtic.mil).

AFRL-RB-WP-TR-2010-3068,V2 HAS BEEN REVIEWED AND IS APPROVED FOR PUBLICATION IN ACCORDANCE WITH THE ASSIGNED DISTRIBUTION STATEMENT.

*//Signature//

THOMAS G. EASON, Project Engineer
Analytical Mechanics Branch
Structures Division

//Signature//

MICHAEL J. SHEPARD, Chief
Analytical Mechanics Branch
Structures Division

//Signature//

DAVID M. PRATT, Technical Advisor
Structures Division
Air Vehicles Directorate

This report is published in the interest of scientific and technical information exchange, and its publication does not constitute the Government's approval or disapproval of its ideas or findings.

*Disseminated copies will show "//Signature//" stamped or typed above the signature blocks.

REPORT DOCUMENTATION PAGE

Form Approved
OMB No. 0704-0188

1. REPORT DATE *(DD-MM-YY)*	2. REPORT TYPE	3. DATES COVERED *(From - To)*
September 2010	Final	22 December 2009 – 26 July 2010

4. TITLE AND SUBTITLE
AIR VEHICLE INTEGRATION AND TECHNOLOGY RESEARCH (AVIATR) Task Order 0015: Predictive Capability for Hypersonic Structural Response and Life Prediction: Phase 1-Identification of Knowledge Gaps, Volume 1–Nonproprietary Version

5a. CONTRACT NUMBER
FA8650-08-D-3857-0015

5b. GRANT NUMBER

5c. PROGRAM ELEMENT NUMBER
0602201

6. AUTHOR(S)
George Tzong, Richard Jacobs, and Salvatore Liguore

5d. PROJECT NUMBER
A0IA

5e. TASK NUMBER

5f. WORK UNIT NUMBER
A0IA0E

7. PERFORMING ORGANIZATION NAME(S) AND ADDRESS(ES)
The Boeing Company
M/C 110-SK56
2600 Westminster Avenue
Seal Beach, CA 90740

8. PERFORMING ORGANIZATION REPORT NUMBER

9. SPONSORING/MONITORING AGENCY NAME(S) AND ADDRESS(ES)
Air Force Research Laboratory
Air Vehicles Directorate
Wright-Patterson Air Force Base, OH 45433-7542
Air Force Materiel Command
United States Air Force

10. SPONSORING/MONITORING AGENCY ACRONYM(S)
AFRL/RBSM

11. SPONSORING/MONITORING AGENCY REPORT NUMBER(S)
AFRL-RB-WP-TR-2010-3068,V1

12. DISTRIBUTION/AVAILABILITY STATEMENT
Approved for public release; distribution unlimited.

13. SUPPLEMENTARY NOTES
Report contains color. PAO Case Number: 88ABW-2010-6345; Clearance Date: 01 Dec 2010.
See technical report AFRL-RB-WP-TR-2010-3068,V2 (eligibility restrictions apply) for proprietary information.

14. ABSTRACT
The Boeing Company investigated current state of the art capability for hypersonic structural response and life prediction. The study focused on identifying current knowledge gaps and limitations in the current methods and tools for design and analysis of reusable, air breathing, Mach 7 hypersonic cruise vehicles made of hot-structure in extreme environments. An open-source reference vehicle, the Technology Experimental Vehicle (TX-V) was refined using an existing Boeing vehicle as a baseline to identify critical regions and associated gaps. Research was completed documenting the methods used for extreme environment analysis on fighter, transport, and commercial aircraft. Additionally, recent and past hypersonic vehicle experience was researched and documented on the National Aerospace Plane (NASP), X-51A, and Hypersonic International Flight Research and Experimentation (HIFiRE) vehicles. Based on the historical and current research completed and the TX-V data provided, a list of knowledge gaps, capabilities needed to overcome these gaps, and predicted benefits if gaps were removed was created.

15. SUBJECT TERMS
life prediction, hot-structure, structural analysis, extreme environments, thermal, acoustic

16. SECURITY CLASSIFICATION OF:			17. LIMITATION OF ABSTRACT:	18. NUMBER OF PAGES	19a. NAME OF RESPONSIBLE PERSON (Monitor)
a. REPORT	b. ABSTRACT	c. THIS PAGE			Thomas G. Eason
Unclassified	Unclassified	Unclassified	SAR	186	19b. TELEPHONE NUMBER *(Include Area Code)* N/A

Standard Form 298 (Rev. 8-98)
Prescribed by ANSI Std. Z39-18

TABLE OF CONTENTS

LIST OF FIGURES

Figure Page

Figure Page

LIST OF TABLES

GLOSSARY

ACCTE	Advanced Ceramic Composites for Turbine Engines
AFRL	Air Force Research Laboratory
AoA	Angle of Attack
ASE	Aeroservoelastic
ATACMS	Army Tactical Missile System
AVIATR	Air Vehicle Integration and Technology Research
BR&T	Boeing Research & Technology
CA	Constant Amplitude
CDR	Critical Design Review
CFD	Computational Fluid Dynamics
CHS	Carbon Hot Structure
CMC	Ceramic Matrix Composite
dB	Decibels
FADEC	Full Authority Digital Engine Control
FEA	Finite Element Analysis
FEM	Finite Element Model
FTS	Flight Termination System
FTV	Flight Test Vehicle
GCU	Guidance Control Unit
GN&C	Guidance, Navigation and Control
GVT	Ground Vibration Test
HFP	High Frequency Phenomena
HIFiRE	Hypersonic International Flight Research and Experimentation
LD&A	Loads, Dynamics & Aeroelasticity

LE	Leading Edge
MPC	Multi-Point Constraint
NASP	National Aerospace Plane
NRF	Nonlinear Response Factor
PDR	Preliminary Design Review
PSD	Power Spectral Density
OASPL	Overall Sound Pressure Level
OML	Outer Mold Line
OTS	Off The Shelf
PWR	Pratt & Whitney Rocketdyne
RMS	Root Mean Square
RSC	Rockwell Science Center
S&C	Stability and Controls
SLT	Structural Loads Test (non-destructive)
SMI	Structural Modal Interaction
SoA	State-of-the-Art
SRA	Sonic Response Analysis
SSC	Structural Sciences Center
TE	Trailing Edge
TPS	Thermal Protection System
TTT	Through the Thickness
TX-V	Technology Experimental Vehicle
USAF	United States Air Force

FOREWORD

The information described in this report was authored by George Tzong, Rich Jacobs, Sal Liguore, and Nicolette Yovanof under the Air Vehicle Integration and Technology Research (AVIATR) contract Delivery Order 15. This project, *Predictive Capability for Hypersonic Structural Response and Life Prediction*, was the Phase I of three on *Identification of Knowledge Gaps*. The work was administered by Air Force Research Laboratory (AFRL) Structural Science Center (SSC) project engineers Thomas G. Eason and Stephen M. Spottswood. The contract work was performed between December 2009 and July 2010. George Tzong was the principal investigator and Nicolette Yovanof was the project manager for this task order.

PREFACE

The purpose of this paper is to document the technical work completed under Air Vehicle Integration and Technology Research (AVIATR) contract Delivery Order 15. This work includes modification and refinement of a reference vehicle to gather data for the identification of knowledge gaps for predictive capability for Hypersonic Structural Response and Life Prediction. This work was completed from December 2009 to July 2010 for the AFRL SSC.

The authors would like to acknowledge the contributions and support of Dr. Bijan Nejad, Dr. Mostafa Rassaian, Mr. Dan Ortega, Dr. Dan Driemeyer, Mr. Ross Rochat, Dr. Kei Lau, Ms. Nicolette Yovanof, Mr. Keith McIver, Mr. Gerry Newkirk, Mr. Dave Bertino, and Mr. John Stoll.

1 SUMMARY

Through the completion of the Phase 1 task order, Boeing researched the rich history of hypersonic vehicles to disclose a list of gaps in the structural analysis and life prediction methods which result in unnecessarily heavy and costly vehicle structures. Fundamental gaps were found in the lack of integrated tool for mechanical flight loads, thermal induced loads, and acoustic environment.

The objective of this Phase I program was to identify gaps in structural analysis and life prediction methods applied to reusable, integrated air vehicle structures for sustained operations in a hypersonic environment. This program focused on areas of the structure where gaps exist in the state of the art (SoA) analysis methods and tools to accurately predict the response and life of the flight vehicle structure to the desired fidelity. The knowledge gaps were identified based on design and analysis issues of current production aircraft (including fighter, transport, and commercial aircraft), recent and past hypersonic vehicle experience (National Aerospace Plane (NASP), X-51A, and Hypersonic International Flight Research and Experimentation (HIFiRE)), and most importantly on a defined Mach 7 hypersonic cruise reference vehicle, called the Technology Experimental Vehicle (TX-V). Table 1 lists the identified gaps and associated critical regions based on a hypersonic vehicle such as TX-V.

Table 1. List Of Gaps and Associated Critical Regions

Gap Description	Critical Vehicle Region
1. Difficult to identify critical thermo-mechanical and acoustic load combinations	Engine nozzle, inlet and duct
2. Difficult to adopt temporal and spatial thermal gradients in panel level linear analysis	Engine nozzle, inlet and duct, wing leading edges, Fwd lower surface
3. Do not account for the coupling between transient thermal and acoustics in linear frequency response analysis	Engine nozzle, flaps and control surfaces, Fwd lower surface, Aft upper and lower surfaces,
4. Cannot accurately include internal loads in panel level analysis	All acreage panels
5. Cannot accurately define thermal and mechanical boundary conditions for detailed panel analysis	All acreage panels
6. Cannot simulate large deformation oscillation or dynamic snap-thru of panels	Aft upper and lower surfaces, flaps and control surfaces
7. Inadequately model accumulated damage and degradation due to high temperatures	Engine nozzle, inlet and duct, wing leading edges, Fwd lower surface
8. Cannot accurately model damping in analysis	All acreage panels
9. Can only approximate acoustic environment using empirical formulas until flight test data is available	Wing leading edge , flaps and control surfaces, Aft upper and lower surfaces
10. Lack the capability to analyze large-order high fidelity models to capture nonlinear, dynamic snap-thru, and high frequency response in coupled extreme environment	Aft upper and lower surfaces, flaps and control surfaces

The result of this study is a list of knowledge gaps and recommended enhancements to the SoA methods, and corresponding structural benefits that would arise from these enhancements. The primary knowledge gaps uncovered in the structural design and analysis of hypersonic hot

structure include prediction of thermal, mechanical, and acoustic design loads and structural sizing and optimization at the vehicle and panel level. Hypersonic acoustic load prediction is at an immature capability level. Understanding the physics and mechanisms through which thermal, mechanical, and acoustic loads couple under hypersonic flow conditions compounds the gaps. Analytical tools capable of addressing coupling between structural response and the thermal-acoustic environments are unavailable. Additionally, material property data for long duration exposure to high temperatures can be difficult to access. Structural and material failure modes have not been adequately characterized. Finally, thermal-mechanical fatigue analysis of advanced hot structure and materials is at an immature capability level.

The recommendations from this study are the selection of four panels for further study in Phase II. These four panels represent the range of technical challenges in detailed panel design and analysis. The selected candidate panels are focused on areas where structural analysis and life prediction knowledge gaps are known to exist. The panels are selected based on severity and uncertainty of the environment and design loads, and those locations which require reduced conservatism in analysis in order to meet design margins. The detailed analysis will result in well-documented test cases that can be used for future development and validation of advanced nonlinear multi-physics analysis methods.

2 INTRODUCTION

2.1 Background

The Predictive Capability for Hypersonic Structural Response and Life Prediction program was sponsored by the Air Force Research Laboratory Structural Sciences Center (SSC) at Wright-Patterson Air Force Base, Ohio. The AFRL program managers were Tom Eason and S. Michael Spottswood. This work was performed under United States Air Force (USAF) contract number FA8650-08-D-3857 DO15 between December, 2009 and July, 2010.

The USAF and The Boeing Company envision a future reusable hypersonic fleet capable of withstanding sustained operations in extreme environments, including combined loading conditions. These extreme environments and combined loading conditions include large magnitude thermal, acoustic, and mechanical loading with large spatial and temporal gradients and nonlinear, coupled interactions between loadings. Durable structures capable of meeting these needs and the ability to accurately and reasonably analyze and predict failure of this structure are key capabilities required to achieve this vision.

The scientific challenge in understanding and analyzing the combined effects of extreme loading on hot-structure is the current focus of research at the AFRL SSC. In order to better understand this challenge, it is important to identify regions where the inability to account for combined loading effects lead to excessive risk and/or weight increase, and the benefits that may stem from addressing these challenges. In order to identify these regions, this project focused on reviewing both historical data and the TX-V baseline hypersonic reference vehicle.

The purpose of the Phase I Predictive Capability for Hypersonic Structural Response and Life Prediction program was to identify gaps in structural analysis and life prediction methods as they apply to reusable, integrated structures for sustained hypersonic operations in an extreme environment. The purpose of the overall three phase program was to uncover the shortcomings in current methods used for design and analysis of hypersonic structures through identification, detailed design, and testing in order to identify areas where conservatism could be reduced to decrease weight and cost without compromising risk. Results will be open source and releasable to the public to drive projects for academic research and collaboration with universities.

2.2 Approach

The Boeing Company reached across the large knowledge base of people and design experiences from previous and ongoing hypersonic vehicle development programs across the enterprise. In particular, the X-43, X-51, HyFly and HIFiRE programs were utilized in support of this AFRL SSC task order. This experience was combined with state-of-the-art design practices to develop a hot structure configuration and define critical panel locations, sizing, and aero-thermal environments based on the Boeing Mach 7 Manta-2025 concept vehicle. Panel configurations were developed using detailed thermal, acoustic, aeroelasticity, and structural sizing analysis expertise. The developed design and environments, along with available data from previous programs and publicly available literature, were used to guide the identification of critical gaps in predictive analysis methodologies and to identify enhancements required to address structural response under extreme environments such that excessive risk and/or structural weight penalties

can be avoided in future hypersonic vehicle development. Figure 1 summarizes the approach for the Phase I task of identifying knowledge gaps that restrict predictive capability as well as the output that will benefit the Phase II detailed design of panels that will be tested in Phase III.

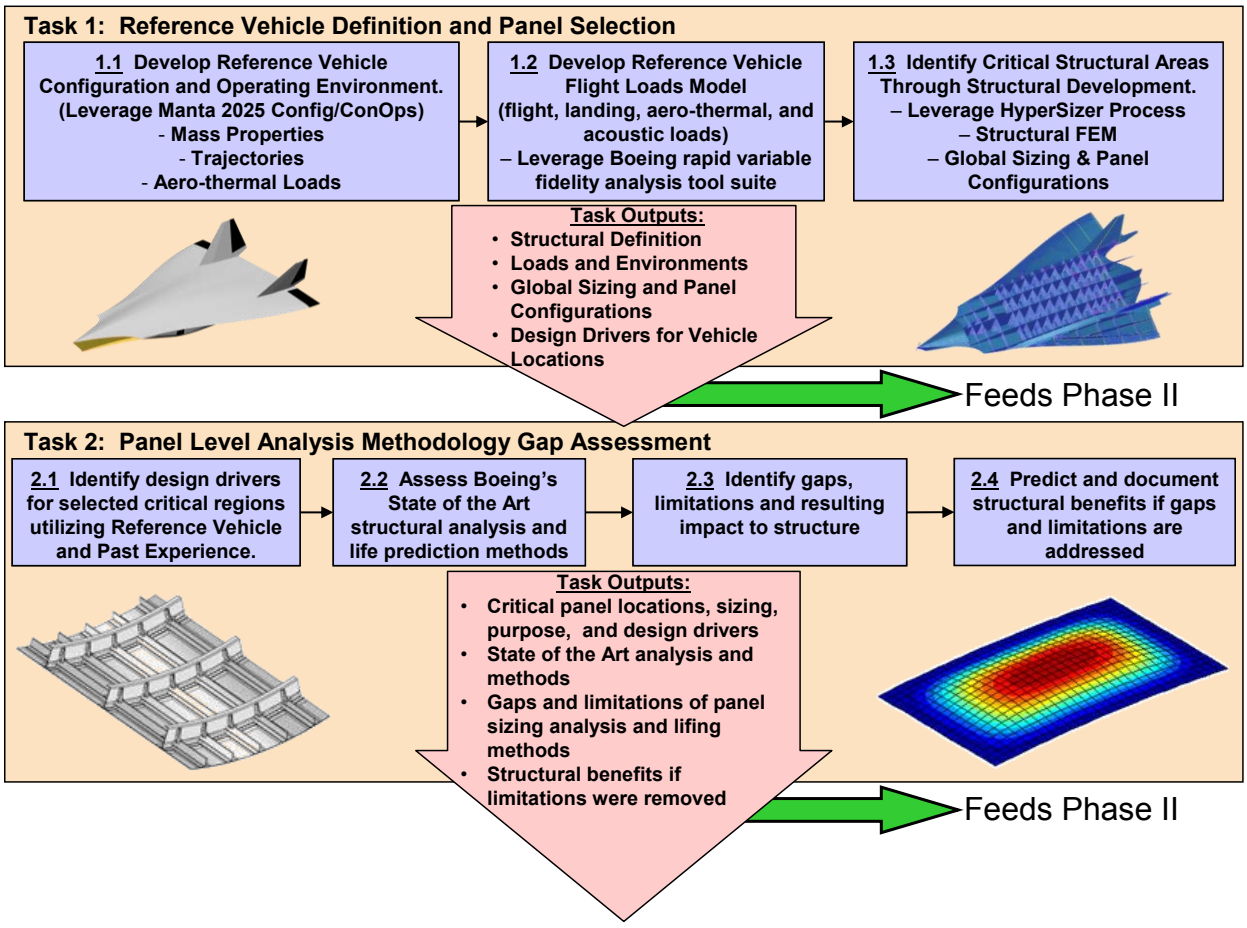

Figure 1. This Project Provides AFRL With a Closed-Concept Hypersonic Vehicle Design That Can Be Used For Open Source Assessments During Phase II.

To support the identification of critical technology gaps and provide a platform for future detailed design of critical regions, a reference vehicle, known as the Technology Experimental Vehicle (TX-V) was necessary to establish a baseline from which trades and assessments can be measured and compared. The Boeing Company used the recently-developed Manta 2025 hypersonic cruise vehicle design to provide a state-of-the-art (SoA) baseline for the study. This concept vehicle was modified to a Mach 5-7 metallic hot structure configuration in order to provide an open-source reference vehicle where results can be used for determination of critical regions for identification of gaps and limitations in predictive methodologies, detailed panel design, and university interactions during subsequent phases of the program. This aggressive approach of developing a reference vehicle from an existing vehicle added risk in the program as such the TX-V that the vehicle design would not close or meet the requirements of the Mach 7 reusable hot-structure. The panel's thermal growth during cruise were exceeding the TX-V substructure capabilities and resulting in grossly overweight panels. To keep within the objective of the study, the panels were sized to a 500 degrees F thermal growth where by closing the

vehicle. Once the reference vehicle baseline was established, identification of critical gaps in structural analysis and life prediction methods were compiled.

2.3 Scope

The team of subject matter experts leveraged panel design concepts and environment data from past and ongoing programs to rapidly ascertain critical thin-gauge, hot-structure regions on the TX-V reference vehicle. Thermal-acoustic and fatigue sizing expertise was then used to assess and document areas where existing analysis methods do not properly account for the non-linear coupling between extreme hypersonic aero-thermal-acoustic environments and the evolving structural state during flight. Documentation was produced that includes a summary of current design practices used to work around analytical tool limitations and an assessment of the excess weight and design margin or risk they introduce. The Phase I effort was broken down into two main tasks:

1. Refining the TX-V Reference Vehicle Baseline – The Boeing Company selected a well-defined hypersonic concept vehicle, the Manta 2025 configuration, as the baseline for reference vehicle development and structural analysis methodology assessment. The existing Manta 2025 vehicle was updated to a closed-concept, thin gauge metallic reference vehicle that provided flight weight structural definition, design drivers, and panel configurations for critical regions of the vehicle. This was accomplished using a combined global-local optimization scheme that efficiently couples thermal, aeroelasticity, and structural sizing analysis results. An existing Manta finite element model (FEM) and computational fluid dynamics (CFD) model were used to enable a rapid metallic panel sizing and critical aero-thermal environments definition. These results were then coupled with flight and engine acoustic environments from semi-empirical models developed from flight test and wind tunnel test data. These critical locations were documented to serve as the basis for the Task 2 detailed thermal-acoustic design methodology gap assessment. The resulting reference vehicle is known as the Technology Experimental Vehicle (TX-V)

2. Design & Analysis Methods Assessment – The Boeing Company utilized the TX-V and flight environments, along with available data from previous hypersonic programs to identify critical gaps and limitations in existing predictive analysis methodologies. The issues involved in non-linear coupling between extreme hypersonic thermal-acoustic environments, evolving material attributes and the resulting structural response and failure modes were identified and documented. The gaps and limitations inherent in our SoA analysis and life prediction methods were then assessed. Also, the structural benefits that could be obtained through increased fidelity of the design of hot structures enabled by removal of the identified gaps and limitations were included. The definition of the gaps associated in the predictive capabilities of hypersonic structural response and life prediction were documented.

   The documentation summarizes: (1) a reference vehicle configuration and panel design concepts; (2) open source, non-proprietary critical panel locations, function, boundary conditions, and sizing criteria; (3) open source, non-proprietary panel aero-thermal-acoustic loads, and structural response; (4) analysis assumptions/limitations leading to design conservatism or risk for these panels; and (5) prediction of structural benefits if gaps and limitations were removed.

3 PROCEDURES

The general purpose of this study is to better understand the current analysis methods for an extreme environment, hypersonic vehicle in preparation for a future Air Force hypersonic fleet. The objective of the Phase I program was to identify gaps in structural analysis and life prediction methods as applied to reusable, integrated structures for sustained operations in a hypersonic environment. The following methods, assumptions, and procedures were considered in this study.

3.1 Task 1 – Procedures

The objective of Task 1 was to establish a reference hypersonic cruise vehicle using metallic hot structure to aid in the identification of critical technology gaps. To support this effort, The Boeing Company selected the 75 ft Mach 7.0 Manta 2025 vehicle to provide a configuration baseline. An aggressive approach was determined to provide necessary panel level data in a relevant environment for gap assessment and future research projects and phases of this program. The hot structure design was derived by transforming this vehicle from a ceramic, Thermal Protection System (TPS) to a hot structure concept by removing the ceramic TPS and applying new materials capable of withstanding the higher temperatures. Representative loads and environments were developed focusing on the bulk panel acreage and disregarding specialty areas requiring more detailed analysis such as leading edges, inlets, and exhaust nozzles due to cost and schedule constraints. Vehicle flight design loads were generated using high fidelity Navier-Stokes computational fluid dynamics (CFD) solutions for maneuver conditions along the mission trajectory at Mach numbers of 0.6, 0.95, 1.8 and 7.0. Wind tunnel data was not available for this application. Figure 2 illustrates the process use to develop the trimmed flight maneuver load conditions.

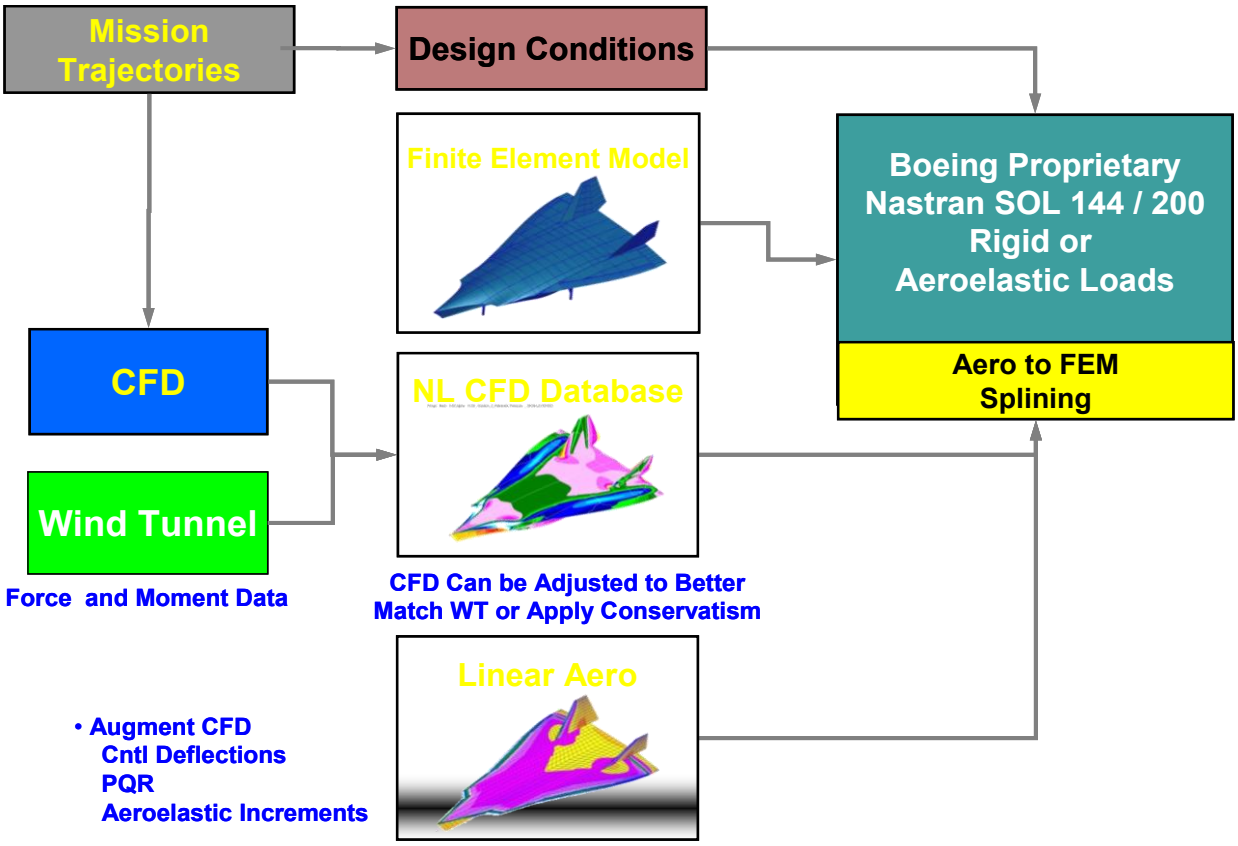

Figure 2. Figure Flight Maneuver Trimmed Loads Process

The Doublet-Lattice Method was used to supply the aerodynamic increments for control surface deflections, and to provide the aeroelastic incremental loads due to structural deformations. This approach enables trimmed and balanced load cases to be developed quickly and easily using CFD data. Key thermal and acoustic environments were determined for the Mach 7.0 cruise mission trajectory for use in structural sizing. Structural sizing/optimization was performed using Nastran Sol 200 and Collier Research's HyperSizer program. Using the developed loads and environments, structural sizing/optimization was performed. Figure 3 presents the loads and structural sizing process used to determine structural sizing.

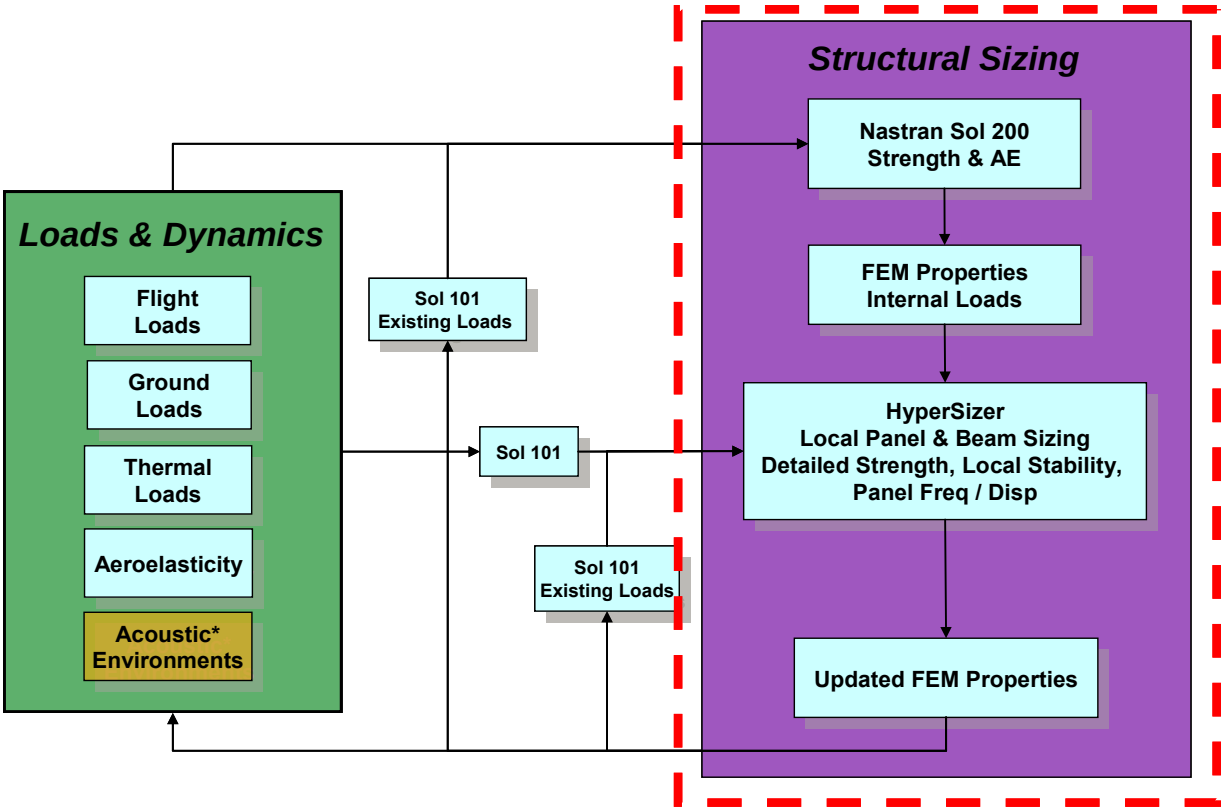

Figure 3. Loads and Structural Sizing Process

The initial sizing was determined using Nastran Sol 200 with critical flight and ground load conditions. This initial sizing was used as input for HyperSizer where thermal loads were added to the critical flight and ground cases. HyperSizer performes detailed panel and beam sizing subject to strength, buckling, and panel frequency constraints. Details of the strength checks performed by HyperSizer are available in Appendix E HyperSizer Strength Checks. Using the newly computed sizing, internal loads were updated using Nastran Sol 101 and fed back into HyperSizer. This loop was performed until convergence. The first cycle through the HyperSizer - Sol 101 loop failed to converge. This was resolved by using a reduced thermal environment. The details of this issue are discussed in section 4.4.3.6.

3.2 Task 2 – Procedures

This task focused on the vehicle's exterior skin panels where SoA methods are inadequate to predict the structural response and life to the desired fidelity. This study leveraged results from the TX-V reference vehicle developed in Task 1 along with hypersonic experience on previous projects to identify gaps and limitations in the predictive methods. Additionally, experience from conventional transport and fighter aircraft was included in the SoA assessment. In addressing these knowledge gaps, The Boeing Company has identified enhancement needs for these methods that will improve structural design by reducing risk and conservatism as well as minimizing weight, and time and costs for vehicle development, support and sustainment.

The methods used to predict the response and life of the structural component depend on the design criteria, environment and loads, function, structural construction and configuration, and

materials and failure modes. Assumptions or shortcuts currently adopted in structural analysis were examined to determine their impact on structural design. The assessment included documentation of assumptions or techniques of the current analysis approach are perceived as a limitation or gap, the current workarounds employed to ensure structural integrity and life; and the causes and affects the workarounds or assumptions will introduce to the system (adding weight, costs, risk, and increasing inspections, etc.). The benefits realized by introducing advanced analysis capabilities to remove assumptions and gaps in predictive methods were discussed.

The panel methodology gap assessment was accomplished using the four step process illustrated in Figure 4 and is described in subsequent sections.

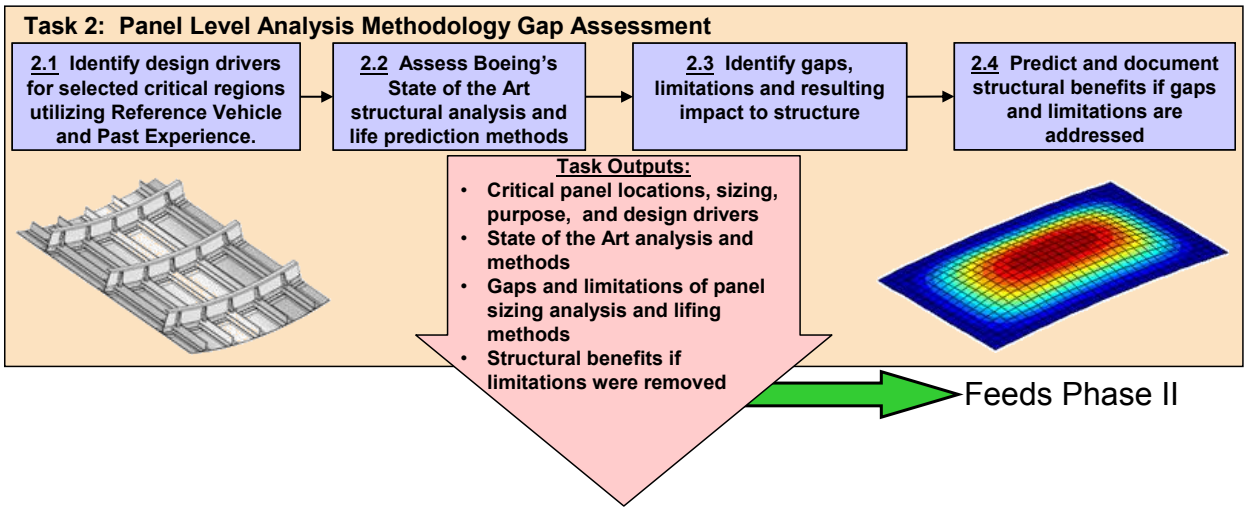

Figure 4. The Panel Level Analysis Methodology Gap Assessment

The TX-V reference vehicle results developed in Task 1 provided closed-concept and open-source data as the starting point for Task 2. These data were used for determination of critical regions for identification of knowledge gaps and limitations in the predictive methodologies and can be used for detailed panel design analysis and university interactions in the following phases of the program.

4 TECHNICAL STUDIES

4.1 Task 1 – Technical Information

4.1.1 Manta Background

The Boeing 75 ft Mach 7 Manta 2025 vehicle was selected to provide a configuration baseline for this study and is shown in Figure 5. From previous studies, scaled vehicle sizes from 32 ft to 135 ft long have been developed on the Manta configuration to assess extended range operation scenarios and reusable flight demonstrator concepts. This vehicle incorporates dual high speed turbine and ram-scramjet engines installed using a three dimensional inward-turning inlet design for efficient air capture. Takeoff and landing are horizontal for aircraft-like operation. Initial sizing of the wing is designed to achieve a planform loading of 55 pounds (lbs) per square foot (sq ft) at take-off.

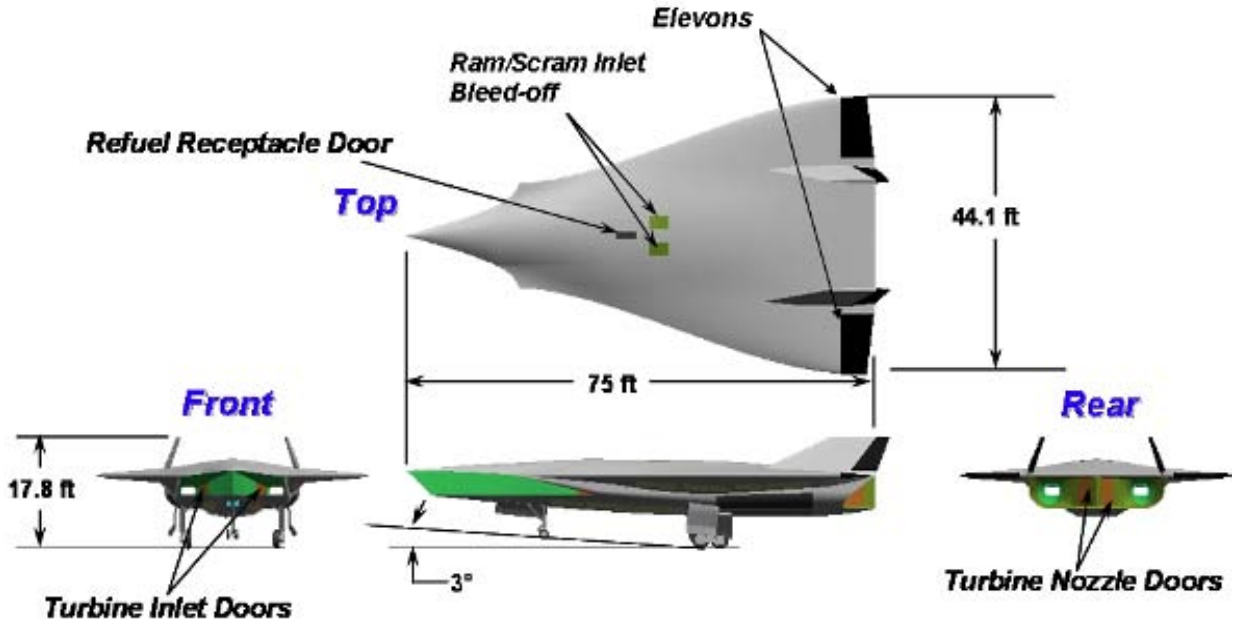

Figure 5. Manta 2025 Hypersonic Cruise Vehicle

Mass properties for the 75 ft Manta 2025 vehicle reveal a take-off gross weight of 184,515 lbs, with an empty weight of 74,387 lbs which includes a 10% weight margin based on the empty weight. The propulsion system and tank arrangements are shown in Figure 6 and Figure 7. The propulsion ducts shown are conceptual at this time.

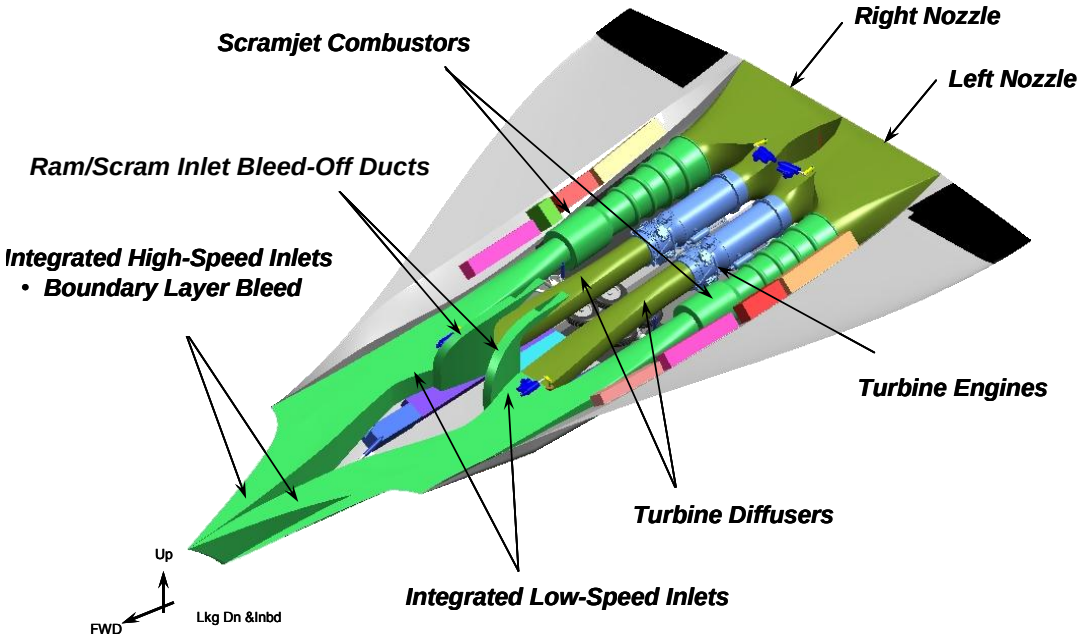

Figure 6. Manta 2025 Propulsion System

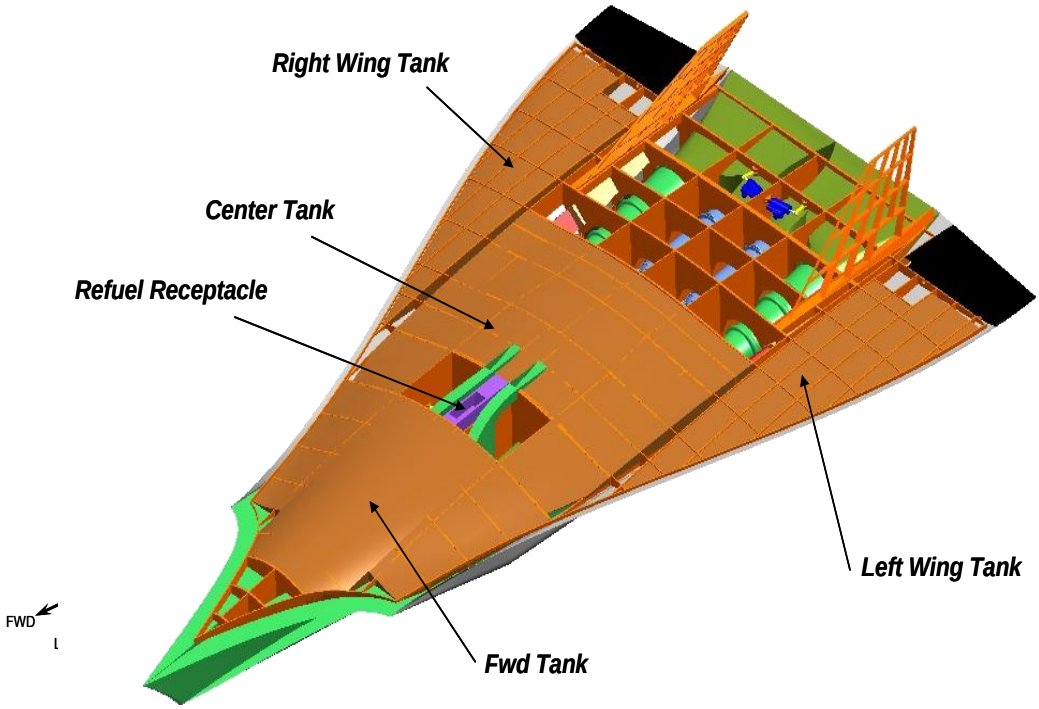

Figure 7. Manta 2025 Fuel Tank Arrangements

The baseline Manta FEM developed during a previous study is shown in Figure 8 with the upper skin removed. This model contains 53,000 nodes and 64,000 elements.

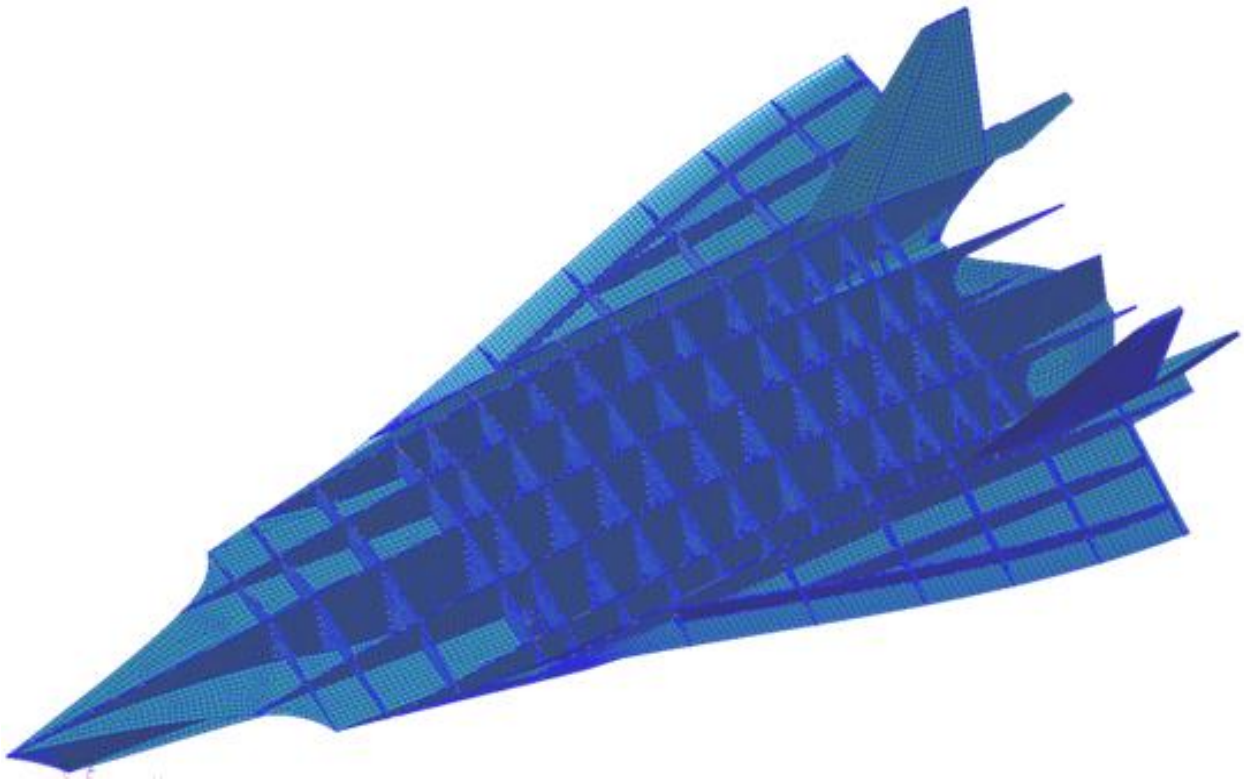

Figure 8. 32 Ft Manta FEM Shown With Upper Skin Removed

The design mission trajectory used for this study is shown in Figure 9. It features a Mach 7 cruise at 95 to 100k ft with a dynamic pressure of 1000 psf. During the acceleration up to Mach 7 the maximum dynamic pressure of 2000 psf is experienced.

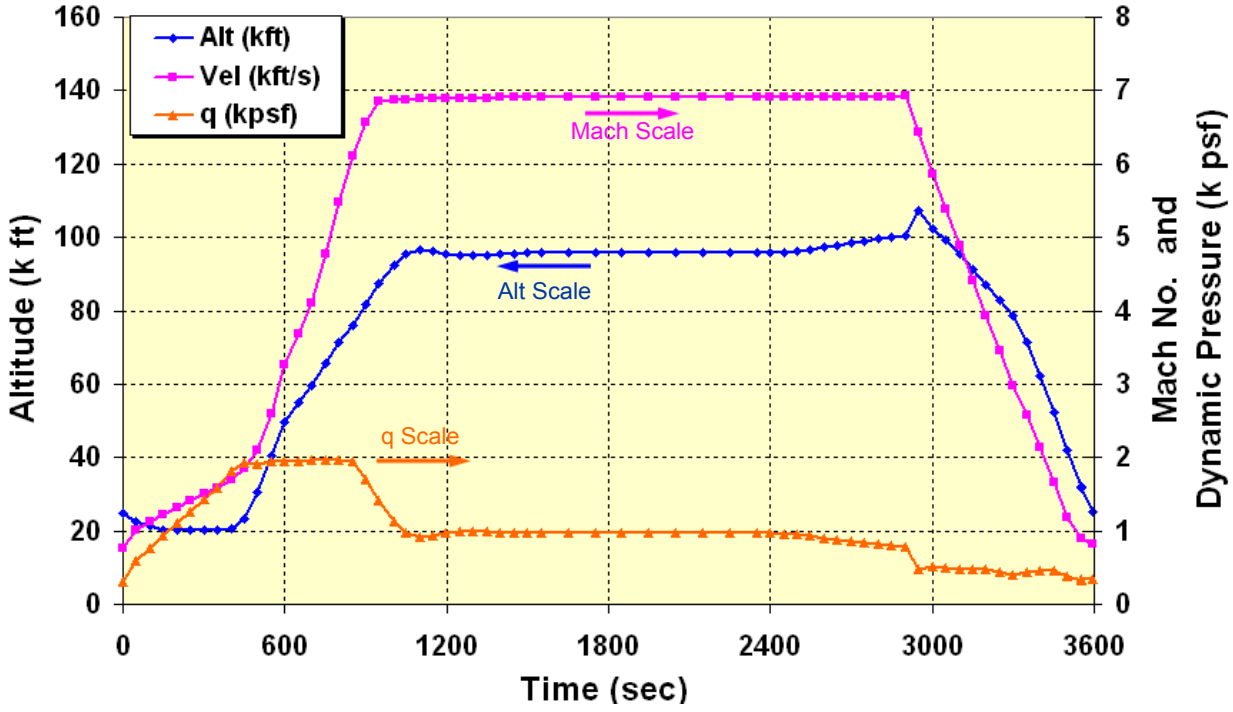

Figure 9. Mach 7 Design Mission Trajectory

Key mission events for the design trajectory are shown in Figure 10 and include:

1) The mission begins with a horizontal runway take-off.
2) Acceleration to the mode transition point using turbine propulsion.
3) Ram/scram jet propulsion is started.
4) Accelerate on Ram/Scramjet to Cruise Mach.
5) Cruise at Mach 7.
6) Unpowered Flight to Subsonic Mach.
7) Re-Start Turbine Engines. Return to a horizontal powered runway landing.

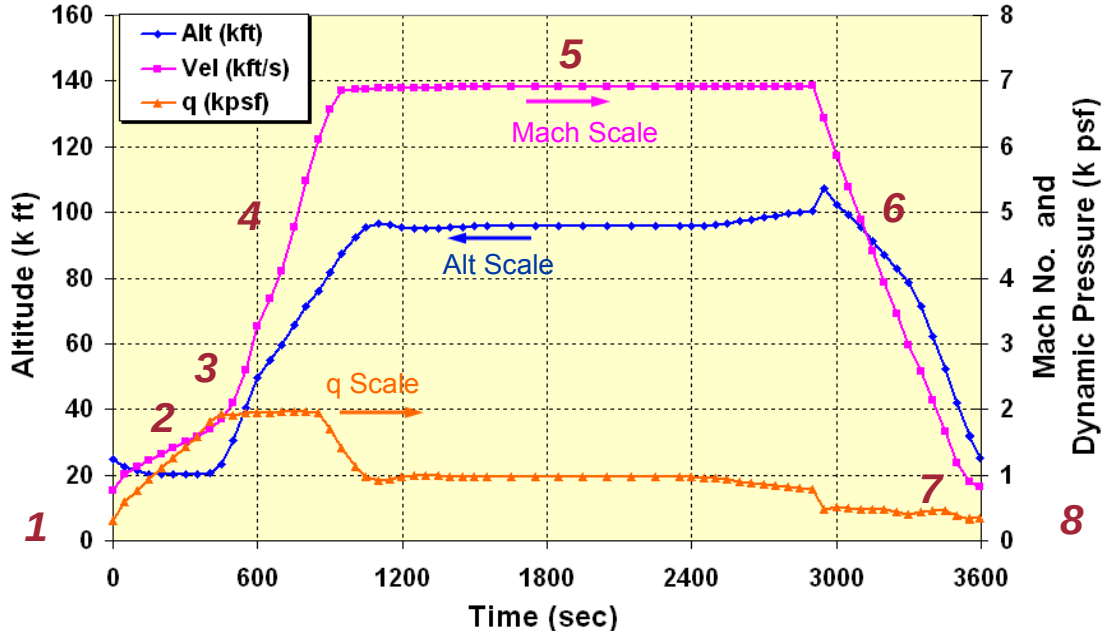

Figure 10. Key Mission Events

Estimated mass properties are shown in Figure 11. The maximum take off gross weight is 184,000 lbs which includes a 5,000 lb payload. The empty weight is 74 k-lbs.

Component		Weight
Structure	**28,959**	
Wing		4,551
Vertical Tail		1,444
Fuselage		19,566
Landing Gear		3,398
Propulsion	**31,510**	
Ramjet		17,452
Turbojet		5,864
Inlet		3,161
Nozzle		2,924
Fuel System		1,352
Misc. Propulsion		758
Subsystems	**6,416**	
Avionics		3,511
Electrical		1,832
Misc. Systems		1,073
Margin		7,437
Empty Weight		**74,318**
Payload		5,000
Usable Fuel		103,543
Unusable/Misc. Useful Load		1,585
Total Take Off Gross Weight		**184,443**

Propellant Fraction: 56%

10% Weight Margin

Figure 11. 75 Ft Manta Mass Properties

4.1.2 TX-V Modifications

The TX-V Finite Element Model (FEM) used in this study was derived by photographically scaling the 32 ft long Manta FEM to a length of 75 ft. Additional structural definition and refinement was then performed. This included creating the elevon and rudder control surfaces, refining the vertical tail mesh with additional spars and ribs, adding a nose and main landing gear and adding fuselage frame caps. To support structural sizing and optimization studies, element property groups were defined and material directions were added for the panel and beam elements. Figure 12 presents the TX-V FEM.

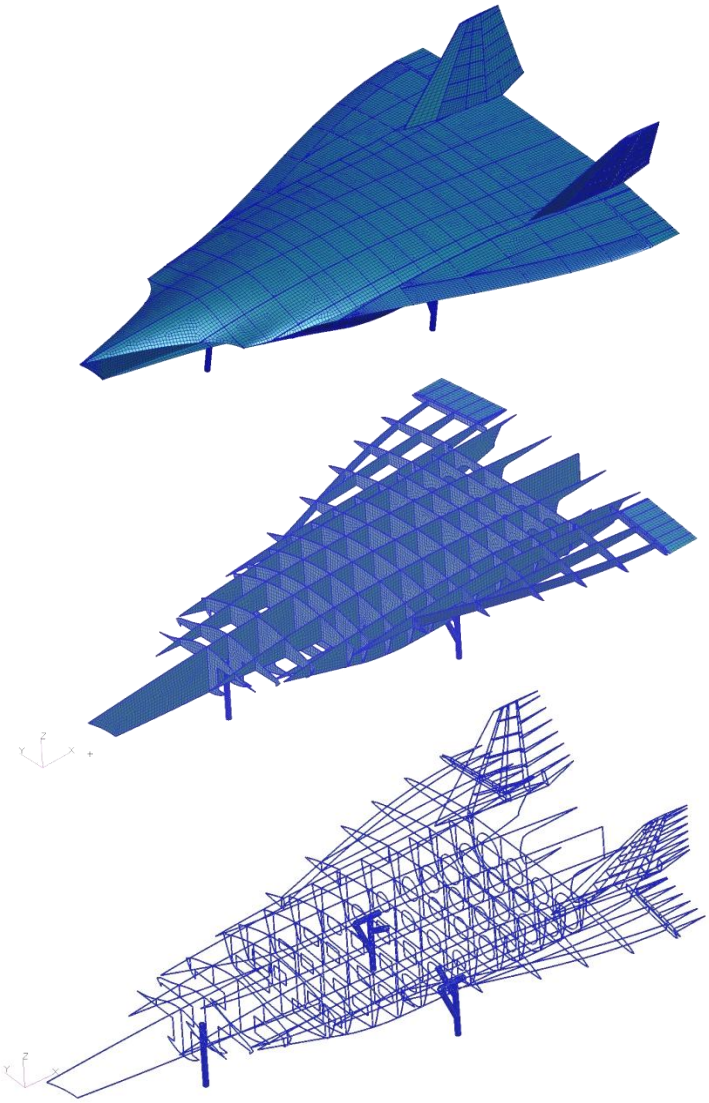

Figure 12. TX-V FEM

Mass properties for non-structural mass items were distributed to the FEM hard points. The hard points included bulkhead and skin and keel and skin intersections. FEM Fuel distributions were created for 5 fuel level variations. These include 16%, 25%, 50%, 75%, and full fuel conditions.

Figure 13 presents the TX-V FEM with the non-structural mass items represented as CONM2 elements.

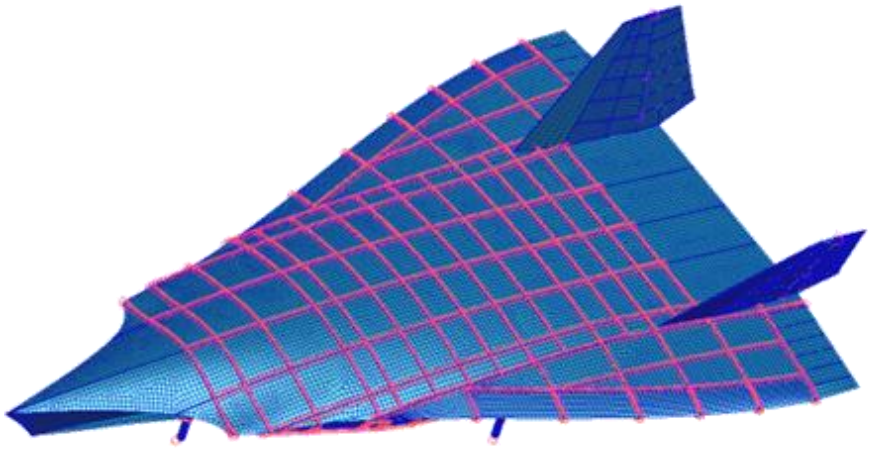

Figure 13. Non-Structural Mass Distribution

To support structural sizing/optimization design regions were created for use in Nastran Sol 200 & HyperSizer. The design regions consisted of 306 Panels zones, and 326 Spar, Rib, Bulkhead, and Keel Caps. Figure 14 shows the exterior skin panel design zones used in this study.

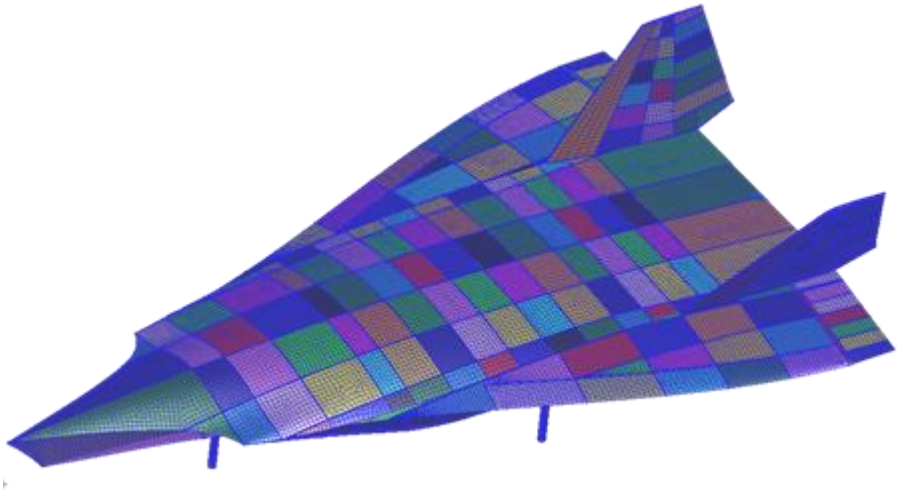

Figure 14. Skin Panel Design Regions

The Manta FEM was modified to the TX-V FEM to support structural sizing for a hypersonic cruise vehicle.

4.1.3 TX-V Results

4.1.3.1 Flight Loads

Distributed aerodynamics data for use in defining flight maneuver conditions was obtained from high fidelity CFD simulations. These were computed using the CFD++ flow solver. A distributed aerodynamic database consisting of four Mach numbers at 0.60, 0.95, 1.80 and 7.00 with three angles of attack at 0^o, 5^o and 10^o was generated. Figure 15 presents the external pressure distribution result for a Mach 0.60 at 10^o Angle of Attack (AoA) condition. A wing vortex and low pressure region can clearly be seen over the wing.

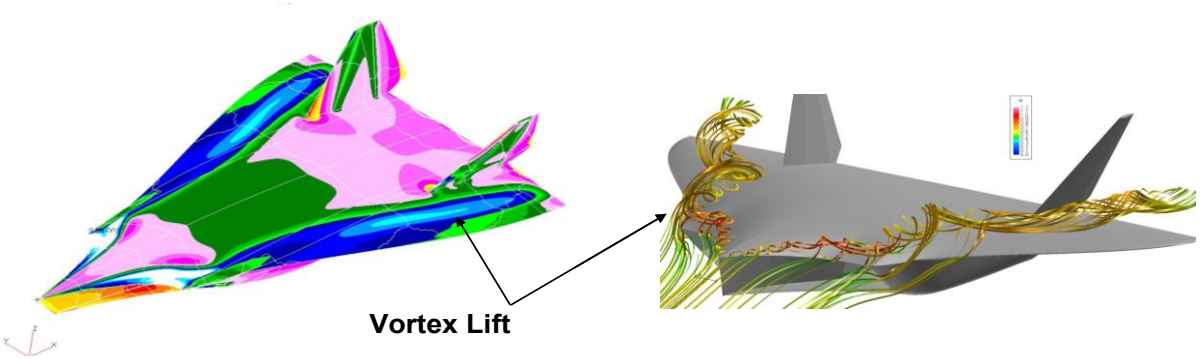

Figure 15. Mach 0.60 Pressure Distribution and Streamlines for 10 AoA

For Mach 7 at a 5^o AoA the pressure coefficient (Cp) distribution is shown in Figure 16.

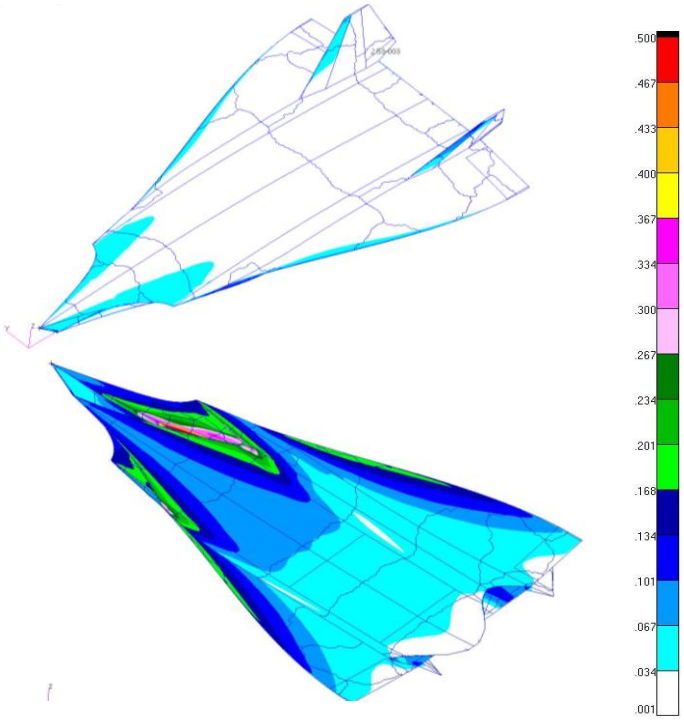

Figure 16. Pressure Coefficient Mach 7 at 5^o AoA

Flight maneuver loads were generated at critical points along the mission trajectory for Mach 0.60, 0.95, 1.80 and 7.00. For each Mach number, trimmed and balance load conditions were created and applied to the FEM and load conditions were created with load factors of -1.0, +1.0 and +2.5g and +1g and 5^{o} sideslip angle. Ground loads were produced following MIL-A-8862 criteria. The maximum sink speed was 10 ft/sec at the maximum design landing weight of 87,000 lbs, and 6 ft/sec for the maximum takeoff weight of 187,000 lbs. Table 2 presents the ground load conditions investigated for this study.

Table 2. Ground Load Condition

3PT LEVEL SPIN UP	3PT BRAKED ROLL N=1.0g
3PT LEVEL SPING BACK	3PT BRAKED ROLL N=1.2g
3PT LEVEL MAX V	2PT BRAKED ROLL N=1.0g
2PT LEVEL SPIN UP	2PT BRAKED ROLL N=1.2g
2PT LEVEL SPRING BACK	UNSYMM BRAKING
2PT LEVEL MAX V	LT TURN-MAX FSMR
2PT TAIL DWN SPIN UP	LT TURN-MAX FSML
2PT TAIL DWN SPRING BACK	REVERSE BRAKING
PT TAIL DWN MAX V	TAXI
1 WHEEL SPIN UP	
1 WHEEL SPRING BACK	
1 WHEEL MAX V	
DRIFT TO RIGHT	

Based on the flight and ground loads, the fuselage vertical bending moment was determined to assess the relative severity. Figure 17 presents the fuselage vertical bending moment for flight and ground environments.

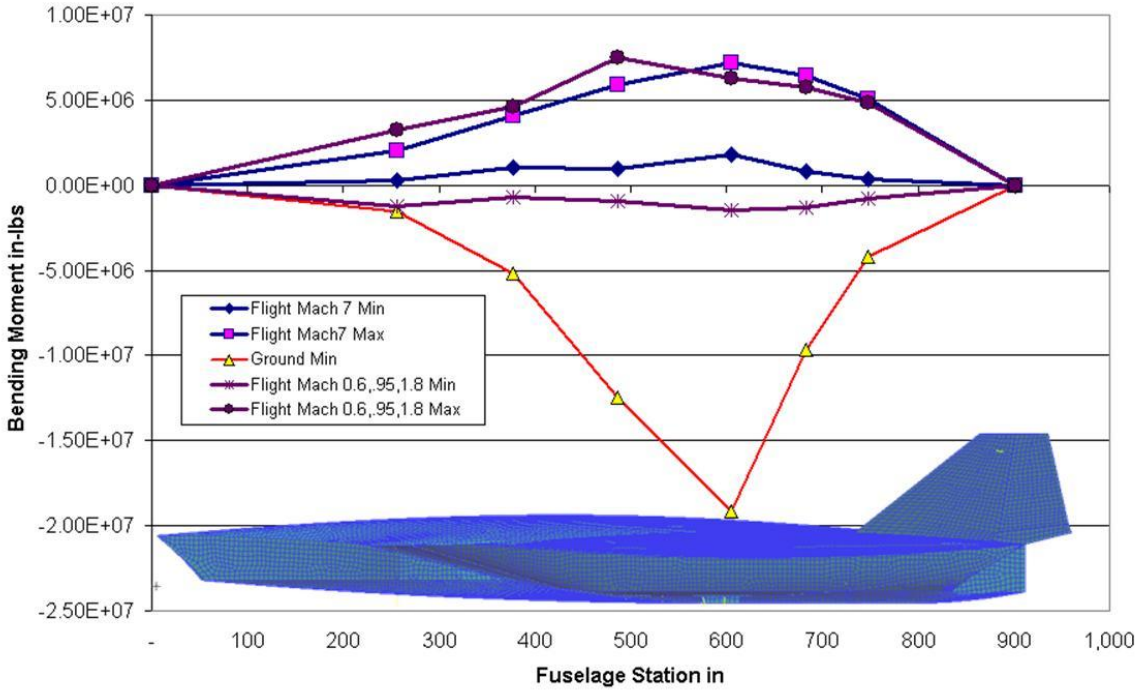

Figure 17. TX-V Fuselage Vertical Bending Moment

A transient thermal analysis was performed to determine the temperature distribution throughout the structure for the Mach 7 mission trajectory.

4.1.3.2 Thermal Math Model (TMM)

A finite difference Thermal Math Model (TMM) was developed from the Finite Element Model used for structural analysis. The TMM is a symmetric model created for the left side of the vehicle with 30,375 thermal nodes. The TMM is shown in Figure 18 without and with the exterior skin. The TX-V vehicle structure is composed of honeycomb sandwich panels made from titanium or inconel materials. The honeycomb panels consist of an upper facesheet, core, and a lower facesheet layers. Each layer can have different properties that must be accounted for in the thermal analysis. For the thermal analysis the honeycomb skin was modeled as 2-D elements with a thermal capacity and conduction comparable to the actual honeycomb skin panels. Thermal conduction was used on all 2-D plate elements. Fuel is stored in the lower fuselage and lower wing areas. Fuel was used as a heat sink. The lower body surface and wing surfaces conducted heat to the fuel mass. All element intersections were assumed to be perfect thermal contact (zero thermal resistance). The upper skin assumed radiation to a space environment. The lower surfaces assumed radiation to an earth environment. The initial structural temperature was assumed to be 100^{o} F.

No subsystem or engine components were included in the thermal analysis as this was out of scope. While including these thermal sources would improve the accuracy it is felt that the fundamental result would not be significantly altered. The TMM was used to produce temperature time histories at the element centroids. For structural analysis temperature data is required at the element corner point nodes. The nodal temperatures were determined by interpolating the element centroid temperatures to the element corner points. Structural temperatures for the right side of the FEM were obtained by mirroring the left side results to the right side.

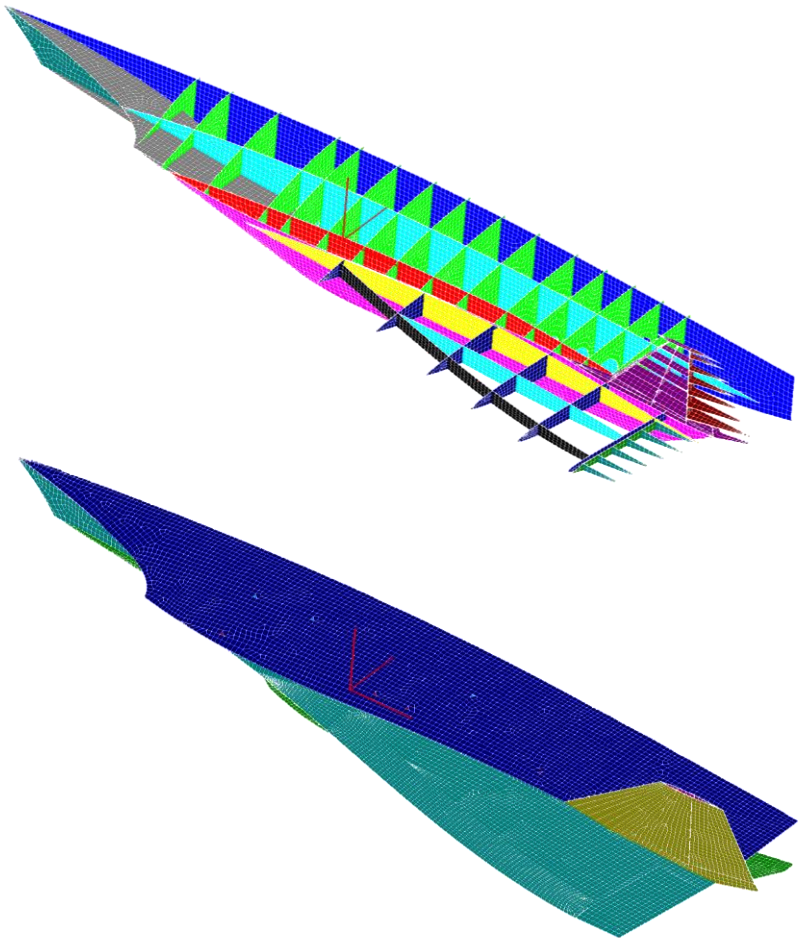

Figure 18. TX-V Thermal Math Model

An existing aeroheating database was leveraged for this effort. The aeroheating model was not an exact match for the TX-V vehicle OML. This required interpolation of the aeroheating data from the aeroheating model to TMM. The existing aeroheating model did not contain accurate aeroheating data for the leading edges. The data for these locations were simply determined by extrapolating from the acreage heating. Since the focus of this effort is to address panel acreage, and not leading edge regions this will not have impact the results.

The temperature time history for the upper and lower fuselage centerline locations is shown in Figure 19. This case illustrates the maximum temperature gradient between the upper and lower surface at this location.

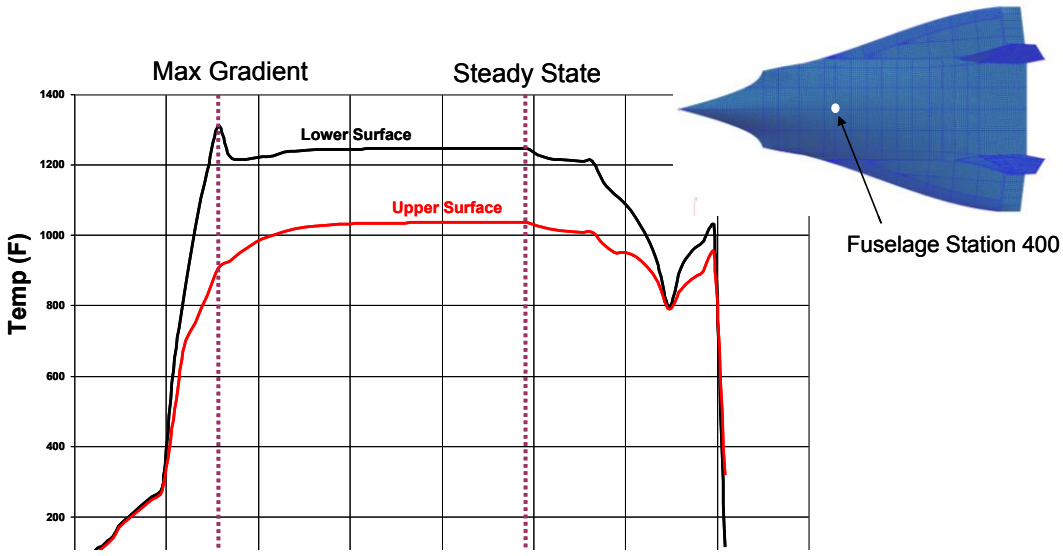

Figure 19. Fuselage Station 400 Temperature vs Time

Figure 20 contains the temperature time history for a point on the wing at station 600. External temperature distributions for t=800 sec, and t=2400 sec are presented in Figure 21 through Figure 22.

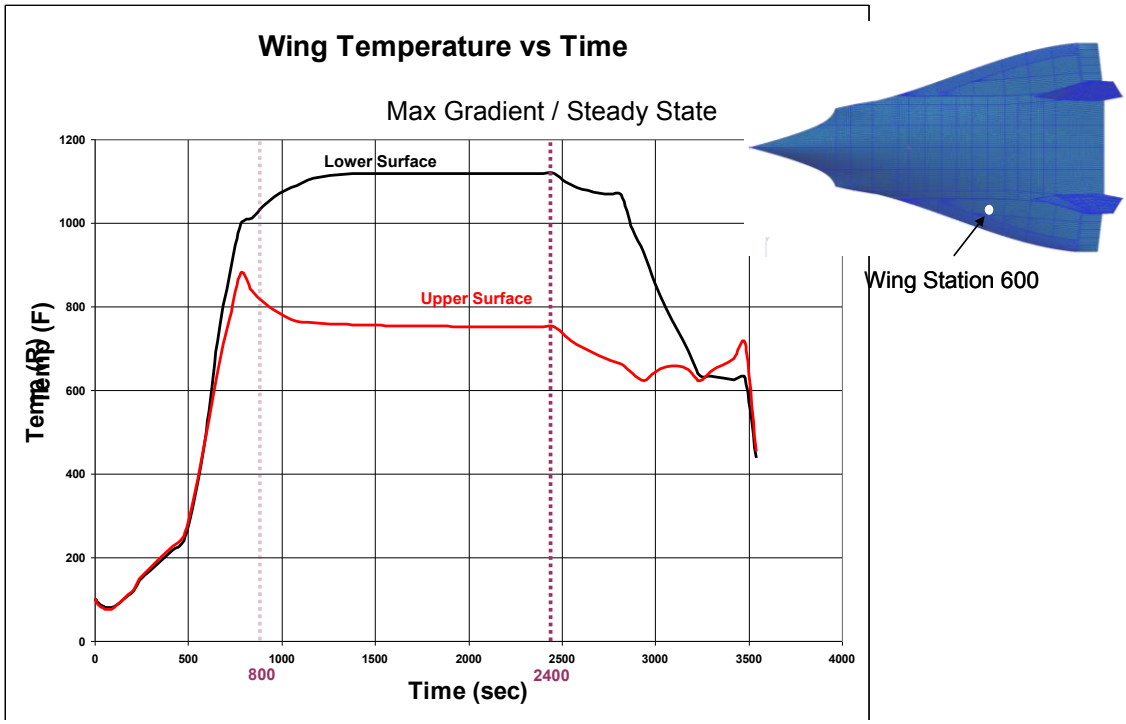

Figure 20. Wing Station 600 Temperature vs Time

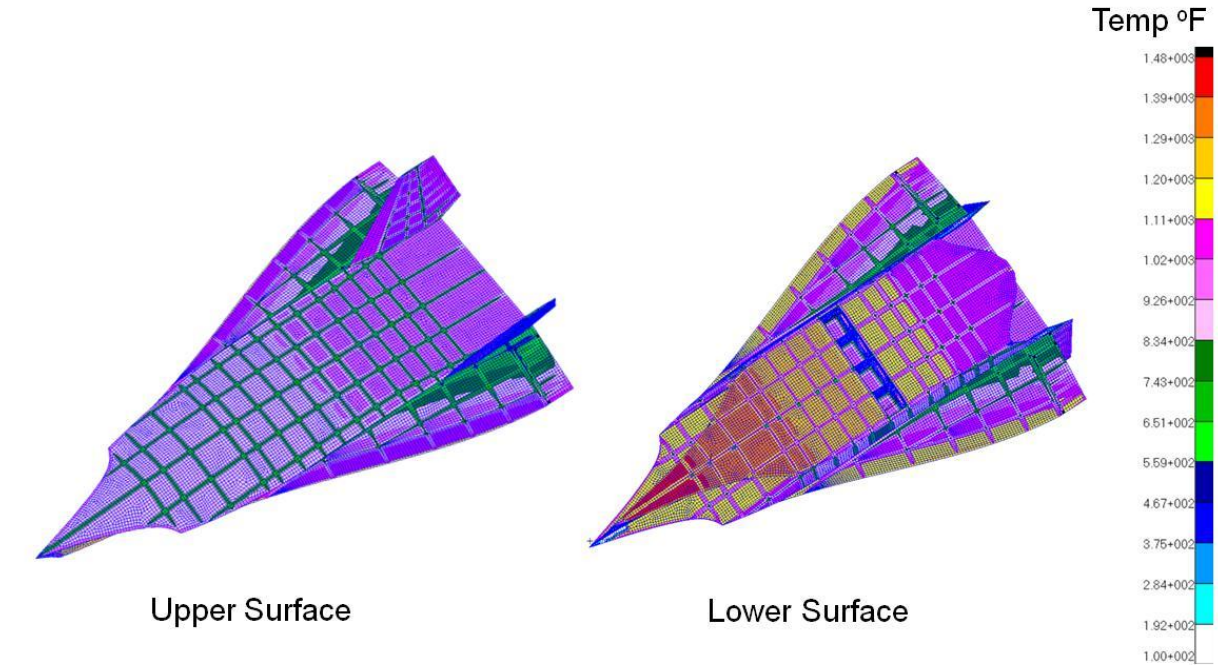

Figure 21. Structural Temperatures at 800 Sec

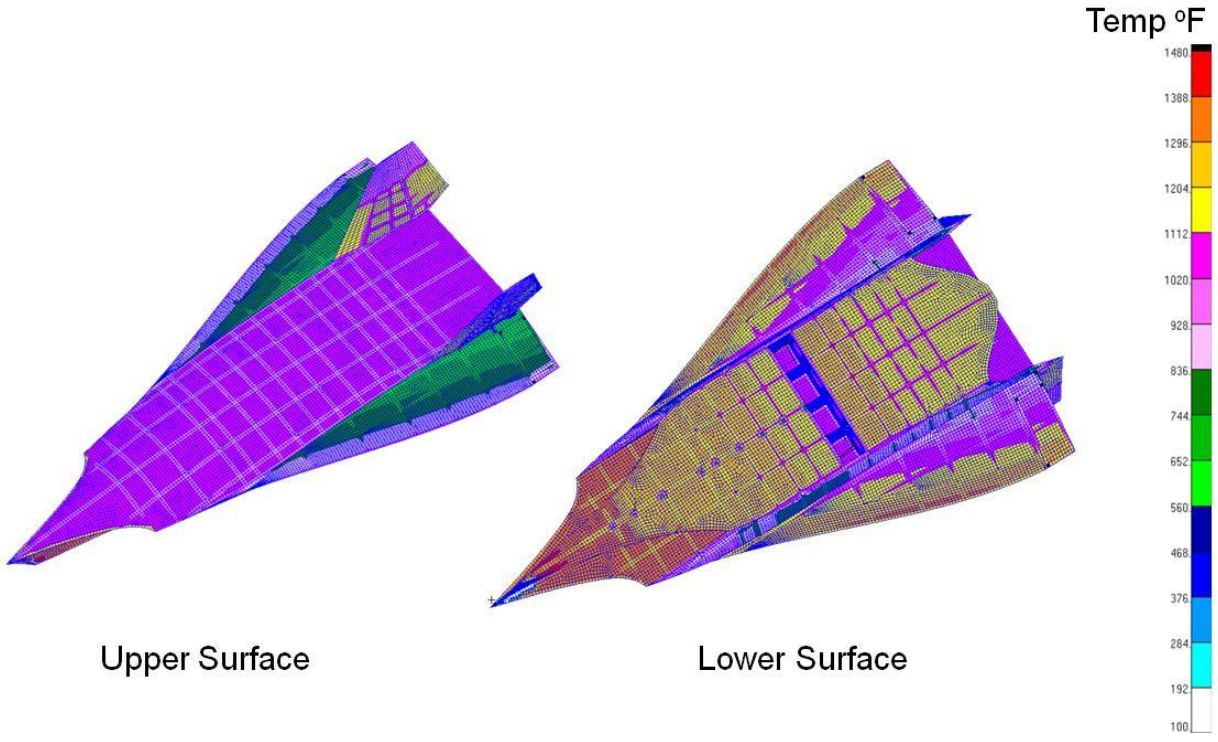

Figure 22. Structural Temperatures at 2400 Seconds

The following are some observations from the TMM analysis.

1. Since the TMM had corresponding elements for every vehicle surface element, the translation from the vehicle model to TMM was straightforward.

2. The vehicle model had many small, irregularly shaped surfaces that created some poorly defined thermal connectors, but since the grid was sufficiently fine the result was minor temperature distortion.

3. Mapping from the aeroheating model to the vehicle model was difficult. The two models were close in overall appearance, however slight differences in wing sweep and wing thickness made mapping difficult. Increased fidelity between aeroheating and vehicle models is desirable.

4. Leading edge temperatures could not be adequately calculated using the available aeroheating model. Separate aeroheating models should be used to calculate vehicle nose and leading edge heating rates when realistic data is required for leading edges.

5. The use of fuel as a heat sink can be a significant component in reducing vehicle temperatures. To accurately take advantage of fuel as a heat sink, the detail heat transfer from internal structure and skin surfaces to fuel tank and fuel should be determined. The details should consider the complex conduction, radiation and convection linkages, and usage rates at different tank areas.

4.1.3.3 Acoustic Loads

The following describes the process used to define the external aero-acoustic loads. Definition started with the general vehicle arrangement. Features were identified that may contribute to acoustics loads and determine appropriate empirical models for the region and flow conditions of interest. Inlets, nozzles, leading edges, surface bumps, all contribute to the loads. Semi-empirical models were applied to the flight trajectory and determine critical acoustic design load conditions for different types of flow including Attached/Turbulent Boundary Layer (A/TBL) and Separated/Turbulent Boundary layer (S/TBL) as shown in Figure 23 . The aero-acoustic loads will be predicted for the given trajectory, Figure 24. Next, CFD results were used to identify areas and conditions when turbulent, vortical, and/or shock induced separated flow conditions exist, Figure 25. Semi-empirical methods were applied to determine acoustic levels and spectrums based on the trajectory. Some of these semi-empirical methods are described in References [1] through [7]. Finally, the vehicle was mapped into regions of similar flow type and levels and all load and design factors were applied. This final load map was used to preliminary size panels in each region of the aircraft. These acoustic loads were then used to develop preliminary design requirements based on acoustic levels. These acoustic design requirements are then used in the preliminary structural sizing. CFD results are used to identify areas and conditions when turbulent, vortical, and/or shock induced separated flow conditions exist.

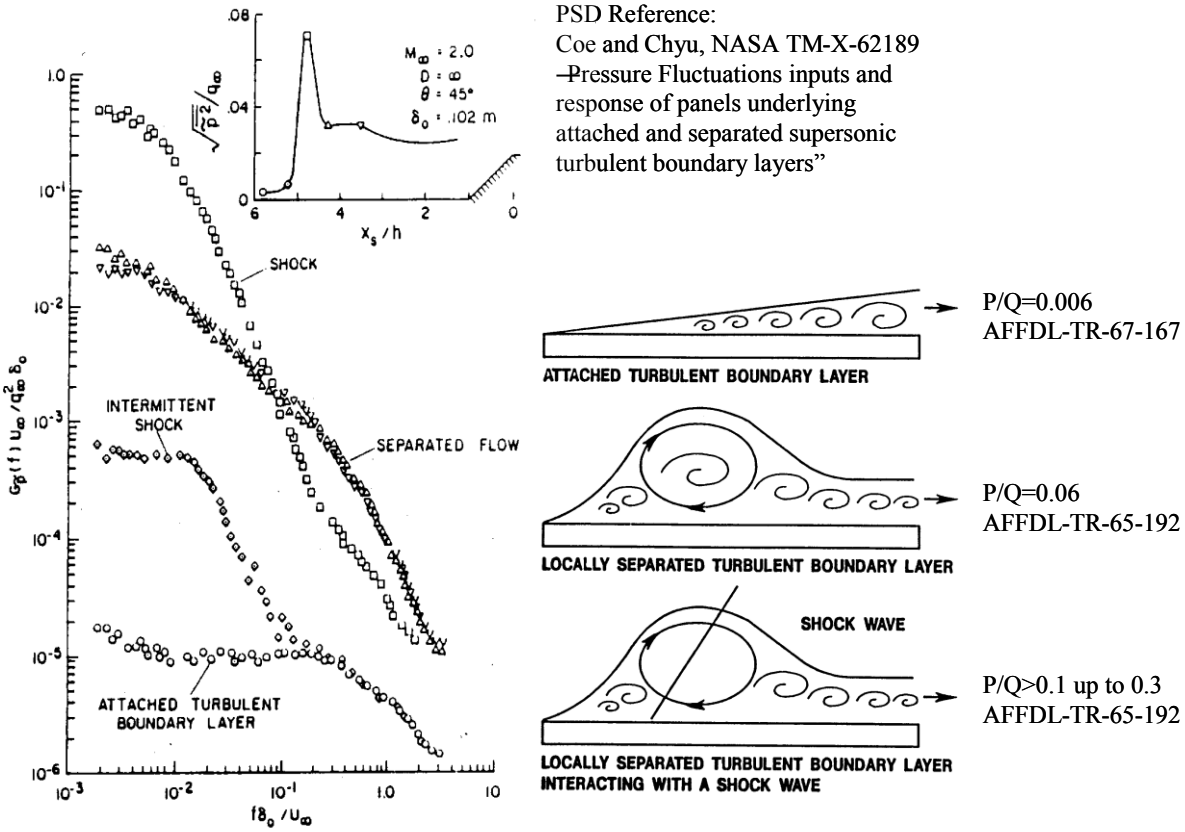

Figure 23. Flow Type and the Reference Empirical Model

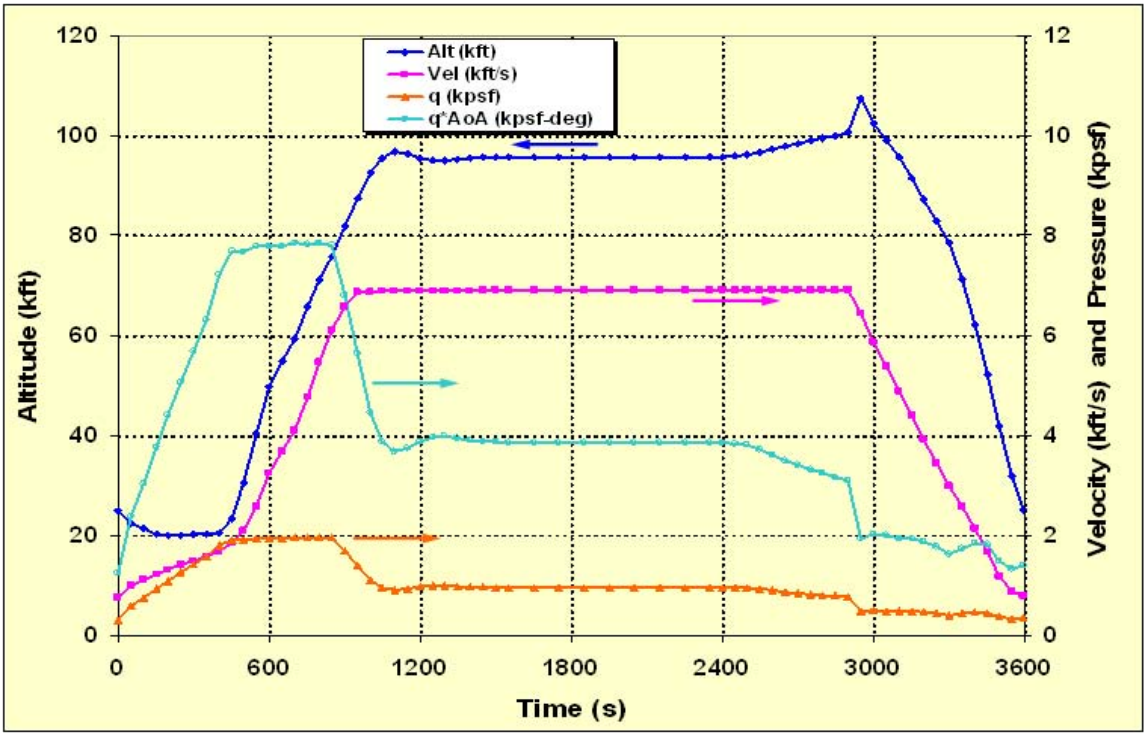

Figure 24. Baseline Trajectory

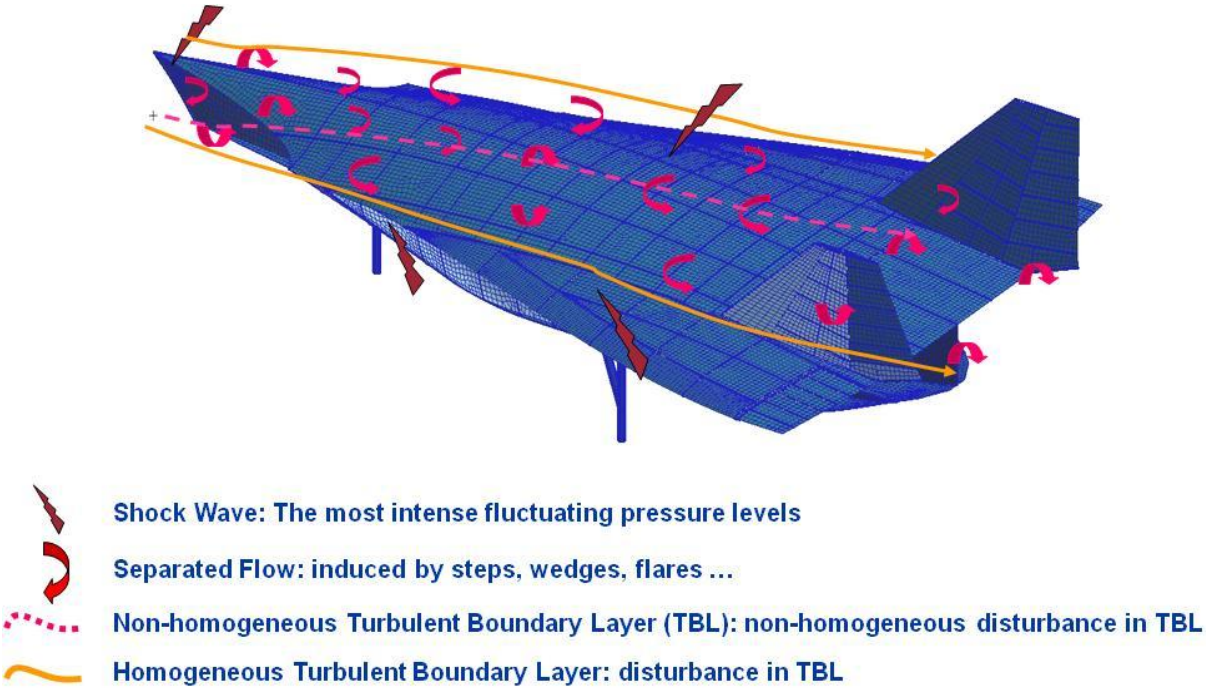

Figure 25. Flow Features Important for Acoustic Predictions

4.1.3.4 Trajectory Analysis

For this analysis, a simple acoustic model was used for two types of flow conditions: Attached/TBL and Separated TBL from Reference [5]. The maximum overall sound pressure levels (OASPL) for A/TBL is encountered at lower altitudes and Mach numbers, and the levels are fairly low (<150dB), as shown in Figure 26. This model is applicable to the majority of the vehicle acreage. In areas of vortex flow, the separated flow model was used. This would be applicable to the wing, aft fuselage and control surfaces. The highest levels occur during the acceleration to cruise condition. The max OASPL approaches 166dB as shown in Figure 26.

$$A/TBL\ OASPL = 16.153 * Ln(Mach) + (150. - Alt * 0.0004)$$
$$S/TBL\ OASPL = 20. * Log(Q) + \left(20 * Log(0.0078/\mathrm{Pr}ef) + 20. * Log((1 + Ca/\theta)^{1/2}\right) \quad \text{(Eqn. 4.1.1)}$$

Mach = Mach Number
Alt = Altitude (ft)
Pref = Reference Pressure 2.9e-9 psi
Q = Dynamic Pressure (psf)
Ca = Leading Edge Cone Angle
θ = Angle of Attack

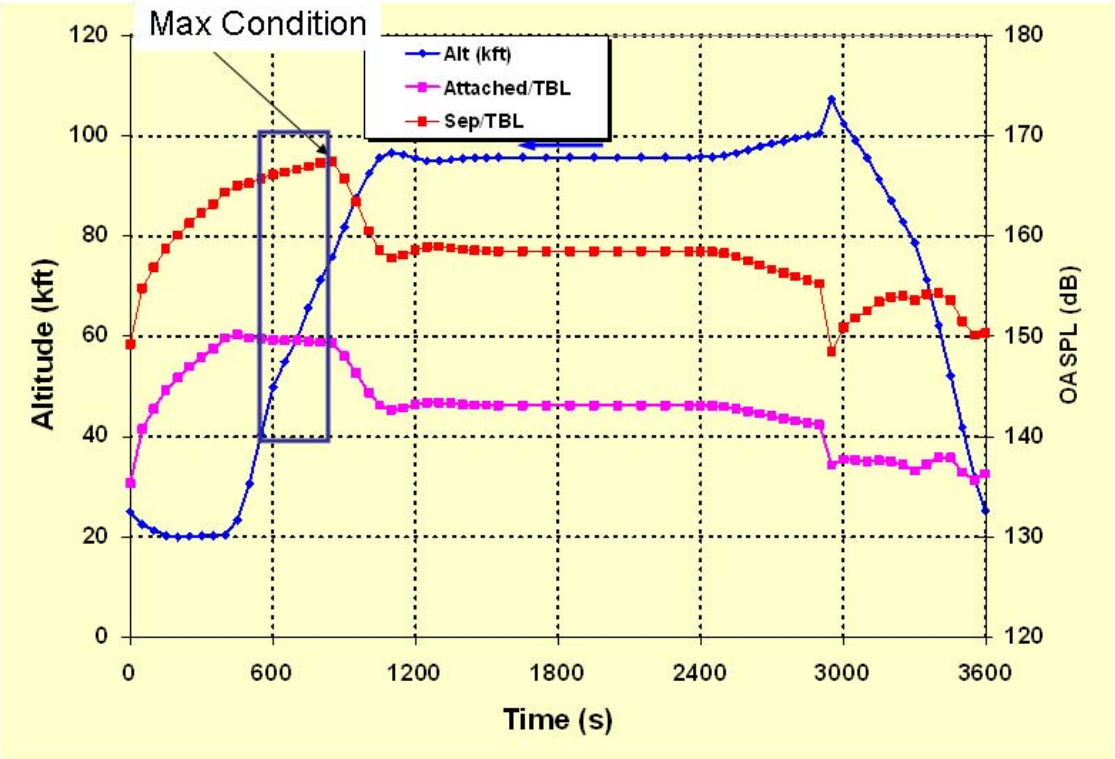

Figure 26. Reference Acoustic Levels for the Baseline Trajectory

4.1.3.5 CFD Guidance

A nonlinear CFD loads database was produced for the 12 conditions identified below:

- Navier-Stokes CFD Using Flow Solver CFD++
- CFD Mesh ~20M Grid Points
- Four Mach No.: 0.60, 0.95, 1.80, 7.00
- Three Angles Of Attack per Mach: 0^o, 5^o, 10^o

The acoustic loads were not based on these solutions; rather these conditions are qualitatively used to define regions of attached, separated, or shock induced flow. At Mach 0.6 and AoA of 10 degrees, there was leading edge vortex lift. The center fuselage regions were assumed to be A/TBL. The region from the wing leading edge to the aft control surfaces was assumed to be S/TBL (where the lifting vortex is pictured below in Figure 27). There are additional contributions if shocks are present. Also, additional contributions were included in the final design loads for the areas in the inlet, near the vertical tails, and exhaust regions. At higher dynamic pressures, the shock was primarily aft based on CFD analysis as shown in Figure 28. The shock induced turbulent boundary layer (SI/TBL) model was used for regions aft of the shock.

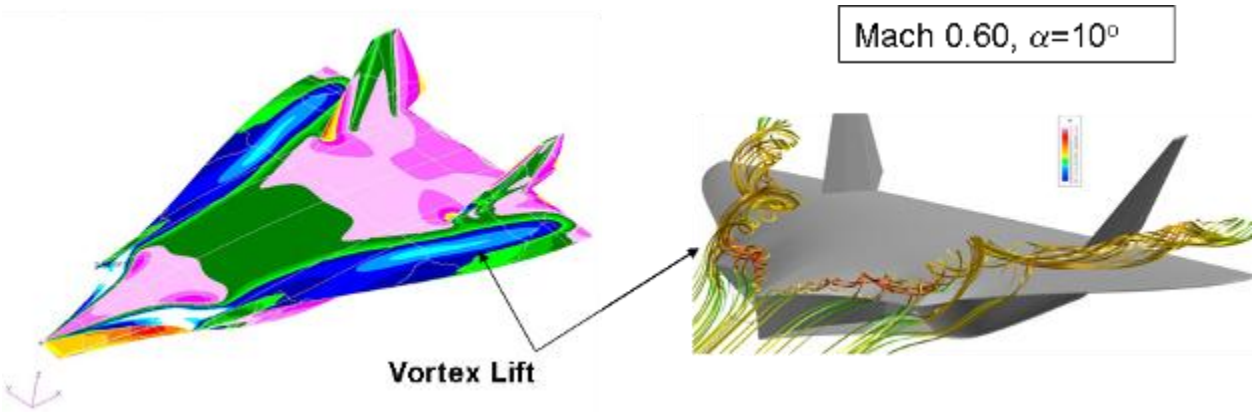

Figure 27. CFD Results

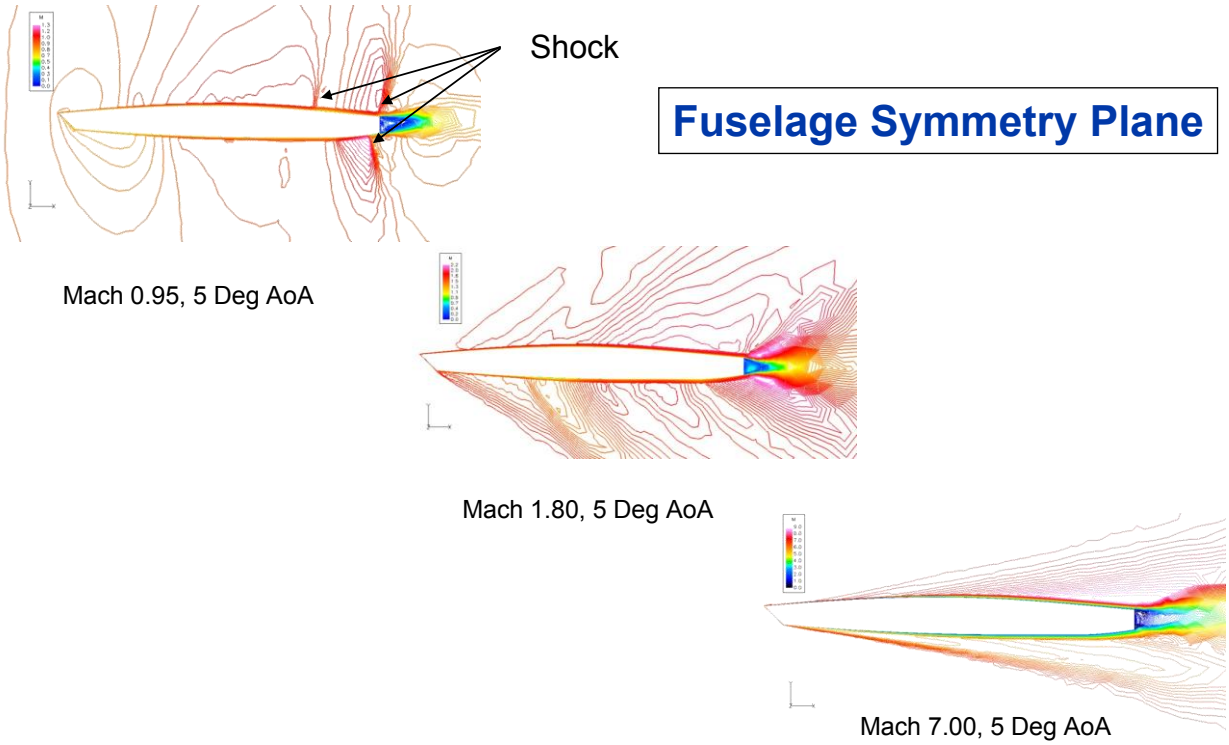

Figure 28. Mach Lines Showing Shock Locations

Based on the CFD results, upper and lower surface regions were defined. For the acreage regions, the Efimtsov model [2] was used to define acoustic levels along a stream line on the vehicle; i.e., OASPL vs. distance from LE. In Figure 29, the Attached/TBL 1/3 Sound Pressure Level (SPL) in the 250Hz band as a function of the distance from leading edge is shown. This stream–line would be from the wing LE to the elevon for the cruise condition in areas of no shocks or vortices. The max A/TBL spectrum is shown in Figure 30. For the aft fuselage and upper and lower wing surfaces of separated flow and shock induced flow separation, Figure 31 shows the 1/3 Octave Band Spectrum for 3 different types of separated flow. The highest curve is for SI/TBL at OASPL=164dB. This curve would be applicable near the local shock waves on the upper and lower surfaces. The lowest curve is for typical separated flow OASPL=159dB. The S/TBL flow type is typical for control surfaces (elevon and rudder), and locations on the aft side lower fuselage when the flow has transitioned from attached/TBL. The middle curve is applicable to regions where there are expansion-compression corners due to forward facing steps on the surface that exceed the local boundary layer thickness. For the TX-V vehicle, it is assumed that gaps and steps will be below this threshold.

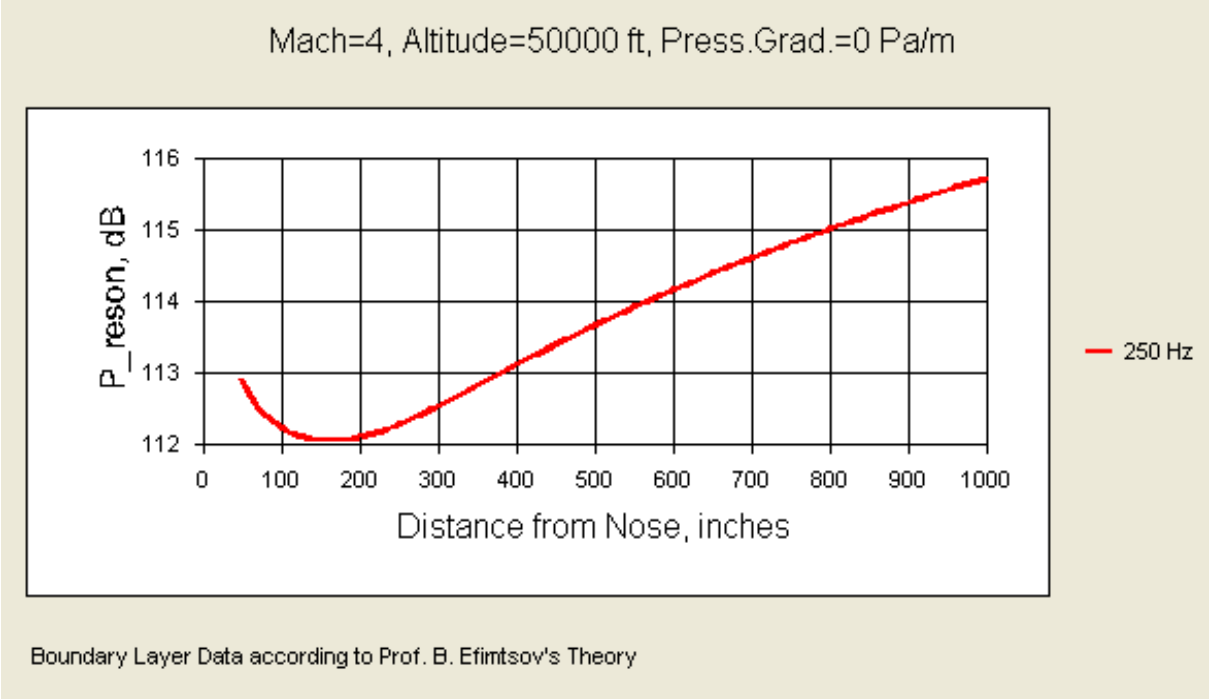

Figure 29. Attached/TBL 250hz 1/3 OCT Band Level as a Function Of Distance From the Leading Edge

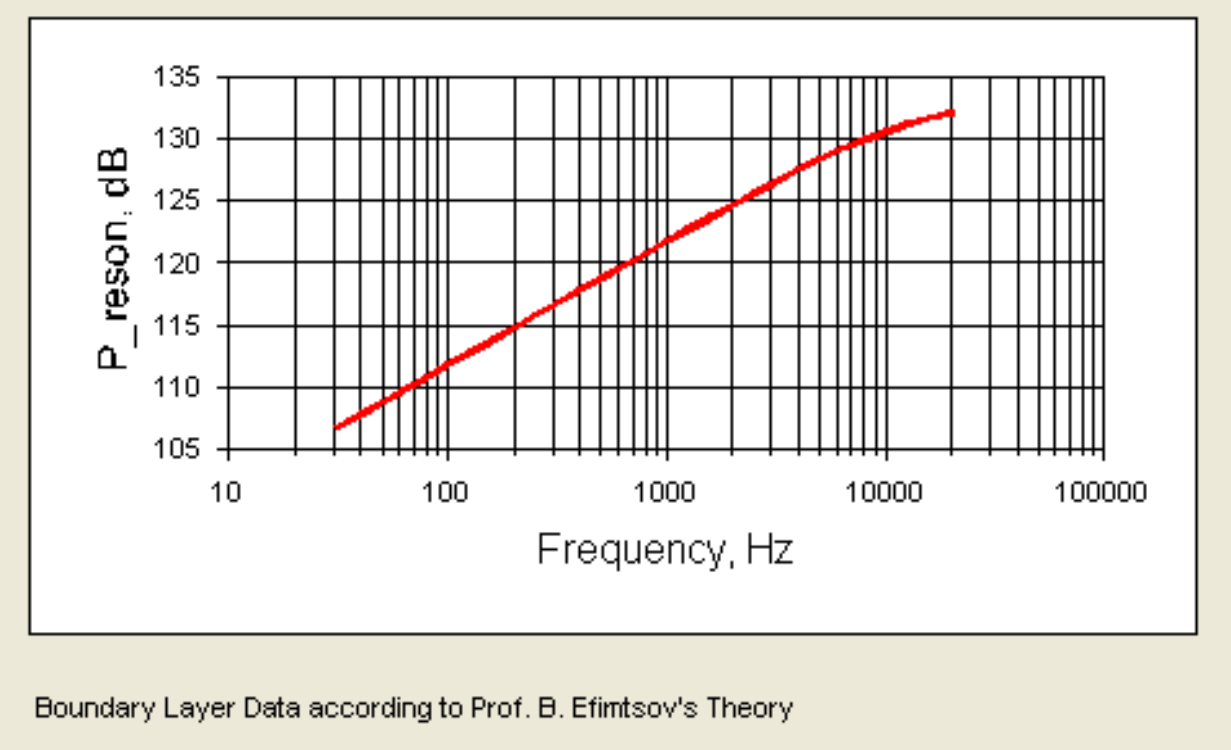

Figure 30. Attached/TBL Spectrum Aft Fuselage, OASPL=140.5 dB

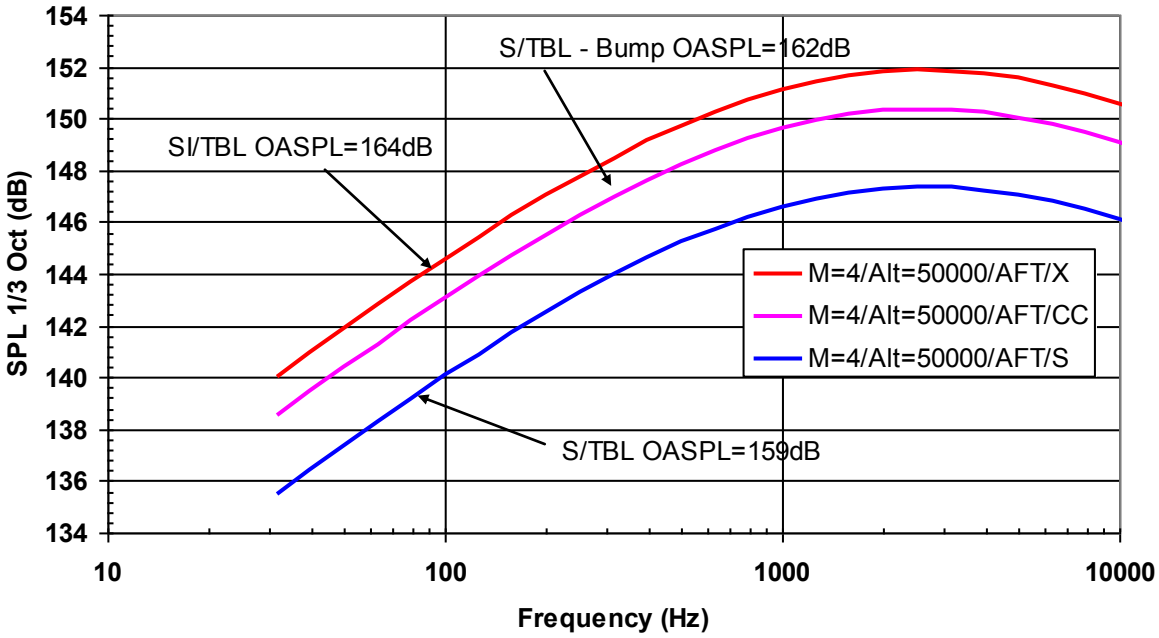

Figure 31. Separated and Shock Induced/TBL Spectrums AFT Fuselage

Based on the streamlined acoustic load predictions, CFD analysis, and empirical models, the acoustic zone maps were developed. Figure 32 and Figure 33 are the upper and lower acoustic zone maps, respectively. Regions of similar flow type and acoustic levels are color coded. Panels within these color coded regions could then be qualitatively evaluated as candidate panels for Phase II. Acoustic regions 1 and 8 used the Efimtsov A/TBL model. The other fuselage and wing LE regions used the S/TBL model. Region 5 on the upper surface uses the SI/TBL model. Region 6 on the upper surface uses the S/TBL model and an additional adjustment of 3.5dB for low frequency (10-60Hz) vortex buffet. On the lower surface, the inlet region included an additional 6 dB over the S/TBL model. This was to account for any bow shock or local inlet shock effects. There is also forward propagating propulsion noise at subsonic speeds. The inlet noise was only estimated for this study, however, the acoustic level increase is consistent with other vehicles. Region 14 had direct exhaust exposure. Again, the acoustic levels were not specifically predicted for the exhaust region in this study, but approximate estimates of acoustic levels were developed based on effective nozzle area and exit flow velocity.

The acoustic levels in the zone maps are design loads. These loads were factored for acoustic fatigue life predictions. A factor of safety of 3.5dB was added to the levels. Acoustic noise levels in TBL flow has considerable uncertainty and a factor of safety is standard design practice for acoustic fatigue to account for uncertainty. Also, the entire flight profile and usage was taken into account and reduced to a single OASPL and duration. The acoustic levels specified on the Zone Maps will produce the same damage as the full trajectory. This is based on Time Compression analysis, assuming titanium fatigue exponent.

The assumptions for the time compression analysis were as follows:

No. of Flights = 300
Flight Time = 1 hr (3600 sec)
Critical Condition = Acceleration from Mach 2.7 to 6.2
Time on Condition= 300 sec
Acoustic Level Correction: ΔdB = -0.75
Total Time = 300 sec/3600 * 300 flight = 25 hrs

For example, consider a panel in Zone 5 on the upper surface. For any simplified acoustic fatigue life prediction, an OASPL=171 dB was assumed and the panel would have to survive for 25 hours at this level.

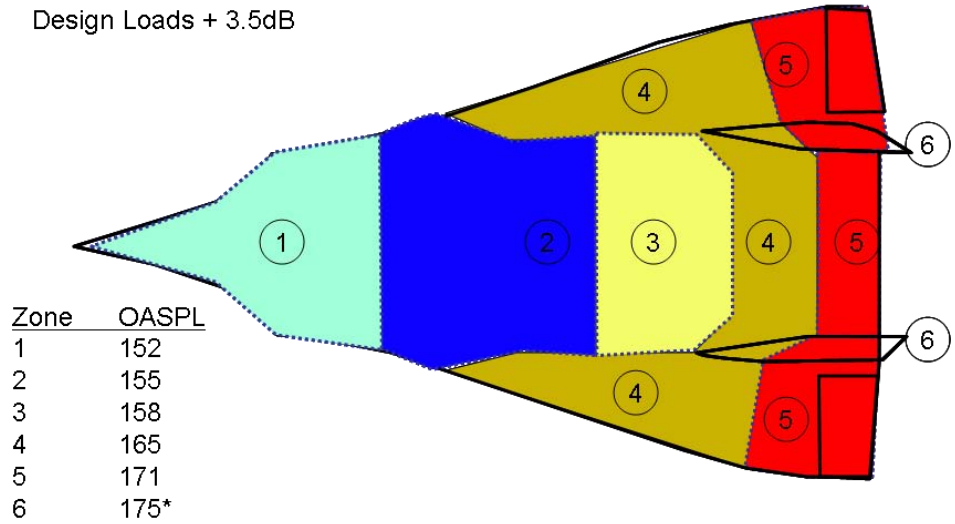

Zone	OASPL
1	152
2	155
3	158
4	165
5	171
6	175*

Figure 32. Upper Acoustic Zone Map

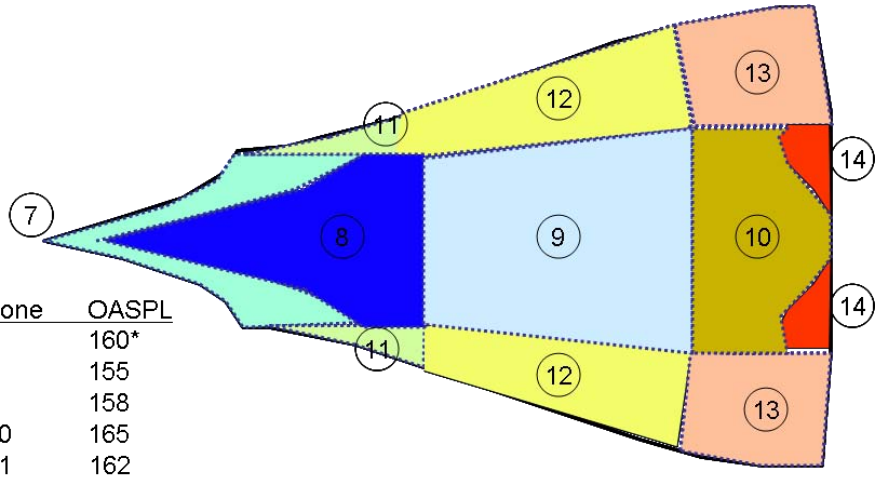

Zone	OASPL
7	160*
8	155
9	158
10	165
11	162
12	161
13	168
14	172**

Figure 33. Lower Acoustic Zone Map

For preliminary sizing, acoustic fatigue was not preformed on any individual panel. Instead, the acoustic design requirements were used to define panel frequency requirements based on acoustic fatigue. Figure 34 shows the results of a spreadsheet parametric analysis for a large range of panel length, width, and thickness of titanium thin gage panels at OASPL=165dB. This same analysis was run at several OASPL to develop the general guidelines below. The red line in the figure represents the frequency requirement at OASPL=165dB.

Panel Frequency Design Guidelines:

- Minimum Fn > 100 Hz (panel flutter and acoustic fatigue requirement)
- Zones OASPL <155dB, Fn>125Hz
- Zones 155dB < OASPL < 160dB, Fn>150Hz
- Zones 160dB < OASPL < 165dB, Fn>200Hz
- Zones OASPL > 165dB, Fn>250Hz

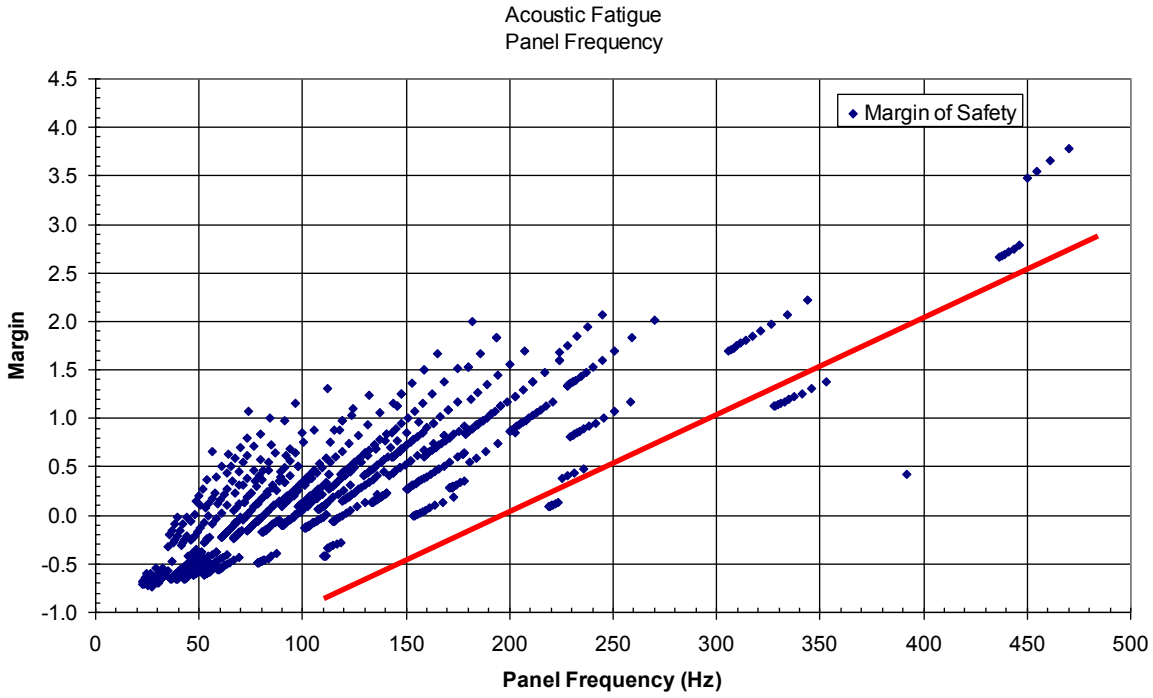

Figure 34. Parametric Analysis Results at OASPL=165dB

A plot of the panel frequency requirement is shown in Figure 35. In general, any panels that do not meet this requirement should be analyzed using detailed panel level FEA. Some additional requirements are given below:

- On all panels that don't meet above criteria, or
- 0.75 < P/Pc < 1.0 for static loads (thermal+Mech), or
- Low static strength margins for bending/compression
- For all panels exposed to acoustic levels OASPL > 165dB

The static loads due to thermal and mechanical loads can cause significant in-plane loads that can change the frequency and mode shapes of panels. If the panel is close to buckling limits, Pc,

then acoustic fatigue can be more critical. Also, if the OASPL is above 165dB then nonlinear acoustic response is likely. This would require detailed analysis.

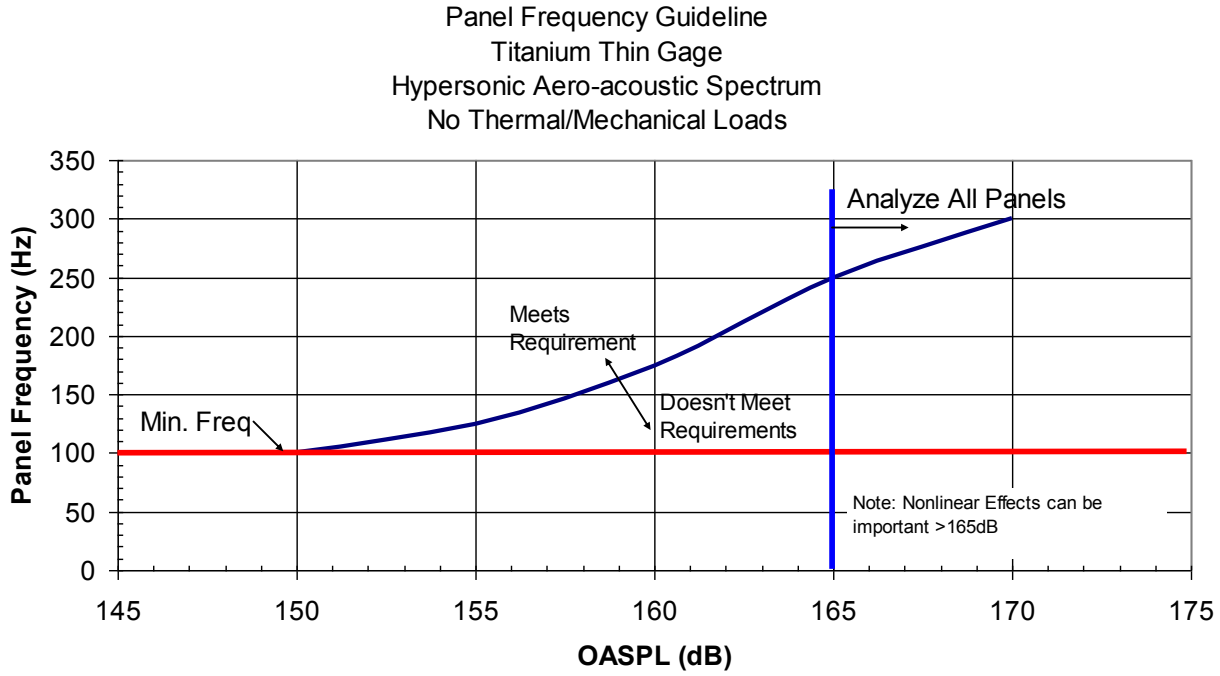

Figure 35. Panel Frequency Requirement Plot

4.1.3.6 Structural Sizing

Structural analysis was performed using MSC.Nastran, and HyperSizer. MSC.Nastran is a general purpose finite element program which solves a wide variety of engineering problems. It is developed, marketed and supported by the MSC.Software Corporation. For the structural sizing task Sol 200 and 101 solution sequences were used. Nastran Sol 200 is a gradient based structural optimization capability used to perform design optimization. Nastran Sol 101 is a linear statics solver which was used to determine internal load distributions, after sizing or external load updates. HyperSizer is a structural sizing program developed by Collier Research, used to perform local panel and beam sizing.

Structural sizing was performed using the global/local Nastran Sol 200 and HyperSizer process outlined in Section 3.1. For this application, Sol 200 was used to determine an initial global sizing subject to strength constraints. The strength constraints in Sol 200 consisted of minimum and maximum principle stress. Internal loads were computed using the Sol 200 sizing results and input into HyperSizer where detailed strength, buckling and panel frequency constraints were applied, and the sizing updated.

Materials were selected based on the thermal temperature results. If the structural temperature was greater than 1000^{o} F then Inconel 718 was used. This occurred primarily on the exterior skin surfaces. The bulkhead and keel structures which were much cooler were made from titanium alloy. Since the material strength allowable is a function of temperature, and the temperature varied over the design zones, the strength allowable was determined by computing the average

design zone temperature and applying the appropriate allowable based on this average temperature.

The Sol 200 load set consisted of the 10 flight maneuver cases shown in Table 3 which included both minimum and maximum fuel conditions. The fuel mass conditions were applied using separate MPC sets. This allowed the mass conditions to be selected at the subcase level which permitted multiple mass conditions to be considered in Sol 200. For the initial Sol 200 sizing the Mach 7 flight loads were not included since the CFD results for Mach 7 were developed using a different mesh output format, and it was not possible to combine these solutions with the others within the schedule constraints. The Mach 7 flight loads were used in HyperSizer. It is not expected this will have a significant effect on the sizing results.

Table 3. Sol 200 Flight Maneuver Conditions

Mach	Nz	Sideslip	Fuel
0.60	-1.0	0	Min
0.60	2.5	0	Min
1.80	-1.0	0	Min
1.80	2.5	0	Min
0.60	-1.0	0	Max
0.60	2.5		Max
0.60	1.0	5	Max
1.80	-1.0	0	Max
1.80	2.5	0	Max
1.80	1.0	5	Max

Conditions for ground loads included the five cases shown in Table 4 which were all produced for the maximum gross take off gross weight condition. A full set of 21 landing and ground handling load conditions were investigated. Landing loads were developed assuming a typical 80% shock strut efficiency.

Table 4. Sol 200 Ground Load Conditions

Description	Fuel
3PT BRAKED ROLL N=1.2g	Max
UNSYMM BRAKING	Max
LT TURN-MAX FSMR	Max
REVERSE BRAKING	Max
TAXI	Max

FEM nodal temperature sets were developed for 2 time points in the mission trajectory. These points represent the maximum thermal gradient between the upper and lower fuselage surfaces, and the maximum steady state temperature condition. The maximum steady state temperature set was selected for the initial Sol 200 sizing based on preliminary HyperSizer results which indicate this case was more critical. The number of thermal cases considered for sizing was intentionally kept small to minimize the effort while still providing representative loading. For a

more detailed analysis many time points along the trajectory would be considered to ensure the critical loading for each structural member is considered for structural sizing. Use of the thermal loads in Sol 200 produced two issues. These issues ultimately prevented the use of thermal loads in Sol 200 for this application. The first issue was due to the use of rigid RBE2 elements. For the TX-V FEM these were used for connecting dissimilar meshes on components such as the wing, vertical tail, control surfaces and fuselage. This is not a desirable modeling approach if time and budget permit more accurate modeling. However, the TX-V FEM was obtained from a previous conceptual level study that did not require accurate results in these locations and creating a more detailed FEM was out of the scope of the current effort. In order to obtain reasonable internal load results when temperature loads are applied, the Lagrange multiplier method should be used for processing the rigid elements. This is easily done for the Sol 101 static analysis, but Nastran Sol 200 does not support this capability. As a test of using Sol 200 with thermal loads the linear method for the RBE2 processing was used in spite of the questionable internal load results. This produced the second issue which prevented the use of thermal loads in Sol 200. Nastran Sol 200 reported that sensitivities for some elements were zero and optimization was not possible. This was not fully investigated but it is believed to be model dependant and due to the use of a cool substructure with high temperature skin panels.

In order to generate an initial sizing, the thermal load was removed from the Sol 200 analysis, and the sizing performed considering only the flight maneuver and ground load conditions. The Sol 200 sizing was performed with consideration of material strength constraints.

The Sol 200 sizing results were used as input for HyperSizer where panel level sizing was performed considering strength, buckling, and panel frequency constraints based on acoustic requirements. The initial sizing was performed using a honeycomb panel concept.

Table 5 contains the load cases used in the HyperSizer assessment. The table presents the load case numbers used by HyperSizer for condition identification. The maximum temperature column indicates the maximum nodal temperature for a load case. The % Total Weight column shows the weight fraction attributed to each load case. Table 5 shows that load case 9 is the sizing load case for nearly the entire structure, 99.4% of the structural weight was sized using loads from this condition. The Weight column gives the total vehicle weight used in generation of the flight and ground load conditions. The thermal load used in Table 5 is for the maximum steady state thermal load. This occurred at time=2400 s at the end of the Mach 7 cruise segment. This thermal case was combined with a Mach 7, +2.5g, symmetric pull up maneuver. Internal loads were computed using Sol 101 with the Lagrange multiplier method. It should be noted that the mechanical contribution to load case 9 was insignificant compared to the thermal portion. Reducing the load factor to a level less than +2.5g would have little effect on the resulting sizing and weight.

Table 5. HyperSizer Mach 7 Load Set

Load Case	Cond	Type	Max Temperature Degrees F	% Total Weight	Mach	Nz g's	Sideslip Angle Deg	Weight lbs
2	Flight	Mechanical	72	0.00%	0.60	-1.0	0	98,190
3	Flight	Mechanical	72	0.00%	0.60	2.5	0	98,190
4	Flight	Mechanical	72	0.00%	1.80	2.5	0	98,190
5	Flight	Mechanical	72	0.50%	1.80	1.0	5.0	98,190
6	Flight	Mechanical	72	0.00%	0.60	2.5	0	185,640
7	Flight	Mechanical	72	0.00%	1.80	2.5	0	185,640
8	Flight	Mechanical	72	0.00%	1.80	1.0	5.0	185,640
9	Flight	Mechanical+Thermal	1721	99.40%	7.00	2.5	0	159,740
10	Ground	Mechanical	72	0.00%	0.10	1.2	0	185,640
11	Ground	Mechanical	72	0.0%	0.10	2.0	0	185,640

Based on the applied loads and constraints in strength, buckling, and frequency, revised structural sizing was determined. Using the newly computed sizing, the internal loads were updated for the mechanical and thermal loading. These new internal loads were then used by HyperSizer to compute updated panel level sizing. The sizing loop was iterated until the structural sizing and weight converged. The initial sizing attempt did not converge as shown by the diverging total weight result shown in Table 6. Each iteration through the Hypersizer and Sol 101 loop resulted in significant weight increase. Additional information on the weight breakdown along with the controlling failure mode is presented in Table 6 for 3 iterations. The sizing was dominated by the Mach 7 thermal load case. Table 6 shows the sizing integration history with the Mach 7 thermal loads.

Table 6. HyperSizer Iteration Weight History for Mach 7 Thermal Loads

Iteration	1	2	3
Weight Total (lb)	43,330	70,410	103,700
Beam, Unit Weight (lb / ft)	2.08	3.34	4.20
Beam, Total Weight (lb)	7,087	11,350	14,290
Panel, Unit Weight (lb / ft^2)	4.26	6.94	10.51
Panel, Total Weight (lb)	36,240	59,060	89,430
Controlling Failure Mode, Strength (lb)	27,750	42,030	51,970
Controlling Failure Mode, Buckling (lb)	2,113	1,042	1,411
Controlling Failure Mode, Local Buckling (lb)	2,907	4,829	4,176

Figure 36 shows the location of panel 712 on the lower surface. HyperSizer determines the material allowables based on the average panel temperature. Since the thermal load case defines nodal temperatures at each node there can be a significant variation in temperature on a panel. For panel 712, the minimum, average, and maximum temperatures are 768.9, 1197.2, and 1237.0^{o} F respectively for the Mach 7 thermal load case at t=2400 sec. The sizing iteration history for this panel is shown in Table 7. For the first iteration panel 712 was sized by frequency requirements dictated by acoustic fatigue guidelines. On the 2nd & 3rd iterations the facesheet gages and core thickness increase significantly with a strength failure mode.

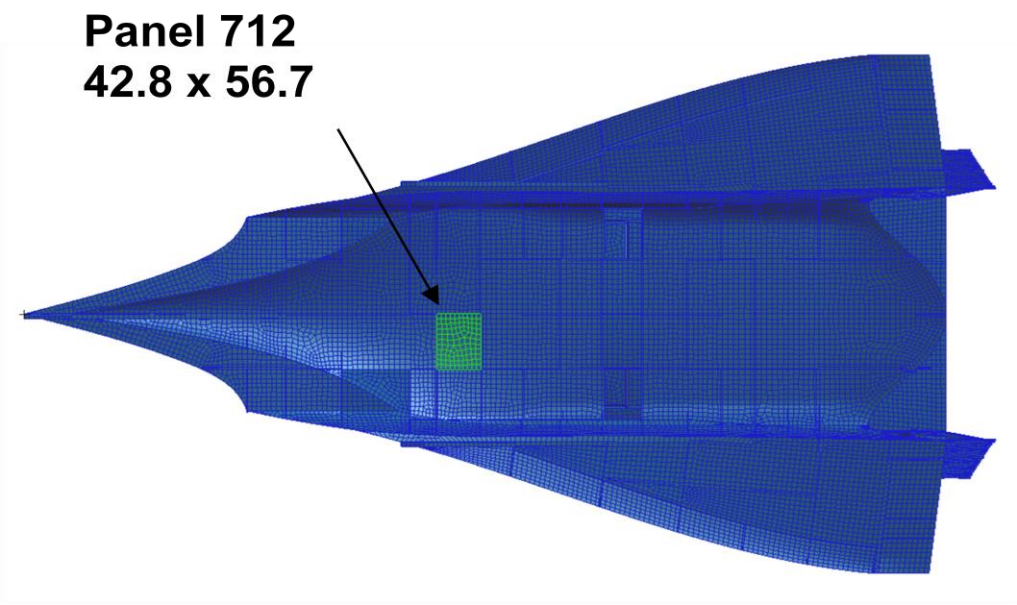

Figure 36. Lower Surface Panel 712

Table 7. Panel 712 HyperSizer Iteration History for Mach 7 Thermal Loads

Iteration	Group / Component	t_{tf}	t_c	Weight	Lowest	Controlling	Controlling
		(in)	(in)	(lb)	MS	Load Case	Failure Mode
1	712 "FUSE_LOWER_RHS.009"	0.034	1.82	73.7	0.299	9	Frequency Limit, Panel or Beam
2	712 "FUSE_LOWER_RHS.009"	0.052	1.82	100.6	0.178	9	Isotropic Strength, Von Mises Interaction Yield Criterion
3	712 "FUSE_LOWER_RHS.009"	0.089	3.01	170.7	0.192	9	Isotropic Strength, Von Mises Interaction Yield Criterion

Upon investigation of the results, several interesting characteristics of the Manta structural configuration were evident. The upper and lower surface skins were very hot and loaded in compression in both the x and y directions while the bulkhead and keel substructures were cool and loaded in tension. Essentially, the substructure being cool and made out of titanium remained fixed expanding very little and constraining the inconel skins that were subjected to high temperatures and attempting to expand.

For a constrained structure subject to severe thermal loading, increasing the cross sectional area in an attempt to reduce stress has no effect since this also increases the thermal load. For a constrained bar subject to thermal loading the stress is calculated by the equation $\sigma = -E\alpha(\Delta T)$. This equation shows that changing the cross sectional area has no effect on the stress. To minimize the internal loads, desirable factors would include a material with a low CTE, sufficiently small ΔT, or attachment fixity that allows for expansion.

A better solution for this problem is to redesign the structural configuration so that the full depth bulkheads and keels are replaced with minimum depth frames and longerons that will heat up and expand along with the skin panels. This was the approach used for one of NASP designs. This was not feasible as it was out of the scope for this effort. The approach taken was to scale down the temperature distribution so that the maximum temperature was reduced to 1050^{o} F. It is estimated this would be roughly equivalent to reducing the cruise Mach number to the Mach 4 to Mach 5 range. The scaled temperature distribution is presented in Figure 37 and Figure 38.

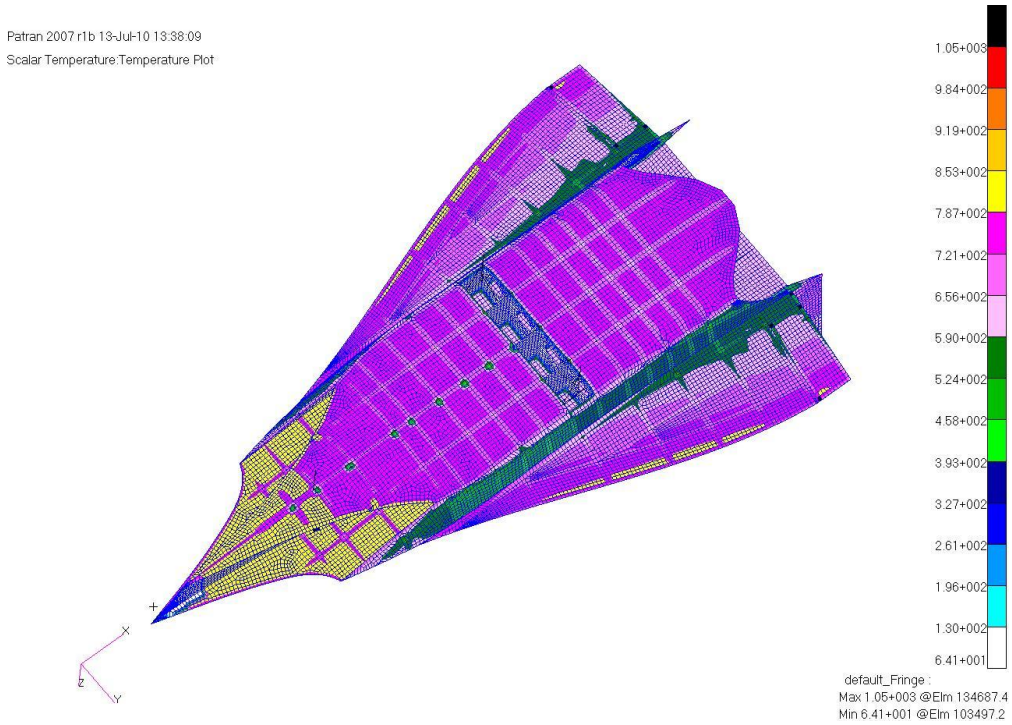

Figure 37. Reduced Lower SurfaceTemperature Distribution

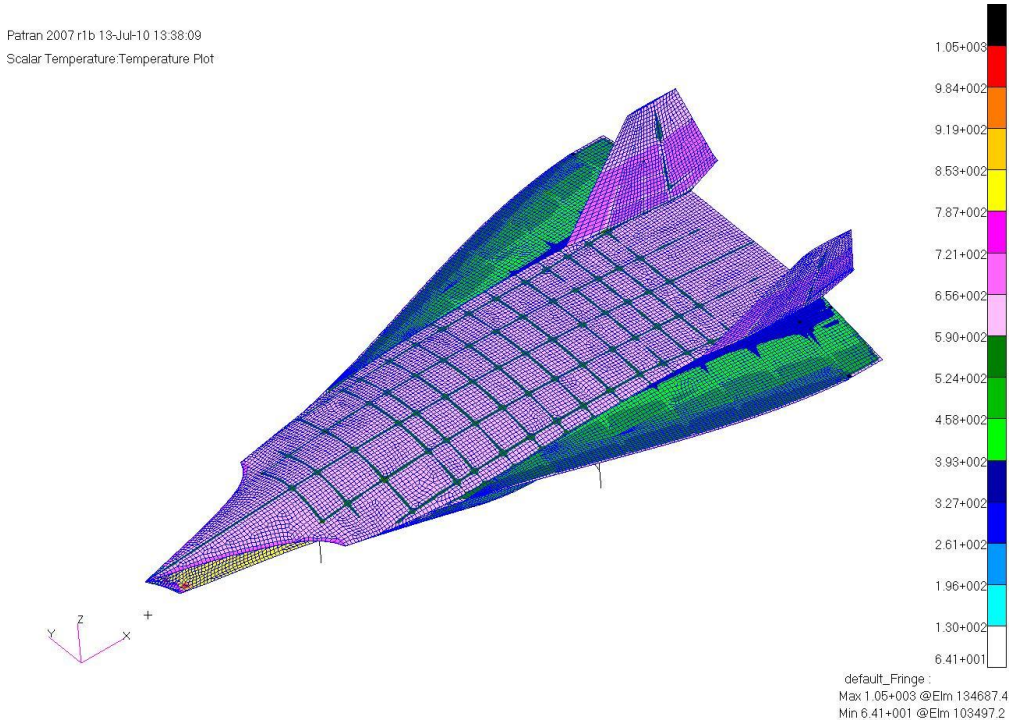

Figure 38. Reduced Upper Surface Temperature Distribution

Table 8 contains the load cases considered for the Hypersizer sizing with the reduced thermal loading. All other load cases were identical to those used in the initial HyperSizer sizing attempt except for the thermal condition.

Table 8. HyperSizer Load Cases with Factored Thermal Condition

Load Case	Cond	Type	Max Temperature Degrees F	% Total Weight	Mach	Nz g's	Sideslip Angle Deg	Weight lbs
2	Flight	Mechanical	72	4.6%	0.60	-1.0	0	98,190
3	Flight	Mechanical	72	0.1%	0.60	2.5	0	98,190
4	Flight	Mechanical	72	0.0%	1.80	2.5	0	98,190
5	Flight	Mechanical	72	0.0%	1.80	1.0	5.0	98,190
6	Flight	Mechanical	72	0.3%	0.60	2.5	0	185,640
7	Flight	Mechanical	72	8.6%	1.80	2.5	0	185,640
8	Flight	Mechanical	72	0.4%	1.80	1.0	5.0	185,640
9	Flight	Mechanical+Thermal	1050	84.5%	7.00	2.5	0	159,740
10	Ground	Mechanical	72	1.1%	0.10	1.2	0	185,640
11	Ground	Mechanical	72	0.4%	0.10	2.0	0	185,640

Using the reduced thermal loading resulted in convergence of the structural sizing. The new results show that load case 9 is still the driving load case accounting for 85.5% of the structural weight. It is believed this result is primarily due to the full depth keel and bulkhead configuration.

Table 9 presents a component weight summary for a honeycomb panel concept. The results show the total component, and unit weights. The honeycomb face sheet thickness and core thickness are presented in Figure 39 and Figure 40. The honeycomb face sheet thickness and core thickness for the fuselage are presented in Figure 41 and Figure 42. The honeycomb panels use the same sizing for both the upper and lower face sheets. Complete panel sizing results for the entire vehicle, with controlling load case and panel failure modes are presented in Appendix A and Appendix AA.

Table 9. Structural Component Weights

Group Panel Weight Summary				
Group	Area (ft^2)	Unit Weight (lb / ft^2)	Weight (lb)	% Total Panel Weight
Fuselage lower skin	925	2.36	2,184	9.2%
Fuselage upper skin	1,330	1.86	2,474	10.5%
Bulkheads	1,451	2.18	3,166	13.4%
Keels	1,473	1.91	2,818	11.9%
Fuselage side skins	466	3.50	1,632	6.9%
Wing skin	737	2.77	2,039	8.6%
Wing spars & ribs	353	1.47	520	2.2%
Engine Inlet	547	2.65	1,447	6.1%
Elevon & rudder control surfaces	378	1.24	468	2.0%
Vertical tails	347	2.05	712	3.0%
Wing & vertical leading edges	504	12.24	6,170	26.1%
Totals	8,510	2.78	23,630	100.0%
Group Beam Weight Summary				
Group	Length (ft)	Unit Weight (lb / ft)	Weight (lb)	% Total Beam Weight
Keel caps	683	1.41	965.6	22.7%
Fuselage vert stiffeners	292	0.88	258.4	6.1%
Bulkhead caps	1,161	0.83	964.9	22.6%
Wing spar/rib caps	553	2.69	1485	34.9%
Elevon/rudder rib/spar caps	623	0.51	315.8	7.4%
Wing & vertical leading edges areas caps	91	3.01	272	6.4%
Totals	3,403	1.25	4,262	100.0%

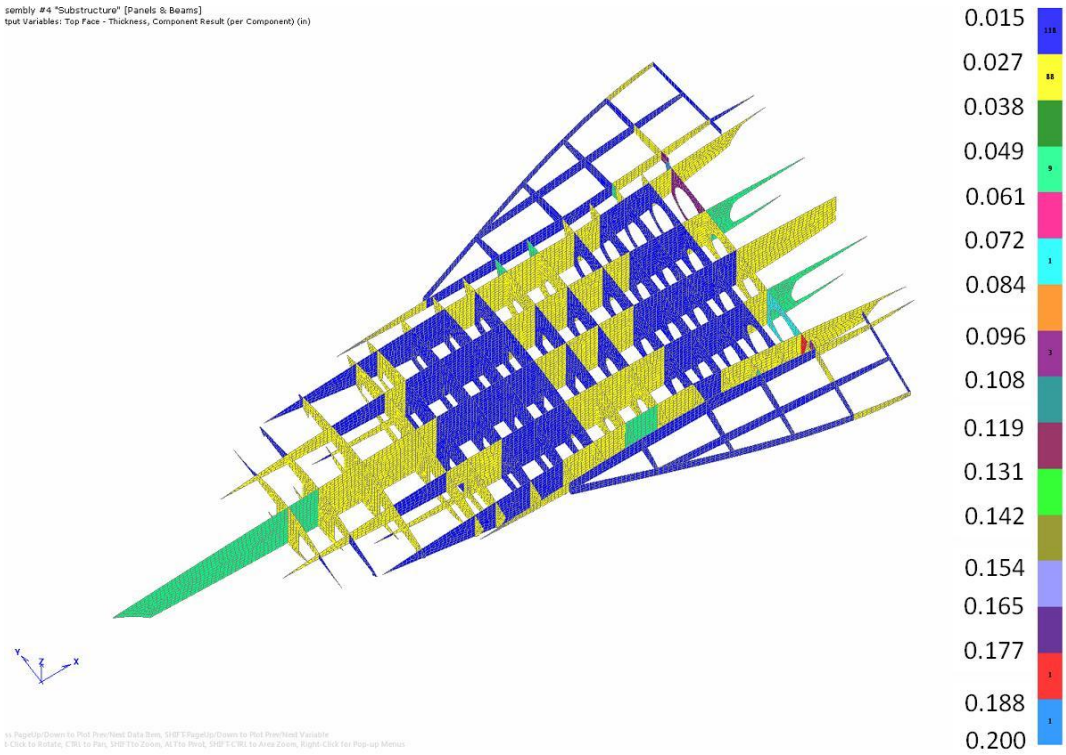

Figure 39. HyperSizer Honeycomb Facesheet Thickness

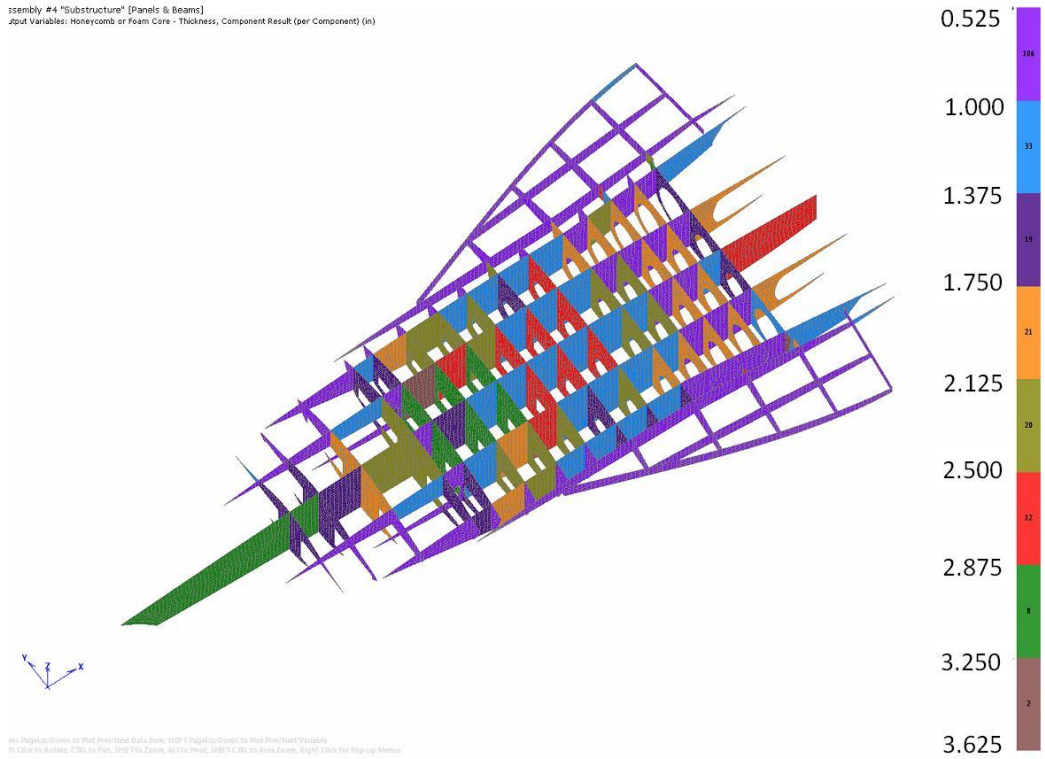

Figure 40. Honeycomb Thickness

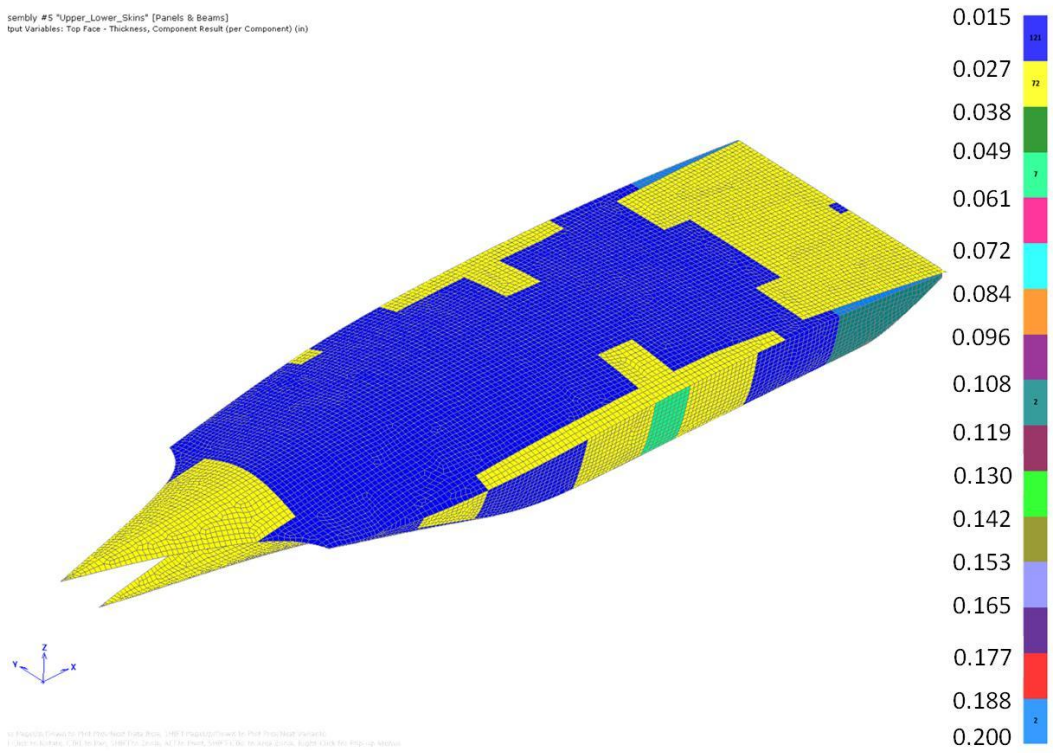

Figure 41. Fuselage Honeycomb Facesheet Thickness

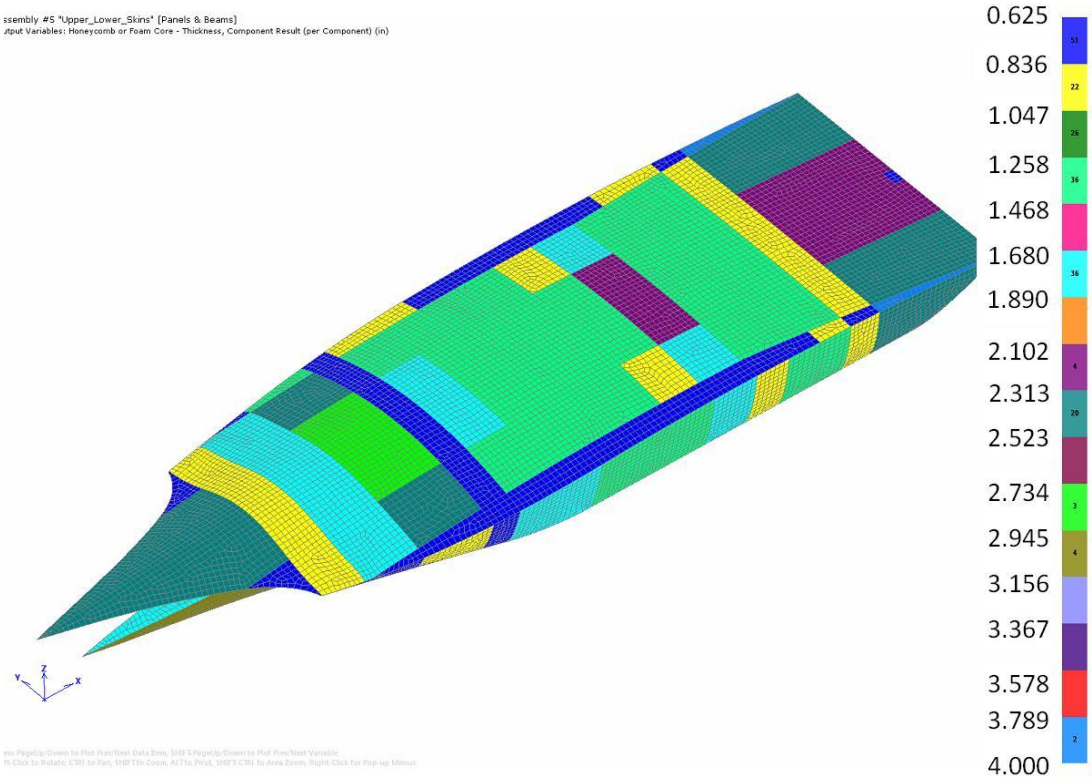

Figure 42. Fuselage Honeycomb Thickness

Representative loads and environments were developed for flight, ground, thermal and acoustic environments. These were applied to the FEM and structural sizing performed for a Mach 7.0 trajectory. This resulted in a non-convergence due to the severe thermal environment, and inability of the TX-V structural configuration to accommodate the structural growth. The structural temperatures were reduced to an equivalent cruise Mach between 4.0 and 5.0 resulting in converged sizing.

In Task 1 the TX-V reference vehicle was established to aid in the identification of critical technology gaps that will impact development of future hypersonic cruise vehicles. To support this ambitious goal, an aggressive approach was undertaken. Data from Boeing's existing Manta project was leveraged, modified, and extended where possible. The vehicle was converted from a ceramic TPS structure to a metallic hot structure by simply replacing the existing TPS with high temperature metallic materials. An existing FEM was scaled, refined, and enhanced to support structural optimization. Representative loads and environments were developed for flight, ground, thermal and acoustic environments. A small CFD database was developed using high fidelity Navier-Stokes CFD simulations to capture the loading from flight maneuvering along the trajectory. Structural temperatures were determined by performing a transient thermal analysis for a Mach 7.0 trajectory. The acoustic environments were defined using empirical methods and used to establish panel frequency requirements. The developed loads and environments were applied to the FEM and used in a structural sizing process. The results showed that the structural sizing was dominated by thermal loading and that this structural configuration is not suitable for a Mach 7 cruise environment. The initial sizing did not converge using the Mach 7 thermal loads. The reason for the non-convergence was due to large thermal expansion of the skin panels and lack of expansion of the substructure the panels attached to. Reducing the structural temperatures to a maximum of 1050^{o} F resulted in a converged solution. It is estimated this would be roughly equivalent to reducing the cruise Mach to the 4 to 5 range. It is very challenging to design a metallic hot structure that can efficiently accommodate the thermal expansion for a Mach 7 thermal environment. This is a primary concern in defining the structural layout. A design that avoids large temperature gradients and provides for a uniform expansion at high temperature will be key objectives. For Phase II, FEM refinement and/or a reduced coefficient of thermal expansion will be used to close the design at the vehicle level for a Mach 7.0 cruise trajectory. In the detailed panel design task the full coefficient of thermal expansion will be used with design features such as increased fastener spacing and scallops in the frame attachment to allow non-rigid boundary conditions.

4.2 Task 2 – Technical Information

4.2.1 Boeing State-of-the-Art Methods

4.2.1.1 State-of-the-Art Analysis and Life Prediction Methods for Hypersonic Panels

Due to the complicated extreme environment of hypersonic structures, there are limitations or gaps in the application of the current State-of-the-Art (SoA) methods. These methods are a derivative of methods used for conventional air vehicles. The gaps identified herein are associated with either the structural screening process or the detailed finite element analysis process. For the detailed analysis process, the gaps described are based on the engineer's knowledge in lieu of quantitative data. The hypersonic programs reviewed for this study did not

perform complete detailed combined-environment (loads) analyses utilizing the SoA approach due to time and budget constraints. These programs adopted simplified approaches or took a weight and/or performance penalty to alleviate complex design issues.

In a typical air vehicle design cycle the potential problem areas with low stress and strain margin are identified using simplified panel screening methods. The critical panels are then studied in more details and panel sizing is finalized using a detailed panel-level FE model. In this context a panel is a region enclosed by frames and longerons.

The panel FEA model is built with adequate fidelity to predict the stress distribution within the structure. Fatigue issues typically occur near the edge of the panel and in its frame and longeron attachment structure in areas affected by stress concentration, i.e., fastener holes, bend radii, machined steps, welds, etc. Using structural specimens, The Boeing Company develops strength and fatigue allowables, as shown in Figure 43, for structural features with stress concentration details (e.g., bolted or welded joints), which are then used with a FE model that sufficiently represents the panel configuration.

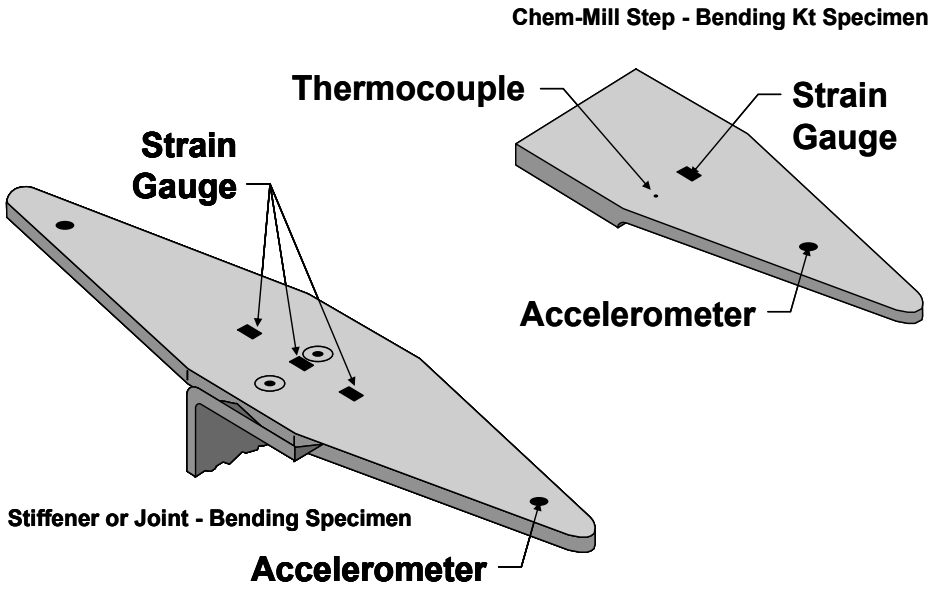

Figure 43. Standard Random High Cycle Fatigue Joint Specimens – Showing Reference Strain Gage Locations

A detailed panel level analysis process is conducted. The type and level of analysis is usually dictated by other resources like man power, expertise, schedule, and funding. The process starts with a linear static and buckling analysis and generates results to ensure the structure meets the acoustic requirements.

The guidelines for performing a detailed nonlinear analysis are subjective. The linear random response analysis and static loads are combined to yield the total response for fatigue and strength calculations.

4.2.1.2 Linear SoA Best Practice

Typically in a linear SoA best practice analysis, detailed panel-level analysis is first conducted as linear quasi-static analysis. The thermo-mechanical internal loads, extracted from the vehicle level analysis, are applied to the panel boundaries. If applicable, the steady state pressure loads, temperature, and/or thermal gradient effects through the panel thickness are applied and the resulting stress distribution in the panel structure is established.

If acoustic environment is present, a linear dynamic structural-acoustic analysis is conducted in frequency domain with the fluctuating air pressure, as defined by the sound pressure, power spectral density (PSD), applied to the panel external surfaces. The Sonic Response Analysis (SRA) process described in the following section is commonly used at The Boeing Company for this purpose. Aero-acoustic loads are typically modeled as a traveling progressive wave. Hence, the acoustic fluctuating pressure is partially correlated over the surface of skin panel.

From this type of response analysis, the PSD functions for stress in the areas of interest are recovered. The area moments of the predicted PSD stress are then calculated and used for establishing the extreme value statistics of stress response due to acoustic input. Quasi-static and dynamic stresses are superimposed on these results. Duration (or time at condition) of the acoustic environment, expected number of zero crossings (calculated from the stress PSD), along with the assumption of Gaussian distribution on the response process are then used to compute the fatigue spectrum (stress levels vs. number of cycles). The resulting fatigue spectrum along with the established allowable is used to assess the structural integrity of the panel at locations of interest.

4.2.1.3 Boeing Sonic Response Analysis (SRA) Tool

To assess the integrity of a variety of product including subsonic, supersonic and hypersonic aircraft, space launch and re-entry systems, and rotorcraft, The Boeing Company has developed a finite element based vibro-acoustic analysis method in the NASTRAN/PATRAN environment, Sonic Response Analysis (SRA). This method includes the challenging feature to evaluate the effect of preload to response of structures. Figure 44 shows an overview of the SRA process for analyzing a structure exposed to quasi-static load coupled with noise and vibration environment.

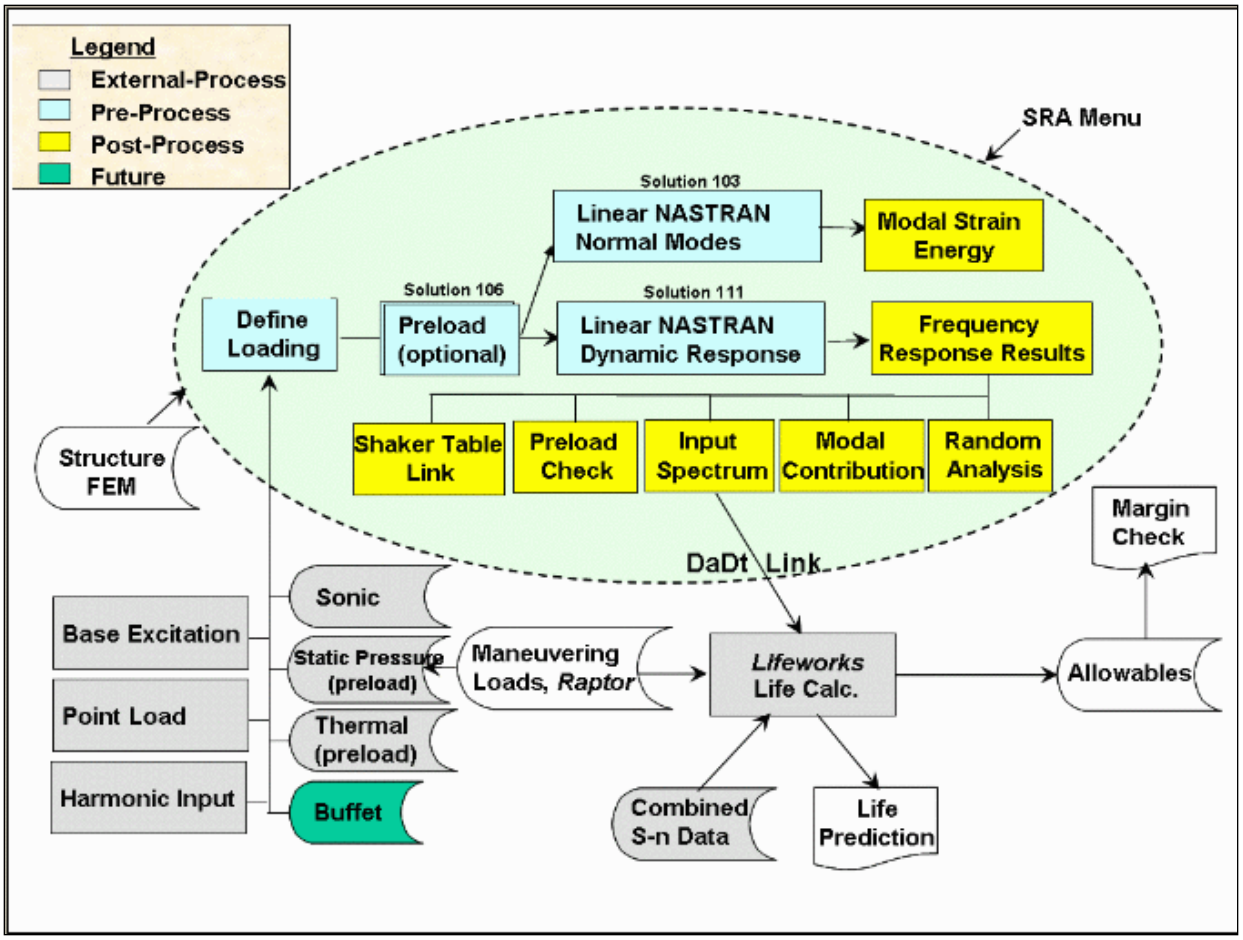

Figure 44. The Boeing Sonic Response Analysis Process

This tool uses a NASTRAN input deck to perform a frequency analysis coupled with thermal and/or pressure preload. The numerical results include spectral densities of physical response, root mean square values, and fatigue damage for a variety of vibration and thermal conditions.

The preload has a direct effect on the frequencies of vibration modes. Under quasi-static preload, a new deformed equilibrium is generated by *"follower"* forces different than the unloaded position producing a shift in modal characteristics. If the loads are not significant, the linear differential stiffness matrix can be included to modify the modes and frequencies. Otherwise, the nonlinear stiffness matrix corresponding to strains and temperatures of the design condition will be used for the modal analysis. This preload effect has been included in the SRA analysis process, which uses NASTRAN Sol 106 (nonlinear static solution) and Sol 111 (frequency response analysis) in conjunction with the modal superposition method. In Sol 106, as FE model deforms for the preload, the stiffness is updated continuously until the convergence achieves. The stiffened mode shapes and frequencies are then calculated. Sol 111 restarts from Sol 106 to calculate the response of structure using the modal superposition. The stress calculation due to mode shapes is purely linear and does not account for any large displacement effects. In addition, the current capability of SRA only allows local buckling while the global buckling cannot be exceeded.

4.2.1.4 Thermal/Acoustic Fatigue Analysis

Acoustic fatigue is caused by the resonant structural response, which is generally above 100 Hz. This causes very high accumulation of stress cycles that can be greater than $1x10^6$ cycles. The slope of the S-N curve is much flatter in the high cycle range than in the low cycle. Therefore, small changes in stress response can lead to significant difference in fatigue life. It is critical that analysis methods accurately predict the stress response. The accuracy of the methods has a direct bearing on the required conservatism through knock-down factors. The endurance limit is shown in Figure 45.

High cycle fatigue can be analyzed using the linear elastic fatigue methods since the stress response is usually in the linear range. If the acoustic loading causes nonlinear stress (plastic deformation), the structure is inadequately designed. Root mean square (RMS) fatigue methods are the most common. These methods use RMS S-N data instead of CA (Constant Amplitude) data. Miners Rule is also used to predict accumulated damage for Finite Life methods. But, Infinite Life (or RMS endurance limit) methods are commonly used for high cycle fatigue.

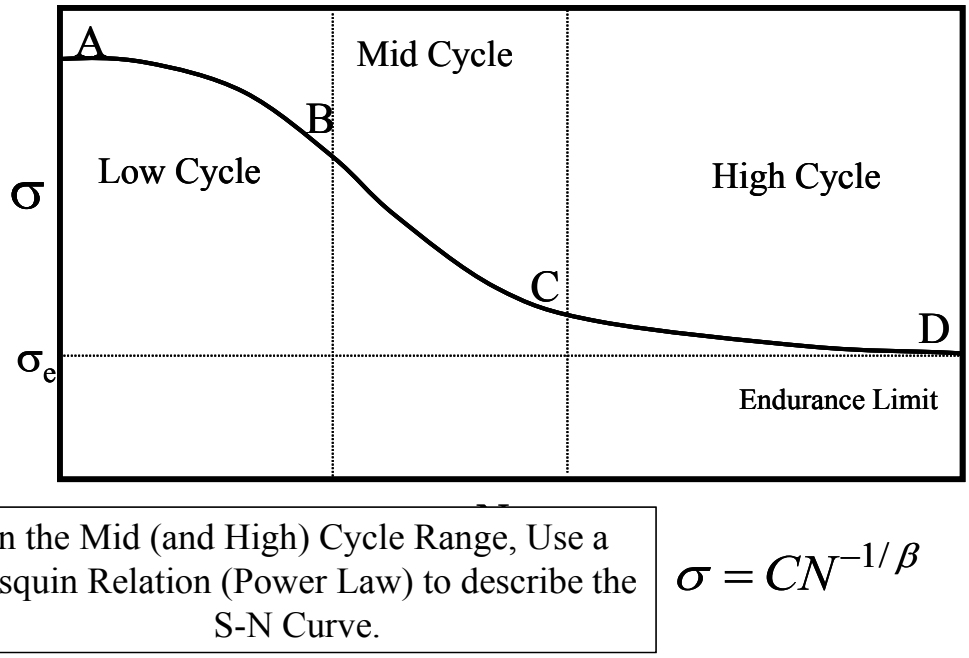

Figure 45. Definition of the Endurance Limit

RMS S-N data is derived from material coupon fatigue tests. There are several types of specimens that are used to quantify the fatigue behavior. The most common one is the bending beam type coupon. This can be either a 1st bending mode or 2nd bending mode specimen. The 1st bending mode specimen is used to characterize certain joint fatigue details. While the 2nd bending specimen is ideal for K_t=1.0, R=-1 type characterization. These tests are performed using narrow band, random base excitation on a shaker in Figure 46.

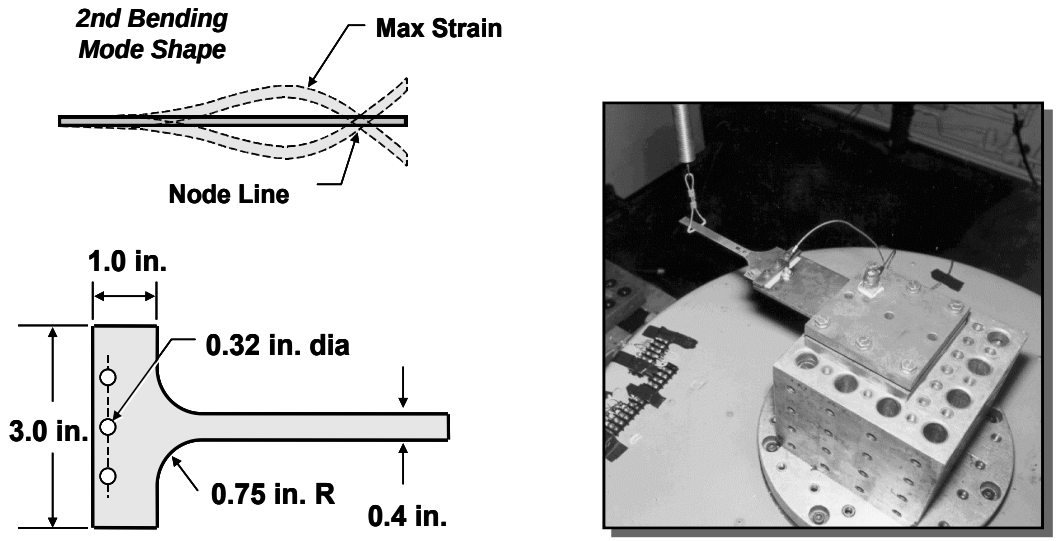

Figure 46. Random Vibration Beam Setup

RMS S-N data is fundamentally different from CA data, as shown. CA data is characterized by Max Stress or Stress Range, Figure 47. RMS fatigue data is characterized by standard deviation in the response average over time.

A few fundamentals of RMS fatigue analysis are:

- There is no exact damage equivalency of sine to random
- Peak value for a random event is tied to the type of event
    - White noise has the highest Peak to RMS (> 6)
    - Narrow-band (uni-modal) has the lowest Peak to RMS (~ 2.5 – 3.5)
    - Static bias or offset skews Peak to RMS
- Different random characteristics can have the same RMS but do not accumulate damage at the same rate
- Fatigue is defined by the stress history of the materials

Aircraft structure response tends to be uni-modal with 3 to 3.5 sigma peak stress excursions relative to RMS. This is so that the peaks are assumed to be within this range and the uni-modal material properties test using random excitation are developed for the same range.

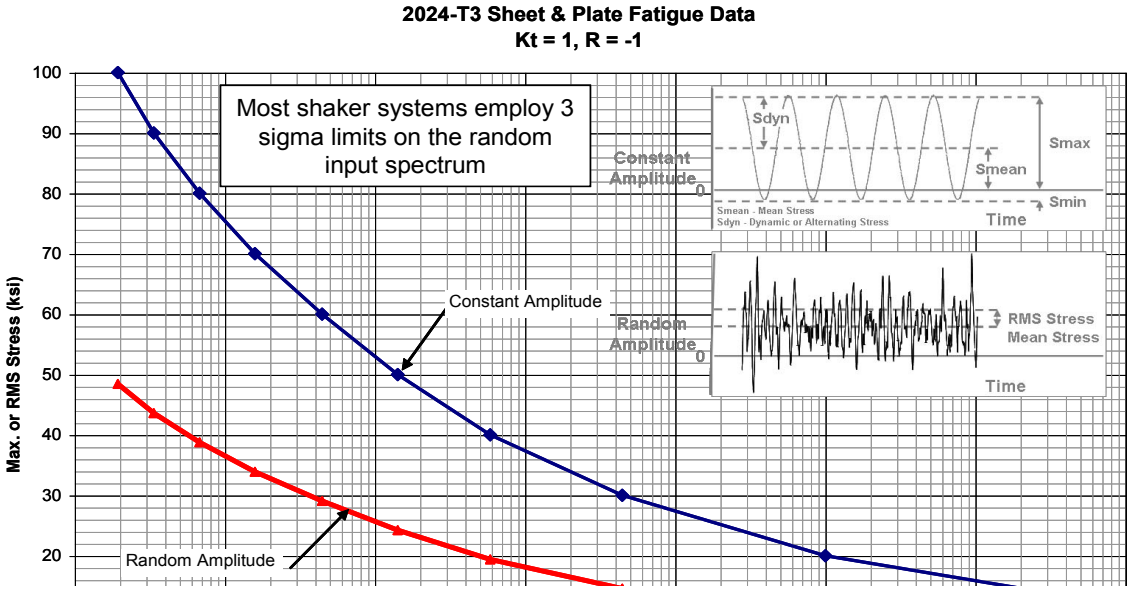

Figure 47. Comparison of Constant and Random Amplitude S-N Data

4.2.1.5 Nonlinear Effects to SoA Best Practice

The application of the SoA methods to analyze panels in thermal-acoustic environment is affected by the loads and associated structural response.

When the geometric stiffness effects due to internal loads are significant, the structural-acoustic analysis is conducted using the differential stiffness matrix calculated for the deformed structure under the quasi-static internal loads. In this modification of only the stiffness matrix used in the structural-acoustic analysis, the dynamic analysis stays linear and is conducted in the frequency domain.

In the presence of high mechanical, thermal, and/or acoustic loading, the linear frequency response analysis with detailed panel model cannot correctly predict the stress distribution due to large geometric and material nonlinearities of the panel. For instance, when a thin flat panel undergoes large displacement and develops membrane response, the linear normal modes response is no longer a good approximation of internal stresses. Nonlinear transient dynamic analysis is conducted to address various nonlinearity related concerns, in which the time-domain realization (5 to 7 cases) of sound pressure PSD is used and the extreme value statistics are typically established directly from the predicted transient stress response. It should be noted that the tools available to conduct nonlinear transient dynamic analysis to investigate structural response under high thermal and acoustic loads environment are not considered best practice design tools, but they do provide insight and help form a basis for engineering judgment.

Generally, the degree of nonlinearity in the response can be estimated from the Nomograph as in Figure 48. The figure shows the degree of nonlinearity from the RMS linear response for flat-rectangular clamped edge panel under uniform acoustic loading. The Nonlinearity Response Factor (NRF) is the ratio of the nonlinear center panel displacement to the linear response. The figure is intended to show that as a panel becomes larger (B=width) or thinner (T=thickness), the geometric nonlinearity becomes a factor. Considering that small differences in RMS stress (10%) can equate to a factor of 2 in fatigue life. This factor in fatigue life increases substantially at RMS stress levels near the endurance limit. Hence, uncertainty in acoustic levels, modal damping, and temporal correlation of acoustic loads has an important effect on the accuracy of structural response prediction.

Step 1: Calculate (b/Et^2)
Step 2: Find Curve
Step 3: Determine 1/3 Oct SPL

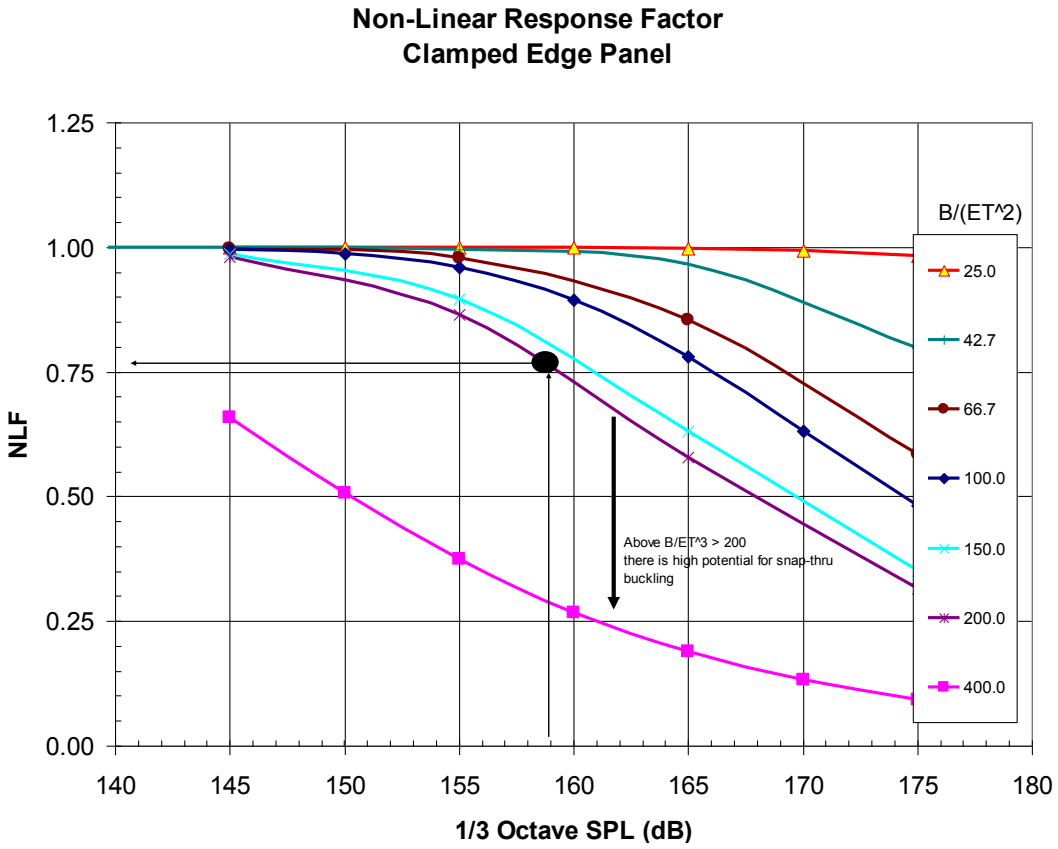

Figure 48. Nonlinearity Response Factor for Clamped Flat Rectangular Panels

Static loads including aerodynamic pressure and internal thermo-mechanical loads can have a large effect on the frequency, mode shapes, and response of acoustic excited structures. A large pressure load on a thin gage panel causes nonlinear (membrane) stiffening. The first effect is on the natural frequency of the panel. Pressure loads have a larger effect on lower order modes than on higher order modes. The following example in Figure 49 shows the effect of pressure load on the fundamental frequency of a thin gage, curved panel with an aspect ratio of A/B = 2, a slenderness ratio of B/t = 143, and a curvature ratio of $B^2/ R t = 10.5$. The figure shows that frequency ratio, frequency at pressure / frequency at zero pressure, increases with positive

pressure. At negative pressures, the panel softens and the frequency ratio decreases and reaches a minimum at buckling. At increasing negative pressures, the panel is post-buckled and the frequency ratio starts to increase.

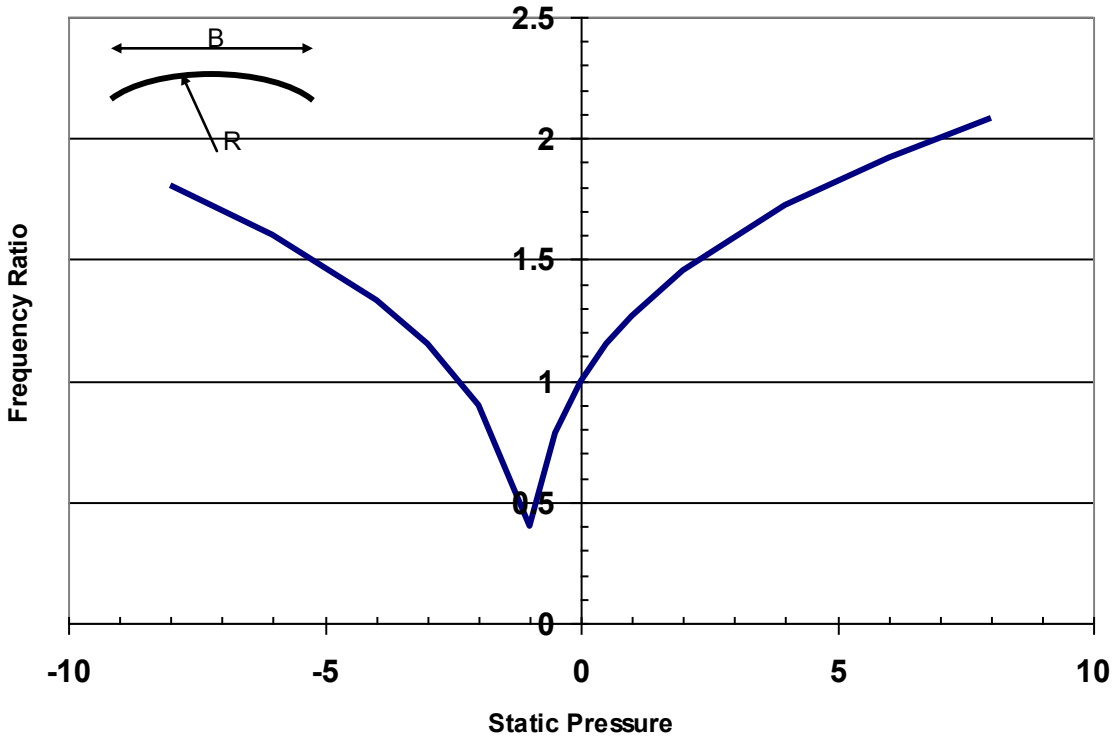

Figure 49. Effect of Static Pressure on Frequency

4.2.2 Historical Research

4.2.2.1 Thermal-acoustic Analysis of National Aerospace Plane (NASP) Panels

To meet the goal of developing affordable and sustainable hypersonic structures in combined extreme environments, the methodologies adopted by the NASP program to design and analyze panels for thermal-acoustic loads have been investigated. Four panels were selected from the NASP historical data documented in Reference 8 at the locations of forebody, ramp, horizontal and vertical stabilizers, and aft-nozzle. The details including function, location, structural design concept, and design environment were examined for thermal-acoustic analysis shown in Table 10, Figure 50, and Figure 51.

Table 10. Detailed Data of NASP Panels

Panel Function/ Purpose	Forebody Panel	Ramp Panel	Engine Nozzle Panel designed to dissipate heat	Horizontal & Vertical Stabilizers
Panel Position/ Region	Lower surface at about 20ft from nose (total vehicle length of 100ft)	Lower surface at about 55ft from nose; at location air is compressed into engines	2 panels evaluated; one at 15ft aft of engine combustor (high thermo-mechanical loads), and another one at 7ft aft (peak acoustic loads)	Located at about 90ft from nose
Structural Concept (as shown in Figure 54)	Integral blade-stiffened carbon-carbon (C-C) skins attached to underlying carbon-carbon frames & longerons	Single-faced corrugated skin protected by C-C blade-stiffened skin panel (metallic structure protected by passively cooled heat shields)	Actively cooled Ti-matrix composites carrying hydrogen coolant	Single-faced corrugated skin panels from Ti matrix composites
Panel Geometry (Aspect Raito, Curvature) and dimensions	Flat with bolted flange on two sides to C-C frames; 34”X20" with longer side attached to substructure	Designed for free thermal expansion; flat with bolted flange on two sides to C-C frames; 34”X20" with longer side attached to substructure	48"X48" flat panels	NA
Specifications (thickness, dimensions, spacing, etc)	Skin thickness =.115 in, Blade stiffener: height=2.0in, thickness= .115in, spacing=6 in	Skin thickness =.045 in, Blade stiffener: height =1.25in, thickness= .065in, spacing=10in	Skin thickness (15ft/7ft) =.016/.016in; total height =.83/1.08in, heat exchanger height =.08/.08 in, weight =42.4/51.7lb	Skin thickness =.030/.045in, corrugated stiffener: height =2.5/1.7in, thickness=.015in, pitch =1.7/1.5in

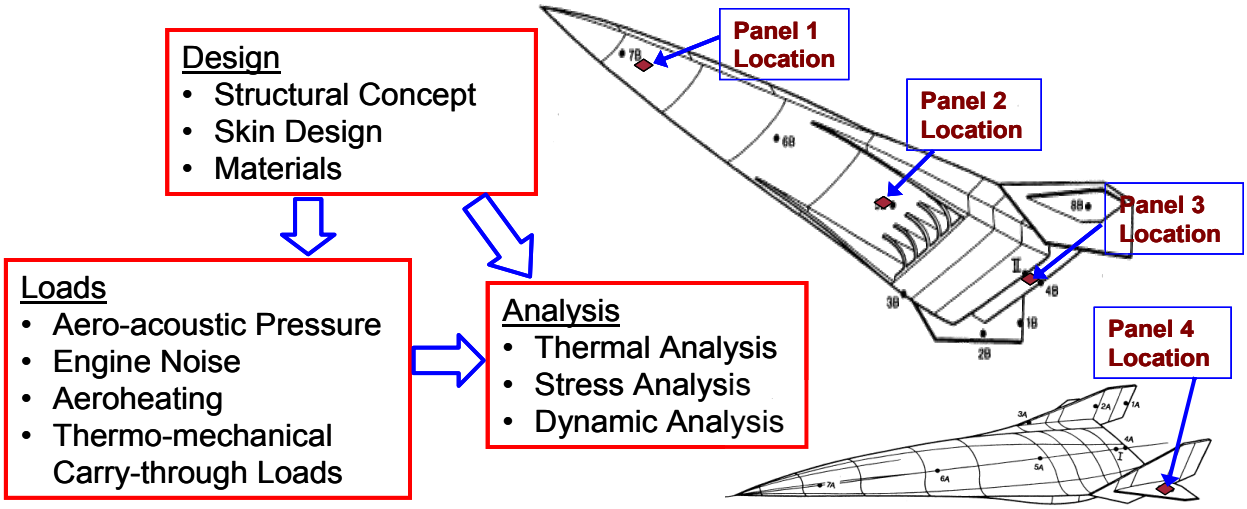

Four Panels were investigated

1. Forebody panel: 20 ft from nose on lower surface
2. Ramp panel: 60 ft from nose on lower surface
3. Actively cooled panel: 95 ft from nose
4. Horizontal stabilizer: 90 ft from nose

Figure 50. Locations of Panels on NASP for SoA Assessment

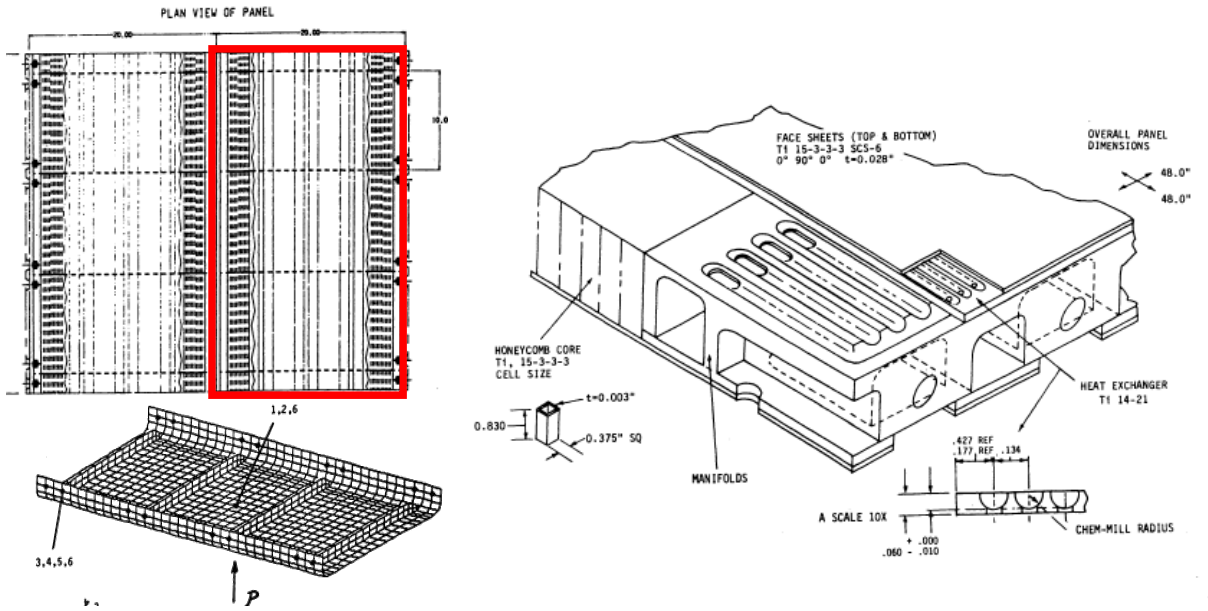

(a) Fore-body and Ramp **(b) Engine Nozzle Areas**

Figure 51. Structural Concepts for Fore-body, Ramp, and Engine Nozzle Areas

The NASP analysis methods closely resemble the Boeing SoA methods. A comprehensive analysis procedure can be found in Reference 8 for the analysis of NASP engine nozzle panels. The panels were designed with actively cooled features to remove excessive heat from engine

combustion and reduce temperatures to outer face sheet of a titanium sandwich structure that composed the panels.

The analysis was divided into two steps to predict structural response and fatigue life of the panels. First, the panel was evaluated over the entire trajectory using the classical plate theory. The resulting static and dynamic stress responses were input to a simple fatigue model to identify critical load conditions. The thermo-mechanical loads were predicted at the vehicle level for 14 design points in the flight trajectory including taxi, ascent, cruise, and descent. The local thermo-mechanical in-plane loads, acoustic loads, temperatures and thermal gradients for each condition were applied to panels. The 2nd step involved detailed structural finite element (FE) analysis to refine response prediction with critical loads identified in the first step. The responses were then fed into the fatigue model to evaluate fatigue life. The panel level thermal analysis was also performed to obtain temperature distribution and thermal gradient, which was able to be captured accurately at the vehicle level thermal analysis.

Similar to the sizing optimization of the TX-V in Task1 with HyperSizer, the panel weight was minimized prior to the FE analysis with thermo-mechanical loads and a panel optimization program using face-sheet thickness, ply orientation, and sandwich depth as design variables and face sheet strength, panel buckling, core dimpling, and delamination as design constraints.

Utilizing the stresses obtained with thermo-mechanical in-plane loads, thermal gradients, and acoustic loads approximated by using the Miles equation, critical loads were identified as those having the largest combined static and dynamic stress ratios defined as

$$r = \frac{\sigma_s}{F_{tu}} + \frac{\sigma_a}{S_n} \qquad \text{(Eqn. 4.2.1)}$$

where σ_s is the static stress, F_{tu} the ultimate tensile strength, σ_a the acoustic RMS stress, and S_n the fatigue allowable.

It was determined that the critical acoustic load case was during take-off when both rocket and scramjet engines operate jointly with ground reflection. The following table, Table 2, summarizes analyses conducted on different panels, which varies slightly between panels for their individual design conditions.

Table 11. Analysis Data of NASP Panels

Panel Function/ Purpose	Forebody Panel	Ramp Panel	Engine Nozzle Panel designed to dissipate heat	Horizontal & Vertical Stabilizers
Mechanical Internal loads Case and Nx, Ny, Nxy , Mx, My, Mxy	Strength and buckling checked for ascent (Flight Condition 2) with Nx = 1221(lb/in), Ny= -207, Nxy=85; and for Condition 9 with Nx = 1914, Ny= 756, Nxy=-202; Mx, My and Mxy are from aerodynamic pressure equally distributed on panel	Pressure loads of 1.23 psi and temperature loads for Condition 3 (OML T=50F) were selected; No preload considered since the panel was not designed for carry-thru loads	NA	Thermo-mechanical carry-thru loads are significant higher than forebody and ramp panels (values not available); buckling is a concern; temperature is very high.
Acoustic OASPL and Design Conditions	Take-off condition: acoustic loads are from the operation of both rocket and scramjet engines plus ground reflection (most severe 150-160dB)	Take-off condition: computed for 165dB; most severe 160-170dB	Take-off condition: 175dB	Engine acoustic loads of 160 to 170dB; peak oscillating shock pressure of 1.5psi equivalent to 175dB
Boundary Conditions	Thermal: outer surface was subjected to aeroheating & radiation; the inner surface was insulated; Structural Dynamics: boundaries were constrained for all rotations and z-translation @ 24 fasteners along flanges on both sides, and z-translation along normal sides; Strength & Buckling: boundaries were constrained for all rotations and z-translation @ 24 fasteners, and y-rotation along normal sides	Thermal: same as forebody; Structural: boundaries were constrained for all rotations and z-translation @16 fasteners alongside flanges, and x & y-translations and z-rotation at panel center to avoid rigid-body motion (normal side edges were free)	Thermal: 2D analysis for thru-thickness thermal gradient; Structural: simple supported along the centerline of edges	NA
Materials	C-C pa nel made of 0/90deg fabrics sandwiched between 2 outer 45deg fabrics	same as forebody	Ti-matrix Composites	NA
Geometry and Modeling	Panel dimension of 34"X20" with 6-2” blade stiffeners; modeled with 2D QUAD elements	Panel dimension of 34"X20" with 4-1.25” blade stiffeners; modeled with 2D QUAD elements	Thermal: 2D finite difference model; Structural: Panel face sheet, heat exchanger, honeycomb, manifolds and edge closeouts were modeled by solid elements	NA
Analysis Tool and Type	Thermal: PATRAN P/Thermal; Buckling & Dynamic: NASTRAN	Thermal: PATRAN P/Thermal; Buckling & Dynamic: NASTRAN	Buckling & nonlinear stress: NASTRAN	NA

The finite element analyses included NASTRAN linear static, nonlinear static, modal and acoustic. Modal analysis was performed with an updated stiffness matrix including preload

effects from nonlinear static analysis, similar to the Boeing SoA approach. A specific 2-D thermal analysis was conducted for the engine nozzle panel to retrieve thru-the-thickness (TTT) thermal gradients. The thermal gradient at the center of panel at Mach 12 was then used for the entire panel. As a result, the static stress due to thermal gradient was 20 times higher than that by thermo-mechanical loads. Several conservative elements were identified in the analysis for engine nozzle panels that include:

- 2-D thermal analysis was used to extract the TTT thermal gradient and did not consider the thermal conduction spatially,
- A uniform TTT thermal gradient was assumed throughout the panel with data at the panel center for analysis resulting in very high thermal stresses increasing design weight,
- A combination of acoustic loads at takeoff and thermal gradient at Mach 12 was conservative to evaluate the panel fatigue life , and
- Using the Mile's equation for equivalent static acoustic loads added weight to the design.

A similar analysis approach was used for other panels including the forebody and ramp panels, both with integral-stiffened carbon-carbon skins, in which the ramp skin panel was not designed to carry thermo-mechanical loads from the vehicle analysis.

For fore body and ramp panels, the detailed FE analysis started with using thermal analysis tool P/Thermal in PATRAN with heat flux profiles derived from generic trajectories and associated turbulent heating rates. The heat flux was assumed to be uniform on the panel surface. The aeroheating for two free-stream dynamic pressures, 1000 and 2600 psf, were studied. The temperatures for the 2600-psf case exceeded 3000^{o}F. However, when the turbulent boundary layer turned into laminar after the first five minutes of flight, the flow re-laminarization resulted in much lower temperatures, approximately 1200^{o}F for the fore body and 800^{o}F for the ramp panel. The use of turbulent heating in thermal analysis for the entire trajectory was therefore conservative. In addition, the TTT thermal gradient was considered to be negligible allowing 2-D QUAD elements to be used.

Similar to an engine nozzle panel, the fore body panel in-plane loads from flight maneuvers, inertia, and thermal were obtained from a vehicle analysis for 14 design points with different outer mold line (OML) temperatures and pressures in the flight trajectory. The critical load case was Flight Condition 2 during ascent with highest mechanical stresses and $T=200^{o}$F, and Flight Condition 9 in cruise with highest thermal stresses, $T=1825^{o}$F. This condition, with maximum inplane loads Nx, Ny and Nxy, was selected in combination with temperature from panel level thermal analysis. The aerodynamic pressures were imposed on the exterior skin of panel. The FE model contained skins, stiffeners, flanges, skin-flange transition, and fasteners that were constrained as boundary conditions. The buckling analysis was performed to ensure the stability of panel.

The dynamic analysis used static mean preload , vibration modes, and linear frequency response with aeroacoustic loads to evaluate fatigue. NASTRAN nonlinear static analysis was performed with preload and pressure to update stiffness matrix for modal analysis. Additionally, linear material properties without accounting for temperature effect were used for conservatism.

From the NASP study, the following table, Table 12, identifies the design drivers for each panel region and gaps that are associated with the analysis approach.

Table 12. Design Driver for NASP Panels

Panel Function/ Purpose	Forebody Panel	Ramp Panel	Engine Nozzle Panel designed to dissipate heat	Horizontal & Vertical Stabilizers
Design Drivers	In the mechanical load check, the outer ply near the outmost fastener failed at MS=-.17; Otherwise large positive margin was found; e.g., MS=3.29 for laminate ultimate strength; Buckling and sonic acoustic response were not of concern	Highest RMS stress observed on the upper side of middle stiffener and center of middle bay, exceeding fatigue allowable; Strength was not a concern	High acoustic-fatigue stress ratio at take-off (thru approximate panel evaluation method) was identified; High TTT thermal gradient induced stresses 20 times higher than thermo-mechanical loads; Inner face sheet is more prone to fatigue than outer due to compressive stress from aero pressure reducing stress on outer surface; The critical location are at the face sheets of panel center	There were high temperature (2500F) and/or high acoustic loads 175dB due to shock heating, which may require active cooling design; In-plane thermo-mechanical are significantly higher than forebody panel, hence buckling is a concern

The following gaps are identified from the NASP analysis and are also commonly observed in today's hypersonic, as well as conventional, vehicle programs:

- Use of conservative combinations of high inplane thermo-mechanical loads with high acoustic environment: for example the acoustic condition during takeoff was combined with thermo-mechanical loads in ascent for the evaluation of forebody panel, which produces the stress level that is less likely to occur
- Not including temperature-dependent materials in static strength, buckling, and dynamic analyses for the forebody panel is not necessarily conservative as claimed
- Approximation in boundary condition selections (e.g., constrained z-translation along edges to next panel for forebody panel) and evenly distribution of preload along the edge of panel affects the model stiffness and hence frequencies and mode shapes. This was applied for forebody, engine nozzle panels
- Using the Miles equation to generate quasi-static acoustic loads was conservative
- Use of conservative turbulent heating assumption for both forebody and ramp panels resulted in much higher temperatures than the real case
- Use 2-D thermal gradient at panel center for the entire nozzle panel was too conservative

4.2.2.2 X-51A Wave Rider

X-51A Wave Rider data can be found in the Boeing proprietary appendix.

4.2.2.3 Hypersonic International Flight Research and Experimentation (HIFiRE)

HIFiRE is a joint program between the United States AFRL and Defense Department of Australia. The objective of the program is to demonstrate the control of a non-powered hypersonic vehicle in a ballistic re-entry trajectory at Mach 8. The HIFiRE program is a series of

10 investigations of fundamental hypersonic air vehicle and propulsion technologies deemed critical to the realization of next generation Air Force aerospace systems. Each research effort will culminate with a flight experiment to be launched under representative flight conditions (Reynolds number and Mach) while employing low-cost sounding rockets.

HIFiRE-4, a more recent design, has a wing-body type configuration shown in Figure 52. The wing is primarily made of solid metal with cavities for equipment storage and the body is cylindrical shell structure with a thickness of 0.125 in, which does not contain any structural layout. Conventional metallic materials including Aluminum for the majority of wing and body and Copper for the nose tip and leading edge of wing are used. Since HIFiRE-4 is designed to fly at a ballistic reentry trajectory, as shown in Figure 53 and Figure 54, it flies most of the time at Mach Number lower than 3 and low dynamic pressure around 100 psf with few opportunities for turbulent boundary layer, strong shock or intensive acoustic loads to be generated. As a result, the acoustic environment was not considered in the structural evaluation.

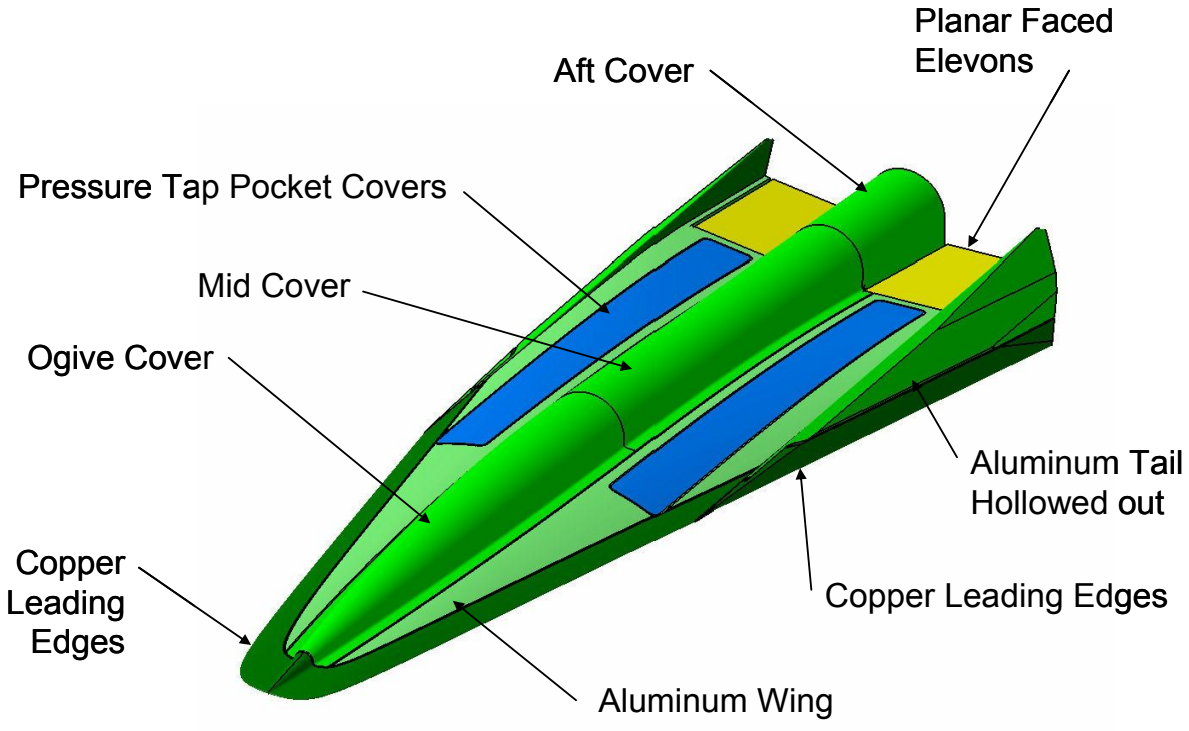

Figure 52. HIFiRE Geometry and Component Layouts

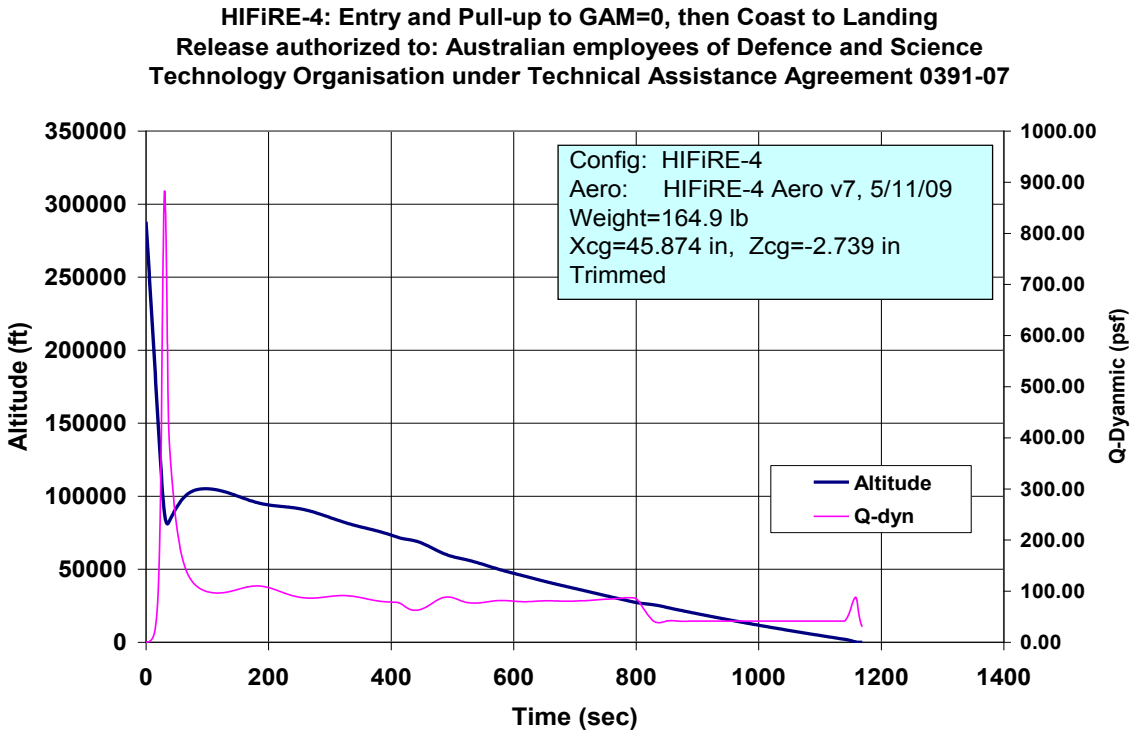

Figure 53. HIFiRE-4 Entry Trajectory, Altitude and Dynamic Pressure

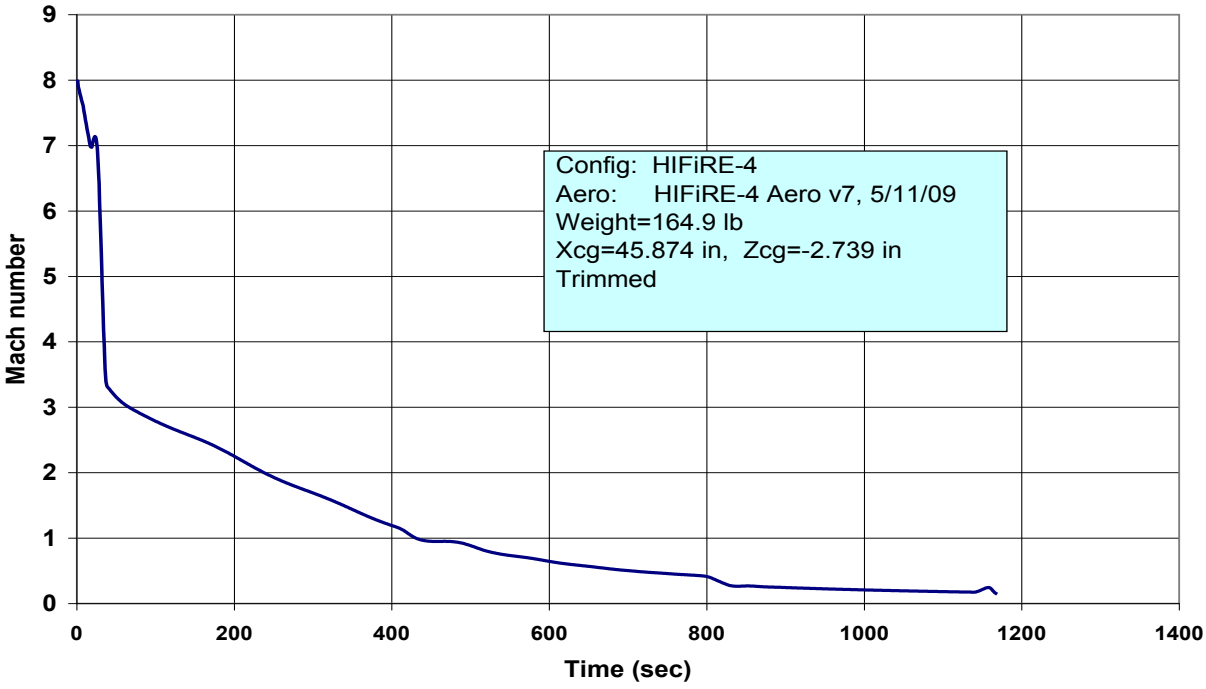

Figure 54. HIFiRE-4 Entry Trajectory, Mach No.

For HIFiRE 4, the aeroheating data was generated by engineering methods in the aeroheating code MINIVER, and 1-D Convective heating and Ablation Program CHAP. CHAP is a Boeing proprietary code designed to predict the temperature distribution and ablation of TPS thickness on the re-entry vehicle surface. Both MINIVER and CHAP were integrated into an automated aeroheating/TPS design and sizing module developed based on the Model Center of Phoenix Integration Company. The aeroheating analysis started with inputs of vehicle geometry and flight trajectory including Mach Number, altitude, angle of attack and control surfaces trim schedule, and was executed with the Model Center tool. Neither CFD solutions nor aerothermal wind tunnel data were used due to the aggressive plan. The MINIVER only approach was deemed adequate for the short flight duration and all metallic airframe design. The thermal design was primarily driven by the material thermal capacitance of the airframe. The aeroheating results were then mapped to the surface of 3-D model for thermal analysis with SINDA. Nonlinear structural analysis with temperature-dependent material properties was completed with pressure loads and temperatures converted from the thermal model using a Boeing general mapping procedure.

Figure 55 shows the tail fin surface heating at 27 seconds and the temperature distribution at 34 seconds during the space reentry. The flight reaches peak aerodynamic heating at 27 seconds of entry and the peak airframe temperature lags 7 seconds and reaches peak at 34 seconds. The temperature range is moderate, i.e., less than 500°F, during reentry.

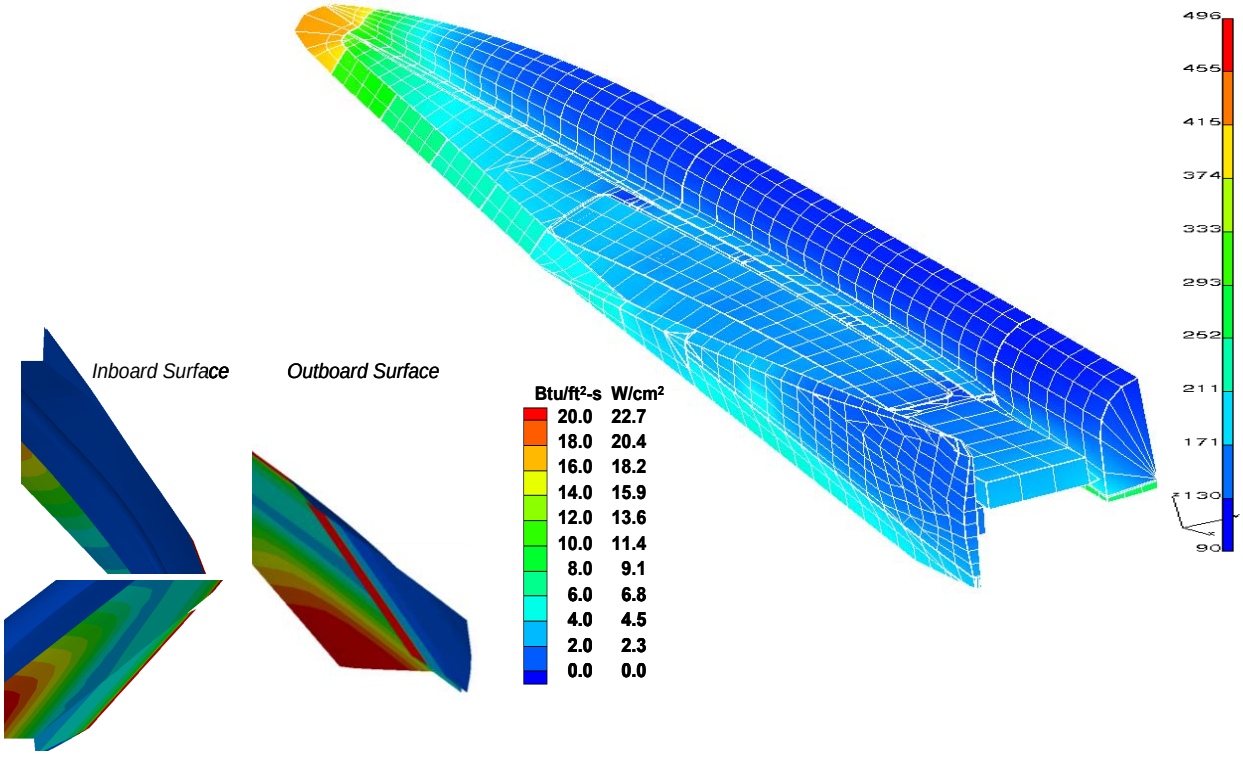

Figure 55. Tail Fin Surface Heating and Temperature Distribution on Thermal Model

Since the vehicle is designed for a one-time flight test, only the load case combining maximum temperature and maximum aerodynamic pressure, which is the design driver for the vehicle structure, was used for static structural analysis. The analysis concluded that neither the vehicle

strength nor the performance due to deflection under loads was a concern. The von Mises stress of majority of vehicle is lower than 28ksi except for bolt connected areas that are modeled with rigid connection elements introducing fictitious high stresses. Figure 56 shows the finite element structural model composed of solid elements and von Mises stress distribution in the model. No acoustic analysis was performed on the HIFiRE structure, since the wing, vertical stabilizers, leading edges and control surfaces are primarily machined solid metals and the dynamic pressure (100psf) during reentry is not high.

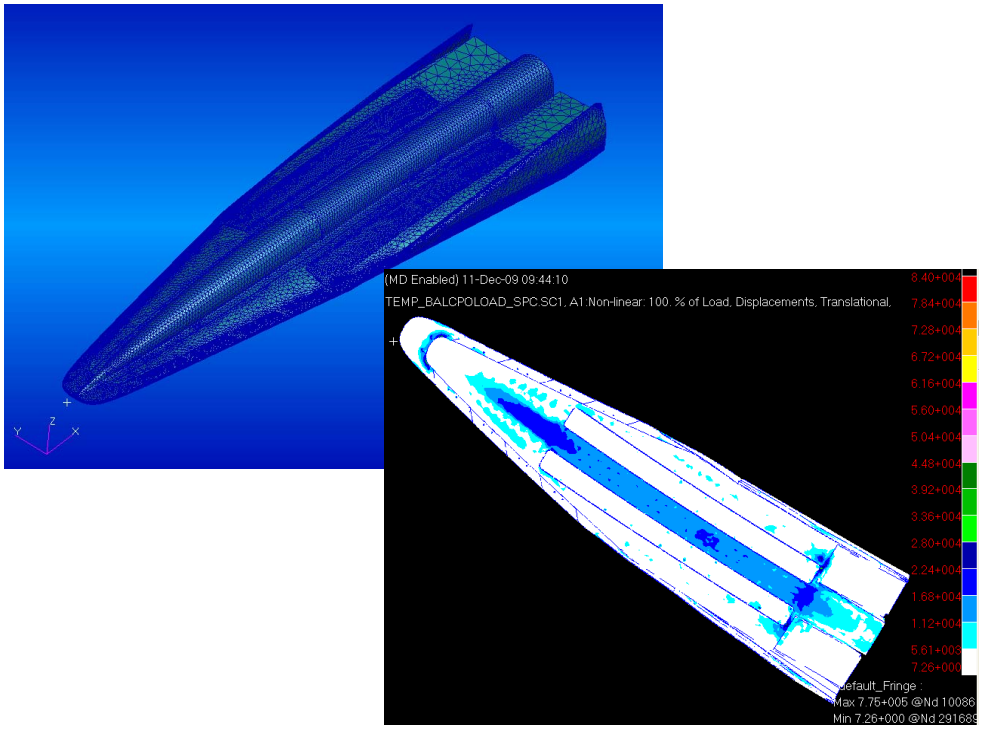

Figure 56. Finite Element Model and Stress Distribution on Lower Surface of Structure at 34 second of Space Entry

The primary gap in the HIFiRE analysis was that the structure was not designed for thermal-acoustic environment with the assumption that the flight maneuver and thermal loads was the design driver.

The summary for the HIFiRE structural development includes:

1. Structural dynamic response and therefore fatigue life was not a concern due to low dynamic pressure in flight and the use of solid metals for wing, vertical stabilizer and control surfaces
2. Temperature was not very high. Therefore material change due to temperature did not significantly affect the response
3. A —conservative" combination of maximum aerodynamic and temperature loads and resulting low stresses indicated that the structure may be over-designed. Therefore, excessive structural weight could be removed by introducing thin gage panel design and using advanced design and analysis methods.

4.2.2.4 Fighter Aircraft Example

Aircraft that fly aggressively low altitude or high-angle of attack maneuvers will experience high acoustic loading in the presence of external stores. These high acoustic loads can lead to premature acoustic fatigue in thin gage metallic structure. The majority of structure that cracks due to the acoustic loads are thin gage metallic structure; such as, fuselage skins, access doors, non-load carrying fairings, and leading edges, and secondary support structure; such as stiffeners, stringers, shear clips, and brackets. In thin gage metallic structure, cracking tends to occur at stress discontinuities arising from chem-mill radii or at fastener holes. The out-of-plane bending response of a panel causes the highest stresses and bending moments to occur at or near the edges of the panels where such features as chem-mills, fastener holes, and support structure are located. Figure 57 is a summary of the panel geometry, boundary conditions, loads, and design drivers.

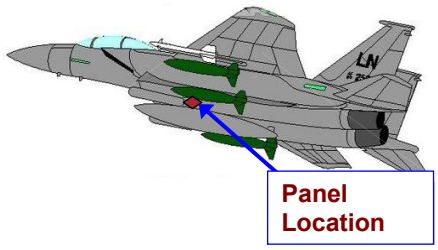

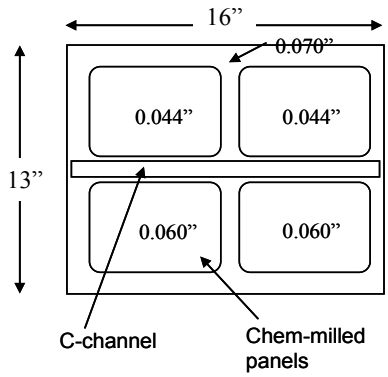

- Locations and Purpose:
  - Lower surface Nacelle exterior panel
- Structural Concept:
  - Thin gage metallic stiffened panel
- Specifications:
  - 16”X13” aluminum 2024-T6, Skin thickness=.070” w/ chem-milled pockets to 0.04 and 0.06”,
- Mechanical & thermal preload
  - Aerodynamic: Ps=3psi
  - Thermal: 40F
- Acoustic loads:
  - Max Q condition: 165dB
- Boundary Conditions:
  - Clamped along all edges (support by bulkheads and stringers)
- Dynamic/thermal analysis:
  - Linear Random Frequency with static preloads
- Design Drivers:
  - High acoustic-fatigue stresses during high speed low altitude maneuvers
  - High static pressure loads due to local shocks from electronic pods

Figure 57. Panel Summary

During the early design of the F-15E attack aircraft; there were several lower fuselage skin panels that were experiencing cracking. The F-15E was a ground attack version of the F-15C/D air-superiority fighter. This version of the F-15 carried more external stores on both the wing and fuselage stations, which included the ground terrain following LANTIRN and FLIR pods. During high speed and low altitude conditions, the entire lower fuselage is awash in complex flow around these external stores. The complex flow separation and shocks increased acoustics by 12dB (exceeding previous worst case design conditions). One panel in particular that was directly behind the LANTIRN pod was experiencing cracking. The panel was 16 in by 13 in, 0.071 in thick, with 0.06- and 0.04-in chem-milled pockets. The skin panel was supported by a bulkhead along long edges and a heavy blade stringer on the short edges. Also, there is a C-channel stiffener that splits the panel. It was this stiffener that was fatigue critical. However,

this wasn't obvious from initial observations. The stiffener would fail at the end supports where it bolted to the blade stringers. The crack would propagate into the stiffener, and eventually cracks would form in the skin. Initially, it wasn't known if the skin or stiffener failed first. A more complete description on the analysis and testing of the panel can be found in Appendix C.

The knowledge gaps identified for this application include:

- There were high level uncertainty in the aeroacoustic loads behind external stores
- Static pressure loads due to local shock can vary depending on shock position. The static pressure loads had large effect on the dynamic response
- Thermal loads and effects were unknown. Thermal environment depends on altitude, Mach Number, and worldwide locations (operating environment)
- Acoustic levels were high enough to cause nonlinear skin panel response.

4.2.2.5 Transport Aircraft Fuselage Skin

In 2006 during a routine visual inspection, a number of indications were found on an aircraft fuselage outer skin that suggested potential fatigue damage. The subject location was on the side of aircraft just forward of the wing to body interface. At least one more subsequent visual inspection of same model aircraft yielded a similar damage indication in the same fuselage area. This aircraft, which is referred to as Subject Aircraft or SA, uses the thruster reversal during its landing maneuvers to reduce speed and bring the SA to stop on the airfield. The thruster reversal may be used when the engine power is on its full setting and results in direct impingement of jet engine out-flow on the fuselage in the areas that potential fatigue damage was spotted. The damage area consists of individual panels with approximately 9.5 inch longeron spacing and 24 inch frame spacing, respectively. The skin thickness in the area varies between 0.061 and 0.090 inch.

To reduce the problem to a reasonable size for numerical analysis, a four frame by five longeron grid of fuselage along with associated frames and longeron structures were modeled in NASTRAN using 2D plate-shell elements, Figure 58. The modeled grid represents the fuselage side just forward of the wing to body interface, which is the primary impingement area during thrust reversal. Fine mesh in the FE model was used in the zones with strain gage instrumentation during the flight test. For the strain gage locations on the middle panel, panel thickness variation was modeled precisely. Other panels were modeled with the average panel thickness. To derive the forcing function for analysis, the measured pressure fields at two symmetrical locations at each side of SA from the flight test with max thrust reversal condition were averaged and fitted in the frequency domain by a piece-wise linear curve.

The linear frequency response FE analysis was conducted using the Sonic Response Analysis (SRA) procedure. The analysis process is schematically shown in Figure 59. Figure 60 shows typical analysis results for the fuselage acceleration PSD and the accumulated acceleration plots. The measured acceleration is also shown. In an attempt to improve the correlation between the analytical predictions and the measured strains and accelerations, various reasonable implementations of boundary conditions, damping, cross-correlation between input PSD, and fuselage skin to frame and /longeron connection stiffness were investigated. However, within the limits of linear analysis, poor correlation between the measured and the predicted acceleration and strain responses was observed.

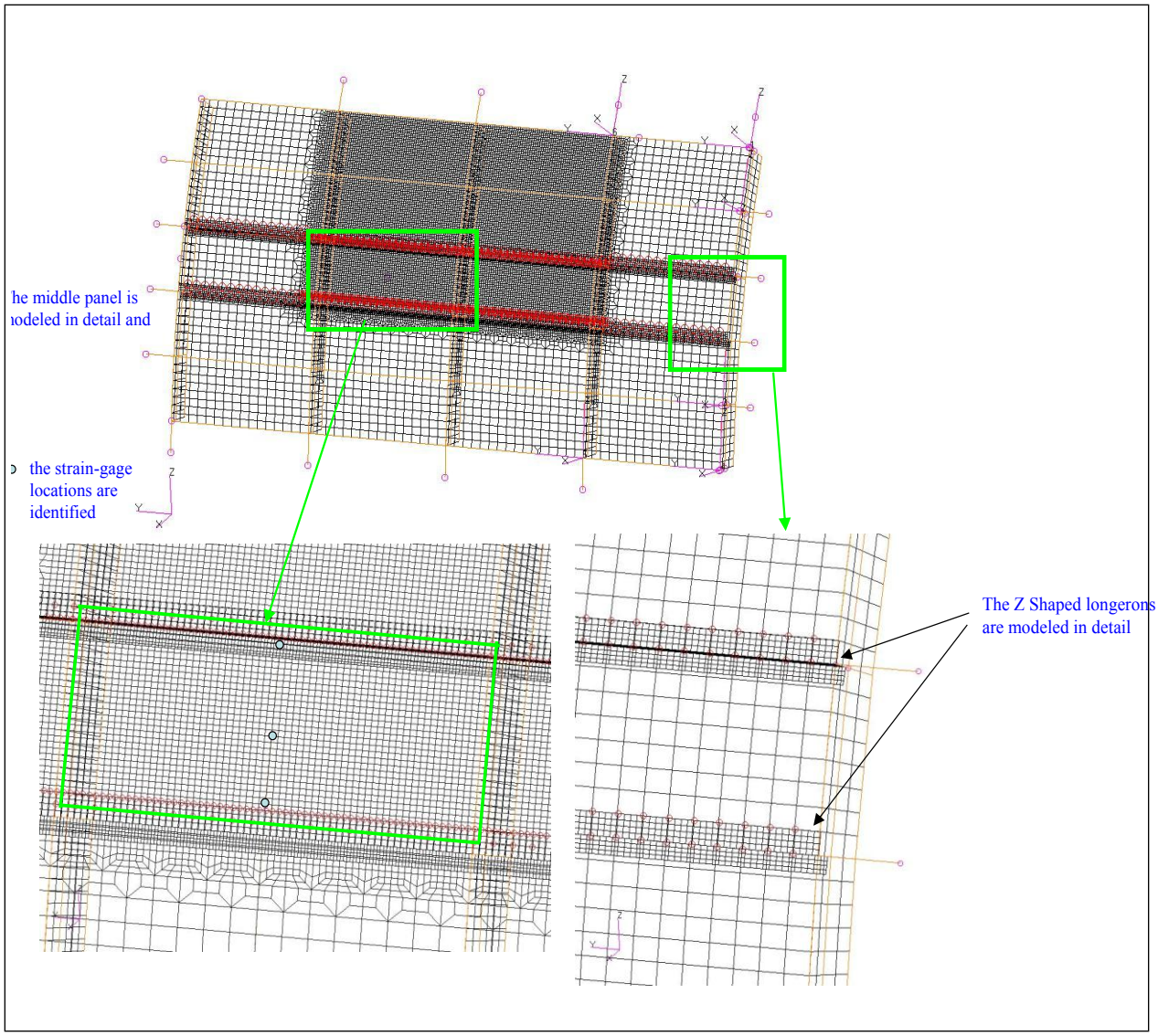

Figure 58. Finite Element Model of the Primary Thrust Reversal Impingement Area

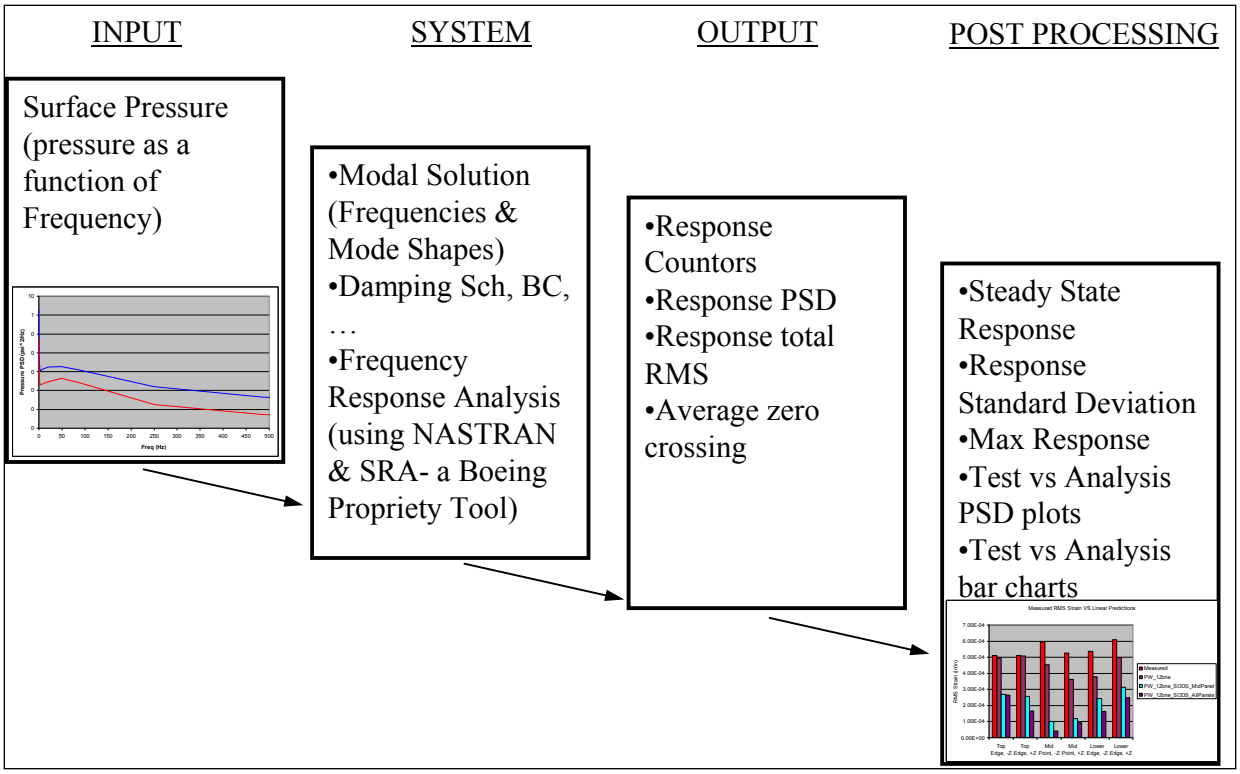

Figure 59. Analysis Process

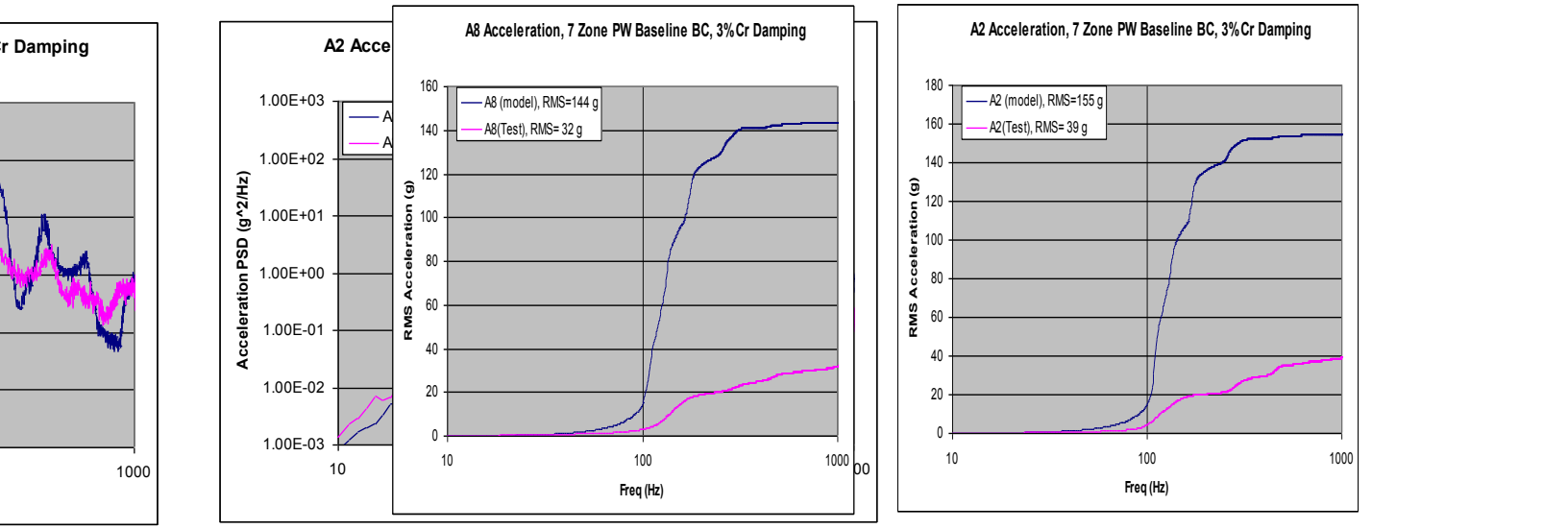

Figure 60. Comparison Between Measured and Predicted Responses

A number of collaborating evidences suggested strong nonlinear effects:

Non-Gaussian Response: Statistical analysis of a the input process as measured by the pressure gages showed that the Skewness (S) and Kurtosis (K) values for the pressure environment were close to the theoretical values for a Gaussian process (S=K=0). However, the output process, as measured by the strain gages, with typical Skewness of more than 0.5 and Kurtosis of more than

3, was far from a Gaussian distribution, Figure 61. Since a linear system will produce a Gaussian output from a Gaussian input, it is concluded that the system (structure) has behaved nonlinearly.

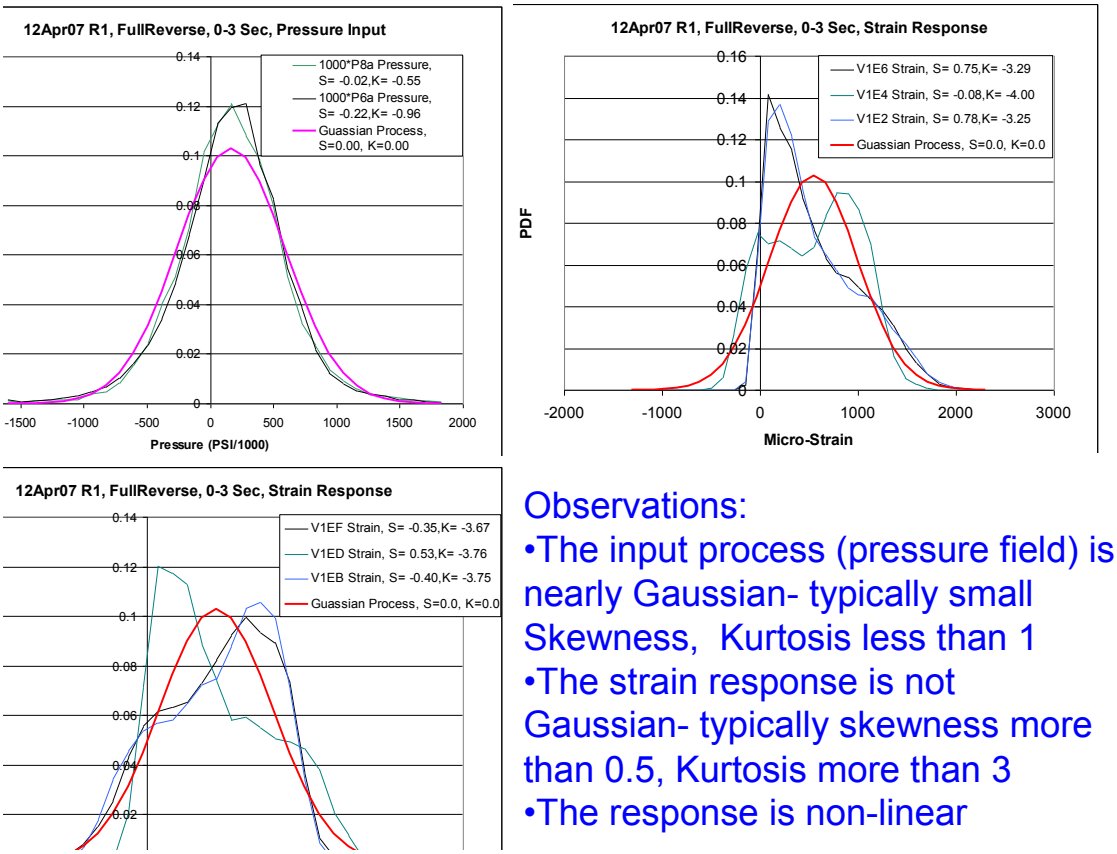

Figure 61. Probability Density Function (PDF) of Measured Input (Pressure) and Output (Strain)

Panel buckling under steady state pressure (Ps~1.5 psi) and temperature environments ($\Delta T>30F$) during thrust reversal: The pressure gage data was low pass filtered at 100 Hz and the resulting maximum pressure was used in a linear buckling analysis using the same FE model. Analysis predicted panel buckling at a fraction of the low pass filtered pressure. As expected a similar analysis performed using the combined thermal and pressure environment confirmed the finding.

Large displacement effects on fuselage skin: Standard deviation of the predicted panel deformation was approximately the same as panel thickness suggesting that the large displacement/membrane action in the fuselage skin was significant and small displacements/rotation assumption and linear analysis does not apply.

Nonlinear contact between fuselage skin and frame/longeron: Based on linear analysis results, full contact or no-contact assumption at the fuselage skin to longeron flange interface had sizable impact on the strain gage predictions.

In general the linear analysis predictions did not correlate well with the measured data. The general lack of correlation was attributed to non-liberalities in the structural system as listed in the above. Further nonlinear analysis with advanced tools was recommended but was not performed due to time and budget considerations under the transport aircraft program.

A more complete description of the analysis and findings for the transport aircraft study can be found in Appendix D.

The gap of the transport aircraft analysis was that the nonlinear effects identified above could not be analyzed with the SoA methods.

4.2.2.6 Aft Fairing Heat Shield Example

As an example of the SRA applications, The Boeing Company, Rockwell Science Center (RSC), and ATK Space Systems in a joint contract with AFRL [10] performed studies for the Advanced Ceramic Composites for Turbine Engines (ACCTE) on a 777 aft fairing heat shield design. Figure 62 shows the design and location of the heat shield. The objective of the study was to demonstrate the feasibility of Ceramic Matrix Composite (CMC) material as a substitute to Titanium for heat shield part that is exposed to high temperature gradient combined with acoustic environment.

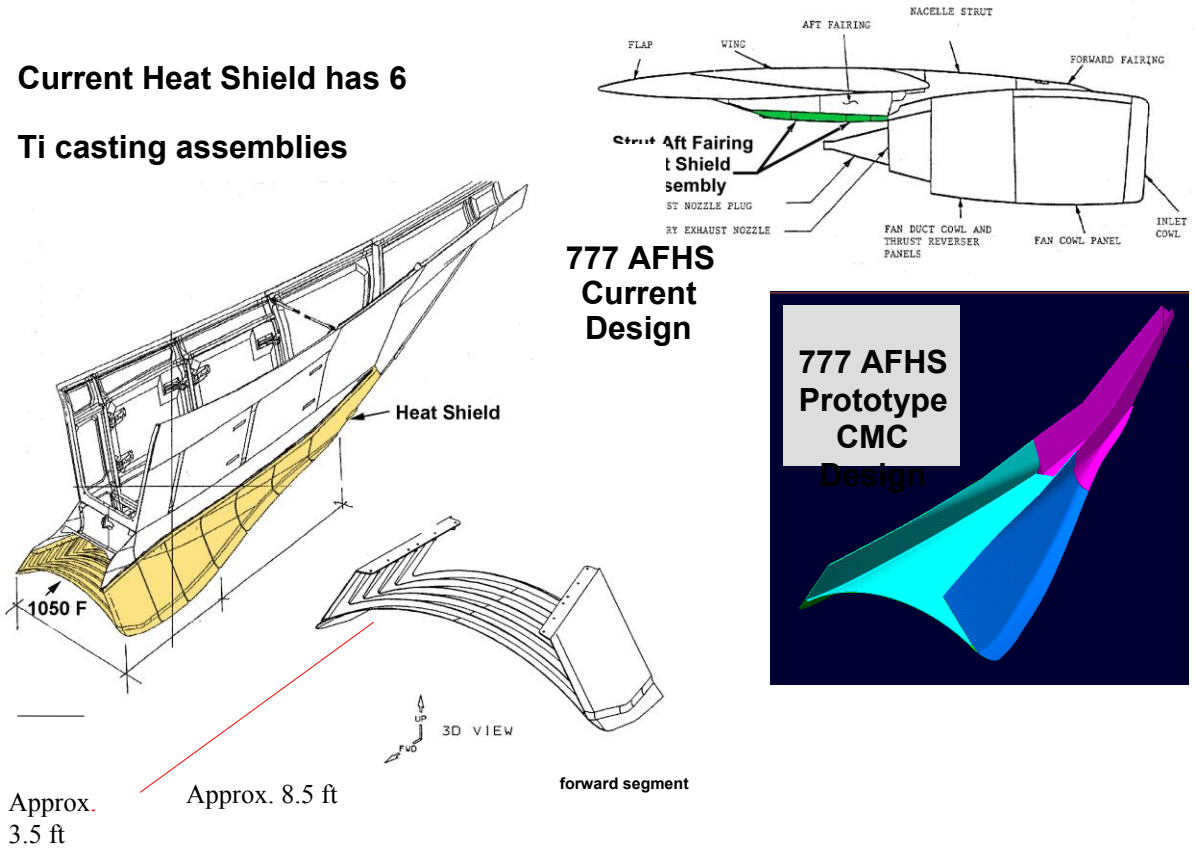

Figure 62. Location of 777 Aft Fairing Heat Shield on Aircraft

The four flight conditions that were considered in this study were idle, take-off, climb and cruise with plume and fan fluid temperatures and convective coefficients. The steady state idle case resulting in the highest heat shield temperatures was used. Boundary conditions at upper edges in contact with the strut fairing are assumed to be 130°F. Internal heat shield surfaces also radiated to this 130°F condition. A radiation boundary condition was applied to the outer surfaces of the heat shield with a radiation source temperature of 70°F. The lower surface of the heat shield received uniform convective heating from the plume. Similarly, the outboard side experiences convection from the fan air flow. Figure 63 shows the temperature distribution on the heat shield with peak temperature of 1180°F and large temperature gradient.

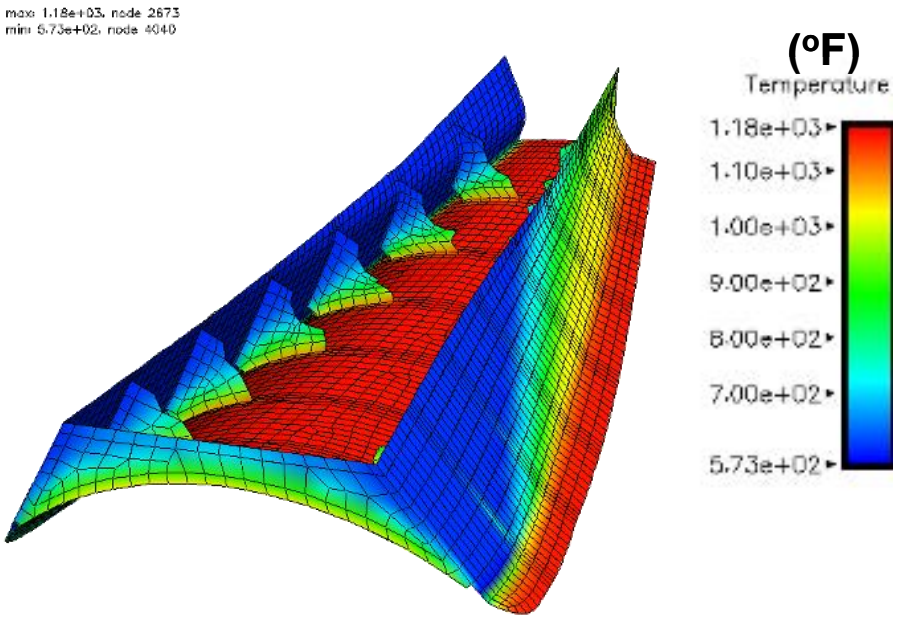

Figure 63. Temperature Distribution Due to Hot Day Idle Conditions

The acoustic environment is shown in Figure 64. The range of frequency is from 50 to 1250 Hz with peak 1/3 octave sound pressure level SPL at 1000Hz. Figure 65 shows the fringes of predicted axial stress component due to combined loads at natural frequencies.

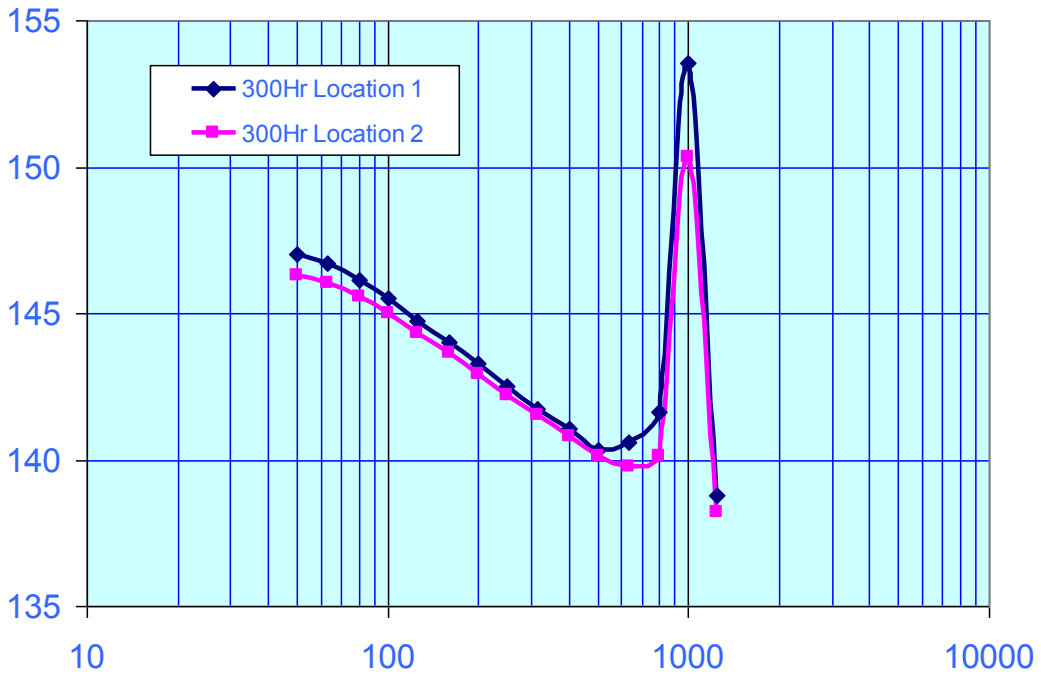

Figure 64. Acoustic Environment at Two Locations On Aft Fairing Heat Shield With Significant Blade Passage Frequency Influence

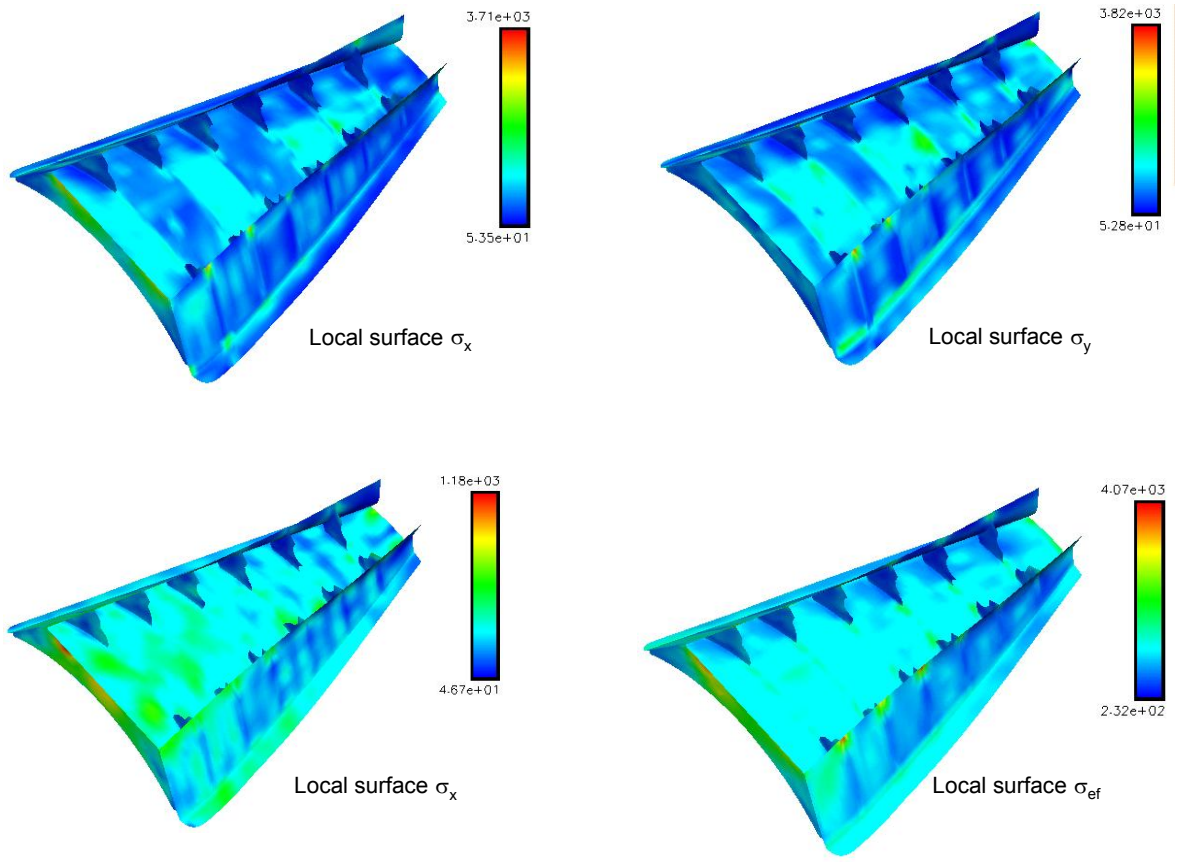

Figure 65. Acoustic Stresses at Natural Frequencies

This study was conducted using the finite element codes TOPAZ3D for thermal analysis and NIKE3D for mechanical stress analysis, both developed by the Lawrence Livermore National Laboratory. The same FEM consists of 3800 shell elements with typical element dimensions of 1 inch was used for both heat transfer and stress analyses. The FEA code read each output without the need for modification. The FEA was run separately and in sequence from TOPAZ3D to NIKE3D and then to SRA.

Various joining concepts, as shown in Figure 66, were considered in the CMC design. The ―t clip" was used in tests for validation of the SRA approach. Comparisons of analytical prediction and experimental data from the t-clipped were made with reasonable agreement, which validated the dynamic analysis methods. Fatigue analysis of the heat shield was conducted using the S-N curve developed from the t-clipped joint dynamic testing. It was however concluded that the CMC materials with pi-joints design provides a lower weight design for heat shield with positive fatigue margin.

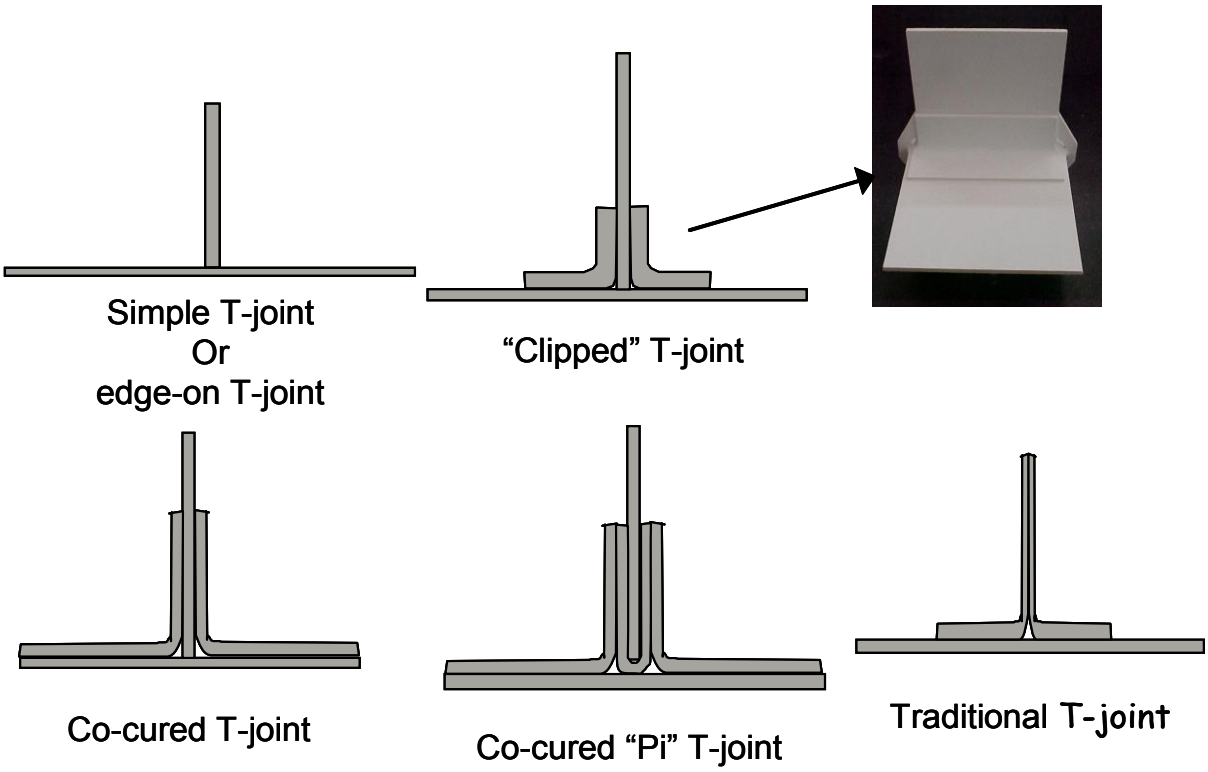

Figure 66. Joint Concepts for CMC Design

The following assumptions and/or gaps were revealed from using the Boeing SRA process in this study:

- The reference geometry was used in the thermal analysis to generate temperature distribution for nonlinear static analysis prior to vibro-acoustic analysis
- Uniform thermal boundary conditions including a convective heating on the underside of aft heat shield and a radiation to outer surfaces were assumed, which may result in higher temperature distribution than that in the real operation
- Linear frequency response analysis adopted in the SRA process does not account for the coupled thermal and acoustic environment.

4.2.3 TX-V Results

4.2.3.1 Identification of Design Drivers for Critical Regions for Reference Vehicle

The TX-V was divided into different regions based on their locations and functions. They included the wings, vertical stabilizers, control surfaces, nozzles, inlet, and forward and aft body surfaces of the vehicle. An expert review was performed on the regions with data containing temperature distribution at time steps of 800 and 2400 seconds into the flight trajectory, aerodynamic pressure at Mach Numbers of 0.95 and 7.0, altitude of 90,000 ft and AOA of approximately 12 degrees, and various acoustic pressure levels. The reviewing process evaluated the data associated with each region and qualitatively categorized the severity and intensity of different types of loads. After the critical regions were identified, a representative panel from each critical region was selected for preliminary analysis using engineering methods

as described in Boeing Appendix D (part of Linear SoA Best Practice). The evaluation contained panel related data of locations, functions, structural concepts, dimensions and sizing, temperature, temperature-dependent frequency, and acoustic loads.

A process was developed for ranking the critical regions of the reference vehicle and for identifying candidate panels for detailed analysis. This two-step process is shown in Figure 67. The first step is to consider the environments and loads obtained from the vehicle-level study, Figure 68. The procedure is to overlay the contour plots of external loads including aerodynamic pressure, temperature, and acoustics and utilizes the structural response stress and internal loads. For the applied external loads, certain criteria, included in the following discussion, are used to rank the environments in each vehicle region. For the structural response loads, the criteria at the region level are mainly areas of high concentrations or hot spots.

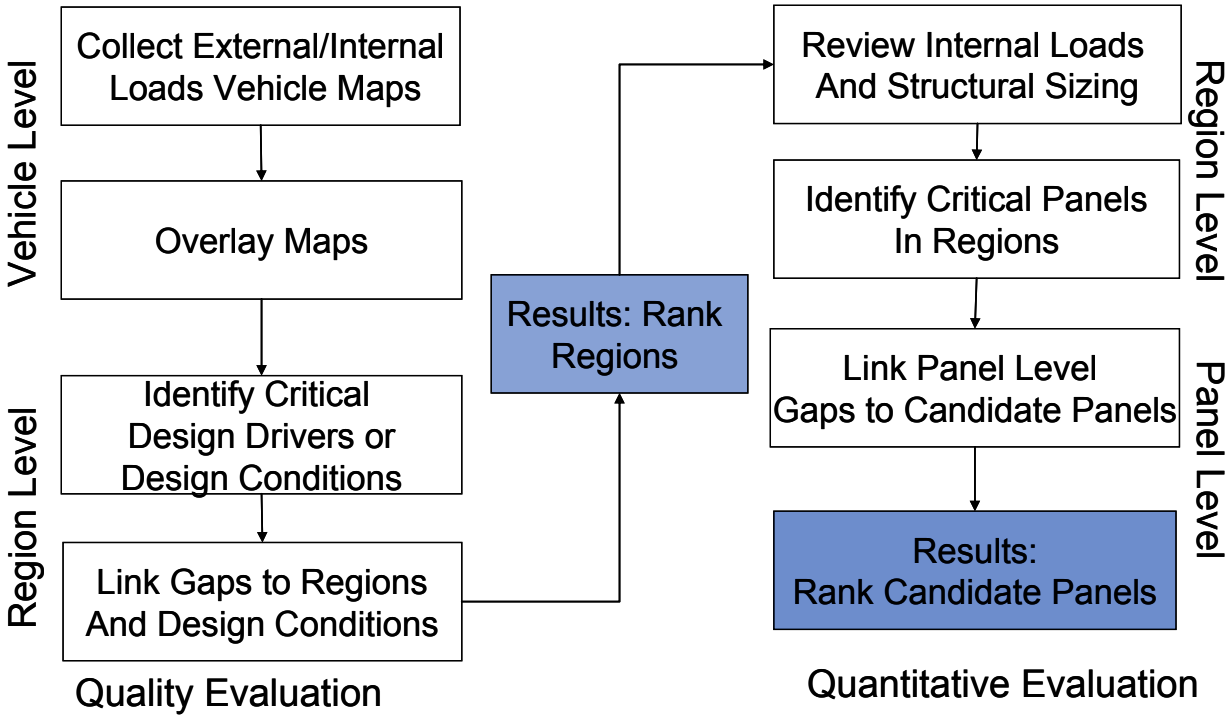

Figure 67. Critical Region/Structure Identification Process

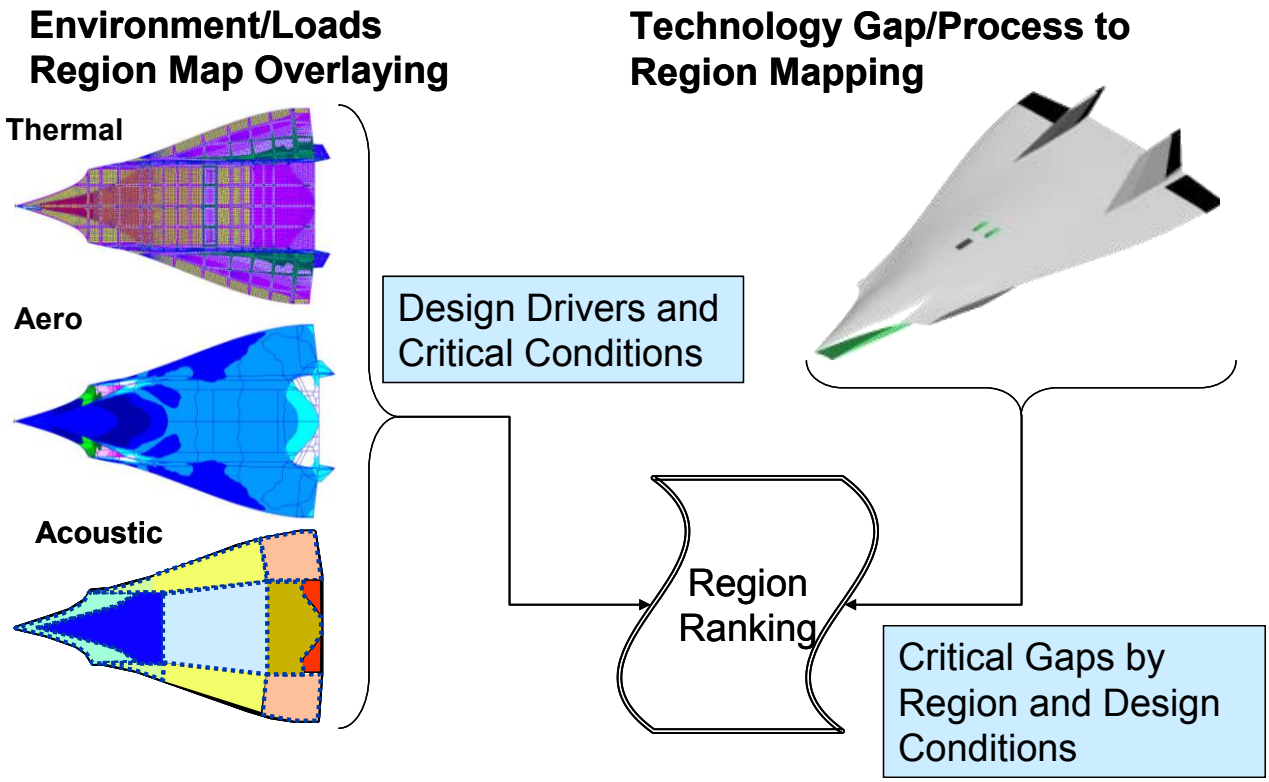

Figure 68. Step I: Candidate Panel Selection - Vehicle Level to Region Process

The TX-V vehicle was primarily designed with the metallic materials inconel and titanium as shown in Table 13. The temperature and stress requirements for both materials are listed below in Table 14. These requirements were used only for a qualitative assessment of risk. Above these stress levels, the nonlinear material stress-strain relationship begins, and above these temperature levels there is a significant degradation in strength allowable and material stiffness. The risk criteria for each material system are also given.

Table 13. Inconel and Titanium Properties

Material	Temperature, F	Stress, ksi
Inconel	1200	45
Titanium	800	70

Table 14. Temperature Requirements

Risk	**Titanium Temperature Criteria**	**Inconel Temperature Criteria**
Low	< 600 F	< 1000 F
Med	600 F < T < 1000 F	1000 F < T < 1400 F
High	T > 1000 F	> 1400 F

The general criteria for acoustic loading are given below in Table 15. When OASPL is below 155dB, the acoustic loads generally do not cause any fatigue issues. Above 165 dB it can potentially be a design driver. For example, the structural response, especially the thin gage structure, can be significantly nonlinear. However, the nonlinear behavior does not necessarily equate to acoustic fatigue design problems.

Table 15. Acoustic Criteria

Risk	**Acoustic Criteria**
Low	< OASPL=155dB
Med	155dB < OASPL < 165 dB
High	OASPL > 165dB

Figure 69 shows that wing and vertical tail leading edges had the highest temperatures, as well as the inlet and forward fuselage lower skins where the temperature was in excess of 1400 F for the Mach 7 design point. The critical regions for the acoustic loads were the upper and lower aft fuselage regions, Figure 70. Based on these maps the critical regions, the design drivers and conditions were identified in Figure 71. This resulted in the Vehicle Region Rankings shown in Figure 72. The regions were ranked by most challenging or highest risk due to uncertainty and magnitude of the design loads, maturity of design concepts for detailed design, and the expected level of complexity in the panel level analysis. The critical regions are the exhaust, inlet and control surface structures. This was consistent with the NASP study. However, the TX-V vehicle does not have a complete structural definition in these regions, i.e., lack of bulkheads and frames, gross approximation of the geometry, using large panels, and assuming a sandwich construction. Although the regions were ranked as the highest risk, lack of sufficient panel configuration definition prevented them from being used in Step II evaluation. The regions that had adequate structural definition and still had high risk ranking for either thermal, mechanical and/or acoustic loads include the wing structure, aft lower fuselage, and upper mid fuselage. The panels for Step II panel evaluation were selected from these regions.

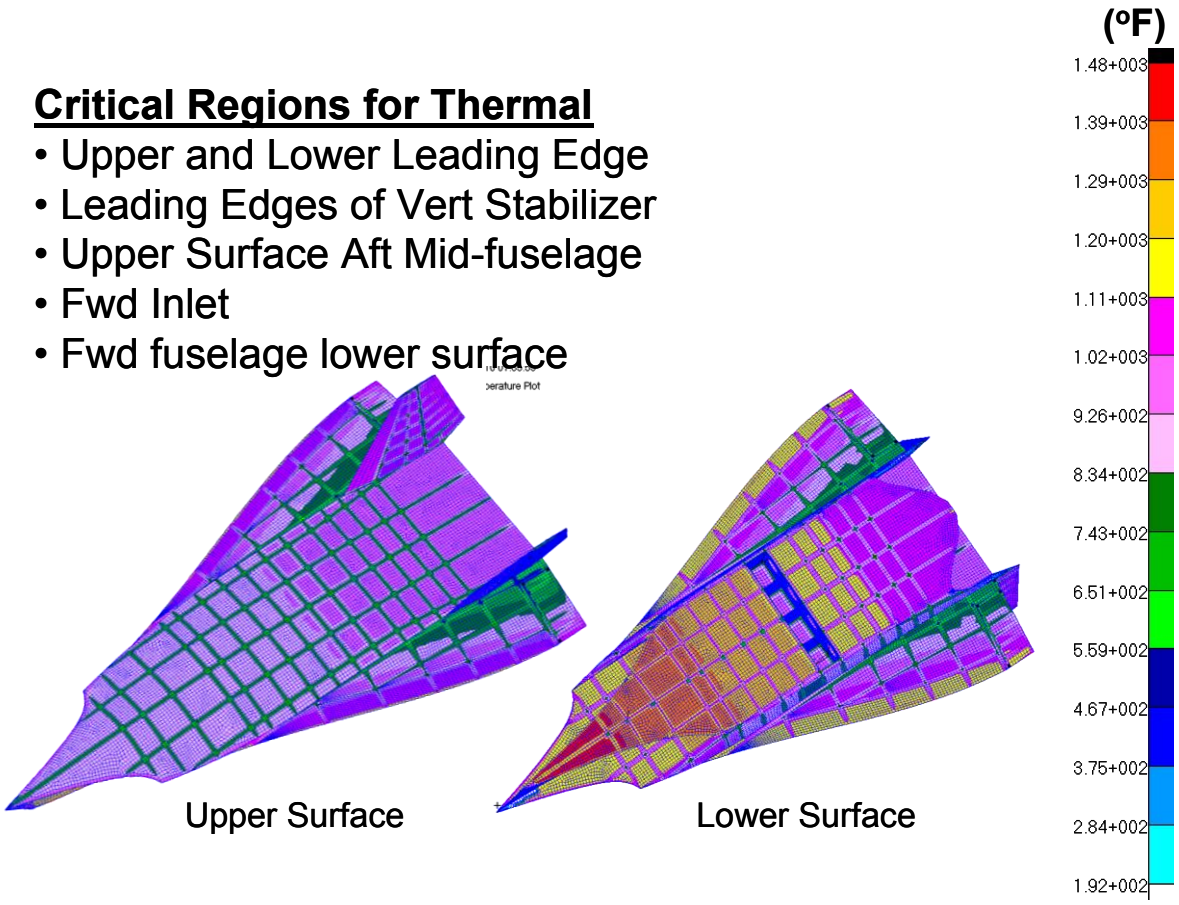

Figure 69. Critical Regions for Thermal at Mach 7

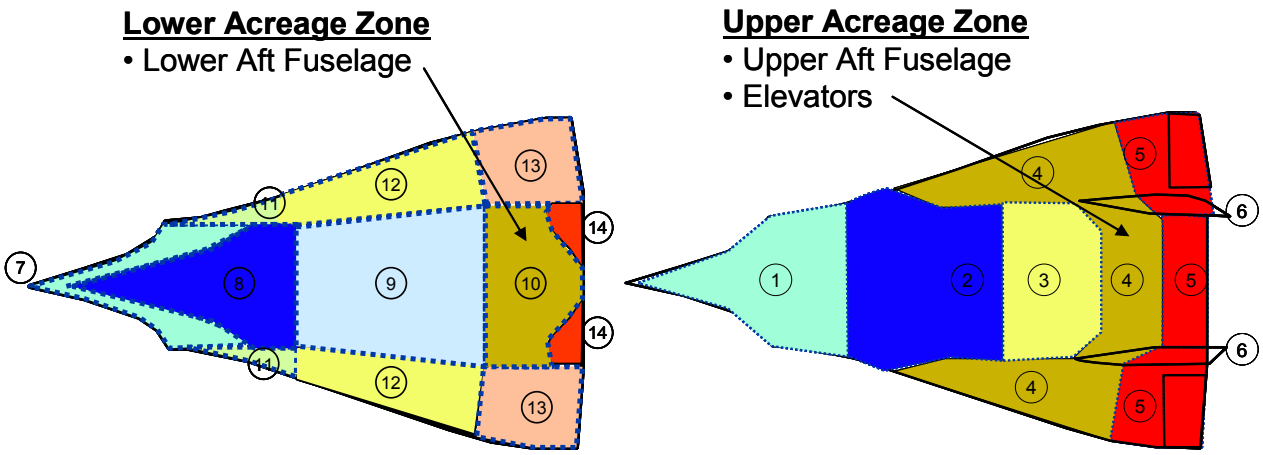

Figure 70. Critical Regions for Acoustic at Max Q

Region	Thermal	Aero/Mechanical	Acoustic/Buffet	Design Driver
Exhaust / Nozzle	HIGH	HIGH	HIGH	High thermal loads, worst case combined loads at Max Thrust and longest exposure to engine noise
Inlet / Duct	HIGH	HIGH	MOD	High Thermal, high pressure, at max Q, hammer shock conditions
Control Surfaces V-Tail, Flaps	MOD	HIGH	HIGH	High aero/maneuver loads, high acoustics and buffet loads during high AOA
Wing LE	HIGH	MOD	MOD	High thermal, active cooling, High aero/maneuver loads, buffet loads during high AOA
AFT Upper/Lower	MOD	MOD	HIGH	High acoustics during max Q accent, engine noise, shocks separated flow
Wing Structure	MOD	HIGH	MOD	High aero/maneuver loads, buffet loads during high AOA
FWD Lower	HIGH	MOD	MOD	High Thermal loads at Max Q, aero/maneuver loads during high AOA
MID Lower	MOD	HIGH	LOW	High mechanical ground loads, Inlet Spillage
FWD/MID Upper	LOW	MOD	LOW	Maneuver Carry Thru Loads

Figure 71. Critical Regions by Loads and Design Drivers

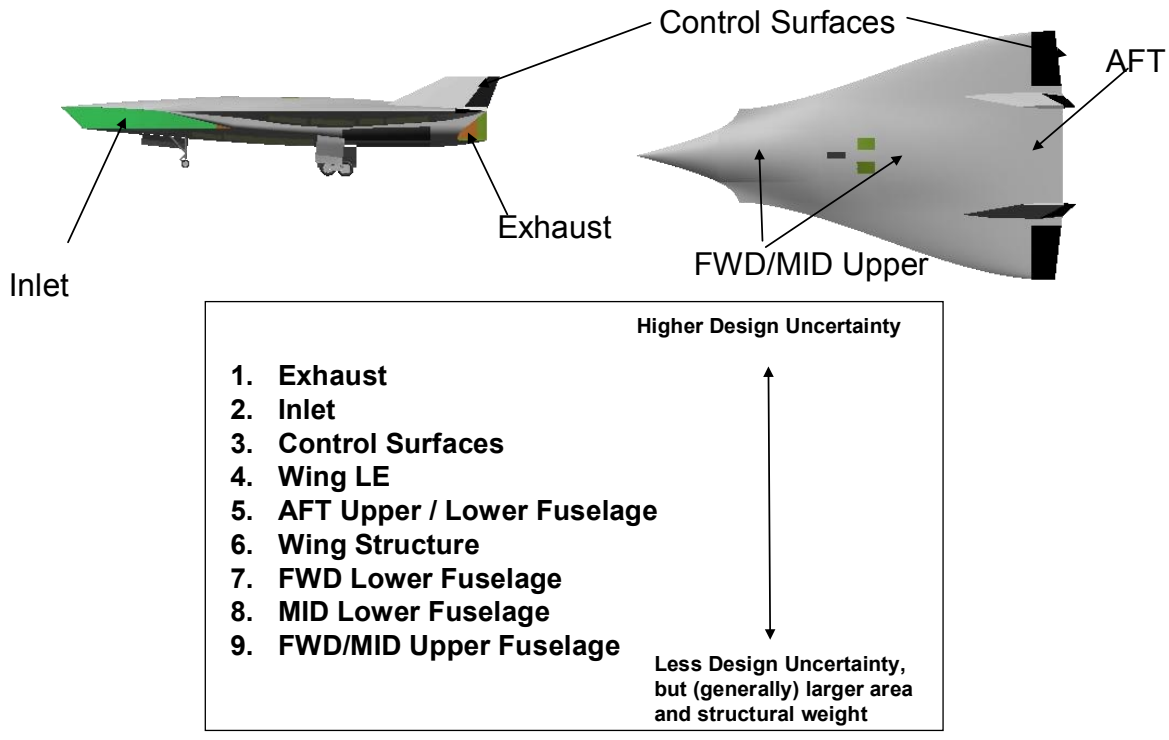

Figure 72. Vehicle Region Ranking

In Step II the panel selection process primarily used the structural sizing results shown in Figure 73. The panels identified for each region were based on large positive or negative margins;

maximum levels of external loads (environment maps); and locations that traditionally require more attention in detailed design. The following specific criteria were used to identify panels: for thermal/mechanical loading:

1. Thermal/mechanical buckling margin,
2. Thermal/mechanical stress margins
3. Thermal knock-down on strength allowables

And for acoustic loading:

1. Frequency limits,
2. Nonlinearity
3. Acoustic fatigue life
4. Regions of shocks

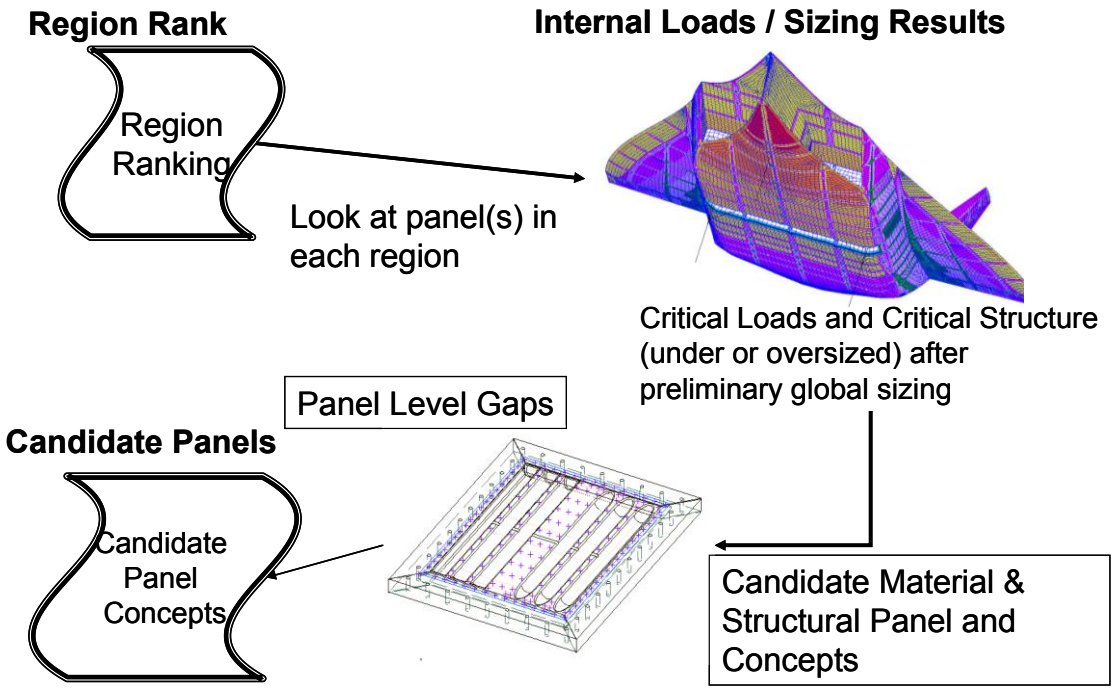

Figure 73. Step 2: Candidate Panel Selection - Region to Panel Level Process

In order to identify specific panels, the critical thermal and acoustic load conditions had to be determined at the panel level. This data came from the Task 1 sizing analysis, in which Hypersizer performed structural optimization analysis with 11 thermal/mechanical load cases. This load case #9 is the primary design driver for 85% of the vehicle acreage as shown Table 16. This is to be expected as load case #9 contains both a 2.5g mechanical load and a thermal load. The star indicates that the load case was active for sizing in HyperSizer and this was true for all but load case #1, which was the thermal case.

Table 16. Structural Sizing Load Cases used in Phase I (* Indicates Case was Active for Sizing in HyperSizer)

Available Load Cases

Load Case	Mechanical Load Set	Thermal Load Set	Weight (lb)	% Total	Description
1		1050			structural temp 2400s
2*	100		1285	4.60%	m.60 q -1g 16f
3*	101		32.46	0.10%	m.60 q 2.5g 16f
4*	104		9.238	0.00%	m1.80 q 2.5g 16f
5*	105		0	0.00%	m1.80 q 1g 5 beta
6*	201		91.83	0.30%	m.60 q 2.5g ff
7*	204		2395	8.60%	m1.80 q 2.5g ff
8*	205		98.77	0.40%	m1.80 q 1g 5 beta ff
9*	703	1050	23570	84.50%	Mach 7, 2.5g, 2000q, 159,740 lbs
10*	1015		307.6	1.10%	3 Point Braked Roll Nz = 1.2g
11*	1022		104.5	0.40%	taxi m

The panels in each region were selected based on the following requirements:

1. Select panels from a vehicle region where material property changed due to thermal loads and high aeroacoustic loads are primary concern.
2. Select panels from a vehicle region where transient and/or quasi-static thermal and mechanical loading and material property changes drove the design.
3. Select panels from a vehicle region where the combination of high aerodynamic loads, thermally induced stress, and material property change caused aeroelastic stability to be of primary concern.
4. Select panels from a vehicle region where the combination of all extreme-environments (aeroacoustic, material property change, thermally induced stress, and mechanical loading) drove the design.

For these load scenario requirements, the following data in Table 17 are the identified critical conditions, design drivers, and vehicle regions.

Table 17. Critical Conditions and Design Drivers for Each Requirement

Requirement	Critical Design Condition	Primary Design Driver	Vehicle Application Region
1	Max Q (dynamic pressure)	Acoustic Fatigue during Transient High Thermal and Aero-Acoustic conditions	Upper/Lower AFT Fuselage
2	Mach 7, Lf=2.5g (Load Factor)	Thermal Buckling, thermal stresses, and thermal degradation due to Steady State High Thermal and Mechanical Loads	Wing LE, Vert Stabilizer LE
3	Mach 7, L=2.5g	Panel Flutter due to High Compressive Internal Loads due to high thermal and/or mechanical loads	Mid Upper fuselage, lower fwd fuselage
4	Mach 7, Lf=2.5g	Complex design / failure modes (thermal / mechanical and acoustic fatigue) due to High Combined Thermal, Mechanical and Acoustic conditions	Wing LE, Control Surfaces, Vertical Stabilizer, wing/fuselage skin panels

These panels that were identified based on the four requirements encompass the most critical design challenges and knowledge gaps for hypersonic vehicle structural design and analysis. The panels are depicted in Figure 74 and Figure 75. They are the upper and lower surface acreage panels, respectively. Each panel is referenced to the primary design requirement (loading scenario) listed in Table 5. No panels from the Inlet and Exhaust regions were included since the environments and the primary design load conditions are not completely characterized, and their structural layouts are not defined sufficiently.

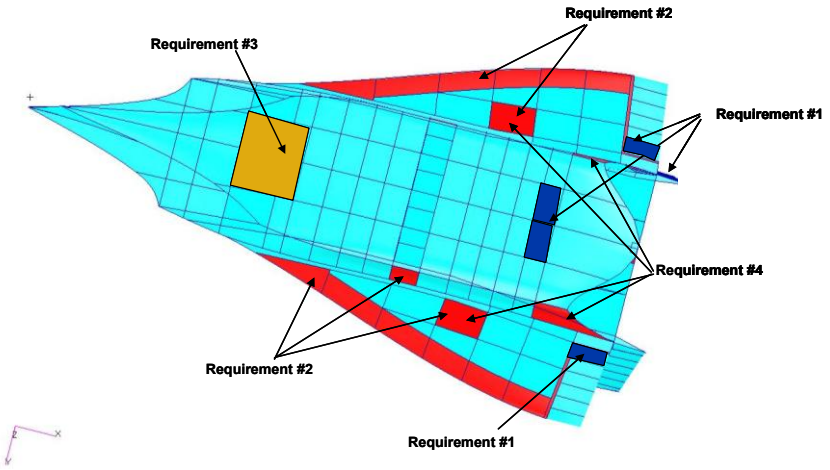

Figure 74. Load Case #9 – Critical Panels Lower Surface

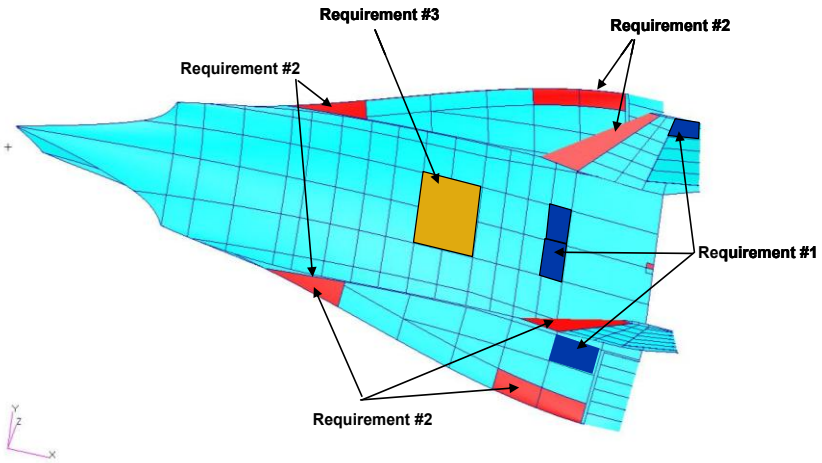

Figure 75. Load Case #9 – Critical Panels Upper Surface

The panels that are specifically critical for combined loading are shown in Figure 76.

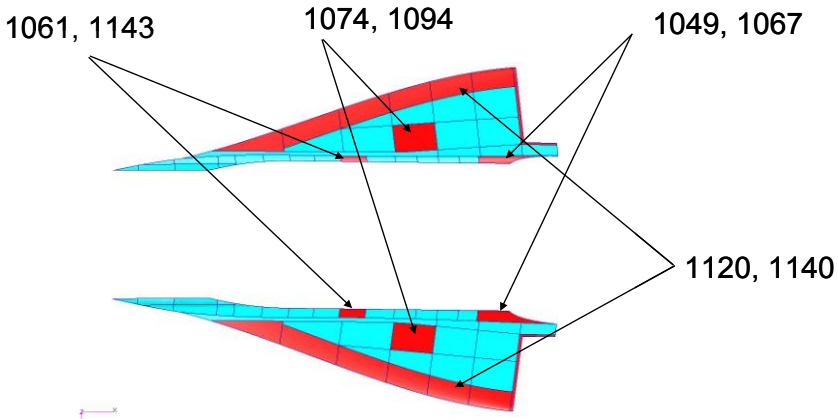

Figure 76. Critical Panel for Combined Thermal/Mechanical Load (Panel IDs Shown)

5 RESULTS AND DISCUSSION

Upon completion of the state of the art structural analysis and life prediction methods assessment, the gaps and limitations to the current analysis and life prediction approaches were identified. Any assumptions or shortcuts that were made in order to perform analyses were examined in order to determine why the assumption is made and what the impact to the analysis or the structure would be if the assumption is negated or modified. Any techniques of the current analysis approach that were perceived as a limitation or a gap, what the current workaround is in order to guarantee the structural integrity and structural life of the system, and what the cause and effects of our workarounds that will introduce conservatism to the system (added weight, costs, risk, increased inspections, etc.) were identified.

5.1 TX-V Gaps Identified

During the development of the TX-V reference vehicle several challenges and gaps were encountered. Removing these gaps would lead to improved designs, decreased weight and conservatism, and reduced cycle time and cost.

One of the key capabilities that could reduce cycle time and cost was use of an integrated multidisciplinary analysis & optimization process. The process used for this project contained some degree of integration, but could be more fully integrated to streamline data transfer between analysis disciplines, and computer systems. As an example the Sol 200 and loads analysis was performed on a Linux cluster to take advantage of enhanced computing performance. However, the detailed sizing was done using HyperSizer on a PC. This required manual data transfer which prevented the process from running in an automated fashion. Another benefit of an integrated process is that it allows user to cycle through the analysis process to update results or to investigate the impact changes that may have on the design in a timely manner. For this study structural temperatures were developed using a thermal model with assumed structural gages, and materials. Once the structure had been sized it would have been desirable to cycle though the thermal analysis and update the structural temperatures based on the resulting sizing. With a more integrated process this would be a much faster, easier, and less expensive task.

For this project an aeroheating database based on engineering methods was used. This approach works well for initial studies but lacks the fidelity required to support more detailed phases. One approach to improve aeroheating predictions is to employ High fidelity CFD based aeroheating simulations. These can be used to "anchor" and correct the engineering methods so that more accurate aeroheating data can be generated for an entire trajectory. While the accuracy of CFD aeroheating results are significantly better than engineering methods, there exists too much uncertainty with respect to heating for complex flow regions. Improved accuracy is required. The solution time for CFD aeroheating methods is too long, and needs to be reduced. Complete trajectory simulations are not necessarily required, but it is desirable to have tools that provide aeroheating data quickly for use in supporting configuration development as well as supporting thermal-structural analysis.

As the project progresses to more detailed phases, improved thermal-structural analysis methods will be required to enable realistic analysis for the range of hot-structure panel concepts that

might be considered for future hypersonic cruise vehicles. In the past, on projects such as the X-43A, 3-D solid thermal and structural analysis models were used to analyze and design the hot structure components. This was successful, but those components were small and relatively simple. Applying the same approach for a 75 ft. hypersonic cruise vehicle would be challenging and may not be possible.

The results of this effort showed that the thermal environment was the primary design driver for most of the structure. One of the key challenges encountered during the thermal analysis was modeling of the fuel and accounting for the changing fuel levels. The fuel mass is a large heat sink and can having a significant effect on the structural temperatures. Improved methods for integrating fuel mass and varying fuel levels into the thermal analysis process are needed.

For this project many panels were driven by panel frequency requirements dictated by acoustic concerns. Part of that was due to the scaling of the FEM model to 75 ft which resulted in larger panel sizes than would normally be used. However, the acoustic environment is key driver, and improved methods are needed to predict the aeroacoustic environment as well as to address engine acoustics and ground reflection.

HyperSizer panel boundary conditions for buckling analysis are limited to free, fixed or simply supported. This limitation often results in conservative buckling assessment resulting in overdesigned panels.

When performing structural sizing using Nastran Sol 200 or HyperSizer the key drivers for determining panel sizing are the design loads and temperatures. Since these are not constant, and may vary considerably over the panel, it is difficult to determine what values should be used. In Nastran Sol 200 the worst element load is typically used. This can be overly conservative if only a small region or single element experience that load. HyperSizer performs a statistical analysis of the panel element loads and attempts to come up with a less conservative more realistic load, based on a user selected design load level. It would be desirable to have a similar capability in Sol 200.

Nastran Sol 200 does not currently support multistate controllers. Multistate controllers can be used to model nonlinear variation of forces such as exterior pressure distributions from CFD solutions which are used to generate trimmed flight load conditions. Multistate controllers are currently supported in Sol 144. Having this capability available in Sol 200 is more efficient and would require less time.

It was not possible to run Sol 200 using the Lagrange multiplier method with the TX-V model. This feature is available in Sol 101 static analysis and is required to obtain reasonable results if rigid elements are present and temperature loads are applied.

5.2 Knowledge Gaps, Capabilities Required to Address Gaps, & Benefits if Gaps are Addressed

The knowledge gaps identified in this section address the following key questions in bold:

- **The rationale for the identified gap, i.e., what analysis assumptions result in this gap?**

- What is the function or intended purpose of the structural component?
- Where is this component used?
- How was the component sized? For example, strength vs. stability considerations.
- A description of the environment/loads and boundary conditions for the component.
- **The process used/would be used to address the identified gap if current practices were utilized.**

Detailed information at the panel level of the structural components function, location and environment are included in Section 5.3.

The followings gaps were identified from the evaluation of panels on the TX-V and the assessment of the SoA method on thermal-mechanical and acoustic analysis from past conventional and hypersonic air vehicle projects described in Section 4.2.2. The assumptions made to fill the gaps and their impacts to vehicle design are included. Additionally, the following discussion includes suggestions to the future development of advanced methods for hypersonic structures in combined extreme environment. The capabilities are expected to address the gaps discussed above and are suitable for the coupled analyses of aero-thermal, thermal, loads and dynamics, and acoustic disciplines. Finally, the envisioned structural benefits once the above advanced methods and tools are introduced into engineering design for hypersonic structures are also included.

1. ***It is difficult to identify the critical design load combination for thermo-mechanical and acoustic loads. The SoA assumes that the worst case loading scenario meets and exceeds the design requirements. The workaround is accomplished by using the worst combinations of loads from different trajectory points.***

The trajectory of a hypersonic vehicle is highly transient, and the external loads are known to be strongly coupled. Since the flight maneuver loads and thermal loads are determined separately, design load cases are generally based on worst combinations of loads at specific trajectory points. For example, the critical design condition used for the TX-V sizing optimization includes 2.5G flight maneuver loads in ascent at Mach=7, and q=2,000psf, with temperatures at 2400 sec in cruise. This approach can be conservative causing increases the vehicle weight. This kind of combination is typical for structural sizing. When the approach is used in fatigue life prediction, it could significantly over-predict structural response and conservatively estimate structure integrity and life, which leads to an unnecessarily heavy structure.

The advanced capabilities required to address this gap include:

1. New capability to couple aeroheating/CFD, thermal, and structural analyses with acoustic pressure and large static internal loads is needed to predict critical design loads and accurate structural response and life.

The predicted structural benefits if this gap is addressed include:

1. Accurate response and life prediction for hypersonic structures, such as critical locations and stresses on the panel, can be obtained. This will lead to robust structural design, e.g., use of advanced materials and innovative structural concepts, and expand design space for the vehicle. An efficient design also helps increase the vehicle operational range, speed, payloads, maneuverability, and survivability, and satisfy the mission requirements.

2. Reduce weight by helping allow the optimization of structure to meet all design constraints.
3. Reduce uncertain/risk in loads, design and modeling with direct coupling techniques for thermal, CFD, structural and acoustic disciplines and better definitions of boundary conditions and damping.
4. Reduce maintenance time and cost by being able to pin-point critical locations on structure and accurately predict structural response that optimize the inspection interval and improve vehicle reliability throughout its design life.
5. Efficient fabrication and assembly methods can be incorporated early in the design cycle and interacted with structural design to achieve an optimal vehicle meeting design, time and cost constraints.

2. ***The temporal and spatial thermal gradients are difficult to adopt in the panel level linear analysis. The assumption causing the gap in this SoA method is that the maximum temperature and thermal gradient are used for the critical thermal load conditions. The work-around is to use maximum temperature or thermal gradient for the panel.***

The linear frequency response analysis cannot account for the time varying and accumulation effects of thermal, residual stress and/or damage effects during the flight. In addition, both the structural and thermal analyses performed at vehicle level use a low fidelity model. The low fidelity FEM lacks the spatial refinement to accurately determine thermal loads over local sections of the vehicle, especially thru the thickness. Also, the FEM does not model the substructure to panel attachments. Assumptions need to be made as to the compliance and thermal resistance and expansion of these attachments. Hence, there is considerable uncertainty in the spatial and temporal definitions of thermal loads used in detailed panel-level FEA. The impact to structural design includes redundant weight for conservatism, as well as higher risk due to the approximation in predicting response.

The advanced capabilities required to address this gap include:

1. Efficient large-order analysis tools such as NLROM are needed to solve complex and high fidelity FE structural dynamic problems, simulate dynamic snap-thru under intensive aeroacoustic fluctuated pressure, capture high frequencies and large deformation nonlinear response of panels, and address issues such as high CPU time and large computer memory. It will allow a robust detailed nonlinear transient response analysis to alleviate the risk of under-designing panels. If NLROM can be further developed with optimization techniques, e.g., optimization with a response surface approach, it will revolutionize today's engineering design approach and significantly expand the design space.
2. An efficient and accurate analysis method to highly temporal and spatial thermal gradient in calculation is needed.
3. The capability to interface with and take advantage of advanced thermal, structural, CFD, and acoustic analysis tools can help engineers expedite the design validation and trade study.

The predicted structural benefits if this gap is addressed include:

1. Accurate response and life prediction for hypersonic structures, such as critical locations and stresses on the panel, can be obtained. This will lead to robust

structural design, e.g., use of advanced materials and innovative structural concepts, and expand design space for the vehicle. An efficient design also helps increase the vehicle operational range, speed, payloads, maneuverability, and survivability, and satisfy the mission requirements.
2. Reduce design and analysis time, and therefore cost, by allowing quick turnaround for trade study of materials and structural concepts, and avoiding unnecessary analysis of non-critical panels.
3. Reduce weight by helping allow the optimization of structure to meet all design constraints.
4. Reduce maintenance time and cost by being able to pin-point critical locations on structure and accurately predict structural response that optimize the inspection interval and improve vehicle reliability throughout its design life.
5. Efficient fabrication and assembly methods can be incorporated early in the design cycle and interacted with structural design to achieve an optimal vehicle meeting design, time and cost constraints.

3. ***The linear frequency response analysis adopted in SoA does not account for the coupling between transient thermal and vibro-acoustic analyses. The linear analysis is conducted with the assumption of a constant thermal condition. The workaround is to ignore the coupling, use the thermal as the preload, and then factor in the acoustic response.***

At high temperatures in turbulent boundary layer flow fields, there is a coupling between the flow, surface temperature and unsteady component of the pressure field. Some empirical models in Reference 5 have the temperature coupling terms. There is however no standard method to predict this coupling using CFD. The structural deformation further complicates the effect. No coupling introduces uncertainties to the applied loads and requires conservative factors of safety. Use of conservative acoustic loads result superimposed with worst load combinations in an excessively heavy structure.

The advanced capabilities required to address this gap include:
1. New capability to couple aeroheating/CFD, thermal, and structural analyses with acoustic pressure and large static internal loads is needed to predict critical design loads and accurate structural response and life.
2. The capability to interface with and take advantage of advanced thermal, structural, CFD, and acoustic analysis tools can help engineers expedite the design validation and trade study.

The predicted structural benefits if this gap is addressed include:
1. Accurate response and life prediction for hypersonic structures, such as critical locations and stresses on the panel, can be obtained. This will lead to robust structural design, e.g., use of advanced materials and innovative structural concepts, and expand design space for the vehicle. An efficient design also helps increase the vehicle operational range, speed, payloads, maneuverability, and survivability, and satisfy the mission requirements.
2. Reduce weight by helping allow the optimization of structure to meet all design constraints.

3. Reduce uncertain/risk in loads, design and modeling with direct coupling techniques for thermal, CFD, structural and acoustic disciplines and better definitions of boundary conditions and damping.
4. Reduce maintenance time and cost by being able to pin-point critical locations on structure and accurately predict structural response that optimize the inspection interval and improve vehicle reliability throughout its design life.
5. Efficient fabrication and assembly methods can be incorporated early in the design cycle and interacted with structural design to achieve an optimal vehicle meeting design, time and cost constraints.

4. ***The panel evaluation and FE analysis need to properly include internal loads. The assumption is to use uniformly distributed loads along the boundaries of the panel FEM. The workaround is to ignore the internal loads in the panel evaluation process and the effect of using uniformly distributed loads along the boundaries of panel FEM.***

The effect of internal loads to the frequencies and mode shapes are not currently included in the panel evaluation method. In the FE analysis, the internal loads are approximately distributed along the panel boundaries based on the analyst's experience, which may result in inaccurate modal analysis and subsequent stress and displacement response, especially when the internal load magnitudes are high. Impact of the approximation includes weight increase, higher risk, and more frequent maintenance due to inaccurate response prediction.

The advanced capabilities required to address this gap include:
1. An efficient and accurate analysis method to include large thermo-mechanical internal loads in calculation is needed.
2. The capability to interface with and take advantage of advanced thermal, structural, CFD, and acoustic analysis tools can help engineers expedite the design validation and trade study.

The predicted structural benefits if this gap is addressed include:
1. Accurate response and life prediction for hypersonic structures, such as critical locations and stresses on the panel, can be obtained. This will lead to robust structural design, e.g., use of advanced materials and innovative structural concepts, and expand design space for the vehicle. An efficient design also helps increase the vehicle operational range, speed, payloads, maneuverability, and survivability, and satisfy the mission requirements.
2. Reduce design and analysis time, and therefore cost, by allowing quick turnaround for trade study of materials and structural concepts, and avoiding unnecessary analysis of non-critical panels.
3. Reduce weight by helping allow the optimization of structure to meet all design constraints.
4. Efficient fabrication and assembly methods can be incorporated early in the design cycle and interacted with structural design to achieve an optimal vehicle meeting design, time and cost constraints.

5. ***Defining the thermal and mechanical boundary conditions for the detailed panel analysis remains a challenge due to primary reliance on subject matter experts (SME) past***

experience on similar analyses/efforts. The assumption is using prior experience and test scenarios will establish a conservative condition if the test scenarios show results below the allowable. A typical workaround would allow the SME to perform test scenarios and use experience to guide a boundary condition selection. For a project like X-51A, both fixed and hinged boundary conditions were used to ensure the response of structure was bounded. The two boundary conditions were both below the allowable.

The selection is generally based on the stiffness of surrounding structure and the analyst's experience. A substructure or super element approach can be used to model the boundaries, if the design of surrounding structure is available. Otherwise, fixed, hinges, or spring-supported boundary conditions must be chosen. Also, unveiled by a recent study [Reference 9] the inplane forces induced by elastically restrained panel boundary conditions could result in significantly different aero-heating predictions and subsequent thermal and structural response. The impact of this gap and then the assumption made would be inaccurate but conservative response prediction, which translates into additional structural weight.

The advanced capabilities required to address this gap include:

1. Guideline to select proper boundary conditions for thermal and structural analysis of panels is necessary.
2. The capability to interface with and take advantage of advanced thermal, structural, CFD, and acoustic analysis tools can help engineers expedite the design validation and trade study.

The predicted structural benefits if this gap is addressed include:

1. Reduce weight by helping allow the optimization of structure to meet all design constraints.
2. Reduce uncertain/risk in loads, design and modeling with direct coupling techniques for thermal, CFD, structural and acoustic disciplines and better definitions of boundary conditions and damping.
3. Efficient fabrication and assembly methods can be incorporated early in the design cycle and interacted with structural design to achieve an optimal vehicle meeting design, time and cost constraints.

6. ***The linear frequency response analysis does not account for large deformation oscillation or dynamic snap-thru of panel. The assumption is that the response will be linear and that there will not be large deformation oscillation or dynamic snap-thru. The workaround is to superimpose the static and dynamic solutions.***

The assumption may not be accurate when the vehicle with thin structural panels is operated in extreme thermal-acoustic environments. In the linear frequency response methods, thermal preload effects can be included to predict the random acoustic response. However, for hypersonic thin-gauge panels, the structure may be near or above the thermal buckling limit that causes the acoustic response to be nonlinear. The assumptions, judgment and adjustments made to the linear methods to approximate nonlinear transient response of structural panels when the thermal and/or acoustic loads are high add conservatism as well as risk to the resulting structure that can lead to added weight but more frequent inspections and maintenance to the structure.

The advanced capabilities required to address this gap include:

1. Efficient large-order analysis tools such as NLROM are needed to solve complex and high fidelity FE structural dynamic problems, simulate dynamic snap-thru under intensive aeroacoustic fluctuated pressure, capture high frequencies and large deformation nonlinear response of panels, and address issues such as high CPU time and large computer memory. It will allow a robust detailed nonlinear transient response analysis to alleviate the risk of under-designing panels. If NLROM can be further developed with optimization techniques, e.g., optimization with a response surface approach, it will revolute today's engineering design approach and significantly expand the design space.
2. The capability to interface with and take advantage of advanced thermal, structural, CFD, and acoustic analysis tools can help engineers expedite the design validation and trade study.

The predicted structural benefits if this gap is addressed include:

1. Accurate response and life prediction for hypersonic structures, such as critical locations and stresses on the panel, can be obtained. This will lead to robust structural design, e.g., use of advanced materials and innovative structural concepts, and expand design space for the vehicle. An efficient design also helps increase the vehicle operational range, speed, payloads, maneuverability, and survivability, and satisfy the mission requirements.
2. Reduce design and analysis time, and therefore cost, by allowing quick turnaround for trade study of materials and structural concepts, and avoiding unnecessary analysis of non-critical panels.
3. Reduce weight by helping allow the optimization of structure to meet all design constraints.
4. Reduce maintenance time and cost by being able to pin-point critical locations on structure and accurately predict structural response that optimize the inspection interval and improve vehicle reliability throughout its design life.
5. Efficient fabrication and assembly methods can be incorporated early in the design cycle and interacted with structural design to achieve an optimal vehicle meeting design, time and cost constraints.

7. ***The accumulated damage and degradation due to exposure to high temperature environments is inadequately modeled in the SoA approach. The assumption is that degradation and accumulated damage can be simulated by knockdown factors. The workaround is to use knockdown factors for both materials and allowable.***

In the SoA, material change due to temperature is accounted for by using knock-down factors. Strength and fatigue allowables are adjusted based on measured static property data. However, thermal degradation of material properties and failure mode changes due to long term duration (in flight) and long term exposure (over the life) cannot be included in the SoA method. The conservative design approach using thermal knockdown generally leads to over-estimated structural response and weight.

The advanced capabilities required to address this gap include:

1. New method is needed to include effects of material degradation, failure mode change, and residual stress and their damage accumulations throughout vehicle service history.
2. The capability to interface with and take advantage of advanced thermal, structural, CFD, and acoustic analysis tools can help engineers expedite the design validation and trade study.

The predicted structural benefits if this gap is addressed include:

1. Accurate response and life prediction for hypersonic structures, such as critical locations and stresses on the panel, can be obtained. This will lead to robust structural design, e.g., use of advanced materials and innovative structural concepts, and expand design space for the vehicle. An efficient design also helps increase the vehicle operational range, speed, payloads, maneuverability, and survivability, and satisfy the mission requirements.
2. Reduce weight by helping allow the optimization of structure to meet all design constraints.
3. Reduce maintenance time and cost by being able to pin-point critical locations on structure and accurately predict structural response that optimize the inspection interval and improve vehicle reliability throughout its design life.
4. Efficient fabrication and assembly methods can be incorporated early in the design cycle and interacted with structural design to achieve an optimal vehicle meeting design, time and cost constraints.

8. ***Accurately predicting damping for analysis is a challenge due to lack of data. The assumption is that a low damping value, such as 1.6%, over-predicts the structural response. The workaround is to use a low damping value and accept the conservatism.***

A damping factor of 1.6% is generally used for integral and newly assembled metallic structures. Hypersonic vehicles that operate in extreme temperature environment may have a higher damping in local panels due to aerodynamic flow, thermal expansion of joints, changes in material properties to thermal loads, and nonlinear geometric response. A conservative use of low damping leads to much higher response, and hence heavier structural design.

The advanced capabilities required to address this gap include:

1. Accurately modeling structural damping by considering material degradation, level of deformation, contact surfaces, micro-cracking, and vehicle service history is needed for structural response and life prediction.
2. The capability to interface with and take advantage of advanced thermal, structural, CFD, and acoustic analysis tools can help engineers expedite the design validation and trade study.

The predicted structural benefits if this gap is addressed include:

1. Reduce weight by helping allow the optimization of structure to meet all design constraints.
2. Reduce uncertain/risk in loads, design and modeling with direct coupling techniques for thermal, CFD, structural and acoustic disciplines and better definitions of boundary conditions and damping.

3. Efficient fabrication and assembly methods can be incorporated early in the design cycle and interacted with structural design to achieve an optimal vehicle meeting design, time and cost constraints.

9. ***The acoustic environment can only be approximated using established empirical formulas at the beginning of the design phase until flight test can be conducted. The assumption is that the empirical formulas will provide sufficient data for initial panel sizing. The workaround for the preliminary design phase is to add a factor of safety (FS) to be conservative.***

Typically the prediction of these loads relies on empirical models when CFD or measured data do not exist. To perform the linear response analysis, an analyst needs the magnitude and time/spatial correlation characteristics of the loading, which are generally not available and assumptions have to be made. For hypersonic flows, the condition of high temperatures compounds the effects of acoustics loads. Since the OASPL, PSD, and spatial correlation of the acoustic environment are subjected to a high degree of uncertainty, a FS of 3.5dB is added to the worst case design conditions, which results in a heavier structure.

The advanced capabilities required to address this gap include:

1. A new method is needed to reduce the level of uncertainties in acoustic load prediction.
2. The capability to interface with and take advantage of advanced thermal, structural, CFD, and acoustic analysis tools can help engineers expedite the design validation and trade study.

The predicted structural benefits if this gap is addressed include:

1. Reduce weight by allowing the optimization of structure to meet all design constraints.
2. Reduce uncertain/risk in loads, design and modeling with direct coupling techniques for thermal, CFD, structural and acoustic disciplines and better definitions of boundary conditions and damping.
3. Efficient fabrication and assembly methods can be incorporated early in the design cycle and interacted with structural design to achieve an optimal vehicle meeting design, time and cost constraints.

10. ***An efficient design and analysis method to analyze large-order models with a high fidelity mesh to capture nonlinear, dynamic snap-thru, and high frequency response in coupled thermal-acoustic environment is cost and schedule prohibitive for programs. The assumption is a heavier weight design will account for these factors in an effort to save time and cost. The workaround is to use the linear response analysis approach.***

If the design needs to be investigated with a nonlinear transient response approach using either implicit or explicit method, it would be costly and time-consuming. The approach is adopted sometimes for challenging design environment or structural weight reduction, but is not part of the SoA methods.

The advanced capabilities required to address this gap include:

1. Efficient large-order analysis tools such as NLROM are needed to solve complex and high fidelity FE structural dynamic problems, simulate dynamic snap-thru under intensive aeroacoustic fluctuated pressure, capture high frequencies and large deformation nonlinear response of panels, and address issues such as high CPU time and large computer memory. It will allow a robust detailed nonlinear transient response analysis to alleviate the risk of under-designing panels. If NLROM can be further developed with optimization techniques, e.g., optimization with a response surface approach, it will revolute today's engineering design approach and significantly expand the design space.
2. The capability to interface with and take advantage of advanced thermal, structural, CFD, and acoustic analysis tools can help engineers expedite the design validation and trade study.

The predicted structural benefits if this gap is addressed include:

1. Accurate response and life prediction for hypersonic structures, such as critical locations and stresses on the panel, can be obtained. This will lead to robust structural design, e.g., use of advanced materials and innovative structural concepts, and expand design space for the vehicle. An efficient design also helps increase the vehicle operational range, speed, payloads, maneuverability, and survivability, and satisfy the mission requirements.
2. Reduce design and analysis time, and therefore cost, by allowing quick turnaround for trade study of materials and structural concepts, and avoiding unnecessary analysis of non-critical panels.
3. Reduce weight by helping allow the optimization of structure to meet all design constraints.
4. Reduce maintenance time and cost by being able to pin-point critical locations on structure and accurately predict structural response that optimize the inspection interval and improve vehicle reliability throughout its design life.
5. Efficient fabrication and assembly methods can be incorporated early in the design cycle and interacted with structural design to achieve an optimal vehicle meeting design, time and cost constraints.

5.3 Critical Regions Identified

Five panels are selected based on the requirements. They are summarized in Figure 77 through Figure 81 including the geometric parameters, critical load case, design driver, boundary conditions, internal loads, acoustic loads, thermal loads, and acoustic fatigue life. This summary is obtained from the Hypersizer analysis results and quick acoustic fatigue analysis evaluation. Table 18 lists the loads, failure modes, and design requirements associated with these panels.

Table 18. Panel Data Summary

Panel ID	Design Condition	Thermal Load*	Acoustic Load#	Failure Mode	Requirement
705	9	771	155	Stress@	#2
837	1	620	158	Buckling	#3
849	1	618	165	Buckling	#2
736	1	703	165	Buckling	#2
782	1	703	168	Buckling/Acoustic Fatigue	1# or #4

* Thermal Loads are scaled by 1.5 from Mach 7 condition.

Acoustic loads include all design factors.

@ Mechanical loads are for 2.5g maneuver.

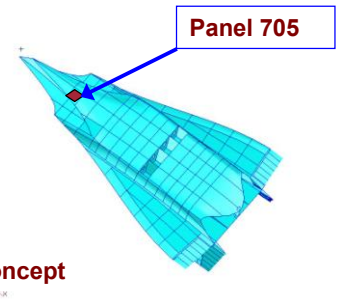

Critical Load Case

Load Case	Description
9*	Mach 7, 2.5g, 2000q, 159,740 lbs

Design Load Case and Lowest Margin of Safety

Load Case	MS	Component	Lim/Ult	Failure Mode
9	.11	705	Ult	Sandwich Flat-wise Tension w/ Interlaminar Shear Interaction

Panel/Beam Loads Table

Load Type	Factor	Nx lb/in	Ny lb/in	Nxy lb/in	Mx lb-in/in	My lb-in/in	Mxy lb-in/in	Qx lb/in	Qy lb/in
STRENGTH	Limit	-456.48	-512.98	-314.74	-680.83	-737.90	-205.73	-136.11	-123.88
	Ultimate	-383.74	-593.94	-378.74	-1019.94	-981.72	-235.66	-189.82	-161.53
BUCKLING	Limit	-276.79	-211.02	-118.08	-241.99	-333.49	-91.46	-47.29	-46.09
	Ultimate	-204.05	-247.82	-147.00	-361.69	-441.57	-107.09	-65.74	-60.04

Component Dimensions

Component ID	t_{tf} (in)	t_c (in)	H (in)	Unit Weight (lb / ft²)	Area (ft²)	Weight (lb)
705	0.0335	1.222	1.289	2.205	11.48	25.33

Honeycomb Materials

2	Honeycomb "Ti-3Al-2.5V_.002_3/16"

Face Sheet Materials

1	Titanium "Ti-6Al-4V KMAT1%301"

Size and Boundary Condition

X-span (in)	Y-span (in)	BC
38	44	simple

OML Temperature

Load Set = 1	771 F @ 2400 sec

Acoustic Loads and Fatigue

A/TBL	OASPL=155dB
fn	169 hz
Life	1.6e10 hrs

Figure 77. Panel 705 Forward Lower Fuselage

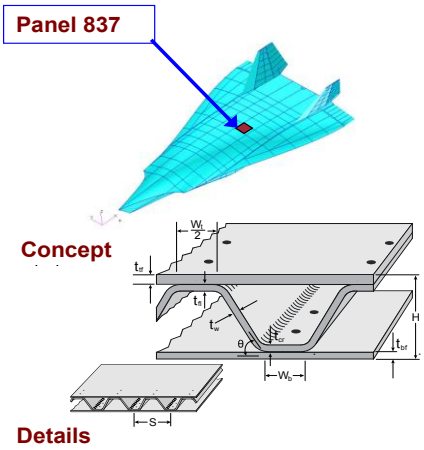

Critical Load Case	
Load Case	Description
1	Thermal Load case at 2400 sec - Steady State Cruise

Design Load Case and Lowest Margin of Safety				
Load Case	MS	Component	Lim/Ult	Failure Mode
1	.14	111	Lim	Local Buckling- Interaction

Panel/Beam Loads Table									
Load Type	Factor	Nx lb/in	Ny lb/in	Nxy lb/in	Mx lb-in/in	My lb-in/in	Mxy lb-in/in	Qx lb/in	Qy lb/in
STRENGTH	Limit	-917.00	-1077.70	138.50	108.77	166.56	200.10	32.10	17.80
	Ultimate	-1006.00	-1076.55	145.75	79.16	179.83	224.15	33.65	19.20
BUCKLING	Limit	-917.00	-1077.70	54.77	-67.63	36.60	84.62	11.00	4.70
	Ultimate	-1006.00	-1076.55	58.16	-108.94	45.39	96.43	11.50	5.05

Component Dimensions													
Comp ID	t_{tf} (in)	t_w (in)	t_{bf} (in)	H (in)	S (in)	w_b (in)	θ (°)	w_t (in)	t_{fl} (in)	t_{cr} (in)	Unit W (lb/ ft²)	Area (ft²)	W (lb)
111	0.0523	0.0256	0.02	1.417	2	0.5	77.5	0.915	0.025	0.025	2.884	1	2.884

OML Temperature	
Load Set = 1	Temp=620 F TTgrad = 100 F/in

Acoustic Loads and Fatigue	
S/TBL	OASPL=158dB
fn	143 hz
Life	1.5e6 hrs

Materials	
2	Titanium "Ti-6Al-4V

Size and Boundary Condition		
X-span (in)	Y-span (in)	BC
40	56	fixed

Figure 78. Panel 837 Mid Upper Fuselage

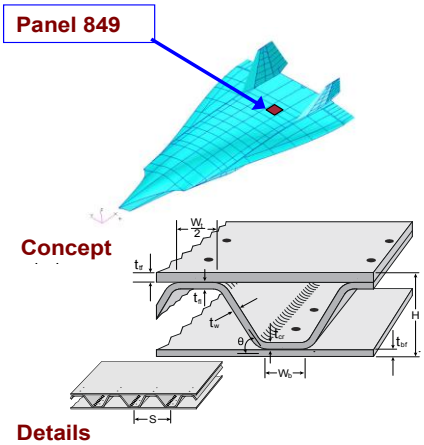

Critical Load Case	
Load Case	Description
1	Thermal Load case at 2400 sec - Steady State Cruise

Design Load Case and Lowest Margin of Safety				
Load Case	MS	Component	Lim/Ult	Failure Mode
1	.44	110	Lim	Local Buckling- Interaction

Panel/Beam Loads Table									
Load Type	Factor	Nx lb/in	Ny lb/in	Nxy lb/in	Mx lb-in/in	My lb-in/in	Mxy lb-in/in	Qx lb/in	Qy lb/in
STRENGTH	Limit	-740.00	-1080.00	-413.60	-54.72	-176.91	-243.92	-10.30	-8.68
	Ultimate	-763.50	-1110.00	-429.90	-61.58	-182.36	-240.88	-9.95	-8.52
BUCKLING	Limit	-608.00	-701.00	-132.60	-3.72	-5.71	-90.52	-4.10	2.98
	Ultimate	-631.50	-731.00	-148.90	-17.08	-18.56	-97.28	-3.95	3.03

Component Dimensions														
Com ID	t_{tf} (in)	t_w (in)	t_{bf} (in)	H (in)	S (in)	w_b (in)	θ (°)	w_t (in)	w_{cs} (in)	t_{fl} (in)	t_{cr} (in)	Unit (lb / ft²)	Area (ft²)	Weig (lb)
110	0.078	0.0355	0.0275	1.675	2	1.25	76.6	0.02808	-0.00423	0.0355	0.0355	4.255	1	4.255

OML Temperature	
Load Set = 1	Temp=618 F TTgrad = 100 F/in

Acoustic Loads and Fatigue	
SI/TBL	OASPL=165dB
fn	266 hz
Life	1.6e4 hrs

Materials	
2	Titanium "Ti-6Al-4V

Size and Boundary Condition		
X-span (in)	Y-span (in)	BC
30	56	fixed

Figure 79. Panel 849 Aft Upper Fuselage

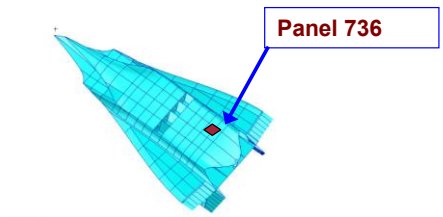

Critical Load Case

Load Case	Description
1	Thermal Load case at 2400 sec - Steady State Cruise

Design Load Case and Lowest Margin of Safety

Load Case	MS	Component	Lim/Ult	Failure Mode
1	.00	113	Lim	Local Buckling- Interaction

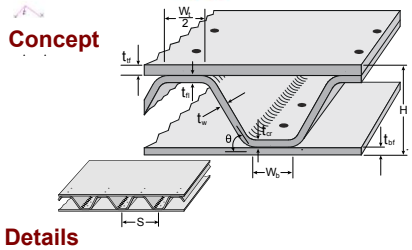

Panel/Beam Loads Table

Load Type	Factor	Nx lb/in	Ny lb/in	Nxy lb/in	Mx lb-in/in	My lb-in/in	Mxy lb-in/in	Qx lb/in	Qy lb/in
STRENGTH	Limit	-447.00	-522.00	569.30	576.92	861.76	527.55	160.00	26.60
	Ultimate	-414.00	-449.00	571.45	626.38	929.64	544.32	167.50	29.90
BUCKLING	Limit	-468.00	-586.00	151.60	258.77	286.75	161.58	54.00	10.80
	Ultimate	-445.50	-545.00	152.40	291.65	313.63	168.36	57.00	11.70

Component Dimensions

Component ID	t_{tf} (in)	t_w (in)	t_{bf} (in)	H (in)	S (in)	w_b (in)	θ (°)	w_t (in)	t_{fl} (in)	t_{cr} (in)	Unit (lb / ft²)	Area (ft²)	Weigh (lb)
112	0.0601	0.0256	0.029	1.15	2.5	1	81.25	1.181	0.0256	0.0256	3.069	1	3.069

OML Temperature

Load Set = 1	Temp=703 F TTgrad = 100 F/in

Acoustic Loads and Fatigue

S/TBL	OASPL=165dB
fn	278 hz
Life	2.8e3 hr

Materials

2	Titanium "Ti-6Al-4V

Size and Boundary Condition

X-span (in)	Y-span (in)	BC
30	30	fixed

Figure 80. Panel 736 Aft Lower Fuselage

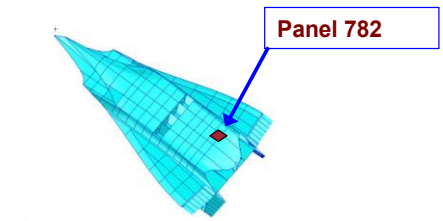

Critical Load Case

Load Case	Description
1	Thermal Load case at 2400 sec - Steady State Cruise

Design Load Case and Lowest Margin of Safety

Load Case	MS	Component	Lim/Ult	Failure Mode
1	.010	112	Lim	Local Buckling- Interaction

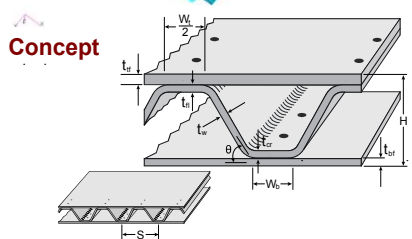

Panel/Beam Loads Table

Load Type	Factor	Nx lb/in	Ny lb/in	Nxy lb/in	Mx lb-in/in	My lb-in/in	Mxy lb-in/in	Qx lb/in	Qy lb/in
STRENGTH	Limit	-447.00	-522.00	569.30	576.92	861.76	527.55	160.00	26.60
	Ultimate	-414.00	-449.00	571.45	626.38	929.64	544.32	167.50	29.90
BUCKLING	Limit	-468.00	-586.00	151.60	258.77	286.75	161.58	54.00	10.80
	Ultimate	-445.50	-545.00	152.40	291.65	313.63	168.36	57.00	11.70

Component Dimensions

Component ID	t_{tf} (in)	t_w (in)	t_{bf} (in)	H (in)	S (in)	w_b (in)	θ (°)	w_t (in)	t_{fl} (in)	t_{cr} (in)	Unit (lb / ft²)	Area (ft²)	Weigh (lb)
112	0.0601	0.0358	0.02	1.417	2	1	81.25	0.5996	0.03583	0.0358	3.593	1	3.593

OML Temperature

Load Set = 1	Temp=703 F TTgrad = 100 F/in

Acoustic Loads and Fatigue

SI/TBL	OASPL=168dB
fn	211 hz
Life	169 hrs

Materials

2	Titanium "Ti-6Al-4V

Size and Boundary Condition

X-span (in)	Y-span (in)	BC
30	56	fixed

Figure 81. Panel 782 - Aft Lower Fuselage

The data documented in Table 19 details the gaps for the five identified panels addressing the following key questions in bold:

- The rationale for the identified gap, i.e., what analysis assumptions result in this gap?
- **What is the function or intended purpose of the structural component?**
- **Where is this component used?**
- **How was the component sized? For example, strength vs. stability considerations.**
- **A description of the environment/loads and boundary conditions for the component.**
- The process used/would be used to address the identified gap if current practices were utilized.

Table 19. Function, Location, Sizing, and Environment of Components Demonstrating Identified Gaps

	1	2	3	4	5
Panel ID	705	837	849	736	782
Functions/Intended Purpose	High Temperature Material Change	High Mechanical Load and Aeroelastic Stability	Mechanical and Acoustic Load	High Temperature and Mechanical Loads	High Temperature and Acoustic Loads
Component Locations	Lower FWD Fuselage	Upper MID Fuselage	Upper AFT Fuselage	Lower AFT Fuselage	Lower AFT Fuselage
Structural Configuration	Honeycomb	Corrugated	Corrugated	Corrugated	Corrugated
Material	Ti-6Al-4V	Ti-6Al-4V	Ti-6Al-4V	Ti-6Al-4V	Ti-6Al-4V
Boundary Conditions	Pinned	Fixed	Fixed	Fixed	Fixed
OASPL (dB)	155	158	165	165	168
OML Temp (deg F)	771	620	618	703	703
Critical Load Case	Mach 7, Maneuver 2.5g	Thermal Load at Mach 7	Thermal Load at Mach 7	Thermal Load at Mach 7	Thermal Load at Mach 7
Design Driver/Sizing Criterion	Sandwich Strength	Local Buckling	Local Buckling	Local Buckling	Acoustic Fatigue
Margin of Safety	0.11	0.14	0.04	0.00	-0.5

For Phase II, the focus will be on critical panels in the acreage regions of the vehicle that meet the following requirements for the study. These requirements are based on these loading scenarios:

1. A vehicle region where material property changes and high aeroacoustic loads are primary concern
2. A vehicle region where transient and/or quasi-static thermal and mechanical loading and material property changes drive the design
3. A vehicle region where the combination of high aerodynamic loads, thermally induced stress, and material property change cause aeroelastic stability to be of primary concern
4. A vehicle region where the combination of all extreme-environments (aeroacoustic, material property change, thermally induced stress, and mechanical loading) drive the design.

6 CONCLUSIONS

In Task 1 of this study, the TX-V reference vehicle was established to aid in the identification of critical technology gaps that will impact development of future hypersonic cruise vehicles. An existing hypersonic vehicle was leveraged and converted from a ceramic TPS structure to a metallic hot structure by replacing the existing TPS with high temperature metallic materials. During the structural sizing analysis the sizing failed to converge for a Mach 7 trajectory. The results showed that the thermal loads were driving the design for most of the vehicle structure. The results also revealed important design considerations for metallic hot structure subject to severe thermal environments. For Phase I, a reduced thermal environment was used to obtain convergence. In Phase II, a Mach 7 trajectory will be used along with refinement of the FEM and/or reduced coefficient of thermal expansion to simulate a more compliant structure that meets the needs of this program.

In the Task 2 effort, the Boeing SoA methods for detailed analysis of structural panels in thermal-acoustic environment were assessed with different hypersonic and conventional air vehicle programs, as well as the TX-V reference vehicle. In each program, the knowledge gaps were identified. This was translated to the TX-V to determine the benefit if the gaps were removed. A region ranking process was developed to categorize regions on TX-V based on the severity and intensity of respective thermal, mechanical and acoustic loads. Five critical panels and associated data such as function, location, sizing, loads, fatigue life, and design driver were also identified.

The Boeing Company recognizes that use of SoA methods for hypersonic vehicle designs result in excessive use of conservatism with heavy weight and cost penalties. Removing these gaps could significantly improve performance and reduce cost. The Boeing Company is well prepared with the TX-V design and identified panel data to successfully execute Phase II.

7 RECOMMENDATIONS

The recommendations from the Phase I study include the selection of panels for further detailed analysis and evaluation of gaps in the Boeing SoA methods in Phase II. These selected panels should encompass the range of technical challenges identified in Phase I. The panels are selected based on where the structural analysis and life prediction knowledge gaps are known to exist, what the severity and uncertainty of environment and design loads are, and where the conservatisms in the SoA methods need to be reduced.

As identified by the AFRL SSC, The Boeing Company concurs that the regions with the following design environments should be the focus for the detailed panel analysis:

1. A region where material property changes due to thermal loads and high aeroacoustic loads are primary concern.
2. A region where transient and/or quasi-static thermal and mechanical loading and material property changes drive the design.
3. A region where the combination of high dynamic pressure, thermally induced stress, and material property change cause aeroelastic stability to be of primary concern.
4. A region where the combination of extreme-environments (aeroacoustic, material property change, thermally induced stress, and mechanical loading) drives the design.

To enable the design of hypersonic structure in increasingly challenging environments, SoA methods must be enhanced with improved fidelity and quick response to reduce cycle time. The following capabilities are necessary to accomplish this.

1. Multi-physics modeling and analysis methods that allow complex and high fidelity coupling between aerothermal, structure, aeroacoustic, mechanical loads, materials, and structural concepts.
2. Development of advanced methods to minimize uncertainties in design load prediction.
3. Development of complete and comprehensive database and prediction models for hot-structure materials including temperature-dependent and degraded properties, service-history dependent stiffness, failure modes, and damping.
4. Analysis methods that allow the prediction of nonlinear response of structural panels and can be incorporated into the sizing optimization procedure to generate a both globally and locally optimized vehicle structure.

REFERENCES

1. —A Guide for Estimating Aero-acoustic Loads on Flight Vehicles Surfaces," AFFDL-TR-76-91.
2. B.M. Efimtsov, —Characteristics of the field of turbulent wall pressure fluctuations at large Reynolds numbers," *Soviet Physics Acoustics* **28** (1982), pp. 289–292.
3. Coe and Chyu, —Pressure Fluctuations Inputs and Response of Panels Underlying Attached and Separated Supersonic Turbulent Boundary Layers," NASA TM-X-62189
4. Lew H.G., and Laganelli, A.L., —Fluctuating Pressure Loads for Hypersonic Vehicle Structures," WL-TR-91-3057.
5. Laganelli A.L., and Howe, J.R., "Prediction of Pressure Fluctuations Associated with Maneuvering Re-entry Weapons," AFFDL-TR-77-59.
6. Lowson, M.V., —Prediction of Boundary layer Pressure Fluctuations," AFFDL-TR-67-167.
7. Wiley, D.E. and Seidl, M.G., —Aerodynamic Noise Tests on X-20 Scale Models," AFFDL-TR-65-192 Vol II.
8. Blevins, R.D., et al., "Thermo-vibro-acoustic Loads and Fatigue of Hypersonic Flight Vehicle Structure," AFRL-RB-WP-TR-2009-3139, 1989.
9. Culler, A., Crowell, A., McNamara, J., "Studies of Fluid-Structural Coupling for Aerothermoelasticity in Hypersonic Flow," AIAA-2009-2364, 17th AIAA/ASME/ASCE/AHS/ASC Structures, Structural Dynamics, and Materials Conference, May, 2009, Palm Springs, CA
10. Boeing-AFRL Contract; *"Advanced Ceramic Composites for Turbine Engines,"* Contract No. F33615-03-2-5201 (2006).

APPENDIX A – PANEL SIZING RESULTS FOR THE TX-V

Appendix A presents the HyperSizer panel sizing results for the TX-V vehicle for a honeycomb sandwich panel. The first part of Appendix A presents the panel facesheet, and core thicknesses, along with the total panel thickness, unit weight, area, and total panel weight. The top and bottom facesheet thickness were constrained to be the same. The facesheet thickness is only given for the top facesheet. The second half of Appendix A contains groupings of components also referred to as panels in HyperSizer along with margin of safety, critical load case number, and failure mode. Details for the load case numbers are available in the section 4.3.11 structural sizing Table 6.

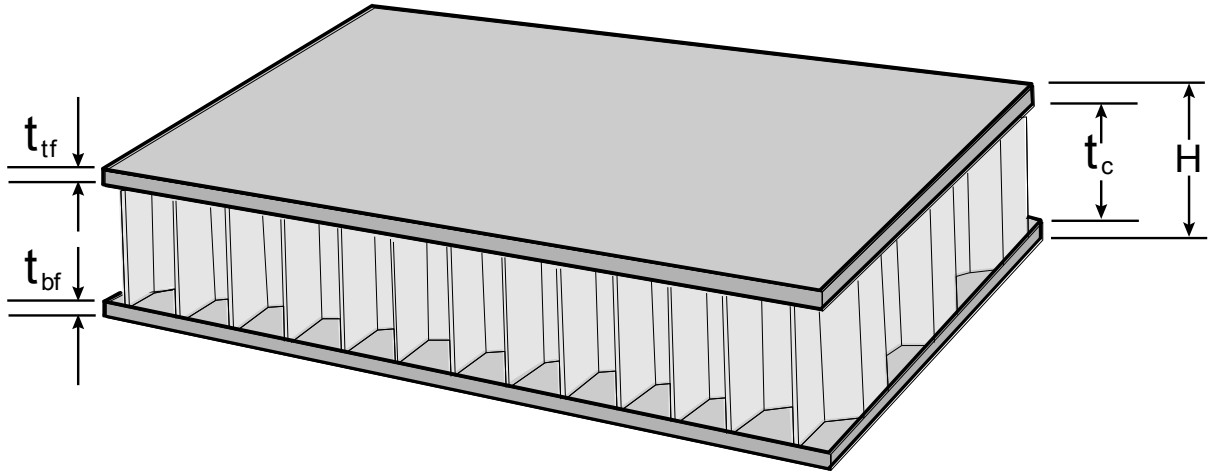

Figure 82. Sandwich Panel Configuration

Component Dimensions						
Component ID	t_{tf} (in)	t_c (in)	H (in)	Unit Weight (lb / ft^2)	Area (ft^2)	Weight (lb)
222	0.077	1.38	1.53	4.10	33.4	136.7
223	0.036	0.63	0.70	1.89	8.5	16.0
224	0.036	0.63	0.70	1.89	7.4	14.1
225	0.015	0.63	0.66	0.95	1.1	1.0
226	0.015	0.63	0.66	0.95	14.2	13.4
227	0.015	0.63	0.66	0.95	10.2	9.7
228	0.015	0.63	0.66	0.95	6.9	6.5
229	0.015	0.63	0.66	0.95	4.2	4.0
230	0.015	0.63	0.66	0.95	2.2	2.1
231	0.118	2.13	2.36	6.30	1.4	8.8
232	0.077	1.38	1.53	4.10	11.7	48.0
233	0.056	1.38	1.49	3.15	12.3	38.6
234	0.036	2.50	2.57	2.66	10.0	26.6
235	0.036	0.63	0.70	1.89	7.7	14.7

236	0.036	0.63	0.70	1.89	5.5	10.4
237	0.015	1.00	1.03	1.10	2.8	3.0
238	0.036	0.63	0.70	1.89	6.1	11.6
239	0.015	0.63	0.66	0.95	9.1	8.6
240	0.036	0.63	0.70	1.89	6.7	12.7
257	0.015	0.63	0.66	0.95	7.6	7.2
258	0.036	0.63	0.70	1.89	7.3	13.8
259	0.015	1.00	1.03	1.10	10.3	11.3
260	0.015	0.63	0.66	0.95	8.9	8.4
261	0.015	0.63	0.66	0.95	7.4	7.0
262	0.015	0.63	0.66	0.95	6.0	5.7
263	0.015	0.63	0.66	0.95	4.1	3.9
266	0.036	1.00	1.07	2.05	8.5	17.3
267	0.036	0.63	0.70	1.89	7.4	14.1
268	0.015	0.63	0.66	0.95	1.1	1.0
269	0.077	2.13	2.28	4.40	11.7	51.6
270	0.056	1.75	1.86	3.30	12.3	40.5
271	0.056	0.63	0.74	2.84	10.0	28.4
272	0.036	0.63	0.70	1.89	7.7	14.7
273	0.036	0.63	0.70	1.89	5.5	10.4
274	0.015	1.00	1.03	1.10	2.8	3.0
275	0.036	0.63	0.70	1.89	6.1	11.6
276	0.015	0.63	0.66	0.95	9.1	8.6
277	0.015	0.63	0.66	0.95	7.6	7.2
278	0.056	1.00	1.11	3.00	7.3	21.8
279	0.015	1.38	1.41	1.25	10.3	12.9
280	0.015	0.63	0.66	0.95	8.9	8.4
281	0.015	0.63	0.66	0.95	7.4	7.0
282	0.015	0.63	0.66	0.95	6.0	5.7
283	0.015	0.63	0.66	0.95	4.1	3.9
705	0.034	3.01	3.08	2.78	11.5	31.9
706	0.034	3.01	3.08	2.78	21.6	59.9
707	0.015	0.63	0.66	0.95	0.9	0.9
708	0.034	3.01	3.08	2.78	26.7	74.1
709	0.034	3.01	3.08	2.78	14.3	39.7
710	0.015	1.22	1.25	1.19	10.4	12.4
711	0.034	3.01	3.08	2.78	9.1	25.3
712	0.034	1.82	1.89	2.29	17.0	38.8
713	0.034	1.82	1.89	2.29	15.8	36.2
714	0.015	3.01	3.04	1.92	0.5	1.0
715	0.015	1.82	1.85	1.44	16.1	23.1
716	0.034	2.42	2.48	2.53	14.9	37.8
717	0.015	0.63	0.66	0.95	1.7	1.6
718	0.015	1.82	1.85	1.44	15.0	21.5
719	0.034	1.22	1.29	2.04	14.0	28.6
720	0.015	0.63	0.66	0.95	1.9	1.8
721	0.034	1.82	1.89	2.29	15.8	36.1
722	0.052	1.22	1.33	2.90	14.9	43.1
723	0.034	0.63	0.69	1.80	2.0	3.6

724	0.071	3.01	3.16	4.48	2.0	8.9
725	0.034	1.82	1.89	2.29	17.4	39.8
726	0.034	2.42	2.48	2.53	16.5	41.9
727	0.034	1.82	1.89	2.29	2.1	4.8
728	0.015	1.22	1.25	1.19	13.3	15.8
729	0.015	1.22	1.25	1.19	12.9	15.4
730	0.015	1.22	1.25	1.19	1.2	1.5
731	0.015	1.22	1.25	1.19	12.8	15.2
732	0.015	1.22	1.25	1.19	13.2	15.8
733	0.034	3.01	3.08	2.78	0.4	1.1
734	0.015	1.22	1.25	1.19	12.8	15.2
735	0.015	1.22	1.25	1.19	13.7	16.3
736	0.034	1.82	1.89	2.29	11.8	26.9
737	0.052	1.22	1.33	2.90	12.6	36.4
738	0.052	2.42	2.52	3.38	44.9	152.0
739	0.052	3.61	3.72	3.87	27.8	107.5
740	0.015	0.63	0.66	0.95	0.5	0.5
741	0.015	2.13	2.16	1.56	3.3	5.2
742	0.015	1.00	1.03	1.10	11.8	13.0
743	0.056	1.00	1.11	3.00	12.7	38.0
744	0.015	0.63	0.66	0.95	2.6	2.4
745	0.036	2.13	2.20	2.51	48.5	121.7
746	0.036	2.50	2.57	2.66	58.1	154.5
747	0.200	4.00	4.40	12.48	5.3	66.0
748	0.015	0.63	0.66	0.95	0.5	0.5
749	0.034	3.01	3.08	2.78	22.6	62.7
750	0.034	3.61	3.68	3.02	22.6	68.2
751	0.034	3.01	3.08	2.78	11.5	31.9
752	0.034	3.61	3.68	3.02	21.6	65.2
753	0.015	0.63	0.66	0.95	0.9	0.9
754	0.034	2.42	2.48	2.53	26.7	67.6
755	0.034	3.01	3.08	2.78	14.3	39.7
756	0.015	1.22	1.25	1.19	10.4	12.4
757	0.034	3.01	3.08	2.78	9.1	25.3
758	0.034	1.82	1.89	2.29	17.0	38.8
759	0.034	1.82	1.89	2.29	15.8	36.2
760	0.034	3.01	3.08	2.78	0.5	1.5
761	0.015	1.82	1.85	1.44	16.1	23.1
762	0.034	2.42	2.48	2.53	14.9	37.8
763	0.034	0.63	0.69	1.80	1.7	3.1
764	0.015	1.82	1.85	1.44	15.0	21.5
765	0.034	1.22	1.29	2.04	14.0	28.6
766	0.015	0.63	0.66	0.95	1.9	1.8
767	0.034	1.82	1.89	2.29	15.8	36.1
768	0.052	1.82	1.92	3.14	14.9	46.7
769	0.034	0.63	0.69	1.80	2.0	3.6
770	0.052	3.01	3.12	3.63	2.0	7.2
771	0.034	1.82	1.89	2.29	17.4	39.8
772	0.034	1.82	1.89	2.29	16.5	37.8

773	0.034	1.22	1.29	2.04	2.1	4.3
774	0.015	1.22	1.25	1.19	13.3	15.8
775	0.015	1.22	1.25	1.19	12.9	15.4
776	0.034	1.22	1.29	2.04	1.2	2.6
777	0.015	1.22	1.25	1.19	12.8	15.2
778	0.015	1.22	1.25	1.19	13.2	15.8
779	0.015	2.42	2.45	1.68	0.4	0.7
780	0.015	1.22	1.25	1.19	12.8	15.2
781	0.015	1.22	1.25	1.19	13.7	16.3
782	0.015	1.82	1.85	1.44	11.8	16.9
783	0.052	1.22	1.33	2.90	12.6	36.4
784	0.052	2.42	2.52	3.38	44.9	152.0
785	0.052	3.61	3.72	3.87	27.8	107.5
786	0.015	0.63	0.66	0.95	0.5	0.5
787	0.036	2.50	2.57	2.66	52.1	138.6
788	0.015	0.63	0.66	0.95	5.3	5.0
789	0.015	0.63	0.66	0.95	5.3	5.0
790	0.036	2.50	2.57	2.66	52.1	138.6
791	0.015	1.00	1.03	1.10	15.5	17.0
792	0.015	1.00	1.03	1.10	13.0	14.3
793	0.015	1.75	1.78	1.41	22.1	31.0
794	0.015	1.75	1.78	1.41	20.9	29.4
795	0.015	0.63	0.66	0.95	1.7	1.6
796	0.015	2.88	2.91	1.87	26.5	49.4
797	0.036	2.13	2.20	2.51	25.2	63.1
798	0.015	1.38	1.41	1.25	6.4	8.1
799	0.015	1.00	1.03	1.10	15.5	17.0
800	0.015	1.00	1.03	1.10	13.0	14.3
801	0.015	1.75	1.78	1.41	22.1	31.0
802	0.015	1.75	1.78	1.41	20.9	29.4
803	0.015	0.63	0.66	0.95	1.7	1.6
804	0.015	2.88	2.91	1.87	26.5	49.4
805	0.036	2.13	2.20	2.51	25.2	63.1
806	0.015	1.38	1.41	1.25	6.4	8.1
807	0.015	0.63	0.66	0.95	10.4	9.8
808	0.015	0.63	0.66	0.95	9.9	9.3
809	0.036	0.63	0.70	1.89	3.4	6.4
810	0.015	1.75	1.78	1.41	17.0	23.9
811	0.015	1.38	1.41	1.25	16.0	20.1
812	0.036	0.63	0.70	1.89	6.2	11.7
813	0.015	1.38	1.41	1.25	16.1	20.2
814	0.015	1.38	1.41	1.25	15.1	18.9
815	0.036	0.63	0.70	1.89	6.2	11.8
816	0.015	1.38	1.41	1.25	15.0	18.8
817	0.015	1.38	1.41	1.25	14.0	17.5
818	0.036	0.63	0.70	1.89	5.8	10.9
819	0.015	1.38	1.41	1.25	15.8	19.8
820	0.015	1.38	1.41	1.25	14.7	18.4
821	0.056	0.63	0.74	2.84	6.0	17.1

822	0.015	0.63	0.66	0.95	10.4	9.8
823	0.015	0.63	0.66	0.95	9.9	9.3
824	0.056	0.63	0.74	2.84	3.4	9.7
825	0.015	1.75	1.78	1.41	17.0	23.9
826	0.015	1.38	1.41	1.25	16.0	20.1
827	0.036	0.63	0.70	1.89	6.2	11.7
828	0.015	1.38	1.41	1.25	16.1	20.2
829	0.015	1.38	1.41	1.25	15.1	18.9
830	0.036	0.63	0.70	1.89	6.2	11.8
831	0.015	1.38	1.41	1.25	15.0	18.8
832	0.015	1.38	1.41	1.25	14.0	17.5
833	0.036	0.63	0.70	1.89	5.8	10.9
834	0.015	1.38	1.41	1.25	15.8	19.8
835	0.015	1.38	1.41	1.25	14.7	18.4
836	0.056	0.63	0.74	2.84	6.0	17.1
837	0.015	1.38	1.41	1.25	15.8	19.8
838	0.036	1.00	1.07	2.05	14.6	29.9
839	0.036	1.38	1.45	2.20	6.0	13.1
840	0.015	2.13	2.16	1.56	17.4	27.2
841	0.015	1.75	1.78	1.41	16.1	22.6
842	0.036	1.00	1.07	2.05	6.5	13.4
843	0.015	1.38	1.41	1.25	13.3	16.7
844	0.015	1.38	1.41	1.25	12.5	15.6
845	0.036	0.63	0.70	1.89	4.7	8.9
846	0.015	1.38	1.41	1.25	12.8	16.0
847	0.015	1.38	1.41	1.25	12.6	15.8
848	0.036	0.63	0.70	1.89	3.9	7.4
849	0.015	1.38	1.41	1.25	12.8	16.1
850	0.015	1.38	1.41	1.25	13.2	16.5
851	0.015	1.38	1.41	1.25	15.8	19.8
852	0.036	1.00	1.07	2.05	14.6	29.9
853	0.015	2.13	2.16	1.56	17.4	27.2
854	0.015	1.75	1.78	1.41	16.1	22.6
855	0.056	0.63	0.74	2.84	6.5	18.6
856	0.015	1.38	1.41	1.25	13.3	16.7
857	0.015	1.38	1.41	1.25	12.5	15.6
858	0.036	0.63	0.70	1.89	4.7	8.9
859	0.015	1.38	1.41	1.25	12.8	16.0
860	0.015	1.38	1.41	1.25	12.6	15.8
861	0.036	0.63	0.70	1.89	3.9	7.4
862	0.015	1.38	1.41	1.25	12.8	16.1
863	0.015	1.38	1.41	1.25	13.2	16.5
864	0.036	0.63	0.70	1.89	3.3	6.3
865	0.015	1.00	1.03	1.10	11.8	13.0
866	0.056	1.00	1.11	3.00	12.7	38.0
867	0.015	0.63	0.66	0.95	2.6	2.4
868	0.036	1.00	1.07	2.05	6.0	12.2
869	0.036	2.13	2.20	2.51	48.5	121.7
870	0.036	2.50	2.57	2.66	58.1	154.5

871	0.200	4.00	4.40	12.48	5.3	66.0
872	0.015	0.63	0.66	0.95	0.5	0.5
873	0.056	3.63	3.74	3.58	103.6	371.0
874	0.036	1.38	1.45	2.02	30.9	62.4
875	0.036	2.13	2.20	2.22	39.6	88.1
876	0.036	0.63	0.70	1.81	16.1	29.1
877	0.036	1.00	1.07	1.91	26.6	51.0
878	0.015	1.00	1.03	0.97	25.5	24.6
879	0.015	1.00	1.03	0.97	23.7	22.9
880	0.036	1.00	1.07	1.91	24.7	47.2
881	0.036	1.00	1.07	1.91	24.2	46.3
882	0.036	1.00	1.07	1.91	25.9	49.5
883	0.015	1.00	1.03	0.97	19.1	18.4
884	0.015	0.63	0.66	0.86	17.8	15.4
885	0.015	0.63	0.66	0.86	17.2	14.8
886	0.036	0.63	0.70	1.81	15.3	27.7
887	0.036	2.50	2.57	2.33	54.2	126.0
888	0.036	0.63	0.70	1.81	5.5	10.0
889	0.036	0.63	0.70	1.81	9.7	17.5
890	0.015	0.63	0.66	0.86	0.4	0.4
891	0.015	1.00	1.03	0.97	16.8	16.2
892	0.036	0.63	0.70	1.81	4.7	8.6
893	0.036	0.63	0.70	1.81	11.2	20.2
894	0.036	1.00	1.07	1.91	24.2	46.3
895	0.036	1.00	1.07	1.91	23.8	45.6
896	0.036	1.00	1.07	1.91	22.5	43.1
897	0.036	1.00	1.07	1.91	23.8	45.5
898	0.036	1.00	1.07	1.91	23.5	45.0
899	0.036	1.00	1.07	1.91	25.3	48.5
900	0.036	0.63	0.70	1.81	18.8	34.0
901	0.015	0.63	0.66	0.86	17.6	15.2
902	0.015	0.63	0.66	0.86	17.0	14.7
903	0.036	0.63	0.70	1.81	15.2	27.5
904	0.077	1.75	1.90	4.01	22.3	89.4
905	0.015	0.63	0.66	0.86	3.3	2.9
906	0.015	0.63	0.66	0.86	14.7	12.7
907	0.015	1.00	1.03	0.97	8.9	8.6
908	0.036	1.00	1.07	1.91	17.7	33.9
909	0.036	1.00	1.07	1.91	19.0	36.4
910	0.036	1.00	1.07	1.91	18.5	35.3
911	0.036	1.00	1.07	1.91	19.7	37.6
912	0.036	1.00	1.07	1.91	19.6	37.6
913	0.036	1.00	1.07	1.91	21.4	41.0
914	0.036	0.63	0.70	1.81	15.8	28.7
915	0.036	0.63	0.70	1.81	14.4	26.1
916	0.015	0.63	0.66	0.86	13.4	11.5
917	0.036	0.63	0.70	1.81	11.1	20.1
918	0.036	1.00	1.07	1.91	24.7	47.2
919	0.036	0.63	0.70	1.81	5.5	10.0

920	0.036	0.63	0.70	1.81	9.7	17.5
921	0.015	0.63	0.66	0.86	0.4	0.4
922	0.015	1.00	1.03	0.97	16.8	16.2
923	0.036	0.63	0.70	1.81	4.7	8.6
924	0.036	0.63	0.70	1.81	11.2	20.2
925	0.036	1.00	1.07	1.91	24.2	46.3
926	0.036	1.00	1.07	1.91	23.8	45.6
927	0.036	1.00	1.07	1.91	22.5	43.1
928	0.036	1.00	1.07	1.91	23.8	45.5
929	0.036	1.00	1.07	1.91	23.5	45.0
930	0.036	1.00	1.07	1.91	25.3	48.5
931	0.015	1.00	1.03	0.97	18.8	18.1
932	0.015	0.63	0.66	0.86	17.6	15.2
933	0.036	0.63	0.70	1.81	15.2	27.5
934	0.077	1.75	1.90	4.01	22.3	89.4
935	0.015	0.63	0.66	0.86	17.0	14.7
936	0.015	0.63	0.66	0.86	3.3	2.9
937	0.015	0.63	0.66	0.86	14.7	12.7
938	0.015	2.50	2.53	1.38	8.9	12.3
939	0.015	2.50	2.53	1.38	17.7	24.4
940	0.036	1.00	1.07	1.91	19.0	36.4
941	0.036	1.00	1.07	1.91	18.5	35.3
942	0.036	1.00	1.07	1.91	19.7	37.6
943	0.056	1.00	1.11	2.86	19.6	56.2
944	0.036	1.00	1.07	1.91	21.4	41.0
945	0.036	0.63	0.70	1.81	15.8	28.7
946	0.036	0.63	0.70	1.81	14.4	26.1
947	0.036	0.63	0.70	1.81	13.4	24.2
948	0.036	0.63	0.70	1.81	11.1	20.1
949	0.036	1.00	1.07	1.91	24.7	47.2
950	0.056	1.38	1.49	3.15	20.4	64.3
951	0.015	1.75	1.78	1.41	4.3	6.1
952	0.036	2.13	2.20	2.51	25.8	64.8
953	0.036	1.38	1.45	2.20	9.4	20.6
954	0.015	0.63	0.66	0.95	0.6	0.6
955	0.036	1.75	1.82	2.35	28.7	67.6
956	0.056	1.00	1.11	3.00	16.6	49.7
957	0.056	0.63	0.74	2.84	2.8	8.0
958	0.036	1.75	1.82	2.35	30.3	71.2
959	0.036	1.38	1.45	2.20	19.7	43.3
960	0.036	1.00	1.07	2.05	3.9	8.0
961	0.015	4.00	4.03	2.33	30.9	71.9
962	0.036	1.38	1.45	2.20	23.4	51.6
963	0.036	0.63	0.70	1.89	5.5	10.4
964	0.015	2.50	2.53	1.71	30.9	53.0
965	0.015	1.75	1.78	1.41	24.9	35.1
966	0.036	0.63	0.70	1.89	6.3	11.9
967	0.015	1.75	1.78	1.41	30.3	42.7
968	0.015	1.75	1.78	1.41	25.4	35.7

969	0.036	0.63	0.70	1.89	6.5	12.3
970	0.036	1.38	1.45	2.20	29.6	65.1
971	0.036	1.38	1.45	2.20	25.4	55.9
972	0.077	3.63	3.78	5.02	6.6	33.3
973	0.036	1.38	1.45	2.20	28.8	63.3
974	0.036	2.50	2.57	2.66	24.7	65.7
975	0.056	1.00	1.11	3.00	6.7	20.1
976	0.015	1.75	1.78	1.41	27.3	38.4
977	0.015	1.38	1.41	1.25	22.2	27.8
978	0.036	2.88	2.95	2.81	6.7	18.9
979	0.015	1.75	1.78	1.41	25.9	36.4
980	0.015	1.38	1.41	1.25	21.0	26.3
981	0.036	0.63	0.70	1.89	5.6	10.6
982	0.015	1.38	1.41	1.25	24.4	30.6
983	0.015	1.38	1.41	1.25	19.7	24.6
984	0.036	1.38	1.45	2.20	4.4	9.7
985	0.015	1.38	1.41	1.25	22.8	28.6
986	0.015	1.38	1.41	1.25	17.9	22.4
987	0.036	0.63	0.70	1.89	3.3	6.3
988	0.077	1.00	1.15	3.94	21.3	84.0
989	0.138	2.88	3.15	7.55	15.9	119.8
990	0.200	4.00	4.40	12.48	2.4	30.5
991	0.056	1.38	1.49	3.15	20.4	64.3
992	0.036	0.63	0.70	1.89	4.3	8.2
993	0.036	3.25	3.32	2.97	25.8	76.7
994	0.036	1.75	1.82	2.35	9.4	22.0
995	0.015	0.63	0.66	0.95	0.6	0.6
996	0.036	2.13	2.20	2.51	28.7	72.0
997	0.056	1.00	1.11	3.00	16.6	49.7
998	0.056	0.63	0.74	2.84	2.8	8.0
999	0.036	1.75	1.82	2.35	30.3	71.2
1000	0.036	1.38	1.45	2.20	19.7	43.3
1001	0.036	0.63	0.70	1.89	3.9	7.4
1002	0.015	3.25	3.28	2.02	30.9	62.5
1003	0.015	2.50	2.53	1.71	23.4	40.2
1004	0.036	0.63	0.70	1.89	5.5	10.4
1005	0.015	2.50	2.53	1.71	30.9	53.0
1006	0.015	1.75	1.78	1.41	24.9	35.1
1007	0.036	0.63	0.70	1.89	6.3	11.9
1008	0.015	1.75	1.78	1.41	30.3	42.7
1009	0.015	1.75	1.78	1.41	25.4	35.7
1010	0.036	0.63	0.70	1.89	6.5	12.3
1011	0.036	1.38	1.45	2.20	29.6	65.1
1012	0.036	1.38	1.45	2.20	25.4	55.9
1013	0.077	2.50	2.65	4.56	6.6	30.2
1014	0.036	1.38	1.45	2.20	28.8	63.3
1015	0.036	2.88	2.95	2.81	24.7	69.5
1016	0.056	1.00	1.11	3.00	6.7	20.1
1017	0.015	1.75	1.78	1.41	27.3	38.4

1018	0.015	1.38	1.41	1.25	22.2	27.8
1019	0.036	3.25	3.32	2.97	6.7	20.0
1020	0.015	1.75	1.78	1.41	25.9	36.4
1021	0.015	1.38	1.41	1.25	21.0	26.3
1022	0.036	0.63	0.70	1.89	5.6	10.6
1023	0.015	1.38	1.41	1.25	24.4	30.6
1024	0.015	1.38	1.41	1.25	19.7	24.6
1025	0.036	0.63	0.70	1.89	4.4	8.4
1026	0.015	1.38	1.41	1.25	22.8	28.6
1027	0.015	1.38	1.41	1.25	17.9	22.4
1028	0.036	0.63	0.70	1.89	3.3	6.3
1029	0.077	1.00	1.15	3.94	21.3	84.0
1030	0.118	2.13	2.36	6.30	15.9	99.9
1031	0.200	4.00	4.40	12.48	2.4	30.5
1032	0.015	0.63	0.66	0.86	1.7	1.4
1033	0.015	0.63	0.66	0.86	5.2	4.5
1034	0.015	0.63	0.66	0.86	2.8	2.5
1035	0.036	1.00	1.07	1.91	5.6	10.8
1036	0.036	1.00	1.07	1.91	13.4	25.7
1037	0.036	1.38	1.45	2.02	1.0	2.0
1038	0.036	1.00	1.07	1.91	8.4	16.0
1039	0.036	1.38	1.45	2.02	16.5	33.2
1040	0.036	1.38	1.45	2.02	16.8	33.8
1041	0.036	1.38	1.45	2.02	16.2	32.8
1042	0.077	2.50	2.65	4.22	17.6	74.1
1043	0.056	2.50	2.61	3.27	17.8	58.4
1044	0.036	2.13	2.20	2.22	19.8	44.0
1045	0.036	1.00	1.07	1.91	15.1	28.8
1046	0.036	1.00	1.07	1.91	14.4	27.5
1047	0.036	1.00	1.07	1.91	14.2	27.1
1048	0.036	1.00	1.07	1.91	12.8	24.5
1049	0.200	2.50	2.90	9.90	34.0	336.8
1050	0.015	0.63	0.66	0.86	1.7	1.4
1051	0.015	0.63	0.66	0.86	5.2	4.5
1052	0.015	0.63	0.66	0.86	2.8	2.5
1053	0.036	1.00	1.07	1.91	5.6	10.8
1054	0.036	1.00	1.07	1.91	13.4	25.7
1055	0.036	1.38	1.45	2.02	1.0	2.0
1056	0.036	0.63	0.70	1.81	8.4	15.1
1057	0.036	1.38	1.45	2.02	16.5	33.2
1058	0.036	1.38	1.45	2.02	16.8	33.8
1059	0.036	1.38	1.45	2.02	16.2	32.8
1060	0.056	1.38	1.49	2.96	17.6	52.0
1061	0.056	2.88	2.99	3.38	17.8	60.2
1062	0.036	1.75	1.82	2.12	19.8	42.0
1063	0.036	1.00	1.07	1.91	15.1	28.8
1064	0.036	1.00	1.07	1.91	14.4	27.5
1065	0.036	1.00	1.07	1.91	14.2	27.1
1066	0.036	1.00	1.07	1.91	12.8	24.5

1067	0.200	4.00	4.40	12.48	34.0	424.5
1069	0.056	1.00	1.11	2.86	13.2	37.7
1071	0.056	1.75	1.86	3.07	21.6	66.2
1072	0.036	0.63	0.70	1.81	5.8	10.5
1074	0.036	1.75	1.82	2.12	19.2	40.6
1075	0.036	1.00	1.07	1.91	12.4	23.8
1077	0.036	0.63	0.70	1.81	5.5	10.0
1078	0.036	1.75	1.82	2.12	19.2	40.7
1079	0.036	1.75	1.82	2.12	17.6	37.4
1081	0.036	0.63	0.70	1.81	7.2	13.1
1082	0.036	1.75	1.82	2.12	19.3	40.9
1083	0.056	2.13	2.24	3.17	20.7	65.5
1085	0.015	0.63	0.66	0.86	6.6	5.7
1086	0.200	4.00	4.40	12.48	4.7	59.2
1087	0.118	3.63	3.86	6.42	17.7	113.9
1089	0.036	1.00	1.07	1.91	13.2	25.2
1091	0.056	1.75	1.86	3.07	21.6	66.2
1092	0.036	0.63	0.70	1.81	5.8	10.5
1094	0.036	1.75	1.82	2.12	19.2	40.6
1095	0.036	1.00	1.07	1.91	12.4	23.8
1097	0.036	0.63	0.70	1.81	5.5	10.0
1098	0.036	1.75	1.82	2.12	19.2	40.7
1099	0.036	1.75	1.82	2.12	17.6	37.4
1101	0.036	0.63	0.70	1.81	7.2	13.1
1102	0.036	1.75	1.82	2.12	19.3	40.9
1103	0.077	2.13	2.28	4.12	20.7	85.0
1105	0.036	0.63	0.70	1.81	6.6	11.9
1106	0.200	4.00	4.40	12.48	4.7	59.2
1107	0.138	1.75	2.03	6.86	17.7	121.5
1109	0.036	1.38	1.45	2.02	13.1	26.5
1111	0.036	2.50	2.57	2.33	21.7	50.5
1112	0.015	1.00	1.03	0.97	5.6	5.4
1114	0.036	2.50	2.57	2.33	19.3	45.0
1115	0.036	1.38	1.45	2.02	12.2	24.7
1117	0.056	0.63	0.74	2.76	4.1	11.4
1118	0.036	2.50	2.57	2.33	19.4	45.1
1119	0.036	2.50	2.57	2.33	17.5	40.6
1121	0.036	1.00	1.07	1.91	6.5	12.5
1122	0.036	2.50	2.57	2.33	19.4	45.1
1123	0.036	2.88	2.95	2.43	20.5	49.9
1125	0.015	0.63	0.66	0.86	6.5	5.6
1126	0.077	1.00	1.15	3.81	4.7	18.1
1127	0.056	1.75	1.86	3.07	7.4	22.6
1129	0.036	1.38	1.45	2.02	13.1	26.5
1131	0.036	2.50	2.57	2.33	21.7	50.5
1132	0.036	0.63	0.70	1.81	5.6	10.2
1134	0.036	2.50	2.57	2.33	19.3	45.0
1135	0.036	1.38	1.45	2.02	12.2	24.7
1137	0.036	0.63	0.70	1.81	4.1	7.5

1138	0.036	2.50	2.57	2.33	19.4	45.1
1139	0.036	2.50	2.57	2.33	17.5	40.6
1141	0.056	0.63	0.74	2.76	6.5	18.0
1142	0.036	2.50	2.57	2.33	19.4	45.1
1143	0.036	2.88	2.95	2.43	20.5	49.9
1145	0.200	4.00	4.40	12.48	6.5	80.6
1146	0.077	2.13	2.28	4.12	4.7	19.5
1147	0.056	1.75	1.86	3.07	7.4	22.6
1148	0.056	1.00	1.11	3.40	7.6	25.8
1149	0.015	0.63	0.66	1.20	14.1	16.9
1150	0.015	0.63	0.66	1.20	9.5	11.5
1151	0.015	0.63	0.66	1.20	14.6	17.6
1152	0.015	0.63	0.66	1.20	9.3	11.2
1153	0.015	0.63	0.66	1.20	7.8	9.3
1154	0.015	0.63	0.66	1.20	11.5	13.8
1155	0.015	0.63	0.66	1.20	8.8	10.6
1156	0.015	0.63	0.66	1.20	6.2	7.4
1157	0.036	0.63	0.70	2.15	9.6	20.6
1158	0.015	0.63	0.66	1.20	8.2	9.9
1159	0.015	0.63	0.66	1.20	5.8	7.0
1160	0.036	0.63	0.70	2.15	6.4	13.8
1161	0.015	0.63	0.66	1.20	6.0	7.2
1162	0.036	0.63	0.70	2.15	4.7	10.2
1163	0.015	0.63	0.66	1.20	1.9	2.3
1164	0.056	1.00	1.11	3.40	7.6	25.8
1165	0.015	0.63	0.66	1.20	14.1	16.9
1166	0.015	0.63	0.66	1.20	9.5	11.5
1167	0.015	0.63	0.66	1.20	14.6	17.6
1168	0.015	0.63	0.66	1.20	9.3	11.2
1169	0.015	0.63	0.66	1.20	7.8	9.3
1170	0.015	0.63	0.66	1.20	11.5	13.8
1171	0.015	0.63	0.66	1.20	8.8	10.6
1172	0.015	0.63	0.66	1.20	6.2	7.4
1173	0.015	0.63	0.66	1.20	9.6	11.5
1174	0.015	0.63	0.66	1.20	8.2	9.9
1175	0.015	0.63	0.66	1.20	5.8	7.0
1176	0.036	0.63	0.70	2.15	6.4	13.8
1177	0.015	0.63	0.66	1.20	6.0	7.2
1178	0.036	0.63	0.70	2.15	4.7	10.2
1179	0.036	0.63	0.70	2.15	1.9	4.1
1180	0.015	0.63	0.66	1.20	0.6	0.7
1182	0.015	0.63	0.66	1.20	5.1	6.1
1184	0.015	0.63	0.66	1.20	6.7	8.0
1185	0.015	0.63	0.66	1.20	2.3	2.8
1187	0.056	2.88	2.99	4.93	1.4	6.8
1188	0.015	0.63	0.66	1.20	6.5	7.8
1189	0.015	0.63	0.66	1.20	3.9	4.7
1191	0.077	1.75	1.90	4.96	1.6	8.1
1192	0.036	0.63	0.70	2.15	5.2	11.1

1193	0.015	0.63	0.66	1.20	4.4	5.3
1195	0.015	0.63	0.66	1.20	1.2	1.4
1196	0.015	0.63	0.66	1.20	2.9	3.4
1197	0.015	0.63	0.66	1.20	2.9	3.5
1199	0.015	0.63	0.66	1.20	0.6	0.7
1201	0.015	0.63	0.66	1.20	5.1	6.1
1203	0.015	0.63	0.66	1.20	6.7	8.0
1204	0.015	0.63	0.66	1.20	2.3	2.8
1206	0.056	1.75	1.86	4.01	1.4	5.5
1207	0.015	0.63	0.66	1.20	6.5	7.8
1208	0.015	0.63	0.66	1.20	3.9	4.7
1210	0.077	1.00	1.15	4.35	1.6	7.1
1211	0.036	0.63	0.70	2.15	5.2	11.1
1212	0.015	0.63	0.66	1.20	4.4	5.3
1214	0.015	0.63	0.66	1.20	1.2	1.4
1215	0.015	0.63	0.66	1.20	2.9	3.4
1216	0.015	0.63	0.66	1.20	2.9	3.5
1218	0.015	0.63	0.66	0.95	6.6	6.3
1219	0.015	0.63	0.66	0.95	5.2	4.9
1220	0.015	0.63	0.66	0.95	3.9	3.7
1221	0.015	0.63	0.66	0.95	2.8	2.6
1222	0.015	0.63	0.66	0.95	1.9	1.8
1223	0.015	0.63	0.66	0.95	1.1	1.0
1224	0.015	1.00	1.03	1.10	0.8	0.9
1225	0.036	0.63	0.70	1.89	12.4	23.4
1226	0.036	0.63	0.70	1.89	35.0	66.4
1227	0.015	0.63	0.66	0.95	32.3	30.6
1228	0.015	0.63	0.66	0.95	28.6	27.1
1229	0.015	0.63	0.66	0.95	24.9	23.6
1230	0.015	0.63	0.66	0.95	21.2	20.1
1231	0.015	0.63	0.66	0.95	8.9	8.4
1232	0.077	3.25	3.40	4.86	3.1	15.3
1233	0.015	0.63	0.66	0.95	3.0	2.9
1234	0.056	1.38	1.49	3.15	2.9	9.2
1235	0.015	0.63	0.66	0.95	2.8	2.7
1236	0.036	1.00	1.07	2.05	2.7	5.6
1237	0.015	0.63	0.66	0.95	2.3	2.2
1238	0.036	0.63	0.70	1.89	28.1	53.3
1239	0.015	1.00	1.03	1.10	28.0	30.8
1240	0.015	1.00	1.03	1.10	28.0	30.8
1241	0.015	1.00	1.03	1.10	28.0	30.8
1242	0.015	1.00	1.03	1.10	27.9	30.7
1243	0.015	0.63	0.66	0.95	22.8	21.6
1244	0.015	0.63	0.66	0.95	12.3	11.6
1245	0.036	3.08	3.15	2.90	78.3	227.0
1246	0.036	3.90	3.97	3.23	78.3	253.3
1247	0.015	0.63	0.66	0.95	0.7	0.7
1248	0.015	0.63	0.66	0.95	0.7	0.7
1249	0.036	3.08	3.15	2.90	67.8	196.5

1250	0.036	2.26	2.34	2.56	67.8	173.8
1251	0.036	2.26	2.34	2.56	26.1	66.8
1252	0.015	0.63	0.66	0.95	9.3	8.8
1253	0.036	2.26	2.34	2.56	26.1	66.8
1254	0.015	0.63	0.66	0.95	9.3	8.8
1255	0.015	0.63	0.66	0.95	3.4	3.2
1256	0.015	0.63	0.66	0.95	3.4	3.2
1257	0.056	0.63	0.74	2.84	11.3	32.0
1258	0.036	1.44	1.52	2.23	11.3	25.1
1259	0.036	2.26	2.34	2.56	32.0	82.2
1260	0.036	2.26	2.34	2.56	25.4	65.1
1261	0.036	1.44	1.52	2.23	8.3	18.4
1262	0.036	1.44	1.52	2.23	10.9	24.2
1263	0.036	1.44	1.52	2.23	10.9	24.2
1264	0.036	1.44	1.52	2.23	8.3	18.4
1265	0.036	2.26	2.34	2.56	25.4	65.1
1266	0.036	2.26	2.34	2.56	32.0	82.2
1267	0.015	0.63	0.66	0.95	1.2	1.1
1268	0.056	1.00	1.11	3.00	15.0	45.0
1269	0.015	3.25	3.28	2.02	1.2	2.4
1270	0.056	1.00	1.11	3.00	15.0	45.0

Appendix AA – Hypersizer Controlling Loads Case and Panel Failure Modes

Component Panel Weight Summary

Group / Component	Lowest MS	Controlling Load Case	Controlling Failure Mode
1 Group 1 Fuselage Lower Skin"			
705 "FUSE_LOWER_RHS.002"	0.033	9	Shear Strength, Y (Transverse) direction {Hexcel}
706 "FUSE_LOWER_RHS.003"	0.022	9	Shear Strength, X (Longitudinal) direction {Hexcel}
707 "FUSE_LOWER_RHS.004"	1.558	9	Sandwich Flatwise Tension w/ Interlaminar Shear Interaction
708 "FUSE_LOWER_RHS.005"	0.198	9	Shear Strength, Y (Transverse) direction {Hexcel}
709 "FUSE_LOWER_RHS.006"	0.065	9	Shear Strength, Y (Transverse) direction {Hexcel}
710 "FUSE_LOWER_RHS.007"	0.315	9	Isotropic Strength, Von Mises Interaction Yield Criterion
711 "FUSE_LOWER_RHS.008"	0.164	9	Wrinkling, Eqn 2, Honeycomb Core, X, Y & Interaction
712 "FUSE_LOWER_RHS.009"	0.167	9	Frequency Limit, Panel or Beam
713 "FUSE_LOWER_RHS.010"	0.090	9	Shear Strength, Y (Transverse) direction {Hexcel}
714 "FUSE_LOWER_RHS.011"	0.030	9	Wrinkling, Eqn 2, Honeycomb Core, X, Y & Interaction
715 "FUSE_LOWER_RHS.012"	0.052	9	Frequency Limit, Panel or Beam
716 "FUSE_LOWER_RHS.013"	0.056	9	Shear Strength, Y (Transverse) direction {Hexcel}
717 "FUSE_LOWER_RHS.014"	0.136	9	Sandwich Flatwise Tension w/ Interlaminar Shear Interaction
718 "FUSE_LOWER_RHS.015"	0.165	9	Frequency Limit, Panel or Beam
719 "FUSE_LOWER_RHS.016"	0.042	9	Frequency Limit, Panel or Beam
720 "FUSE_LOWER_RHS.017"	0.082	9	Isotropic Strength, Von Mises Interaction Yield Criterion
721 "FUSE_LOWER_RHS.018"	0.269	9	Isotropic Strength, Von Mises Interaction Yield Criterion
722 "FUSE_LOWER_RHS.019"	0.036	9	Frequency Limit, Panel or Beam
723 "FUSE_LOWER_RHS.020"	0.041	9	Shear Strength, Y (Transverse) direction {Hexcel}
724 "FUSE_LOWER_RHS.023"	0.061	9	Isotropic Strength, Von Mises Interaction Yield Criterion
725 "FUSE_LOWER_RHS.024"	0.135	9	Frequency Limit, Panel or Beam
726 "FUSE_LOWER_RHS.025"	0.024	9	Shear Strength, Y (Transverse) direction {Hexcel}
727 "FUSE_LOWER_RHS.026"	0.005	9	Shear Strength, Y (Transverse) direction {Hexcel}
728 "FUSE_LOWER_RHS.027"	0.023	9	Frequency Limit, Panel or Beam
729 "FUSE_LOWER_RHS.028"	0.035	9	Frequency Limit, Panel or Beam
730 "FUSE_LOWER_RHS.029"	0.322	9	Shear Strength, Y (Transverse) direction {Hexcel}
731 "FUSE_LOWER_RHS.030"	0.087	9	Frequency Limit, Panel or Beam
732 "FUSE_LOWER_RHS.031"	0.060	9	Frequency Limit, Panel or Beam
733 "FUSE_LOWER_RHS.032"	0.078	9	Shear Strength, X (Longitudinal) direction {Hexcel}
734 "FUSE_LOWER_RHS.033"	0.089	9	Frequency Limit, Panel or Beam
735 "FUSE_LOWER_RHS.034"	0.052	9	Frequency Limit, Panel or Beam
736 "FUSE_LOWER_LHS.035"	0.032	9	Isotropic Strength, Von Mises Interaction Yield Criterion
737 "FUSE_LOWER_LHS.036"	0.387	9	Isotropic Strength, Von Mises Interaction Yield Criterion
738 "FUSE_LOWER_RHS.037"	0.228	9	Frequency Limit, Panel or Beam
739 "FUSE_LOWER_RHS.038"	0.017	9	Isotropic Strength, Von Mises Interaction Yield Criterion
740 "FUSE_LOWER_LHS.039"	0.587	9	Isotropic Strength, Von Mises Interaction Yield Criterion
749 "FUSE_LOWER_RHS.001"	0.147	9	Shear Strength, Y (Transverse) direction {Hexcel}
750 "FUSE_LOWER_LHS.001"	0.069	9	Shear Strength, Y (Transverse) direction {Hexcel}
751 "FUSE_LOWER_LHS.002"	0.051	9	Shear Strength, X (Longitudinal) direction {Hexcel}
752 "FUSE_LOWER_LHS.003"	0.038	9	Wrinkling, Eqn 2, Honeycomb Core, X, Y & Interaction
753 "FUSE_LOWER_LHS.004"	2.361	9	Isotropic Strength, Von Mises Interaction Yield Criterion
754 "FUSE_LOWER_LHS.005"	0.063	9	Frequency Limit, Panel or Beam

755	"FUSE_LOWER_LHS.006"	0.049	9	Shear Strength, Y (Transverse) direction {Hexcel}
756	"FUSE_LOWER_LHS.007"	0.376	9	Isotropic Strength, Von Mises Interaction Yield Criterion
757	"FUSE_LOWER_LHS.008"	0.169	9	Wrinkling, Eqn 2, Honeycomb Core, X, Y & Interaction
758	"FUSE_LOWER_LHS.009"	0.164	9	Frequency Limit, Panel or Beam
759	"FUSE_LOWER_LHS.010"	0.054	9	Shear Strength, Y (Transverse) direction {Hexcel}
760	"FUSE_LOWER_LHS.011"	0.038	9	Shear Strength, X (Longitudinal) direction {Hexcel}
761	"FUSE_LOWER_LHS.012"	0.049	9	Frequency Limit, Panel or Beam
762	"FUSE_LOWER_LHS.013"	0.072	9	Shear Strength, Y (Transverse) direction {Hexcel}
763	"FUSE_LOWER_LHS.014"	0.217	9	Sandwich Flatwise Tension w/ Interlaminar Shear Interaction
764	"FUSE_LOWER_LHS.015"	0.162	9	Frequency Limit, Panel or Beam
765	"FUSE_LOWER_LHS.016"	0.041	9	Frequency Limit, Panel or Beam
766	"FUSE_LOWER_LHS.017"	0.163	9	Sandwich Flatwise Tension w/ Interlaminar Shear Interaction
767	"FUSE_LOWER_LHS.018"	0.244	9	Isotropic Strength, Von Mises Interaction Yield Criterion
768	"FUSE_LOWER_LHS.019"	0.028	9	Isotropic Strength, Von Mises Interaction Yield Criterion
769	"FUSE_LOWER_LHS.020"	0.175	9	Shear Strength, Y (Transverse) direction {Hexcel}
770	"FUSE_LOWER_LHS.023"	0.011	9	Isotropic Strength, Von Mises Interaction Yield Criterion
771	"FUSE_LOWER_LHS.024"	0.135	9	Frequency Limit, Panel or Beam
772	"FUSE_LOWER_LHS.025"	0.007	9	Shear Strength, Y (Transverse) direction {Hexcel}
773	"FUSE_LOWER_LHS.026"	0.083	9	Sandwich Flatwise Tension w/ Interlaminar Shear Interaction
774	"FUSE_LOWER_LHS.027"	0.023	9	Frequency Limit, Panel or Beam
775	"FUSE_LOWER_LHS.028"	0.031	9	Frequency Limit, Panel or Beam
776	"FUSE_LOWER_LHS.029"	0.316	9	Shear Strength, Y (Transverse) direction {Hexcel}
777	"FUSE_LOWER_LHS.030"	0.087	9	Frequency Limit, Panel or Beam
778	"FUSE_LOWER_LHS.031"	0.059	9	Frequency Limit, Panel or Beam
779	"FUSE_LOWER_LHS.032"	0.021	9	Shear Strength, X (Longitudinal) direction {Hexcel}
780	"FUSE_LOWER_LHS.033"	0.088	9	Frequency Limit, Panel or Beam
781	"FUSE_LOWER_LHS.034"	0.052	9	Frequency Limit, Panel or Beam
782	"FUSE_LOWER_RHS.035"	0.049	9	Isotropic Strength, Von Mises Interaction Yield Criterion
783	"FUSE_LOWER_RHS.036"	0.409	9	Isotropic Strength, Von Mises Interaction Yield Criterion
784	"FUSE_LOWER_LHS.037"	0.230	9	Frequency Limit, Panel or Beam
785	"FUSE_LOWER_LHS.038"	0.008	9	Isotropic Strength, Von Mises Interaction Yield Criterion
786	"FUSE_LOWER_RHS.039"	0.025	9	Isotropic Strength, Von Mises Interaction Yield Criterion
2	**Group 2 Fuselage Upper Skin**			
741	"FUSE_UPPER_RHS.040"	0.009	9	Isotropic Strength, Von Mises Interaction Yield Criterion
742	"FUSE_UPPER_RHS.041"	0.085	9	Frequency Limit, Panel or Beam
743	"FUSE_UPPER_RHS.042"	0.085	9	Isotropic Strength, Von Mises Interaction Yield Criterion
744	"FUSE_UPPER_RHS.043"	0.394	9	Isotropic Strength, Von Mises Interaction Yield Criterion
745	"FUSE_UPPER_LHS.044"	0.074	9	Frequency Limit, Panel or Beam
746	"FUSE_UPPER_LHS.045"	0.115	9	Frequency Limit, Panel or Beam
747	"FUSE_UPPER_LHS.046"	-0.180	9	Isotropic Strength, Longitudinal Direction
748	"FUSE_UPPER_RHS.047"	1.375	9	Isotropic Strength, Transverse Direction
787	"FUSE_UPPER_RHS.001"	0.090	9	Frequency Limit, Panel or Beam
788	"FUSE_UPPER_RHS.002"	0.422	9	Frequency Limit, Panel or Beam
789	"FUSE_UPPER_LHS.002"	0.419	9	Frequency Limit, Panel or Beam
790	"FUSE_UPPER_LHS.001"	0.061	9	Frequency Limit, Panel or Beam
791	"FUSE_UPPER_RHS.003"	0.117	9	Frequency Limit, Panel or Beam
792	"FUSE_UPPER_RHS.004"	0.270	9	Frequency Limit, Panel or Beam
793	"FUSE_UPPER_RHS.005"	0.100	9	Frequency Limit, Panel or Beam

794 "FUSE_UPPER_RHS.006"	0.164	9	Frequency Limit, Panel or Beam
795 "FUSE_UPPER_RHS.007"	0.431	9	Isotropic Strength, Von Mises Interaction Yield Criterion
796 "FUSE_UPPER_RHS.008"	0.050	9	Frequency Limit, Panel or Beam
797 "FUSE_UPPER_RHS.009"	0.114	9	Frequency Limit, Panel or Beam
798 "FUSE_UPPER_RHS.010"	0.030	9	Isotropic Strength, Von Mises Interaction Yield Criterion
799 "FUSE_UPPER_LHS.003"	0.116	9	Frequency Limit, Panel or Beam
800 "FUSE_UPPER_LHS.004"	0.267	9	Frequency Limit, Panel or Beam
801 "FUSE_UPPER_LHS.005"	0.100	9	Frequency Limit, Panel or Beam
802 "FUSE_UPPER_LHS.006"	0.164	9	Frequency Limit, Panel or Beam
803 "FUSE_UPPER_LHS.007"	0.607	9	Isotropic Strength, Von Mises Interaction Yield Criterion
804 "FUSE_UPPER_LHS.008"	0.053	9	Frequency Limit, Panel or Beam
805 "FUSE_UPPER_LHS.009"	0.113	9	Frequency Limit, Panel or Beam
806 "FUSE_UPPER_LHS.010"	0.031	9	Isotropic Strength, Von Mises Interaction Yield Criterion
807 "FUSE_UPPER_RHS.011"	0.097	9	Frequency Limit, Panel or Beam
808 "FUSE_UPPER_RHS.012"	0.116	9	Frequency Limit, Panel or Beam
809 "FUSE_UPPER_RHS.013"	0.089	9	Isotropic Strength, Von Mises Interaction Yield Criterion
810 "FUSE_UPPER_RHS.014"	0.197	9	Frequency Limit, Panel or Beam
811 "FUSE_UPPER_RHS.015"	0.041	9	Frequency Limit, Panel or Beam
812 "FUSE_UPPER_RHS.016"	0.614	9	Isotropic Strength, Von Mises Interaction Yield Criterion
813 "FUSE_UPPER_RHS.017"	0.068	9	Frequency Limit, Panel or Beam
814 "FUSE_UPPER_RHS.018"	0.117	9	Frequency Limit, Panel or Beam
815 "FUSE_UPPER_RHS.019"	0.628	9	Isotropic Strength, Von Mises Interaction Yield Criterion
816 "FUSE_UPPER_RHS.020"	0.176	9	Frequency Limit, Panel or Beam
817 "FUSE_UPPER_RHS.021"	0.231	9	Frequency Limit, Panel or Beam
818 "FUSE_UPPER_RHS.022"	0.079	9	Isotropic Strength, Von Mises Interaction Yield Criterion
819 "FUSE_UPPER_RHS.023"	0.095	9	Frequency Limit, Panel or Beam
820 "FUSE_UPPER_RHS.024"	0.153	9	Frequency Limit, Panel or Beam
821 "FUSE_UPPER_RHS.025"	0.345	9	Isotropic Strength, Von Mises Interaction Yield Criterion
822 "FUSE_UPPER_LHS.011"	0.097	9	Frequency Limit, Panel or Beam
823 "FUSE_UPPER_LHS.012"	0.116	9	Frequency Limit, Panel or Beam
824 "FUSE_UPPER_LHS.013"	0.280	9	Isotropic Strength, Von Mises Interaction Yield Criterion
825 "FUSE_UPPER_LHS.014"	0.197	9	Frequency Limit, Panel or Beam
826 "FUSE_UPPER_LHS.015"	0.041	9	Frequency Limit, Panel or Beam
827 "FUSE_UPPER_LHS.016"	0.204	9	Isotropic Strength, Von Mises Interaction Yield Criterion
828 "FUSE_UPPER_LHS.017"	0.068	9	Frequency Limit, Panel or Beam
829 "FUSE_UPPER_LHS.018"	0.118	9	Frequency Limit, Panel or Beam
830 "FUSE_UPPER_LHS.019"	0.367	9	Isotropic Strength, Von Mises Interaction Yield Criterion
831 "FUSE_UPPER_LHS.020"	0.176	9	Frequency Limit, Panel or Beam
832 "FUSE_UPPER_LHS.021"	0.231	9	Frequency Limit, Panel or Beam
833 "FUSE_UPPER_LHS.022"	0.374	9	Isotropic Strength, Von Mises Interaction Yield Criterion
834 "FUSE_UPPER_LHS.023"	0.095	9	Frequency Limit, Panel or Beam
835 "FUSE_UPPER_LHS.024"	0.153	9	Frequency Limit, Panel or Beam
836 "FUSE_UPPER_LHS.025"	0.075	9	Isotropic Strength, Von Mises Interaction Yield Criterion
837 "FUSE_UPPER_RHS.026"	0.095	9	Frequency Limit, Panel or Beam
838 "FUSE_UPPER_RHS.027"	0.038	9	Frequency Limit, Panel or Beam
839 "FUSE_UPPER_RHS.028"	0.040	9	Isotropic Strength, Von Mises Interaction Yield Criterion
840 "FUSE_UPPER_RHS.029"	0.107	9	Frequency Limit, Panel or Beam
841 "FUSE_UPPER_RHS.030"	0.026	9	Frequency Limit, Panel or Beam
842 "FUSE_UPPER_RHS.031"	0.036	9	Isotropic Strength, Von Mises Interaction Yield Criterion

843 "FUSE_UPPER_RHS.032"	0.164	9	Frequency Limit, Panel or Beam
844 "FUSE_UPPER_RHS.033"	0.212	9	Frequency Limit, Panel or Beam
845 "FUSE_UPPER_RHS.034"	0.034	9	Isotropic Strength, Von Mises Interaction Yield Criterion
846 "FUSE_UPPER_RHS.035"	0.231	9	Frequency Limit, Panel or Beam
847 "FUSE_UPPER_RHS.036"	0.247	9	Frequency Limit, Panel or Beam
848 "FUSE_UPPER_RHS.037"	0.697	9	Isotropic Strength, Von Mises Interaction Yield Criterion
849 "FUSE_UPPER_RHS.038"	0.231	9	Frequency Limit, Panel or Beam
850 "FUSE_UPPER_RHS.039"	0.220	9	Frequency Limit, Panel or Beam
851 "FUSE_UPPER_LHS.026"	0.095	9	Frequency Limit, Panel or Beam
852 "FUSE_UPPER_LHS.027"	0.038	9	Frequency Limit, Panel or Beam
853 "FUSE_UPPER_LHS.029"	0.107	9	Frequency Limit, Panel or Beam
854 "FUSE_UPPER_LHS.030"	0.026	9	Frequency Limit, Panel or Beam
855 "FUSE_UPPER_LHS.031"	0.387	9	Isotropic Strength, Von Mises Interaction Yield Criterion
856 "FUSE_UPPER_LHS.032"	0.164	9	Frequency Limit, Panel or Beam
857 "FUSE_UPPER_LHS.033"	0.212	9	Frequency Limit, Panel or Beam
858 "FUSE_UPPER_LHS.034"	0.095	9	Isotropic Strength, Von Mises Interaction Yield Criterion
859 "FUSE_UPPER_LHS.035"	0.231	9	Frequency Limit, Panel or Beam
860 "FUSE_UPPER_LHS.036"	0.247	9	Frequency Limit, Panel or Beam
861 "FUSE_UPPER_LHS.037"	0.278	9	Isotropic Strength, Von Mises Interaction Yield Criterion
862 "FUSE_UPPER_LHS.038"	0.231	9	Frequency Limit, Panel or Beam
863 "FUSE_UPPER_LHS.039"	0.220	9	Frequency Limit, Panel or Beam
864 "FUSE_UPPER_LHS.040"	0.891	9	Isotropic Strength, Von Mises Interaction Yield Criterion
865 "FUSE_UPPER_LHS.041"	0.085	9	Frequency Limit, Panel or Beam
866 "FUSE_UPPER_LHS.042"	0.162	9	Isotropic Strength, Von Mises Interaction Yield Criterion
867 "FUSE_UPPER_LHS.043"	0.047	9	Isotropic Strength, Von Mises Interaction Yield Criterion
868 "FUSE_UPPER_LHS.028"	0.027	9	Isotropic Strength, Von Mises Interaction Yield Criterion
869 "FUSE_UPPER_RHS.044"	0.074	9	Frequency Limit, Panel or Beam
870 "FUSE_UPPER_RHS.045"	0.115	9	Frequency Limit, Panel or Beam
871 "FUSE_UPPER_RHS.046"	-0.130	9	Isotropic Strength, Longitudinal Direction
872 "FUSE_UPPER_LHS.047"	1.160	9	Isotropic Strength, Von Mises Interaction Yield Criterion
5 "Group 5" Bulkhead			
950 "BULKHEAD_RHS.001"	0.208	9	Isotropic Strength, Von Mises Interaction Yield Criterion
951 "BULKHEAD_RHS.002"	0.004	9	Isotropic Strength, Transverse Direction
952 "Component 952"	0.003	9	Isotropic Strength, Von Mises Interaction Yield Criterion
953 "Component 953"	0.004	9	Isotropic Strength, Transverse Direction
954 "Component 954"	0.030	9	Isotropic Strength, Von Mises Interaction Yield Criterion
955 "Component 955"	0.003	9	Isotropic Strength, Transverse Direction
956 "BULKHEAD_RHS.007"	0.004	9	Frequency Limit, Panel or Beam
957 "BULKHEAD_RHS.008"	0.189	9	Isotropic Strength, Von Mises Interaction Yield Criterion
958 "Component 958"	0.123	9	Frequency Limit, Panel or Beam
959 "Component 959"	0.182	9	Frequency Limit, Panel or Beam
960 "Component 960"	0.084	9	Isotropic Strength, Von Mises Interaction Yield Criterion
961 "Component 961"	0.005	9	Wrinkling, Eqn 2, Honeycomb Core, X, Y & Interaction
962 "Component 962"	0.133	9	Frequency Limit, Panel or Beam
963 "Component 963"	0.281	9	Isotropic Strength, Von Mises Interaction Yield Criterion
964 "Component 964"	0.003	9	Wrinkling, Eqn 2, Honeycomb Core, X, Y & Interaction
965 "BULKHEAD_RHS.016"	0.142	9	Wrinkling, Eqn 2, Honeycomb Core, X, Y & Interaction
966 "BULKHEAD_RHS.017"	0.065	9	Isotropic Strength, Von Mises Interaction Yield Criterion

967 "Component 967"	0.013	9	Frequency Limit, Panel or Beam
968 "Component 968"	0.164	9	Isotropic Strength, Von Mises Interaction Yield Criterion
969 "Component 969"	0.180	9	Isotropic Strength, Von Mises Interaction Yield Criterion
970 "Component 970"	0.037	9	Frequency Limit, Panel or Beam
971 "BULKHEAD_RHS.022"	0.176	9	Frequency Limit, Panel or Beam
972 "BULKHEAD_RHS.023"	0.086	11	Shear Strength, Y (Transverse) direction {Hexcel}
973 "Component 973"	0.062	9	Frequency Limit, Panel or Beam
974 "BULKHEAD_RHS.025"	0.030	10	Isotropic Strength, Von Mises Interaction Yield Criterion
975 "BULKHEAD_RHS.026"	0.060	9	Isotropic Strength, Von Mises Interaction Yield Criterion
976 "Component 976"	0.125	9	Frequency Limit, Panel or Beam
977 "BULKHEAD_RHS.028"	0.061	9	Wrinkling, Eqn 2, Honeycomb Core, X, Y & Interaction
978 "BULKHEAD_RHS.029"	0.001	9	Isotropic Strength, Von Mises Interaction Yield Criterion
979 "Component 979"	0.183	9	Frequency Limit, Panel or Beam
980 "BULKHEAD_RHS.031"	0.074	9	Isotropic Strength, Von Mises Interaction Yield Criterion
981 "BULKHEAD_RHS.032"	0.256	9	Isotropic Strength, Von Mises Interaction Yield Criterion
982 "Component 982"	0.046	9	Frequency Limit, Panel or Beam
983 "BULKHEAD_RHS.034"	0.108	9	Frequency Limit, Panel or Beam
984 "BULKHEAD_RHS.035"	0.017	9	Isotropic Strength, Von Mises Interaction Yield Criterion
985 "Component 985"	0.075	9	Isotropic Strength, Transverse Direction
986 "BULKHEAD_RHS.037"	0.166	9	Frequency Limit, Panel or Beam
987 "BULKHEAD_RHS.038"	0.409	9	Isotropic Strength, Von Mises Interaction Yield Criterion
988 "Component 988"	0.070	9	Isotropic Strength, Von Mises Interaction Yield Criterion
989 "BULKHEAD_RHS.040"	0.000	9	Isotropic Strength, Von Mises Interaction Yield Criterion
990 "BULKHEAD_RHS.041"	-0.211	9	Isotropic Strength, Von Mises Interaction Yield Criterion
991 "BULKHEAD_LHS.001"	0.212	9	Isotropic Strength, Von Mises Interaction Yield Criterion
992 "BULKHEAD_LHS.002"	0.984	9	Isotropic Strength, Von Mises Interaction Yield Criterion
993 "Component 993"	0.000	9	Isotropic Strength, Von Mises Interaction Yield Criterion
994 "Component 994"	0.011	9	Isotropic Strength, Von Mises Interaction Yield Criterion
995 "Component 995"	0.185	9	Isotropic Strength, Von Mises Interaction Yield Criterion
996 "Component 996"	0.002	9	Isotropic Strength, Transverse Direction
997 "BULKHEAD_LHS.007"	0.004	9	Frequency Limit, Panel or Beam
998 "BULKHEAD_LHS.008"	0.344	9	Isotropic Strength, Von Mises Interaction Yield Criterion
999 "Component 999"	0.122	9	Frequency Limit, Panel or Beam
1000 "Component 1000"	0.182	9	Frequency Limit, Panel or Beam
1001 "Component 1001"	0.076	9	Isotropic Strength, Von Mises Interaction Yield Criterion
1002 "Component 1002"	0.006	9	Wrinkling, Eqn 2, Honeycomb Core, X, Y & Interaction
1003 "Component 1003"	0.005	9	Wrinkling, Eqn 2, Honeycomb Core, X, Y & Interaction
1004 "Component 1004"	0.235	9	Isotropic Strength, Von Mises Interaction Yield Criterion
1005 "Component 1005"	0.013	9	Wrinkling, Eqn 2, Honeycomb Core, X, Y & Interaction
1006 "BULKHEAD_LHS.016"	0.096	9	Wrinkling, Eqn 2, Honeycomb Core, X, Y & Interaction
1007 "BULKHEAD_LHS.017"	0.070	9	Isotropic Strength, Von Mises Interaction Yield Criterion
1008 "Component 1008"	0.013	9	Frequency Limit, Panel or Beam
1009 "Component 1009"	0.147	9	Wrinkling, Eqn 2, Honeycomb Core, X, Y & Interaction
1010 "Component 1010"	0.222	9	Isotropic Strength, Von Mises Interaction Yield Criterion
1011 "Component 1011"	0.036	9	Frequency Limit, Panel or Beam
1012 "BULKHEAD_LHS.022"	0.176	9	Frequency Limit, Panel or Beam
1013 "BULKHEAD_LHS.023"	0.099	9	Isotropic Strength, Von Mises Interaction Yield Criterion
1014 "Component 1014"	0.062	9	Frequency Limit, Panel or Beam
1015 "BULKHEAD_LHS.025"	0.019	10	Isotropic Strength, Von Mises Interaction Yield Criterion

1016 "BULKHEAD_LHS.026"	0.111	9	Isotropic Strength, Von Mises Interaction Yield Criterion
1017 "Component 1017"	0.125	9	Frequency Limit, Panel or Beam
1018 "BULKHEAD_LHS.028"	0.033	9	Wrinkling, Eqn 2, Honeycomb Core, X, Y & Interaction
1019 "BULKHEAD_LHS.029"	0.008	9	Isotropic Strength, Von Mises Interaction Yield Criterion
1020 "Component 1020"	0.183	9	Frequency Limit, Panel or Beam
1021 "BULKHEAD_LHS.031"	0.088	9	Frequency Limit, Panel or Beam
1022 "BULKHEAD_LHS.032"	0.284	9	Isotropic Strength, Von Mises Interaction Yield Criterion
1023 "Component 1023"	0.046	9	Frequency Limit, Panel or Beam
1024 "BULKHEAD_LHS.034"	0.108	9	Frequency Limit, Panel or Beam
1025 "BULKHEAD_LHS.035"	0.056	9	Isotropic Strength, Von Mises Interaction Yield Criterion
1026 "Component 1026"	0.092	9	Isotropic Strength, Transverse Direction
1027 "BULKHEAD_LHS.037"	0.166	9	Frequency Limit, Panel or Beam
1028 "BULKHEAD_LHS.038"	0.478	9	Isotropic Strength, Von Mises Interaction Yield Criterion
1029 "Component 1029"	0.155	9	Isotropic Strength, Von Mises Interaction Yield Criterion
1030 "BULKHEAD_LHS.040"	0.003	9	Isotropic Strength, Von Mises Interaction Yield Criterion
1031 "BULKHEAD_LHS.041"	0.008	9	Isotropic Strength, Von Mises Interaction Yield Criterion
1267 "BULKHEADa_LHS.001"	0.283	9	Isotropic Strength, Von Mises Interaction Yield Criterion
1268 "BULKHEADa_LHS.002"	0.064	9	Frequency Limit, Panel or Beam
1269 "BULKHEADa_RHS.001"	0.091	6	Shear Strength, X (Longitudinal) direction {Hexcel}
1270 "BULKHEADa_RHS.002"	0.063	9	Isotropic Strength, Von Mises Interaction Yield Criterion
6 "Group 6" Keels			
873 "Component 873"	0.003	9	Isotropic Strength, Longitudinal Direction
874 "Component 874"	0.008	9	Frequency Limit, Panel or Beam
875 "Component 875"	0.098	9	Frequency Limit, Panel or Beam
876 "Component 876"	0.195	9	Isotropic Strength, Von Mises Interaction Yield Criterion
877 "Component 877"	0.045	9	Frequency Limit, Panel or Beam
878 "Component 878"	0.014	9	Frequency Limit, Panel or Beam
879 "Component 879"	0.142	9	Isotropic Strength, Longitudinal Direction
880 "Component 880"	0.176	9	Frequency Limit, Panel or Beam
881 "Component 881"	0.190	9	Frequency Limit, Panel or Beam
882 "Component 882"	0.023	9	Frequency Limit, Panel or Beam
883 "Component 883"	0.226	9	Isotropic Strength, Longitudinal Direction
884 "Component 884"	0.042	9	Frequency Limit, Panel or Beam
885 "Component 885"	0.053	9	Frequency Limit, Panel or Beam
886 "Component 886"	0.340	9	Frequency Limit, Panel or Beam
887 "Component 887"	0.090	9	Frequency Limit, Panel or Beam
888 "Component 888"	0.315	9	Isotropic Strength, Von Mises Interaction Yield Criterion
889 "Component 889"	0.656	9	Isotropic Strength, Longitudinal Direction
890 "Component 890"	0.619	9	Intracell Dimpling, X, Y & Interaction
891 "Component 891"	0.248	9	Isotropic Strength, Longitudinal Direction
892 "Component 892"	0.167	9	Isotropic Strength, Von Mises Interaction Yield Criterion
893 "Component 893"	0.432	9	Isotropic Strength, Von Mises Interaction Yield Criterion
894 "Component 894"	0.090	9	Frequency Limit, Panel or Beam
895 "Component 895"	0.162	9	Frequency Limit, Panel or Beam
896 "Component 896"	0.298	9	Frequency Limit, Panel or Beam
897 "Component 897"	0.188	9	Frequency Limit, Panel or Beam
898 "FUSE_SPAR_WEB_RHS.011"	0.111	9	Isotropic Strength, Longitudinal Direction
899 "Component 899"	0.032	9	Frequency Limit, Panel or Beam

900 "Component 900"	0.067	9	Frequency Limit, Panel or Beam
901 "Component 901"	0.046	9	Frequency Limit, Panel or Beam
902 "Component 902"	0.055	9	Frequency Limit, Panel or Beam
903 "Component 903"	0.067	9	Isotropic Strength, Von Mises Interaction Yield Criterion
904 "Component 904"	0.133	9	Frequency Limit, Panel or Beam
905 "Component 905"	0.615	9	Intracell Dimpling, X, Y & Interaction
906 "Component 906"	0.035	9	Frequency Limit, Panel or Beam
907 "Component 907"	0.180	9	Intracell Dimpling, X, Y & Interaction
908 "Component 908"	0.308	9	Frequency Limit, Panel or Beam
909 "Component 909"	0.292	9	Frequency Limit, Panel or Beam
910 "Component 910"	0.401	9	Frequency Limit, Panel or Beam
911 "Component 911"	0.172	10	Isotropic Strength, Von Mises Interaction Yield Criterion
912 "Component 912"	0.081	10	Isotropic Strength, Von Mises Interaction Yield Criterion
913 "Component 913"	0.120	9	Frequency Limit, Panel or Beam
914 "Component 914"	0.004	9	Shear Strength, X (Longitudinal) direction {Hexcel}
915 "Component 915"	0.226	9	Frequency Limit, Panel or Beam
916 "Component 916"	0.162	9	Frequency Limit, Panel or Beam
917 "Component 917"	0.237	9	Isotropic Strength, Von Mises Interaction Yield Criterion
918 "FUSE_SPAR_WEB_RHS.031"	0.073	9	Frequency Limit, Panel or Beam
919 "Component 919"	0.215	9	Isotropic Strength, Von Mises Interaction Yield Criterion
920 "Component 920"	0.480	9	Isotropic Strength, Von Mises Interaction Yield Criterion
921 "Component 921"	1.278	9	Shear Strength, Y (Transverse) direction {Hexcel}
922 "Component 922"	0.219	9	Isotropic Strength, Von Mises Interaction Yield Criterion
923 "Component 923"	0.232	9	Isotropic Strength, Longitudinal Direction
924 "Component 924"	0.343	9	Isotropic Strength, Von Mises Interaction Yield Criterion
925 "Component 925"	0.090	9	Frequency Limit, Panel or Beam
926 "Component 926"	0.162	9	Frequency Limit, Panel or Beam
927 "Component 927"	0.298	9	Frequency Limit, Panel or Beam
928 "Component 928"	0.188	9	Frequency Limit, Panel or Beam
929 "FUSE_SPAR_WEB_LHS.011"	0.201	9	Frequency Limit, Panel or Beam
930 "Component 930"	0.032	9	Frequency Limit, Panel or Beam
931 "Component 931"	0.216	9	Isotropic Strength, Longitudinal Direction
932 "Component 932"	0.046	9	Frequency Limit, Panel or Beam
933 "Component 933"	0.011	9	Isotropic Strength, Von Mises Interaction Yield Criterion
934 "Component 934"	0.103	9	Isotropic Strength, Von Mises Interaction Yield Criterion
935 "Component 935"	0.055	9	Frequency Limit, Panel or Beam
936 "Component 936"	0.716	9	Intracell Dimpling, X, Y & Interaction
937 "Component 937"	0.035	9	Frequency Limit, Panel or Beam
938 "Component 938"	0.000	9	Intracell Dimpling, X, Y & Interaction
939 "Component 939"	0.024	9	Intracell Dimpling, X, Y & Interaction
940 "Component 940"	0.292	9	Frequency Limit, Panel or Beam
941 "Component 941"	0.347	9	Isotropic Strength, Von Mises Interaction Yield Criterion
942 "Component 942"	0.278	9	Isotropic Strength, Longitudinal Direction
943 "Component 943"	0.333	10	Isotropic Strength, Von Mises Interaction Yield Criterion
944 "Component 944"	0.120	9	Frequency Limit, Panel or Beam
945 "Component 945"	0.100	9	Shear Strength, X (Longitudinal) direction {Hexcel}
946 "Component 946"	0.227	9	Frequency Limit, Panel or Beam
947 "Component 947"	0.208	9	Isotropic Strength, Longitudinal Direction

948 "Component 948"	0.077	9	Isotropic Strength, Von Mises Interaction Yield Criterion
949 "FUSE_SPAR_WEB_LHS.031"	0.073	9	Frequency Limit, Panel or Beam
7 "Group 7" Fuselage Side Skins			
1032 "FUSE_SIDE_RHS.01"	0.679	6	Intracell Dimpling, X, Y & Interaction
1033 "FUSE_SIDE_RHS.02"	0.086	9	Intracell Dimpling, X, Y & Interaction
1034 "FUSE_SIDE_RHS.03"	0.062	9	Intracell Dimpling, X, Y & Interaction
1035 "FUSE_SIDE_RHS.04"	0.155	9	Sandwich Flatwise Tension w/ Interlaminar Shear Interaction
1036 "FUSE_SIDE_RHS.05"	0.182	9	Isotropic Strength, Von Mises Interaction Yield Criterion
1037 "FUSE_SIDE_RHS.06"	0.109	9	Shear Strength, Y (Transverse) direction {Hexcel}
1038 "FUSE_SIDE_RHS.07"	0.176	9	Sandwich Flatwise Tension w/ Interlaminar Shear Interaction
1039 "FUSE_SIDE_RHS.08"	0.090	9	Frequency Limit, Panel or Beam
1040 "FUSE_SIDE_RHS.09"	0.124	9	Frequency Limit, Panel or Beam
1041 "FUSE_SIDE_RHS.10"	0.218	9	Frequency Limit, Panel or Beam
1042 "FUSE_SIDE_RHS.11"	0.117	9	Shear Strength, X (Longitudinal) direction {Hexcel}
1043 "FUSE_SIDE_RHS.12"	0.029	9	Shear Strength, X (Longitudinal) direction {Hexcel}
1044 "FUSE_SIDE_RHS.13"	0.027	9	Isotropic Strength, Von Mises Interaction Yield Criterion
1045 "FUSE_SIDE_RHS.14"	0.056	9	Frequency Limit, Panel or Beam
1046 "FUSE_SIDE_RHS.15"	0.126	9	Frequency Limit, Panel or Beam
1047 "FUSE_SIDE_RHS.16"	0.135	9	Frequency Limit, Panel or Beam
1048 "FUSE_SIDE_RHS.17"	0.302	9	Frequency Limit, Panel or Beam
1049 "FUSE_SIDE_RHS.18"	0.003	9	Isotropic Strength, Longitudinal Direction
1050 "FUSE_SIDE_LHS.01"	0.195	6	Intracell Dimpling, X, Y & Interaction
1051 "FUSE_SIDE_LHS.02"	0.129	9	Intracell Dimpling, X, Y & Interaction
1052 "FUSE_SIDE_LHS.03"	0.006	9	Intracell Dimpling, X, Y & Interaction
1053 "FUSE_SIDE_LHS.04"	0.133	9	Sandwich Flatwise Tension w/ Interlaminar Shear Interaction
1054 "FUSE_SIDE_LHS.05"	0.050	9	Isotropic Strength, Von Mises Interaction Yield Criterion
1055 "FUSE_SIDE_LHS.06"	0.190	9	Shear Strength, Y (Transverse) direction {Hexcel}
1056 "FUSE_SIDE_LHS.07"	0.204	9	Frequency Limit, Panel or Beam
1057 "FUSE_SIDE_LHS.08"	0.092	9	Frequency Limit, Panel or Beam
1058 "FUSE_SIDE_LHS.09"	0.124	9	Frequency Limit, Panel or Beam
1059 "FUSE_SIDE_LHS.10"	0.218	9	Frequency Limit, Panel or Beam
1060 "FUSE_SIDE_LHS.11"	0.052	9	Sandwich Flatwise Tension w/ Interlaminar Shear Interaction
1061 "FUSE_SIDE_LHS.12"	0.004	9	Isotropic Strength, Von Mises Interaction Yield Criterion
1062 "FUSE_SIDE_LHS.13"	0.073	9	Isotropic Strength, Von Mises Interaction Yield Criterion
1063 "FUSE_SIDE_LHS.14"	0.022	9	Isotropic Strength, Von Mises Interaction Yield Criterion
1064 "FUSE_SIDE_LHS.15"	0.127	9	Frequency Limit, Panel or Beam
1065 "FUSE_SIDE_LHS.16"	0.135	9	Frequency Limit, Panel or Beam
1066 "FUSE_SIDE_LHS.17"	0.301	9	Frequency Limit, Panel or Beam
1067 "FUSE_SIDE_LHS.18"	-0.039	9	Isotropic Strength, Longitudinal Direction
8 "Group 8" Wing			
1069 "WING_LOWER_SKIN_RHS.02"	0.122	9	Frequency Limit, Panel or Beam
1071 "WING_LOWER_SKIN_RHS.04"	0.068	9	Frequency Limit, Panel or Beam
1072 "WING_LOWER_SKIN_RHS.05"	0.469	9	Frequency Limit, Panel or Beam
1074 "WING_LOWER_SKIN_RHS.07"	0.005	9	Frequency Limit, Panel or Beam
1075 "WING_LOWER_SKIN_RHS.08"	0.031	9	Frequency Limit, Panel or Beam
1077	1.670	7	Isotropic Strength, Transverse Direction

"WING_LOWER_SKIN_RHS.10"			
1078	0.011	9	Frequency Limit, Panel or Beam
"WING_LOWER_SKIN_RHS.11"			
1079	0.076	9	Frequency Limit, Panel or Beam
"WING_LOWER_SKIN_RHS.12"			
1081	0.330	7	Isotropic Strength, Transverse Direction
"WING_LOWER_SKIN_RHS.14"			
1082	0.013	9	Frequency Limit, Panel or Beam
"WING_LOWER_SKIN_RHS.15"			
1083	0.018	9	Isotropic Strength, Von Mises Interaction Yield Criterion
"WING_LOWER_SKIN_RHS.16"			
1085	0.057	7	Intracell Dimpling, X, Y & Interaction
"WING_LOWER_SKIN_RHS.18"			
1086	0.444	9	Isotropic Strength, Von Mises Interaction Yield Criterion
"WING_LOWER_SKIN_RHS.19"			
1087	0.004	9	Isotropic Strength, Transverse Direction
"WING_LOWER_SKIN_RHS.20"			
1089	0.072	9	Frequency Limit, Panel or Beam
"WING_LOWER_SKIN_LHS.02"			
1091	0.068	9	Frequency Limit, Panel or Beam
"WING_LOWER_SKIN_LHS.04"			
1092	0.468	9	Frequency Limit, Panel or Beam
"WING_LOWER_SKIN_LHS.05"			
1094	0.005	9	Frequency Limit, Panel or Beam
"WING_LOWER_SKIN_LHS.07"			
1095	0.031	9	Frequency Limit, Panel or Beam
"WING_LOWER_SKIN_LHS.08"			
1097	2.110	9	Isotropic Strength, Von Mises Interaction Yield Criterion
"WING_LOWER_SKIN_LHS.10"			
1098	0.011	9	Frequency Limit, Panel or Beam
"WING_LOWER_SKIN_LHS.11"			
1099	0.076	9	Frequency Limit, Panel or Beam
"WING_LOWER_SKIN_LHS.12"			
1101	0.197	9	Isotropic Strength, Transverse Direction
"WING_LOWER_SKIN_LHS.14"			
1102	0.013	9	Frequency Limit, Panel or Beam
"WING_LOWER_SKIN_LHS.15"			
1103	0.157	9	Frequency Limit, Panel or Beam
"WING_LOWER_SKIN_LHS.16"			
1105	0.020	9	Isotropic Strength, Von Mises Interaction Yield Criterion
"WING_LOWER_SKIN_LHS.18"			
1106	-0.082	9	Isotropic Strength, Von Mises Interaction Yield Criterion
"WING_LOWER_SKIN_LHS.19"			
1107	0.031	9	Isotropic Strength, Von Mises Interaction Yield Criterion
"WING_LOWER_SKIN_LHS.20"			
1109	0.096	9	Frequency Limit, Panel or Beam
"WING_UPPER_SKIN_RHS.02"			
1111	0.037	9	Frequency Limit, Panel or Beam
"WING_UPPER_SKIN_RHS.04"			
1112	0.134	9	Intracell Dimpling, X, Y & Interaction
"WING_UPPER_SKIN_RHS.05"			
1114	0.021	9	Frequency Limit, Panel or Beam
"WING_UPPER_SKIN_RHS.07"			
1115	0.076	9	Frequency Limit, Panel or Beam
"WING_UPPER_SKIN_RHS.08"			
1117	0.373	7	Isotropic Strength, Transverse Direction
"WING_UPPER_SKIN_RHS.10"			
1118	0.025	9	Frequency Limit, Panel or Beam
"WING_UPPER_SKIN_RHS.11"			
1119	0.135	9	Frequency Limit, Panel or Beam
"WING_UPPER_SKIN_RHS.12"			
1121	0.177	7	Isotropic Strength, Transverse Direction
"WING_UPPER_SKIN_RHS.14"			
1122	0.030	9	Frequency Limit, Panel or Beam
"WING_UPPER_SKIN_RHS.15"			
1123	0.045	9	Frequency Limit, Panel or Beam
"WING_UPPER_SKIN_RHS.16"			
1125	0.249	7	Intracell Dimpling, X, Y & Interaction
"WING_UPPER_SKIN_RHS.18"			

1126 "WING_UPPER_SKIN_RHS.19"	0.160	9	Isotropic Strength, Von Mises Interaction Yield Criterion
1127 "WING_UPPER_SKIN_RHS.20"	0.040	9	Isotropic Strength, Von Mises Interaction Yield Criterion
1129 "WING_UPPER_SKIN_LHS.02"	0.098	9	Frequency Limit, Panel or Beam
1131 "WING_UPPER_SKIN_LHS.04"	0.038	9	Frequency Limit, Panel or Beam
1132 "WING_UPPER_SKIN_LHS.05"	0.149	9	Frequency Limit, Panel or Beam
1134 "WING_UPPER_SKIN_LHS.07"	0.021	9	Frequency Limit, Panel or Beam
1135 "WING_UPPER_SKIN_LHS.08"	0.076	9	Frequency Limit, Panel or Beam
1137 "WING_UPPER_SKIN_LHS.10"	0.395	9	Isotropic Strength, Von Mises Interaction Yield Criterion
1138 "WING_UPPER_SKIN_LHS.11"	0.025	9	Frequency Limit, Panel or Beam
1139 "WING_UPPER_SKIN_LHS.12"	0.135	9	Frequency Limit, Panel or Beam
1141 "WING_UPPER_SKIN_LHS.14"	0.165	9	Isotropic Strength, Transverse Direction
1142 "WING_UPPER_SKIN_LHS.15"	0.030	9	Frequency Limit, Panel or Beam
1143 "WING_UPPER_SKIN_LHS.16"	0.044	9	Frequency Limit, Panel or Beam
1145 "WING_UPPER_SKIN_LHS.18"	0.773	7	Shear Strength, Y (Transverse) direction {Hexcel}
1146 "WING_UPPER_SKIN_LHS.19"	0.025	9	Isotropic Strength, Longitudinal Direction
1147 "WING_UPPER_SKIN_LHS.20"	0.055	9	Isotropic Strength, Von Mises Interaction Yield Criterion
9 "Group 9" Wing Spars & Ribs			
1148 "WING_SPAR_WEB_RHS.01"	0.127	9	Isotropic Strength, Longitudinal Direction
1149 "WING_SPAR_WEB_RHS.02"	0.408	9	Isotropic Strength, Von Mises Interaction Yield Criterion
1150 "WING_SPAR_WEB_RHS.03"	0.302	9	Isotropic Strength, Longitudinal Direction
1151 "WING_SPAR_WEB_RHS.04"	0.233	9	Frequency Limit, Panel or Beam
1152 "WING_SPAR_WEB_RHS.05"	0.422	9	Isotropic Strength, Von Mises Interaction Yield Criterion
1153 "WING_SPAR_WEB_RHS.06"	0.513	9	Isotropic Strength, Von Mises Interaction Yield Criterion
1154 "WING_SPAR_WEB_RHS.07"	0.291	9	Isotropic Strength, Longitudinal Direction
1155 "WING_SPAR_WEB_RHS.08"	0.423	9	Isotropic Strength, Longitudinal Direction
1156 "WING_SPAR_WEB_RHS.09"	0.277	9	Isotropic Strength, Von Mises Interaction Yield Criterion
1157 "WING_SPAR_WEB_RHS.10"	0.634	7	Isotropic Strength, Longitudinal Direction
1158 "WING_SPAR_WEB_RHS.11"	0.986	9	Isotropic Strength, Longitudinal Direction
1159 "WING_SPAR_WEB_RHS.12"	0.235	9	Isotropic Strength, Von Mises Interaction Yield Criterion
1160 "WING_SPAR_WEB_RHS.13"	0.132	7	Isotropic Strength, Von Mises Interaction Yield Criterion
1161 "WING_SPAR_WEB_RHS.14"	0.730	9	Isotropic Strength, Von Mises Interaction Yield Criterion
1162 "WING_SPAR_WEB_RHS.15"	0.459	9	Isotropic Strength, Longitudinal Direction
1163 "WING_SPAR_WEB_RHS.16"	1.772	7	Isotropic Strength, Longitudinal Direction
1164 "WING_SPAR_WEB_LHS.01"	0.143	9	Isotropic Strength, Longitudinal Direction
1165 "WING_SPAR_WEB_LHS.02"	0.290	9	Isotropic Strength, Transverse Direction

1166 "WING_SPAR_WEB_LHS.03"	0.146	9	Isotropic Strength, Von Mises Interaction Yield Criterion
1167 "WING_SPAR_WEB_LHS.04"	0.233	9	Frequency Limit, Panel or Beam
1168 "WING_SPAR_WEB_LHS.05"	0.388	9	Isotropic Strength, Von Mises Interaction Yield Criterion
1169 "WING_SPAR_WEB_LHS.06"	0.627	9	Isotropic Strength, Von Mises Interaction Yield Criterion
1170 "WING_SPAR_WEB_LHS.07"	0.376	9	Frequency Limit, Panel or Beam
1171 "WING_SPAR_WEB_LHS.08"	0.617	9	Isotropic Strength, Longitudinal Direction
1172 "WING_SPAR_WEB_LHS.09"	0.534	9	Isotropic Strength, Longitudinal Direction
1173 "WING_SPAR_WEB_LHS.10"	0.821	9	Isotropic Strength, Longitudinal Direction
1174 "WING_SPAR_WEB_LHS.11"	0.604	9	Isotropic Strength, Longitudinal Direction
1175 "WING_SPAR_WEB_LHS.12"	0.675	9	Isotropic Strength, Longitudinal Direction
1176 "WING_SPAR_WEB_LHS.13"	1.274	9	Isotropic Strength, Longitudinal Direction
1177 "WING_SPAR_WEB_LHS.14"	0.891	9	Isotropic Strength, Von Mises Interaction Yield Criterion
1178 "WING_SPAR_WEB_LHS.15"	0.275	9	Isotropic Strength, Von Mises Interaction Yield Criterion
1179 "WING_SPAR_WEB_LHS.16"	0.184	9	Isotropic Strength, Longitudinal Direction
1180 "WING_RIB_WEB_RHS.01"	0.798	9	Isotropic Strength, Longitudinal Direction
1182 "WING_RIB_WEB_RHS.03"	0.238	9	Isotropic Strength, Von Mises Interaction Yield Criterion
1184 "WING_RIB_WEB_RHS.05"	0.152	9	Isotropic Strength, Von Mises Interaction Yield Criterion
1185 "WING_RIB_WEB_RHS.06"	0.673	9	Isotropic Strength, Von Mises Interaction Yield Criterion
1187 "WING_RIB_WEB_RHS.08"	0.122	6	Shear Strength, X (Longitudinal) direction {Hexcel}
1188 "WING_RIB_WEB_RHS.09"	0.332	9	Isotropic Strength, Von Mises Interaction Yield Criterion
1189 "WING_RIB_WEB_RHS.10"	0.692	9	Isotropic Strength, Longitudinal Direction
1191 "WING_RIB_WEB_RHS.12"	0.052	3	Isotropic Strength, Longitudinal Direction
1192 "WING_RIB_WEB_RHS.13"	0.761	9	Isotropic Strength, Von Mises Interaction Yield Criterion
1193 "WING_RIB_WEB_RHS.14"	0.672	9	Isotropic Strength, Von Mises Interaction Yield Criterion
1195 "WING_RIB_WEB_RHS.16"	2.113	7	Isotropic Strength, Von Mises Interaction Yield Criterion
1196 "WING_RIB_WEB_RHS.17"	2.209	7	Isotropic Strength, Von Mises Interaction Yield Criterion
1197 "WING_RIB_WEB_RHS.18"	0.914	9	Isotropic Strength, Transverse Direction
1199 "WING_RIB_WEB_LHS.01"	0.933	9	Isotropic Strength, Longitudinal Direction
1201 "WING_RIB_WEB_LHS.03"	0.167	9	Isotropic Strength, Von Mises Interaction Yield Criterion
1203 "WING_RIB_WEB_LHS.05"	0.095	9	Isotropic Strength, Von Mises Interaction Yield Criterion
1204 "WING_RIB_WEB_LHS.06"	0.508	9	Isotropic Strength, Longitudinal Direction
1206 "WING_RIB_WEB_LHS.08"	0.131	6	Isotropic Strength, Longitudinal Direction
1207 "WING_RIB_WEB_LHS.09"	0.439	9	Isotropic Strength, Von Mises Interaction Yield Criterion
1208 "WING_RIB_WEB_LHS.10"	0.913	9	Isotropic Strength, Longitudinal Direction
1210 "WING_RIB_WEB_LHS.12"	0.172	3	Isotropic Strength, Von Mises Interaction Yield Criterion
1211 "WING_RIB_WEB_LHS.13"	0.650	3	Isotropic Strength, Von Mises Interaction Yield Criterion
1212 "WING_RIB_WEB_LHS.14"	0.847	9	Isotropic Strength, Longitudinal Direction
1214 "WING_RIB_WEB_LHS.16"	1.427	7	Isotropic Strength, Transverse Direction
1215 "WING_RIB_WEB_LHS.17"	1.261	9	Isotropic Strength, Longitudinal Direction
1216 "WING_RIB_WEB_LHS.18"	0.446	9	Isotropic Strength, Von Mises Interaction Yield Criterion
10 "Group 10" Intake			
1245 "INTAKE_RHS.01"	0.158	9	Wrinkling, Eqn 2, Honeycomb Core, X, Y & Interaction
1246 "INTAKE_LHS.01"	0.105	9	Shear Strength, Y (Transverse) direction {Hexcel}

1247 "INTAKE_LHS.03"	0.831	9	Shear Strength, X (Longitudinal) direction {Hexcel}
1248 "INTAKE_RHS.03"	0.885	6	Isotropic Strength, Von Mises Interaction Yield Criterion
1249 "INTAKE_RHS.02"	0.112	9	Isotropic Strength, Von Mises Interaction Yield Criterion
1250 "INTAKE_LHS.02"	0.020	9	Isotropic Strength, Von Mises Interaction Yield Criterion
1251 "INTAKE_LHS.04"	0.301	9	Frequency Limit, Panel or Beam
1252 "INTAKE_LHS.05"	0.179	9	Frequency Limit, Panel or Beam
1253 "INTAKE_RHS.04"	0.301	9	Frequency Limit, Panel or Beam
1254 "INTAKE_RHS.05"	0.179	9	Frequency Limit, Panel or Beam
1255 "INTAKE_RHS.06"	0.521	9	Isotropic Strength, Von Mises Interaction Yield Criterion
1256 "INTAKE_LHS.06"	0.873	9	Isotropic Strength, Von Mises Interaction Yield Criterion
1257 "INTAKE_LHS.07"	0.235	9	Frequency Limit, Panel or Beam
1258 "INTAKE_RHS.07"	0.122	9	Isotropic Strength, Von Mises Interaction Yield Criterion
1259 "INTAKE_RHS.08"	0.035	9	Frequency Limit, Panel or Beam
1260 "INTAKE_RHS.09"	0.258	9	Shear Strength, X (Longitudinal) direction {Hexcel}
1261 "INTAKE_RHS.10"	0.169	9	Isotropic Strength, Von Mises Interaction Yield Criterion
1262 "INTAKE_RHS.11"	0.123	9	Isotropic Strength, Von Mises Interaction Yield Criterion
1263 "INTAKE_LHS.11"	0.632	9	Sandwich Flatwise Tension w/ Interlaminar Shear Interaction
1264 "INTAKE_LHS.10"	0.056	9	Isotropic Strength, Von Mises Interaction Yield Criterion
1265 "INTAKE_LHS.09"	0.290	9	Frequency Limit, Panel or Beam
1266 "INTAKE_LHS.08"	0.035	9	Frequency Limit, Panel or Beam
11 "Group 11" Rudder			
1218 "RUDDER_RIB_WEB.01"	0.035	8	Intracell Dimpling, X, Y & Interaction
1219 "RUDDER_RIB_WEB.02"	0.717	7	Isotropic Strength, Von Mises Interaction Yield Criterion
1220 "RUDDER_RIB_WEB.03"	0.171	7	Isotropic Strength, Von Mises Interaction Yield Criterion
1221 "RUDDER_RIB_WEB.04"	0.332	7	Shear Strength, Y (Transverse) direction {Hexcel}
1222 "RUDDER_RIB_WEB.05"	0.663	7	Isotropic Strength, Von Mises Interaction Yield Criterion
1223 "RUDDER_RIB_WEB.06"	0.450	8	Shear Strength, Y (Transverse) direction {Hexcel}
1224 "RUDDER_RIB_WEB.07"	0.051	8	Intracell Dimpling, X, Y & Interaction
1225 "RUDDER_SPAR_WEB.01"	0.324	7	Isotropic Strength, Von Mises Interaction Yield Criterion
1226 "RUDDER_SKIN.01"	0.220	7	Isotropic Strength, Von Mises Interaction Yield Criterion
1227 "RUDDER_SKIN.02"	0.204	9	Frequency Limit, Panel or Beam
1228 "RUDDER_SKIN.03"	0.355	7	Isotropic Strength, Von Mises Interaction Yield Criterion
1229 "RUDDER_SKIN.04"	0.550	9	Frequency Limit, Panel or Beam
1230 "RUDDER_SKIN.05"	0.648	9	Frequency Limit, Panel or Beam
1231 "RUDDER_SKIN.06"	0.605	8	Intracell Dimpling, X, Y & Interaction
1232 "ELEVON_RIB_WEB.01"	0.035	7	Isotropic Strength, Von Mises Interaction Yield Criterion
1233 "ELEVON_RIB_WEB.02"	1.541	7	Isotropic Strength, Von Mises Interaction Yield Criterion
1234 "ELEVON_RIB_WEB.03"	0.033	7	Isotropic Strength, Von Mises Interaction Yield Criterion
1235 "ELEVON_RIB_WEB.04"	1.347	7	Isotropic Strength, Von Mises Interaction Yield Criterion
1236 "ELEVON_RIB_WEB.05"	0.001	7	Isotropic Strength, Von Mises Interaction Yield Criterion
1237 "ELEVON_RIB_WEB.06"	0.691	9	Shear Strength, Y (Transverse) direction {Hexcel}
1238 "ELEVON_SKIN.01"	0.070	9	Frequency Limit, Panel or Beam
1239 "ELEVON_SKIN.02"	0.140	7	Intracell Dimpling, X, Y & Interaction
1240 "ELEVON_SKIN.03"	0.011	7	Intracell Dimpling, X, Y & Interaction
1241 "ELEVON_SKIN.07"	0.251	7	Intracell Dimpling, X, Y & Interaction
1242 "ELEVON_SKIN.08"	0.072	7	Intracell Dimpling, X, Y & Interaction
1243 "ELEVON_SKIN.09"	0.486	9	Frequency Limit, Panel or Beam
1244 "ELEVON_SPAR_WEB.01"	0.376	9	Isotropic Strength, Von Mises Interaction Yield Criterion

Group 12 Elevon/Rudder Cntl Surf

222 "pshell.222"	0.016	9	Isotropic Strength, Longitudinal Direction
223 "pshell.223"	0.066	9	Isotropic Strength, Longitudinal Direction
224 "pshell.224"	0.071	7	Isotropic Strength, Von Mises Interaction Yield Criterion
225 "pshell.225"	3.329	9	Isotropic Strength, Von Mises Interaction Yield Criterion
226 "pshell.226"	0.465	7	Isotropic Strength, Von Mises Interaction Yield Criterion
227 "pshell.227"	1.587	8	Isotropic Strength, Von Mises Interaction Yield Criterion
228 "pshell.228"	1.084	8	Isotropic Strength, Von Mises Interaction Yield Criterion
229 "pshell.229"	0.591	6	Isotropic Strength, Von Mises Interaction Yield Criterion
230 "pshell.230"	0.826	6	Isotropic Strength, Von Mises Interaction Yield Criterion
231 "pshell.231"	0.035	9	Isotropic Strength, Longitudinal Direction
232 "pshell.232"	0.006	9	Isotropic Strength, Von Mises Interaction Yield Criterion
233 "pshell.233"	0.001	9	Isotropic Strength, Von Mises Interaction Yield Criterion
234 "pshell.234"	0.012	9	Isotropic Strength, Von Mises Interaction Yield Criterion
235 "pshell.235"	0.068	9	Isotropic Strength, Von Mises Interaction Yield Criterion
236 "pshell.236"	0.475	9	Frequency Limit, Panel or Beam
237 "pshell.237"	0.075	9	Isotropic Strength, Von Mises Interaction Yield Criterion
238 "pshell.238"	0.451	7	Isotropic Strength, Von Mises Interaction Yield Criterion
239 "pshell.239"	0.359	9	Frequency Limit, Panel or Beam
240 "pshell.240"	0.672	7	Isotropic Strength, Von Mises Interaction Yield Criterion
257 "pshell.257"	0.624	9	Isotropic Strength, Longitudinal Direction
258 "pshell.258"	0.038	7	Isotropic Strength, Von Mises Interaction Yield Criterion
259 "pshell.259"	0.163	9	Isotropic Strength, Von Mises Interaction Yield Criterion
260 "pshell.260"	0.068	9	Frequency Limit, Panel or Beam
261 "pshell.261"	0.245	9	Frequency Limit, Panel or Beam
262 "pshell.262"	0.217	9	Isotropic Strength, Von Mises Interaction Yield Criterion
263 "pshell.263"	0.251	9	Isotropic Strength, Von Mises Interaction Yield Criterion
266 "pshell.266"	0.012	9	Isotropic Strength, Longitudinal Direction
267 "pshell.267"	0.056	7	Isotropic Strength, Von Mises Interaction Yield Criterion
268 "pshell.268"	3.246	9	Isotropic Strength, Von Mises Interaction Yield Criterion
269 "pshell.269"	0.009	9	Isotropic Strength, Von Mises Interaction Yield Criterion
270 "pshell.270"	0.007	9	Isotropic Strength, Von Mises Interaction Yield Criterion
271 "pshell.271"	0.064	9	Frequency Limit, Panel or Beam
272 "pshell.272"	0.044	9	Isotropic Strength, Von Mises Interaction Yield Criterion
273 "pshell.273"	0.476	9	Frequency Limit, Panel or Beam
274 "pshell.274"	0.066	9	Isotropic Strength, Von Mises Interaction Yield Criterion
275 "pshell.275"	0.719	7	Isotropic Strength, Von Mises Interaction Yield Criterion
276 "pshell.276"	0.336	9	Frequency Limit, Panel or Beam
277 "pshell.277"	0.497	9	Isotropic Strength, Von Mises Interaction Yield Criterion
278 "pshell.278"	0.096	9	Isotropic Strength, Von Mises Interaction Yield Criterion
279 "pshell.279"	0.016	9	Isotropic Strength, Von Mises Interaction Yield Criterion
280 "pshell.280"	0.068	9	Frequency Limit, Panel or Beam
281 "pshell.281"	0.245	9	Frequency Limit, Panel or Beam
282 "pshell.282"	0.170	9	Isotropic Strength, Von Mises Interaction Yield Criterion
283 "pshell.283"	0.220	9	Isotropic Strength, Von Mises Interaction Yield Criterion
18 "Group 18" Vertical Tail			
221 "pshell.221"	-0.576	7	Composite Strength, Tsai-Wu Interaction
265 "pshell.265"	-0.618	7	Composite Strength, Tsai-Wu Interaction

1068 "WING_LOWER_SKIN_RHS.01"	-0.704	9	Composite Strength, Tsai-Wu Interaction
1070 "WING_LOWER_SKIN_RHS.03"	-0.582	9	Composite Strength, Tsai-Wu Interaction
1073 "WING_LOWER_SKIN_RHS.06"	-0.456	9	Composite Strength, Tsai-Wu Interaction
1076 "WING_LOWER_SKIN_RHS.09"	-0.433	9	Composite Strength, Tsai-Wu Interaction
1080 "WING_LOWER_SKIN_RHS.13"	-0.632	9	Composite Strength, Tsai-Wu Interaction
1084 "WING_LOWER_SKIN_RHS.17"	-0.406	9	Composite Strength, Tsai-Wu Interaction
1088 "WING_LOWER_SKIN_LHS.01"	-0.683	9	Composite Strength, Tsai-Wu Interaction
1090 "WING_LOWER_SKIN_LHS.03"	-0.573	9	Composite Strength, Tsai-Hahn Interaction
1093 "WING_LOWER_SKIN_LHS.06"	-0.531	9	Composite Strength, Tsai-Hahn Interaction
1096 "WING_LOWER_SKIN_LHS.09"	-0.404	9	Composite Strength, Tsai-Wu Interaction
1100 "WING_LOWER_SKIN_LHS.13"	-0.480	9	Composite Strength, Tsai-Wu Interaction
1104 "WING_LOWER_SKIN_LHS.17"	-0.468	9	Composite Strength, Tsai-Wu Interaction
1108 "WING_UPPER_SKIN_RHS.01"	-0.640	9	Composite Strength, Tsai-Wu Interaction
1110 "WING_UPPER_SKIN_RHS.03"	-0.477	2	Frequency Limit, Panel or Beam
1113 "WING_UPPER_SKIN_RHS.06"	-0.373	2	Frequency Limit, Panel or Beam
1116 "WING_UPPER_SKIN_RHS.09"	-0.206	2	Frequency Limit, Panel or Beam
1120 "WING_UPPER_SKIN_RHS.13"	-0.251	9	Composite Strength, Tsai-Wu Interaction
1124 "WING_UPPER_SKIN_RHS.17"	-0.226	9	Composite Strength, Tsai-Wu Interaction
1128 "WING_UPPER_SKIN_LHS.01"	-0.688	9	Composite Strength, Tsai-Wu Interaction
1130 "WING_UPPER_SKIN_LHS.03"	-0.477	2	Frequency Limit, Panel or Beam
1133 "WING_UPPER_SKIN_LHS.06"	-0.373	2	Frequency Limit, Panel or Beam
1136 "WING_UPPER_SKIN_LHS.09"	-0.206	2	Frequency Limit, Panel or Beam
1140 "WING_UPPER_SKIN_LHS.13"	-0.229	9	Composite Strength, Tsai-Wu Interaction
1144 "WING_UPPER_SKIN_LHS.17"	-0.305	9	Composite Strength, Tsai-Wu Interaction
1181 "WING_RIB_WEB_RHS.02"	0.103	9	Composite Strength, Tsai-Wu Interaction
1183 "WING_RIB_WEB_RHS.04"	0.186	9	Composite Strength, Tsai-Wu Interaction
1186 "WING_RIB_WEB_RHS.07"	0.202	9	Composite Strength, Tsai-Wu Interaction
1190 "WING_RIB_WEB_RHS.11"	0.331	9	Composite Strength, Tsai-Wu Interaction
1194 "WING_RIB_WEB_RHS.15"	0.178	9	Composite Strength, Tsai-Wu Interaction
1198 "WING_RIB_WEB_RHS.19"	-0.448	7	Composite Strength, Tsai-Wu Interaction
1200 "WING_RIB_WEB_LHS.02"	0.324	9	Composite Strength, Tsai-Wu Interaction
1202 "WING_RIB_WEB_LHS.04"	0.172	9	Composite Strength, Tsai-Wu Interaction
1205 "WING_RIB_WEB_LHS.07"	0.270	9	Composite Strength, Tsai-Wu Interaction
1209 "WING_RIB_WEB_LHS.11"	0.057	9	Composite Strength, Tsai-Wu Interaction
1213 "WING_RIB_WEB_LHS.15"	0.296	9	Composite Strength, Tsai-Wu Interaction
1217 "WING_RIB_WEB_LHS.19"	-0.423	7	Composite Strength, Tsai-Wu Interaction

APPENDIX B – F-15 DATA

Aircraft that fly aggressive low altitude or high-angle of attack maneuvers will experience high acoustic loading in the presence of external stores. These high acoustic loads can lead to premature acoustic fatigue in thin gage metallic structure.

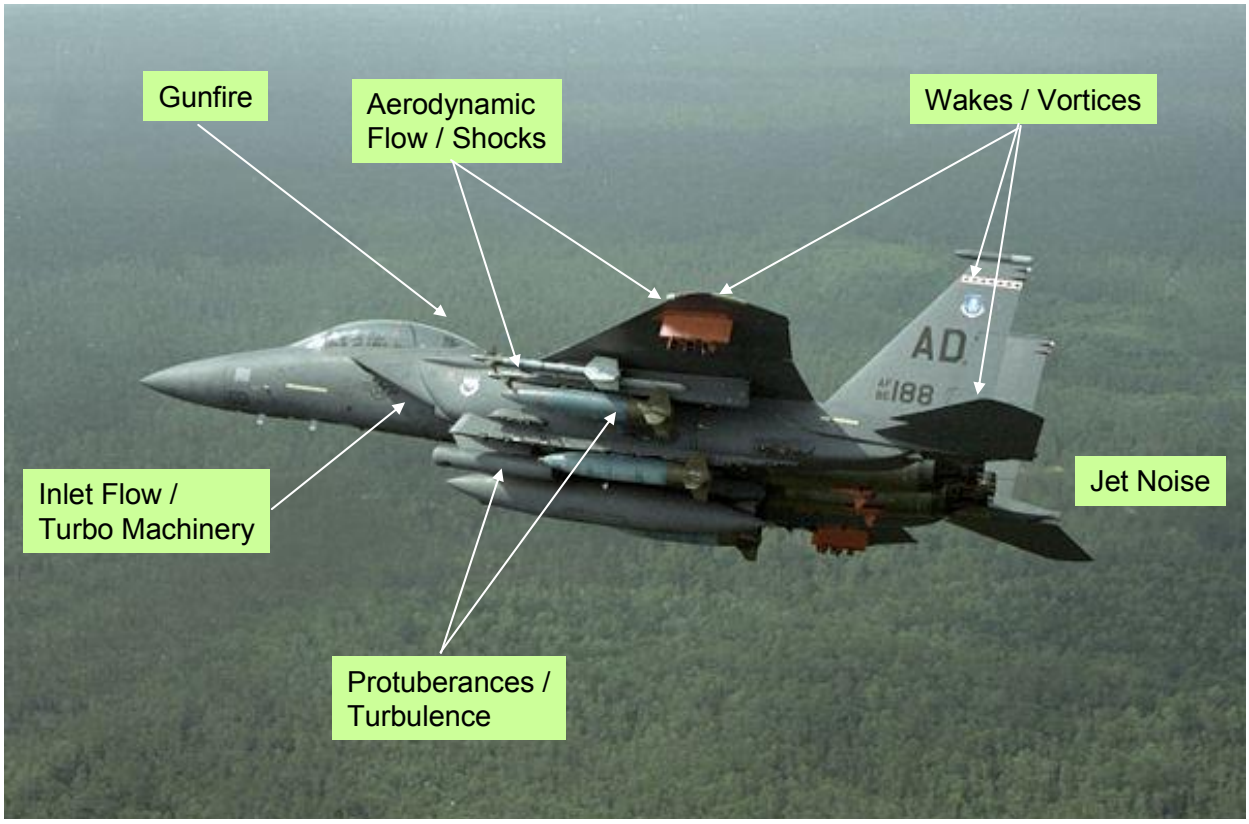

Figure 83. On the Lower Surface, Turbulent Flow Forms Around External Stores.

The majority of structure that cracks due to the acoustic loads are thin gage metallic structure; such as, fuselage skins, access doors, non-load carrying fairings, and leading edges, and secondary support structure; such as, stiffeners, stringers, shear clips, and brackets. In thin gage metallic structure, cracking tends to occur at stress discontinuities arising from chem-mill radii or at fastener holes. The out-of-plane bending response of a panel causes the highest stresses and bending moments to occur at or near the edges of the panels where such features as chem-mills, fastener holes, and support structure are located.

During the early design of the F-15E attack aircraft; there were several lower fuselage skin panels that were experiencing cracking. The F-15E was a ground attack version of the F-15C/D air-superiority fighter. This version of the F-15 carried more external stores on both the wing and fuselage stations, which included the ground terrain following LANTIRN and FLIR pods.

Figure 84. F-15E LANTIRN Pod

During high speed and low altitude conditions, the entire lower fuselage is awash in complex flow around these external stores. The complex flow separation and shocks increased acoustics by 12dB (over previous worst case design conditions.) One panel in particular that was directly behind the LANTIRN pod was experiencing cracking. The panel was 16 in by 14 in, 0.071 in thick, with 0.06- and 0.04-in chem-milled pockets. The skin panel is supported by a bulkhead along long edges and a heavy blade stringer on the short edges. Also, there is a C-channel stiffener that splits the panel. It's this stiffener that was fatigue critical. However, this wasn't obvious from initial observations. The stiffener would fail at the end supports where it bolted to the blade stringers. The crack would propagate into the stiffener, and eventually cracks would form in the skin. Initially, it wasn't known if the skin or stiffener failed first.

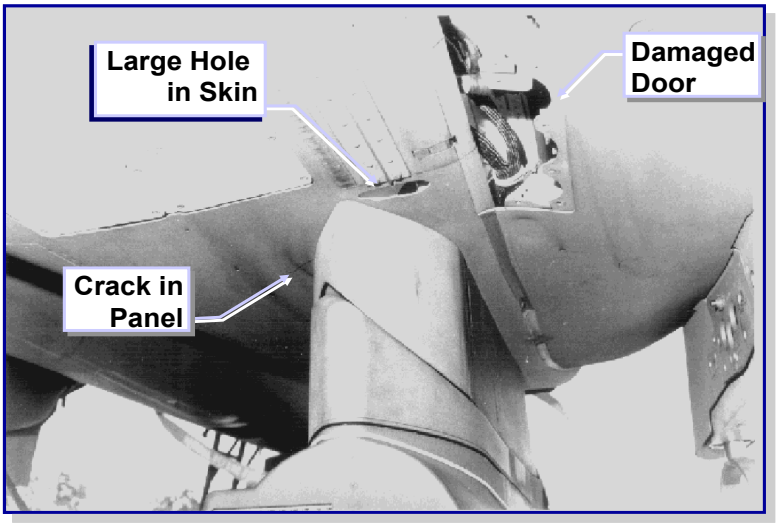

Figure 85. Fatigue Damage

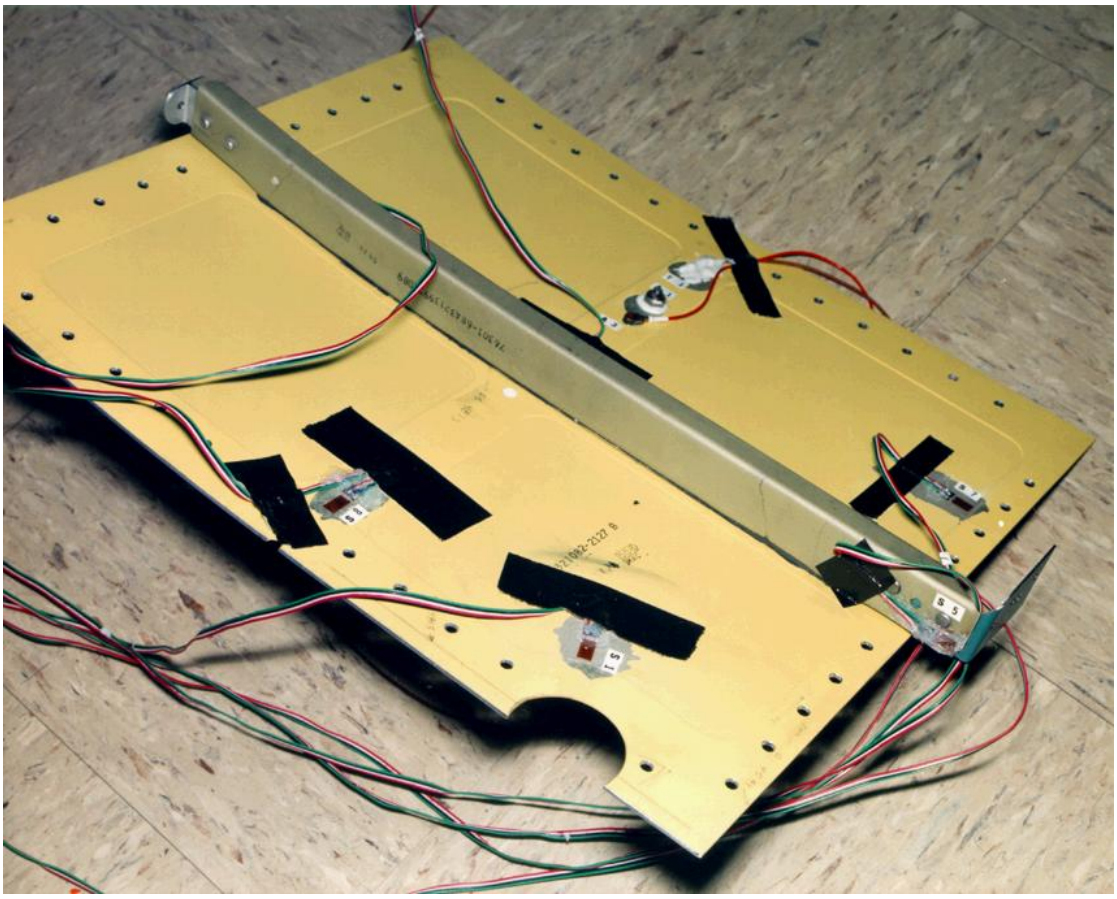

Figure 86. Curved Stiffened Panel Test Case

This is an example of redesigning for acoustic fatigue cracking. First, a FEM was made of the panel, and linear random acoustic response was performed. Linear frequency response methods were used to redesign the skin. The skin was thickened and chem-mill pockets were removed, but this didn't solve the cracking problem. During this early investigation, the environment was not known. With initial redesigns still cracking, a flight test program was initiated that measured the panel environment. The flight test program was able to shed light on the true environments and the critical flight conditions. In the LANTIRN pod configuration, the acoustic loads exceeded OASPL=165dB, and static pressures were exceeding -3psi (suction pressure.) Knowing the flight condition is also important since time-spent-at-condition is critical parameter for fatigue calculations. It turns out, a fighter-attack aircraft; like the F-15, spends about 2 to 4 hrs total time at this condition during its 6000 hr design life. The cracks were occurring after less than 30min of accumulated time. At this point, a laboratory test was designed which would include both acoustic and static pressure effects. Initial testing proved that the baseline design does in fact crack in less than 15 min at 165dB/3psi/75F. The testing demonstrated that the response was very nonlinear. Based on the testing, the stiffener was redesigned. At the time, we did not possess tools required to analyze this type of nonlinear problem.

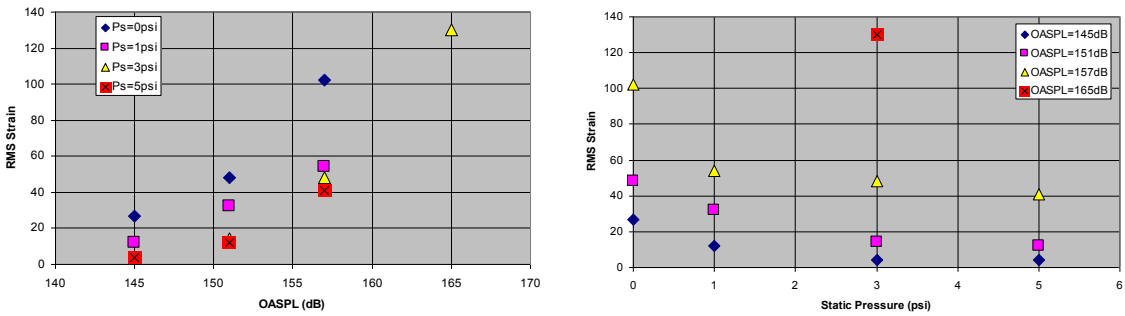

Figure 87. Acoustic Chamber Test Data

Design Environments

During high speed low altitude attack maneuvers, the acoustic level can exceed OASPL=165 dB. In this case, the critical design condition was M=0.95, Alt=3500ft, Q=1175 psf. The max expected acoustic levels are from reference (AFFDL-TR-67-167 and AFFDL-TR-65-192.)

$$OASPL = 20LogQ + 103.0 = 164.4 \text{ dB}$$

And with Shock Interaction, it can be as high as,

$$OASPL = 20LogQ + 107.5 = 168.4 \text{ dB}$$

This is consistent with the flight test measured loads, and the known flow conditions behind the pod.

Also, when shocks are present, the static pressure can be considerable ($\Delta P > 5$psi). The plot below shows the static pressure on the panel for sample of flight conditions. The data below was taken from a single flight during a flight test. The pressure was measured adjacent to the critical panel behind the pod. Note, the pressures can vary from +/- 12 psi. This static pressure alone is enough to cause considerable nonlinear response.

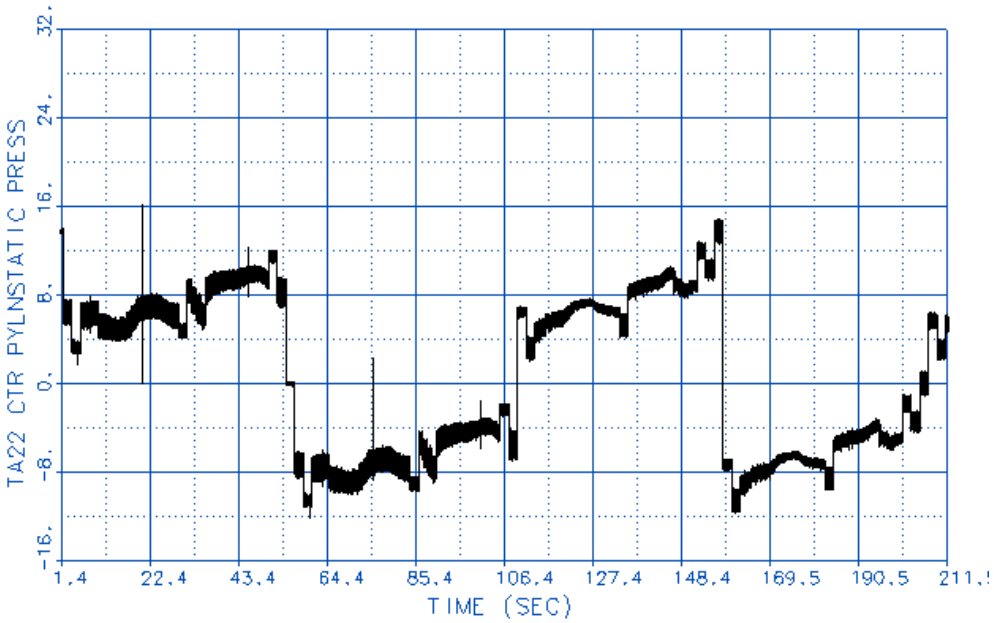

Figure 88. Flight Test Measured Static Pressures Behind Pod

Since, this is a transonic design condition; the temperature is primarily dependent on ambient air temperature conditions (i.e. altitude, season, world wide location). Based on Figure 89, for this critical condition the mean temperature is close to 80F. But, there is the small possibility for temperatures to reach extremes of from T_{Low} =-5F to T_{high}=200F.

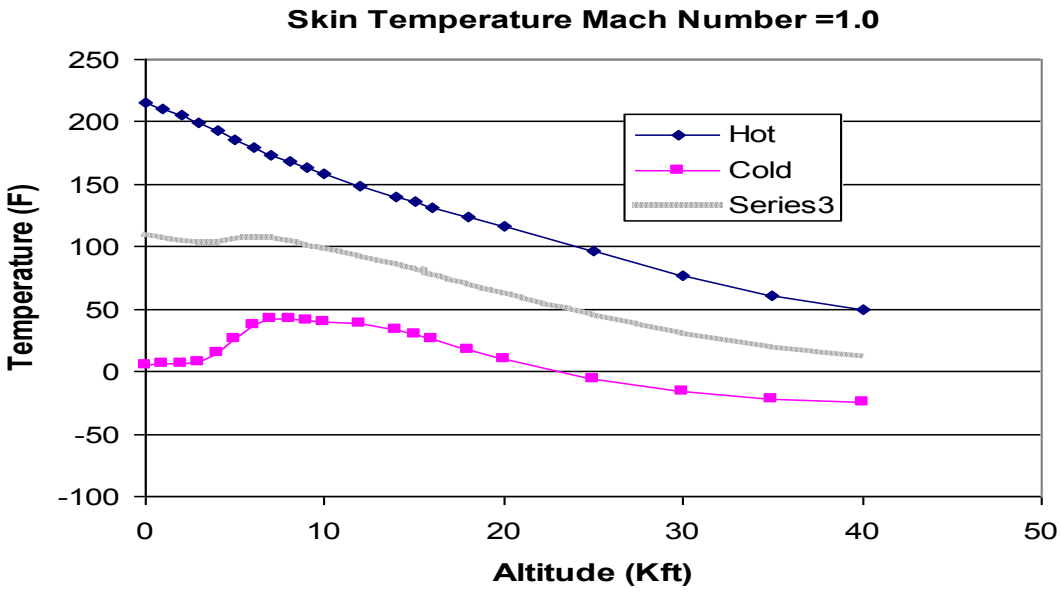

Figure 89. Skin Temperatures From MIL-STD-210

For acoustic fatigue design, a factor of safety of +3.5dB is added to the spectrum. Also, static pressure and thermal loads are assumed worst case. In this case, ΔP=-5psi and ΔT=130 F (200 F – max).

Summary

The following example demonstrates the design and analysis issues of predicting acoustic response and fatigue of aircraft panel subjected to high acoustic loads coupled with high static and mechanical loads. Flight test data was used to identify the critical flight conditions. Mach, Altitude, Load Factor, AoA. Also, external loads (pressure, acoustic, and thermal) were measured or predicted at this critical condition, as well as, the structural response: accelerations and strains. Initial fatigue estimations used approximate solution methods; similar to those found in the Sonic Fatigue Design Guide. For detailed panel level analysis, Linear Random Frequency Response Analysis was performed for Acoustics only, and thermal and static loads were superimposed. The main highlight is the importance of including the static load effects, and using a nonlinear simulation.

Aero-heating analysis	Mil-Std-210, Standard Skin Recovery Model
Thermal analysis	Mil-Std-210, Standard Atmosphere Model
Acoustic loads generation	Empirical, Flight Test Measured
Mechanical/design loads generation	Global Loads FEM, Measured

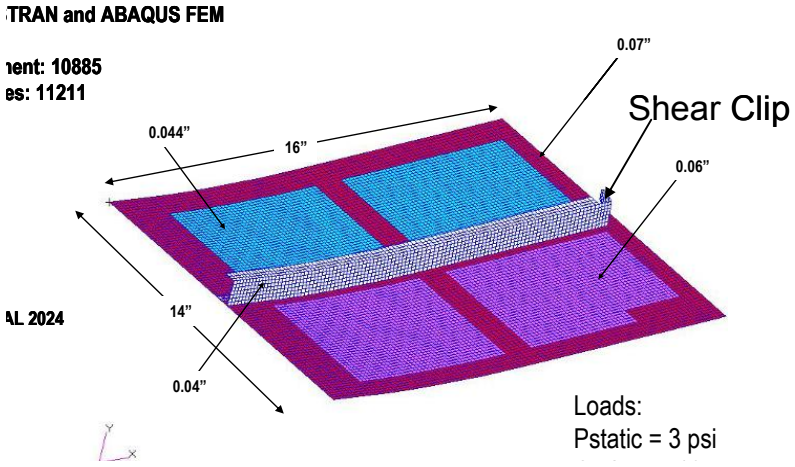

Figure 90. Finite Element Model of Panel

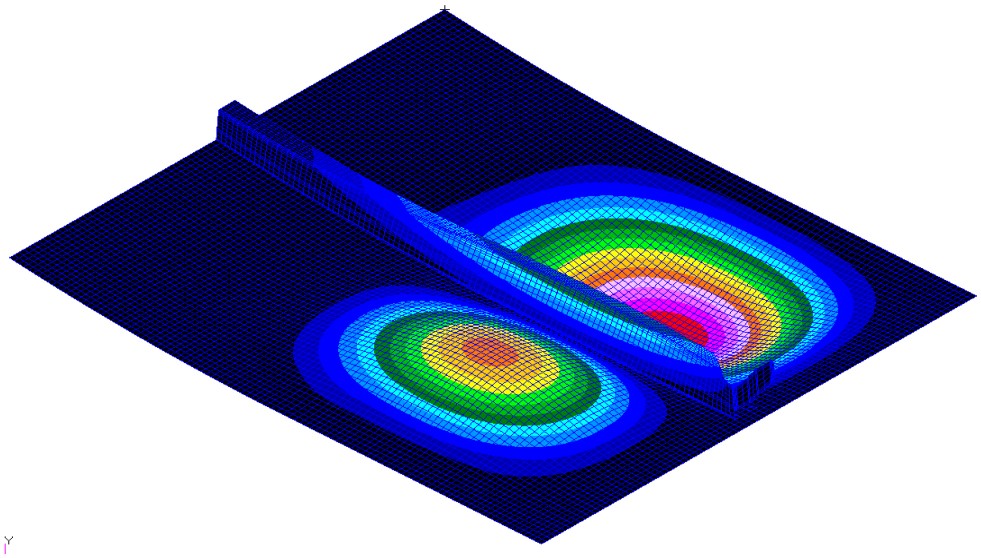

Figure 91. Mode Shape For Baseline Model Mode 1, 281 Hz

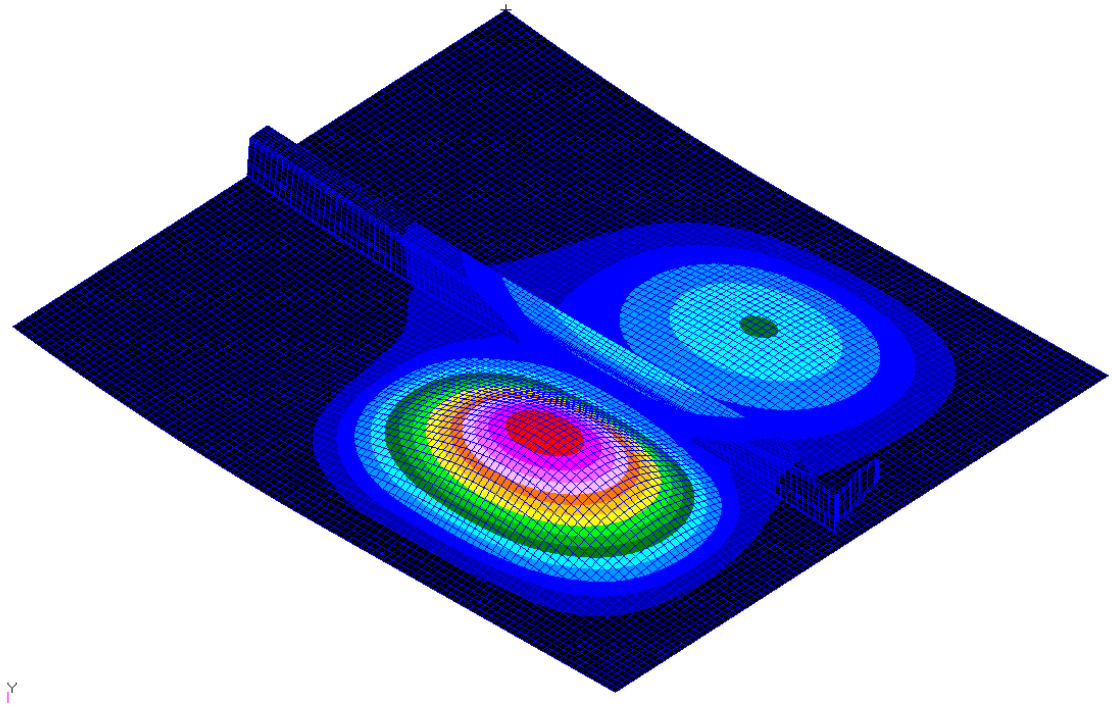

Figure 92. Mode Shape For Baseline Model Mode 2, 334 Hz

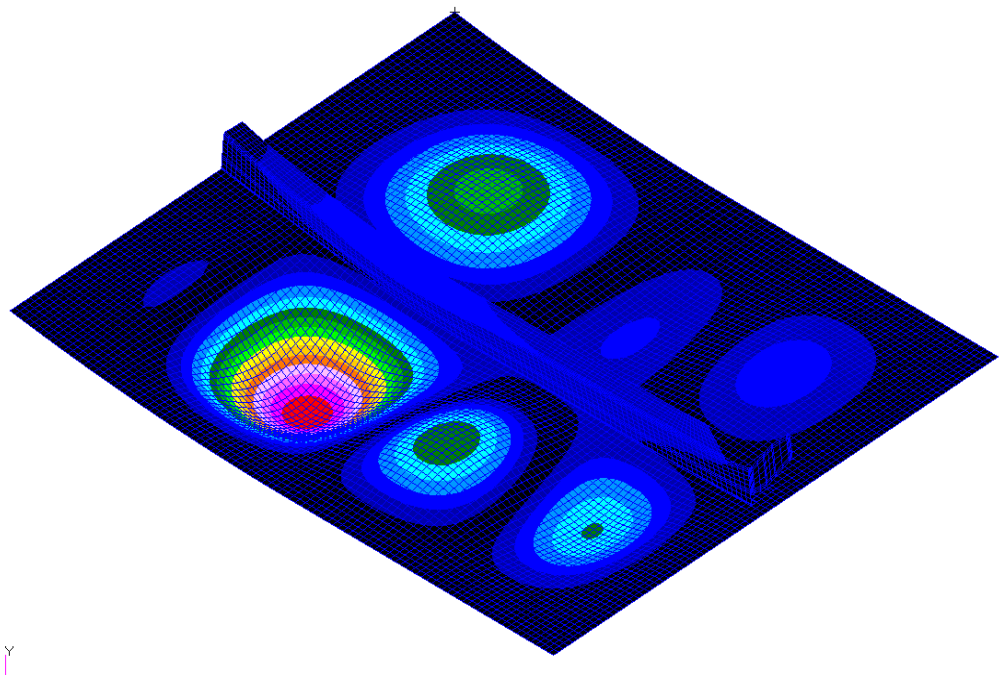

Figure 93. Mode Shape For Baseline Model Mode 6, 568 Hz

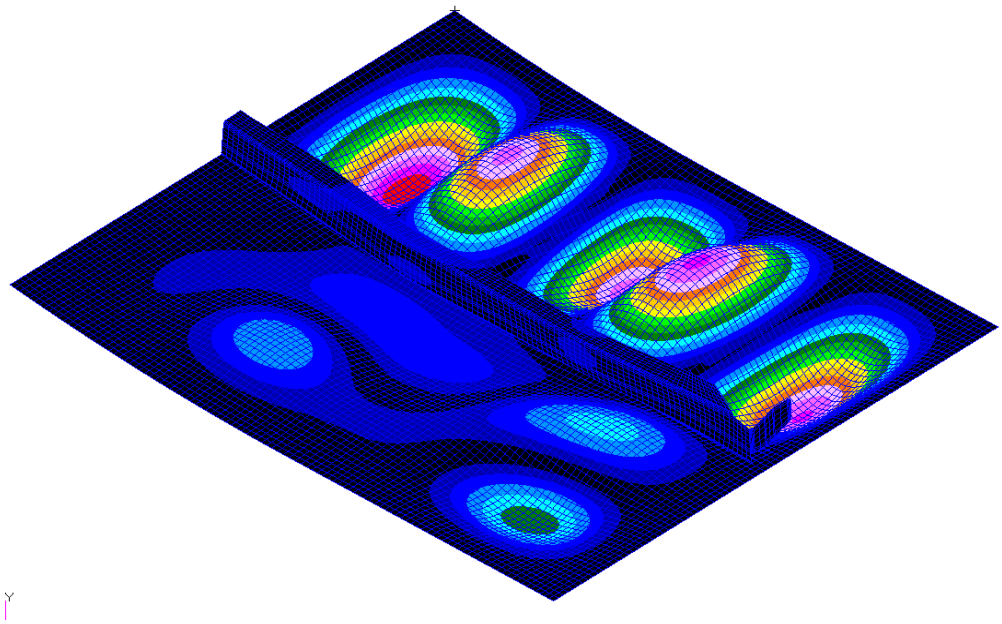

Figure 94. Mode Shape For Baseline Model Mode 14, 873 Hz

The linear NASTRAN results are shown in Figure 95 thru Figure 98. The normal RMS displacement is shown in Figure 95. The center bay displacements are most certainly nonlinear since they are two to three times the skin thickness. The acceleration is shown is Figure 96. The

RMS stress is shown in Figure 97 and Figure 98. The max RMS stress is at the edge of the panel, but there is a hot spot in the integral shear clip. We know from testing that the shear clip is the critical fatigue location.

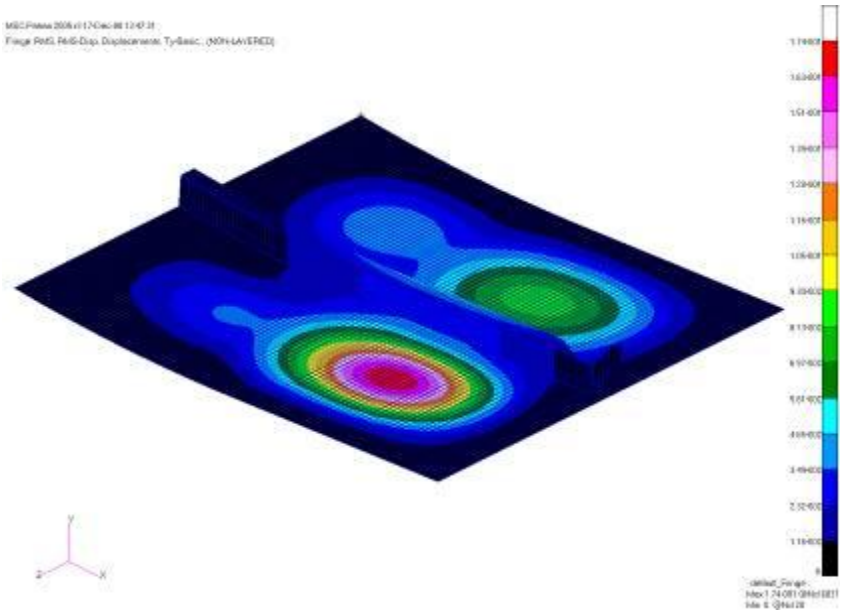

Figure 95. NASTRAN Linear RMS Y-Displacement (Inches)

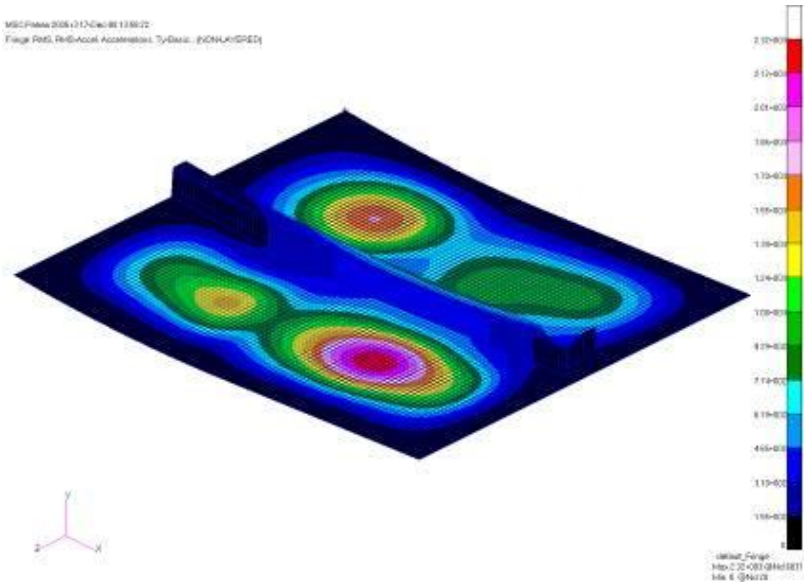

Figure 96. NASTRAN Linear RMS Y-Acceleration (Grms)

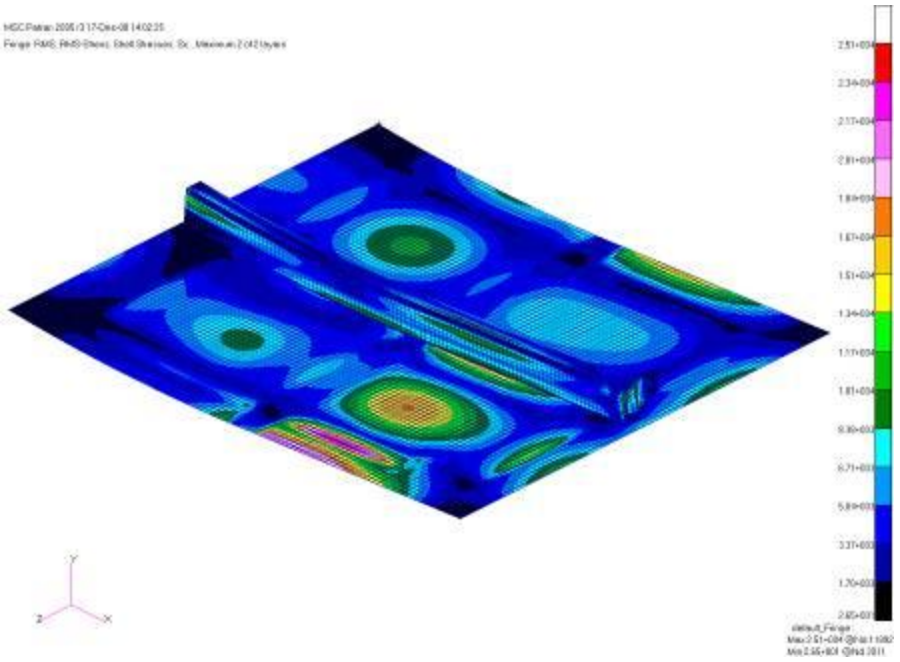

Figure 97. NASTRAN Linear RMS Sx-Stress (psi)

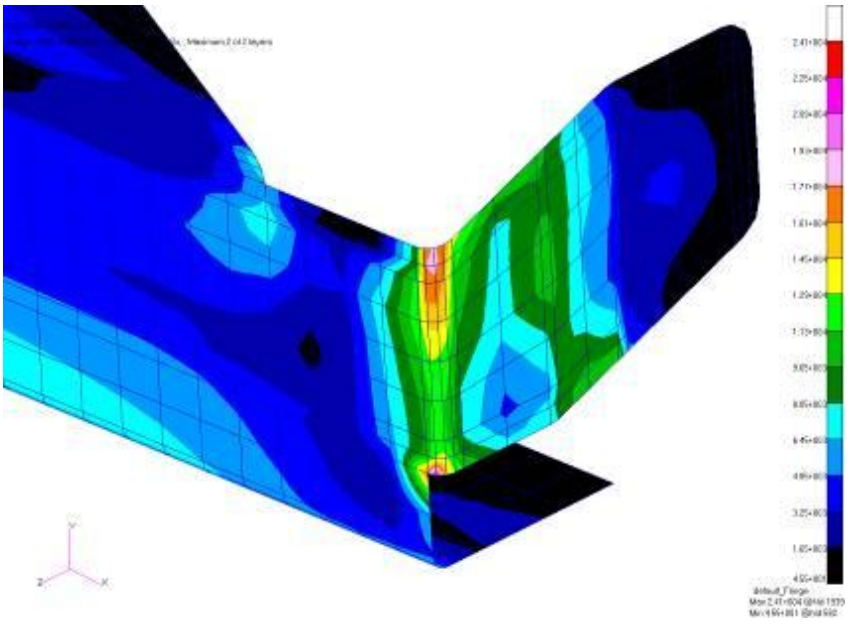

Figure 98. NASTRAN Linear RMS Sx-Stress (psi) (Shear Clip Location)

The reference strain gages (element) and accelerometer (node) locations are shown in Figure 99 and Figure 100. A few comparison PSD between linear random frequency response and nonlinear explicit response are shown in Figure 101 (acceleration in the skin bay) and Figure 102 (stress in the clip). The peaks in the nonlinear response are generally lower with noticeable shifts in frequency. It can be concluded that the linear response is much more conservative.

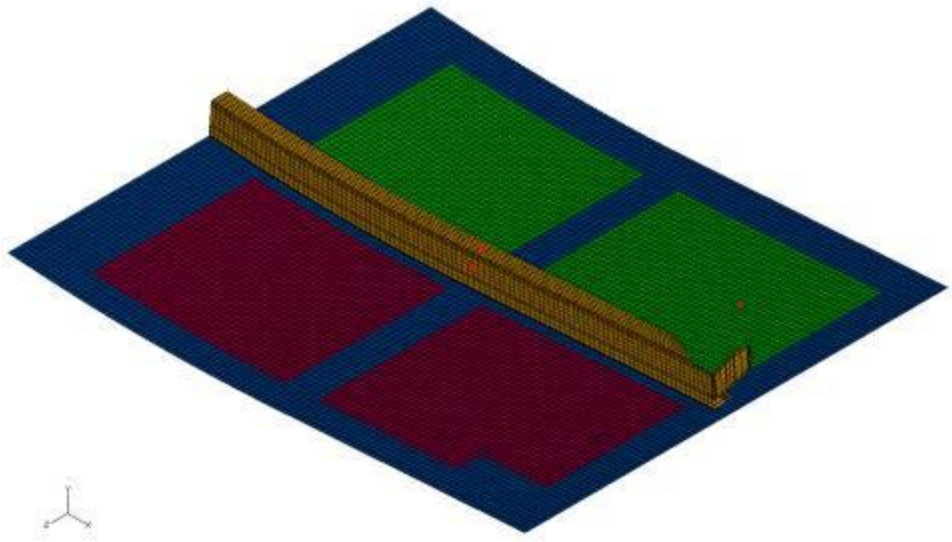

Figure 99. Reference Accelerometer (Node) Locations To Be Used In Study

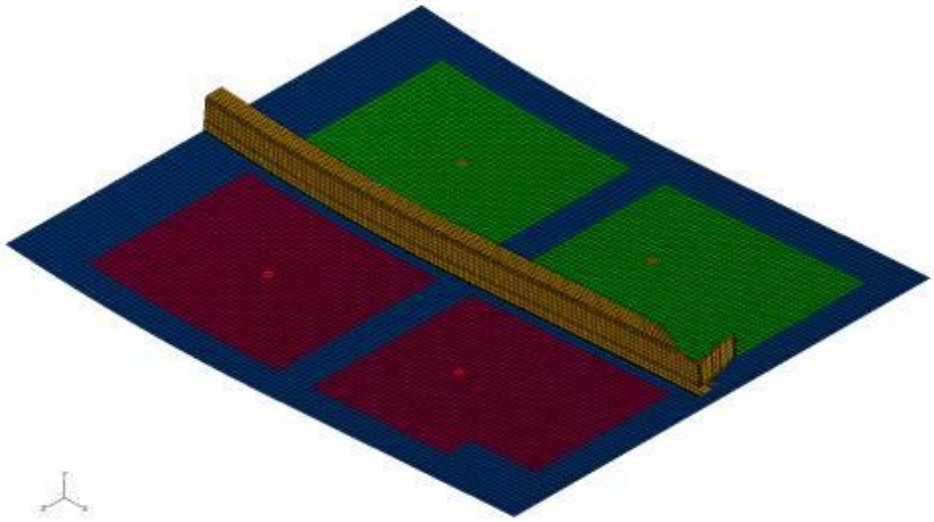

Figure 100. Reference Strain Gage (Element) Locations To Be Used In The Study

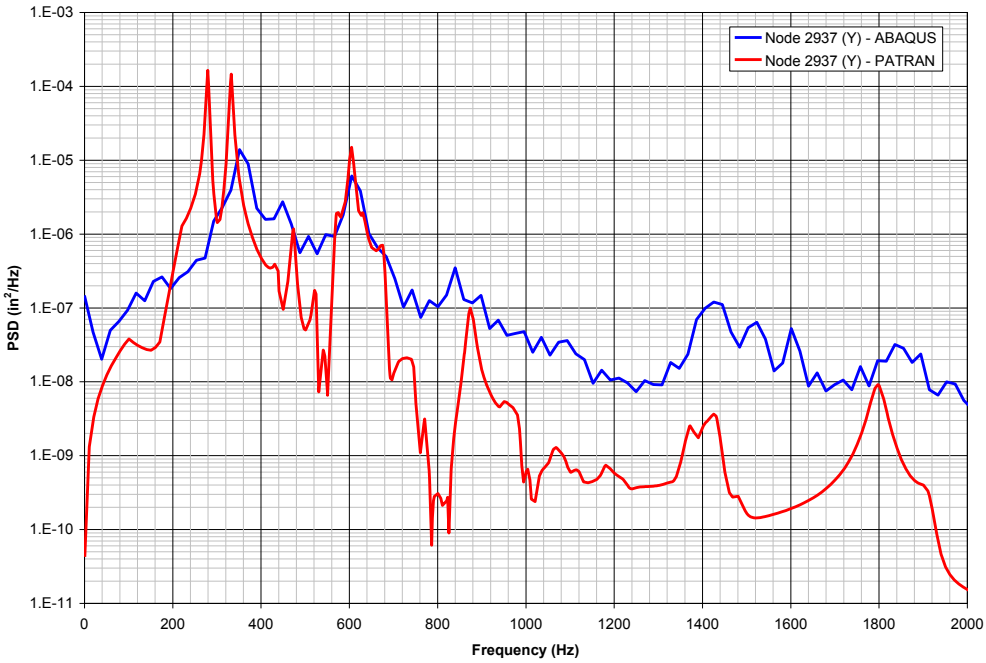

Figure 101. Center Bay (On Skin) Y-Acceleration

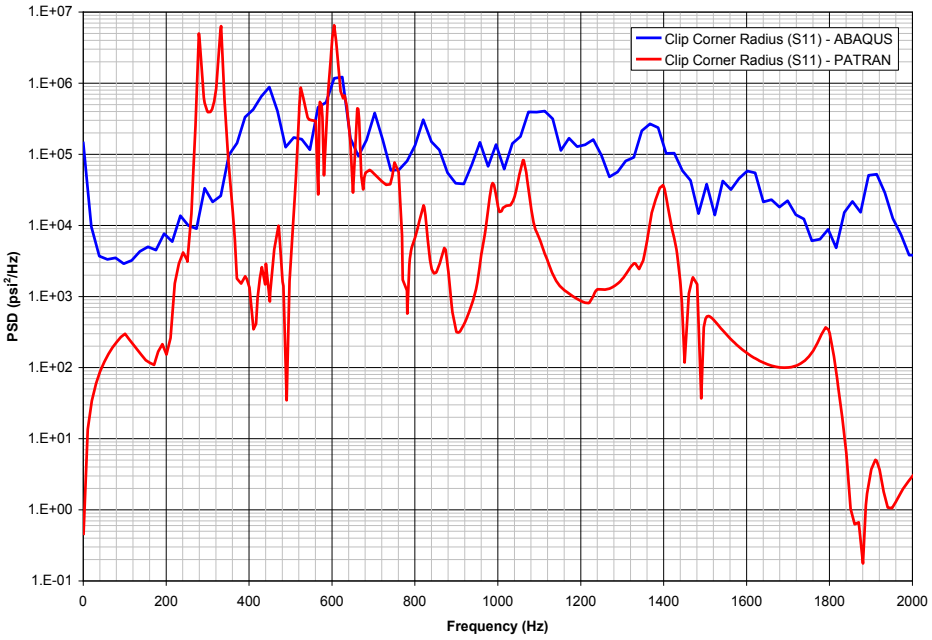

Figure 102. Clip Radius Corner Stress Sx PSD

The NLROM results are compared to the ABAQUS/Explicit solution, as well as to available laboratory test data. Essentially, this is an analysis-to-analysis comparison. The NLROM model used five modes. The acoustic loading was applied as two independent load cases with each applied over half of the panel. This allowed for asymmetric mode response. The load cases are

essentially independent (having no correlation). The damping was set zeta = 0.02. The time integration was □T=1/4000 Hz. The NLROM analysis was run at several OASPL levels, as shown in Figure 103. The general nonlinear stiffening behavior is clearly seen as panel frequencies increase and the peaks broaden. The model was also run with a static preload of 3 psi. The static preload effect on the panel response is shown in Figure 103. The static load also stiffens the panel and changes the mode shapes. As can be seen in the figure, the 600-Hz mode becomes more prominent. The preload effect is more pronounced in Figure 104, which shows the integral shear clip stress. From Figure 105, the linear model does not accurately predict either the magnitude or the spatial distribution of loads and stresses in the panel, so it is evident that a nonlinear simulation is required.

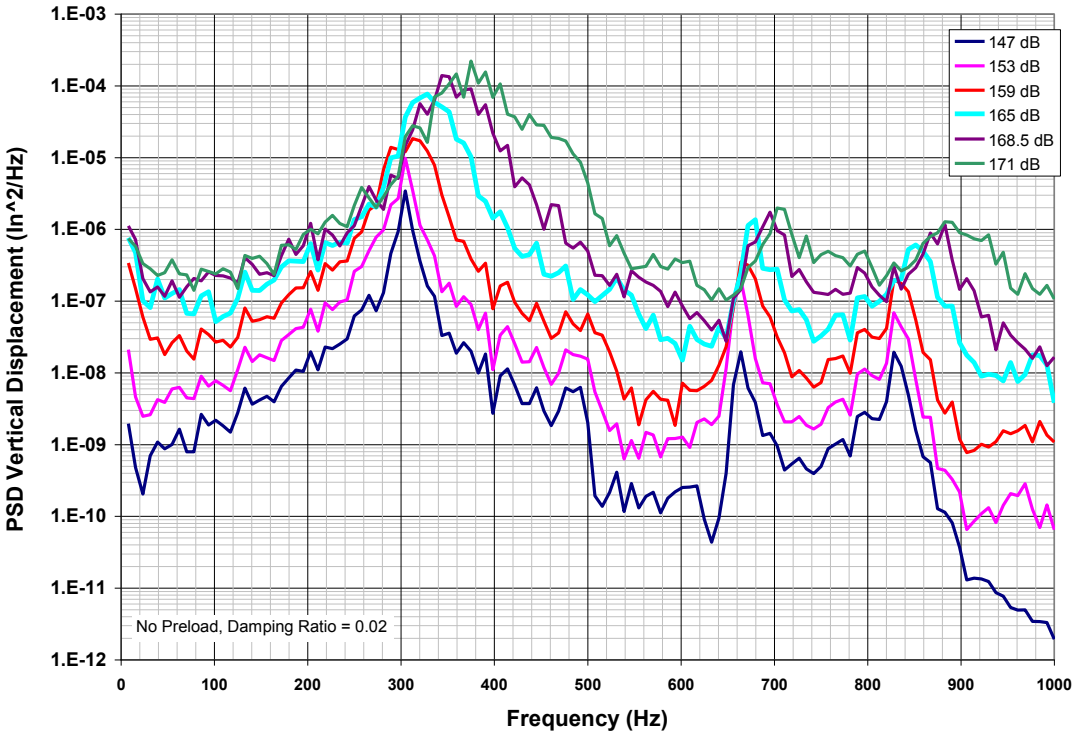

Figure 103. NLROM Simulation at Different Load Levels and Without Preload

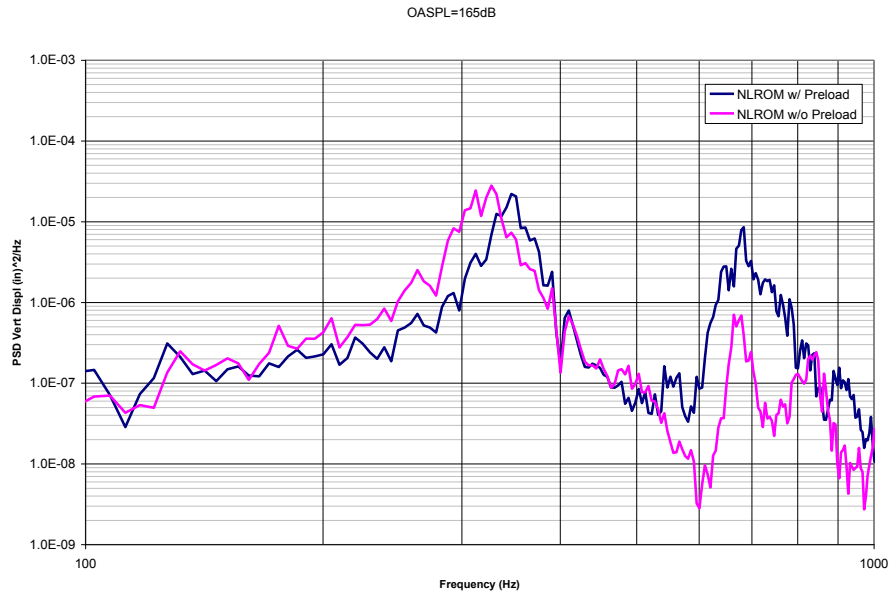

Figure 104. Panel Displacement, NLROM Simulation W/ and W/O 3-Psi Preload

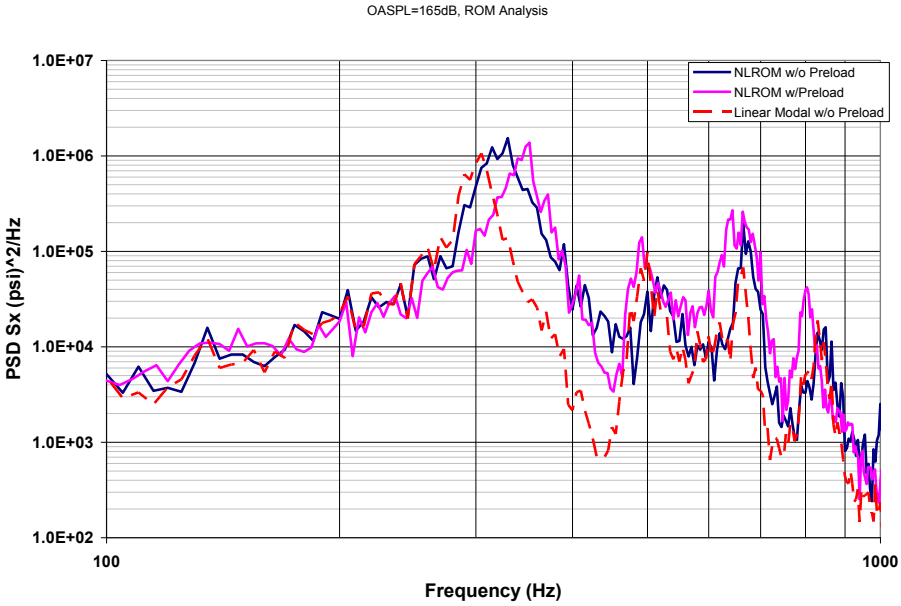

Figure 105. Clip Stress, NLROM Simulation W/ and W/O 3-Psi Preload

The ABAQUS/Explicit and NLROM solutions used the same mesh, boundary conditions, material properties, and damping. The NLROM solution compared well to the ABAQUS/Explicit solution, although there were some differences in the frequencies and mode shapes between the NASTRAN/NLROM model and the ABAQUS/Explicit full-order model. Because the comparison was not as close as it was in the curved panel test case, there were some differences in the response. However, overall the responses in the panel and at the critical stress location in the clip (Figure 106) match very well with the preload.

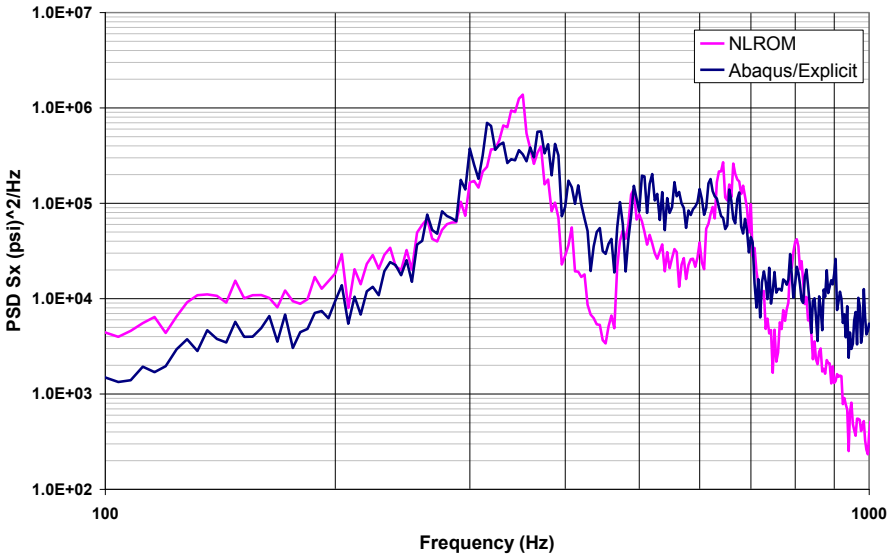

Figure 106. Stress in the Clip at the Edge of Panel, OASPL = 165 dB, Ps=3psi

Fatigue-life prediction is carried out by counting the number of cycles to failure; results are shown in Table 20. The fatigue life as measured in the laboratory tests on several specimens ranged from 1800 to 3200 seconds.

Table 20. Life Prediction Results

	OASPL =165dB Ps=3psi
	Life in Seconds to Failure
NLROM	4319
Full-Order	3705

Lab test data was available for the stiffened curved test panel. The testing was performed in the Progressive Wave Acoustic Facility (Figure 107). An acoustic strain survey was performed on the panel at several combinations of static pressure and acoustic noise levels. Also, all testing was performed at ambient conditions. The panel was then tested to failure at OASPL=165dB and Ps=-3psi. The failure was a crack that initiated in the panel's stiffener integral shear clip, Figure 108. The panel was instrumented with 16 strain gages, three accelerometers, one static pressure transducer, 1 thermocouple, and two control microphones inside chamber, Figure 109. The analysis is compared to the laboratory test data.

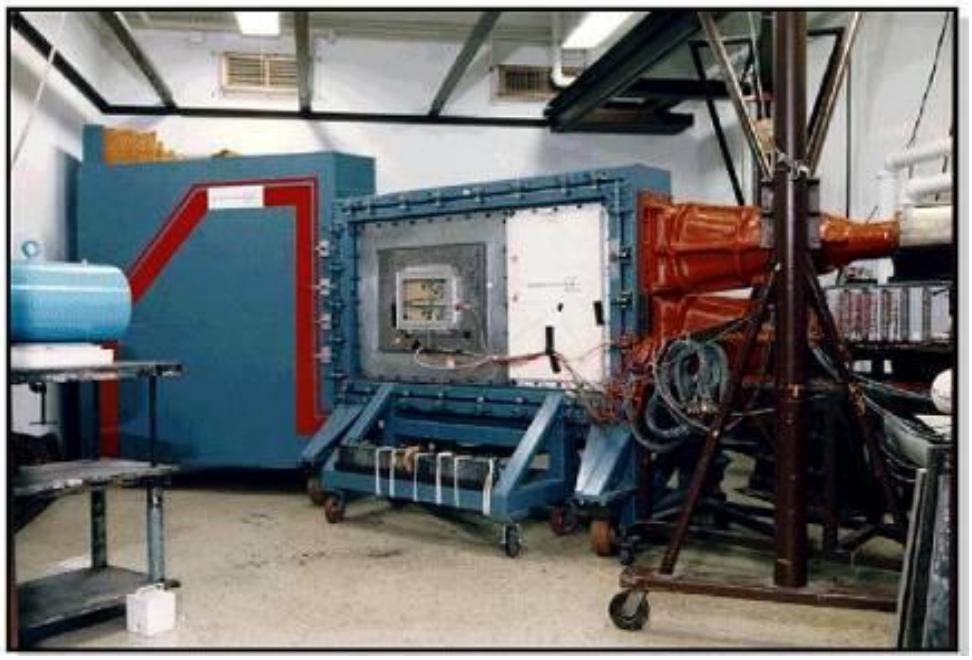

Figure 107. Progressive Wave Chamber

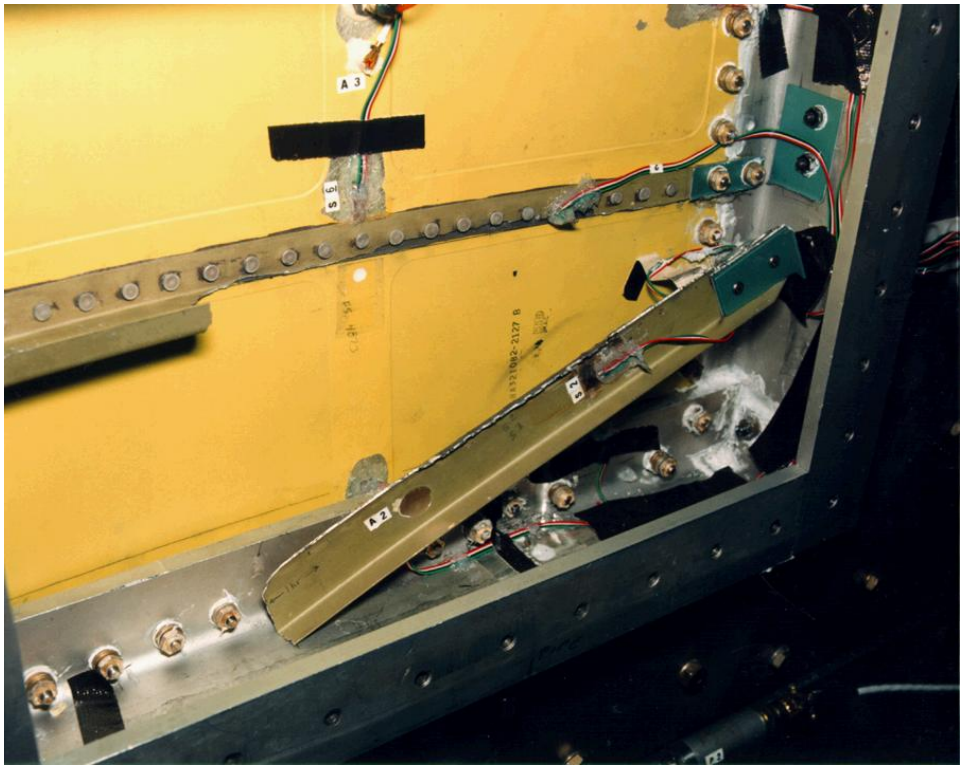

Figure 108. Test Panel Failure Mode

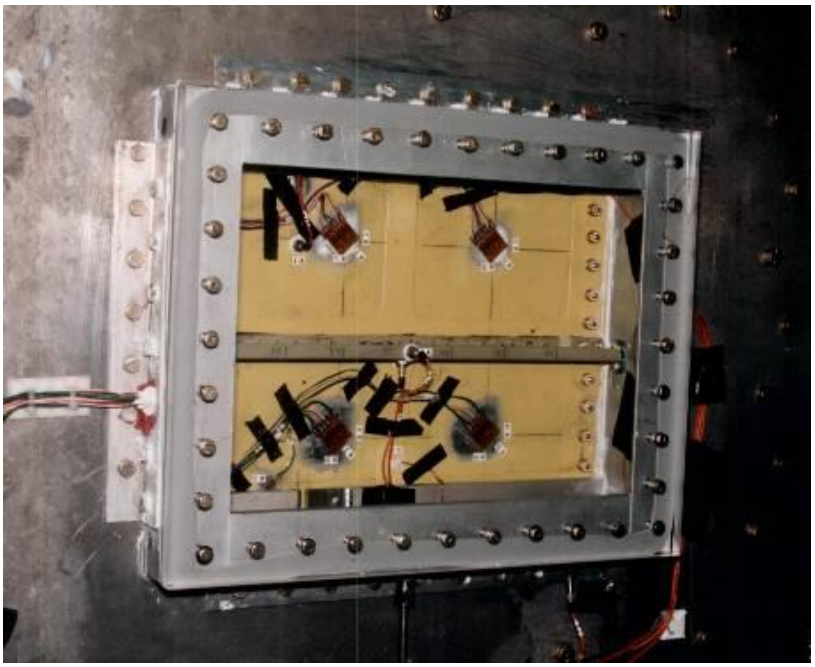

Figure 109. Test Panel Mounted in Facility Side Wall in Pressure Plate Fixture

The panel frequencies are listed below in Table 21. These can be seen in the representative Frequency Response Functions (FRF) shown in Figure 110 and Figure 111.

Table 21. Experimental Panel Frequencies

Mode Number	Frequency (Hz)
1	280.
2	309.
3	414.
4	433.
5	461.
6	515.
7	587.
8	635.
9	679.
10	698.
11	731.
12	792.

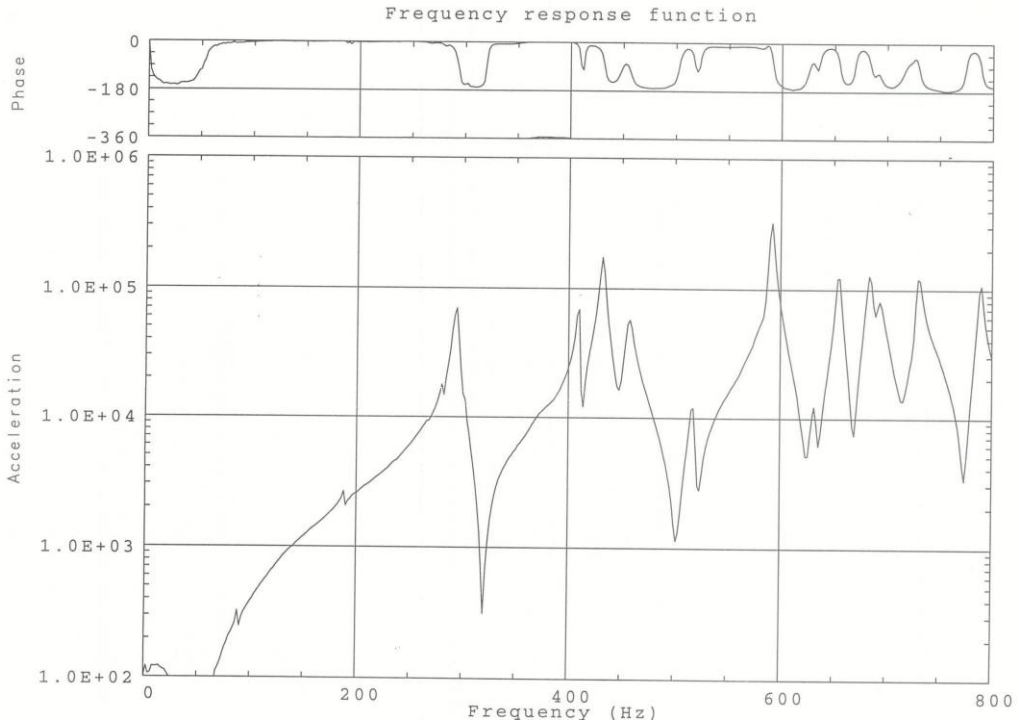

Figure 110. Mid Panel Upper RHS Skin Pocket

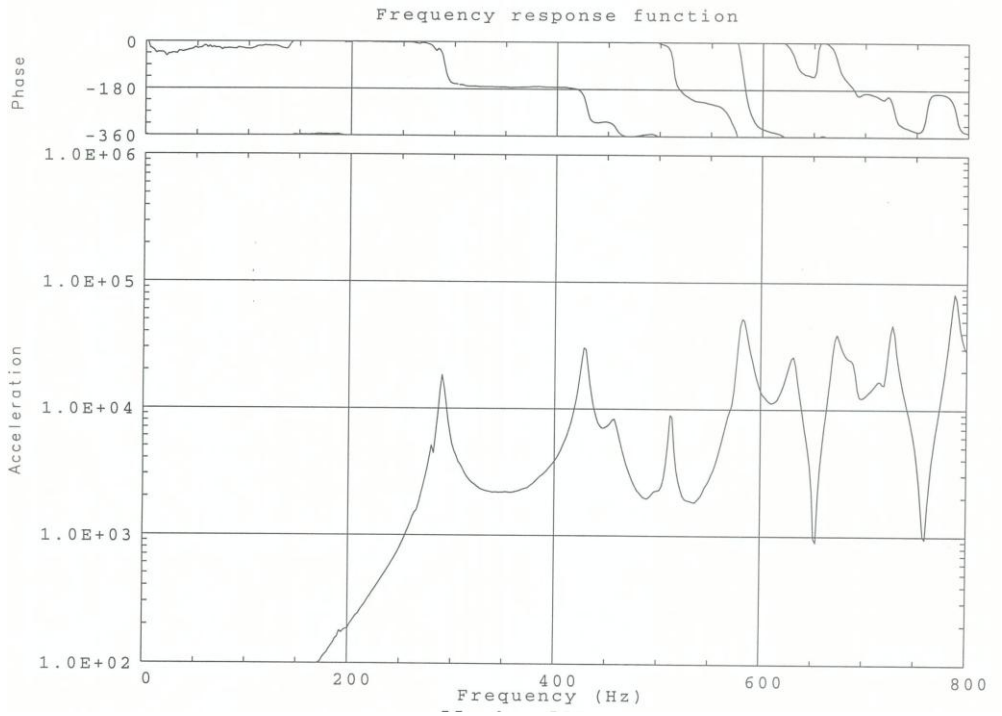

Figure 111. Representative FRF Mid-Stiffener on the Web

The analysis is compared to the lab test data in Figure 112 and Figure 113. The analysis generally captures the same trend in the test data. In Figure 112, the RMS strain in the stiffener

is shown compared to the test data. This was a gage approximately located at the end of the stiffener in the center of the web about 1 inch from the crack location in a lower strain gradient location. The second plot, Figure 113, is from the reference accelerometer in the center of skin pocket. In general, the model does a good job of predicting the RMS trends in the test data.

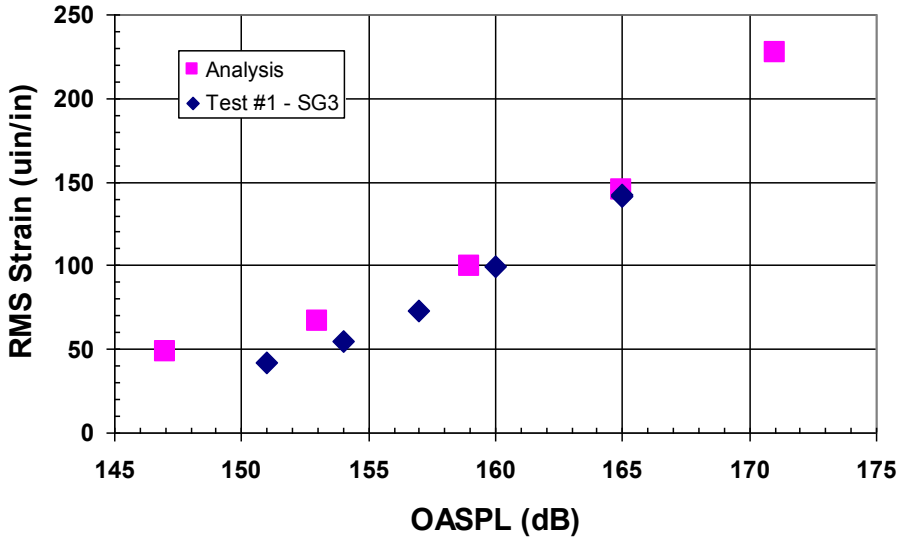

Figure 112. Reference Strain (Sg3) on the Former.

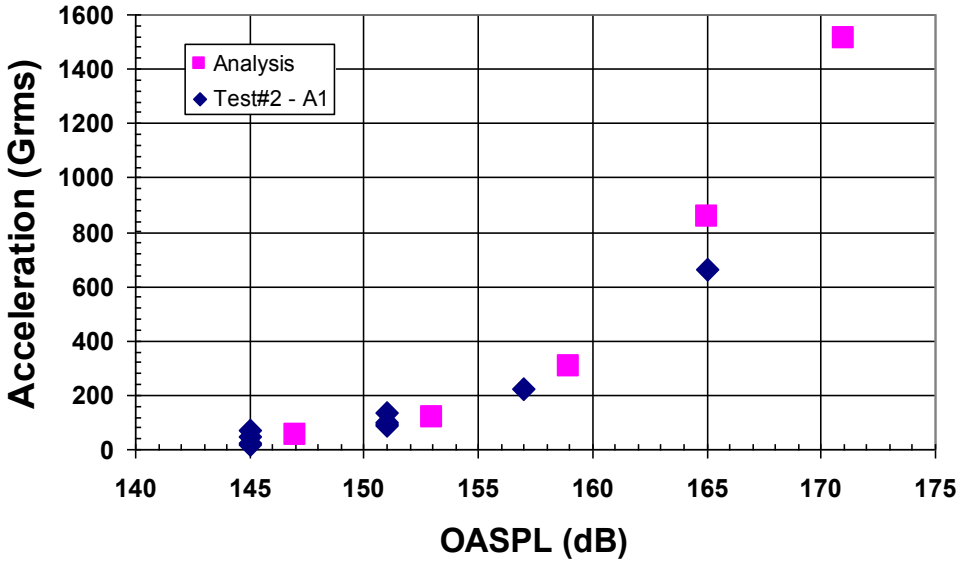

Figure 113. Reference Acceleration (AC1) at the Center of the Panel Bay.

APPENDIX C – TRANSPORT AIRCRAFT DATA

Fatigue Damage Investigation on a Transport Aircraft Fuselage Skin

Background-

In 2006 during routine visual inspection, a number of indications were spotted on an aircraft fuselage outer skin that suggested potential fatigue damage. The subject location was on the side of aircraft just fwd of the wing to body interface. At least one more subsequent visual inspection of same model aircraft, yielded a similar damage indication in the same fuselage area. This aircraft model, which will be referred to as Subject Aircraft or SA, uses thruster reversal during its landing maneuvers to reduce speed and bring the SA to stop on the airfield. The thruster reversal may be used when the engine power is on its full setting and results in direct impingement of jet engine out-flow on the fuselage in the areas that potential fatigue damage was spotted. Subsequent steady state CFD simulations also showed a direct correlation between the maximum overall sound pressure level points during thrust reversal and the locations with observed damage (Figure 114) and supported the initial speculation that the observed damage is a localized phenomenon and is due to increase fluctuating pressure and/or thermal loading from thrust reversal operation. The damage area consists of individual panels with approximately 9.5 by 24 inches longeron and frame spacing, respectively (Figure 115). The skin thickness in the area varies between 0.061 and 0.090 inch.

Two concepts, one for adding passive damping to out-of-plane panel modes using a damping layer, and a second concept for adding stiffness using structural doublers were considered for damage repair and prevention for the remainder of the SA fleet. Original design trades favored the damping layer solution because of its more efficient weight performance. However, flight test pressure measurements (Figure 116) showed that most of the input energy is in frequencies below 100 Hz with a significant steady state component. The flight test consisted of running the SA engines at ideal, half-power, half-power with thrust reversal, full-power, and full-power with thrust reversal with aircraft in parked and taxi positions. Similar to the pressure environment, the measured strain gage response (for the full power with thrust reversal) also showed that most of the response energy is concentrated at frequencies lower than panel's 1st resonance frequency (Figure 117). Since the response below the 1st resonance is governed by the stiffness, and at resonance frequency damping is effective in reducing the response, and above the resonance frequency mass has strong influence on response; it was concluded that added stiffness is needed to reduce the panel strain response.

Analysis-

To reduce the problem to a reasonable size for numerical analysis, a 4 frame by 5 longeron grid of fuselage along with the associated frames and longeron structures were modeled in NASTRAN using 2D plates and shell elements (Figure 118). The modeled grid includes all the panels treated by the Damper Layers and represent the primary impingement area during thrust reversal at longeron numbers greater than L17 (Figure 115). The FE model was refined in the zones with strain gage instrumentation during flight test. For the strain gage locations on the middle panel, panel thickness variation was modeled exactly. Other panels were modeled based

on the average panel thickness. A tap test was conducted to establish the modal characteristics of the panels as installed on the SA, the FE model showed acceptable correlation to the modal tap test results (Figure 119). A similar model of a 5 frame by 7 longeron grid was also generated to study the secondary impingement zone at longeron numbers smaller than L17 on the top surfaces of SA fuselage (Figure 120).

To derive the forcing function for analysis, the measured pressure fields at 2 symmetrical locations at each side of SA from flight test with max thrust reversal condition were averaged and fitted, in the frequency domain, by a piece-wise linear curve.

The linear FE analysis was conducted in frequency domain using Sonic Response Analysis (SRA), a NASTRAN-based Boeing proprietary analysis tool. The analysis process is schematically shown in Figure 121. Figure 122 through Figure 125 show typical analysis results for the fuselage skin, frame, and longeron strain contour plots; response PSD, and accumulated RMS plots. In an attempt to improve on the correlation between the analytical predictions and the measured strains/accelerations, various reasonable implementations of boundary conditions, damping schedule, cross-correlation between input PSDs, and fuselage skin to frame/longeron connection stiffness were investigated.

Four implementations of boundary conditions were considered: (1) Free, (2) Symmetric boundaries where the frames and longerons on the boundary are constrained in tangential /circumferential displacement along with radial and axial rotation, (3) Asymmetric boundary condition, and (4) fixed. The symmetric boundary condition generally improved the correlation. Coupling of the FE model to a reduced boundary stiffness matrix along with modal degrees of freedom was also considered, however, due to practical considerations, this approach was not implemented.

Three methods for specifying the pressure field cross correlation were investigated. (a) A correlated pressure field was applied over the entire 4 frame by 5 loneron bay model, (b) 5 equal but uncorrelated pressure fields were applied to 5 longeron zones, (c) 20 equal but uncorrelated pressure fields were applied to 20 individual panel zones. As expected, case a, does not exit the first group of panel bending (asymmetric) modes where the neighboring panels move in opposing directions. The 1st group of panel modes are excited by methods b and c as it is evident from the 1st PSD peak at below 150 Hz in Figure 126. It is also observed that methods b and c produce almost identical results with minimum 0, average 4%, and maximum 12 % difference in RMS strain prediction and less than 1% difference in RMS accelerations. It was concluded that it is adequate to treat the longeron bays as independent zones (method b).

Observations-

A number of collaborating evidences suggested strong non-linear effects:

1- Non-Gussian Response-

Statistical analysis of a the input process as measured by the pressure gages showed that the Skewness (S) and Kurtosis (K) values for the pressure environment were close to the theoretical values for a Gaussian process (S=K=0). However, the output process, as measured by the strain gages, with typical Skewness of more than 0.5 and Kurtosis of more than 3, was far from a

Gaussian distribution (Figure 126). Since a linear system will produce a Gaussian output from a Gaussian input, it is concluded that the system (structure) has behaved non-linearly.

2- Panel buckling under steady state pressure and temperature environments during thrust reversal-

The pressure gage data was low pass filtered at 100 Hz and the resulting maximum pressure was used in a linear buckling analysis using the same FEM. Analysis predicted panel buckling at a fraction of the low pass filtered pressure. As expected a similar analysis performed using the combined thermal and pressure environment confirmed the finding.

3- Large displacement effects on fuselage skin-

Standard deviation of the predicted panel deformation was approximately the same as panel thickness suggesting that the large displacement/membrane action in the fuselage skin is significant and small displacements/rotation assumption and linear analysis does not apply.

4- Non-linear contact between fuselage skin and frame/longeron-

Based on linear analysis results, full contact or no-contact assumption at the fuselage skin to longeron interface had sizable impact on the strain gage predictions.

In general the linear analysis predictions did not correlate well with the measured data. The general lack of correlation was attributed to non-liberalities in the structural system as listed in the above. Further non-linear analysis was recommended but due was not performed due to time and budget considerations.

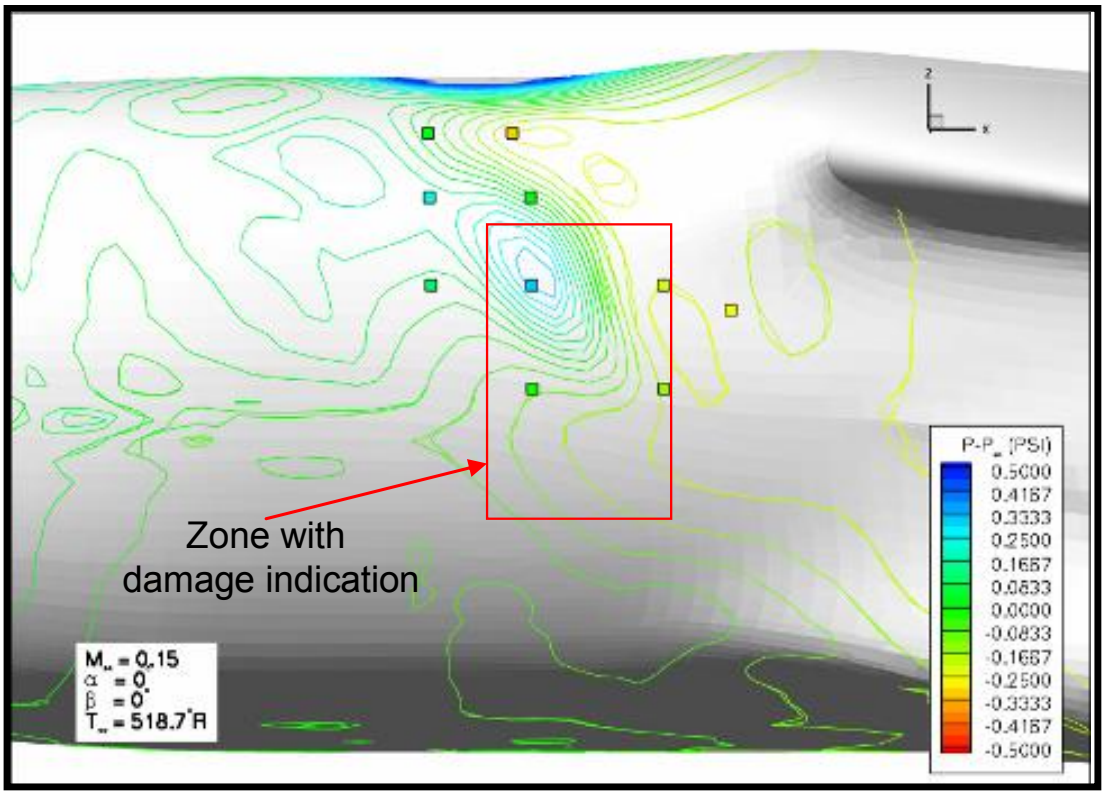

Figure 114. CFD Prediction of Iso-Pressure Contour Lines with Reverse Thrust

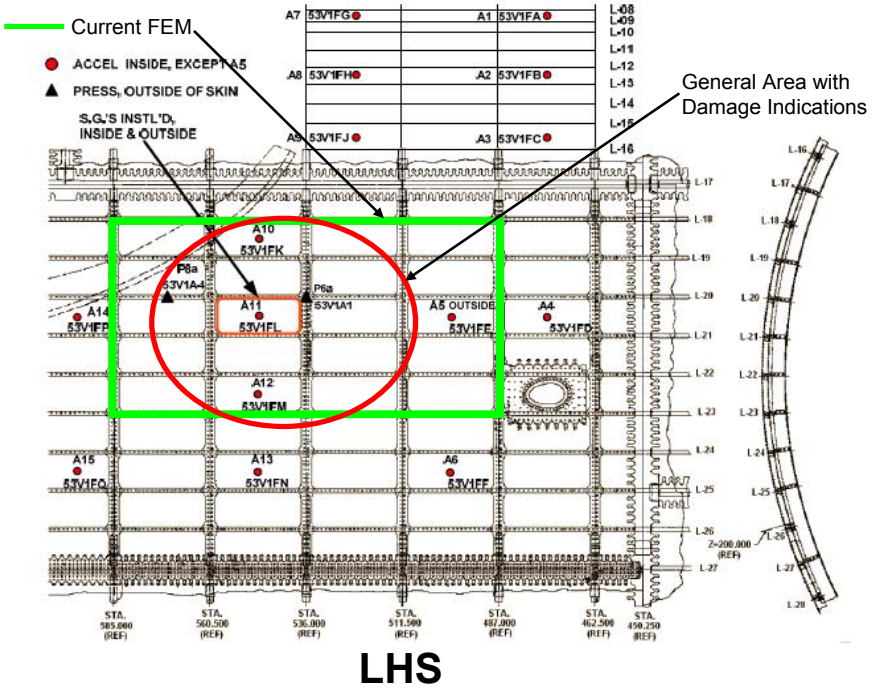

Figure 115. Fuselage General Layout

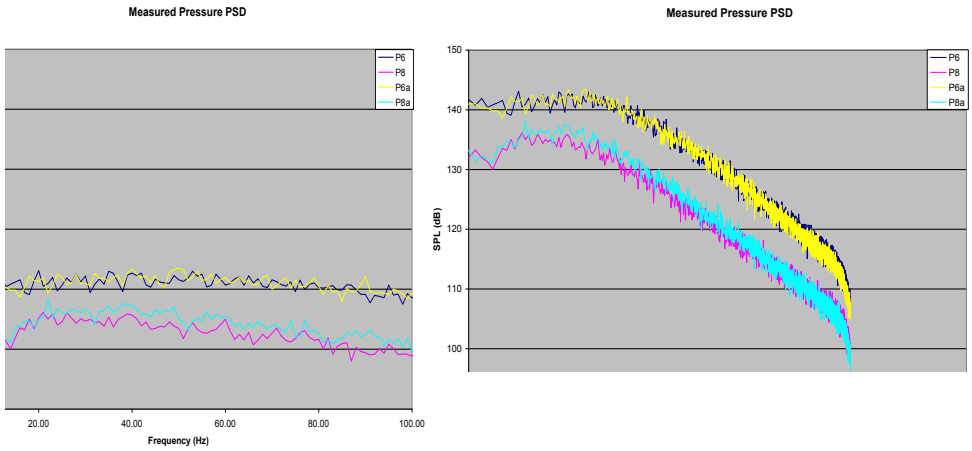

Figure 116. Pressure PSD Measured at Flight Test

The strain data collected from the flight test show no strong influence in strains from the panels natural frequencies

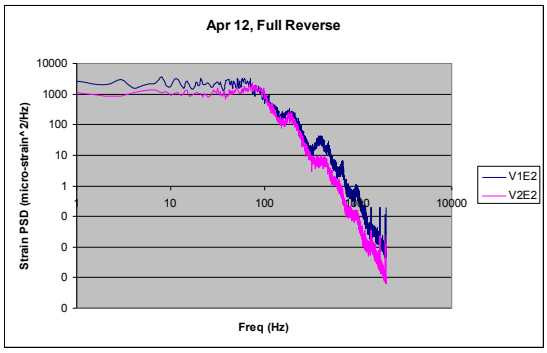

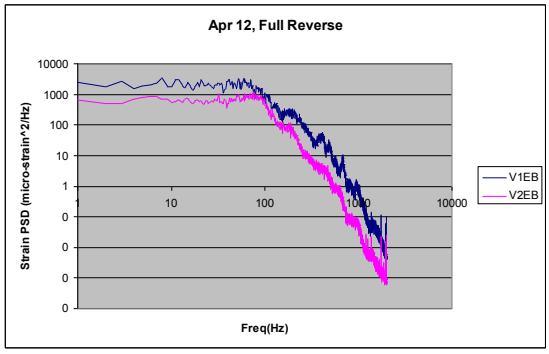

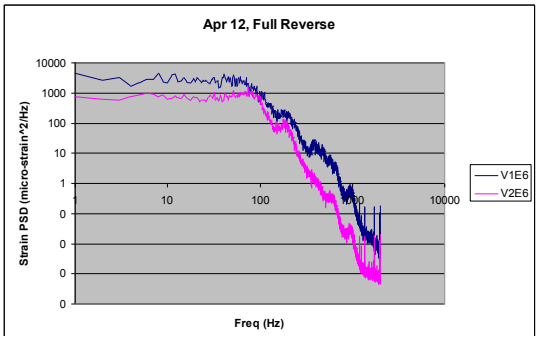

The strain response is highly concentrated in frequencies below the first resonance (well below 120 Hz).

Note: The blue curves are the untreated side.

Figure 117. Flight Test Fuselage Response with Panels Treated with Damping Layer

Figure 118. Finite Element Model of the Primary Thrust Reversal Impingement Area

	Analysis	Tap Test	
Mode No.	Freq (Hz)	Freq (Hz)	% Critical Damping
1	123.48	128.02	6.5
2	126.84	132.42	3.3
3	131.04	133.93	6.6
4	133.67	134.36	3.2
5	135.06	134.87	3.5
6	138.46	139.54	2.9

Figure 119. The Baseline FE Model is in Reasonable Agreement with the Measured Modal Characteristics of the "As Installed" Panels

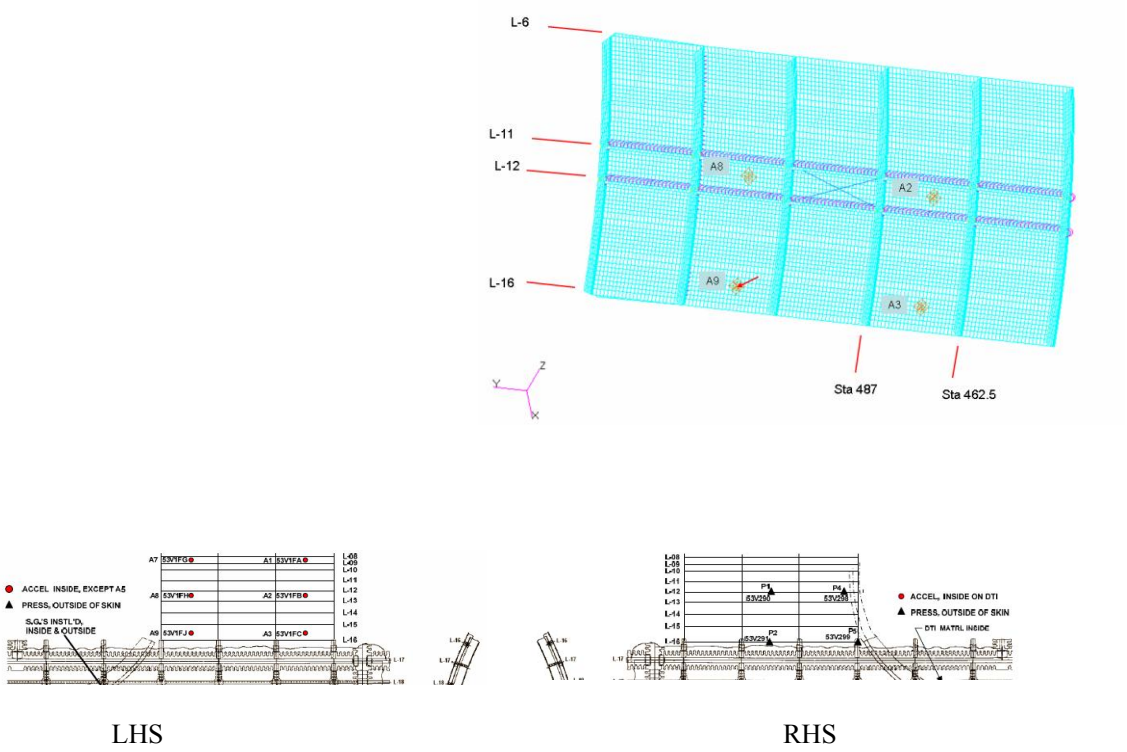

Figure 120. FE Model of the Secondary Thrust Reversal Impingement Zone

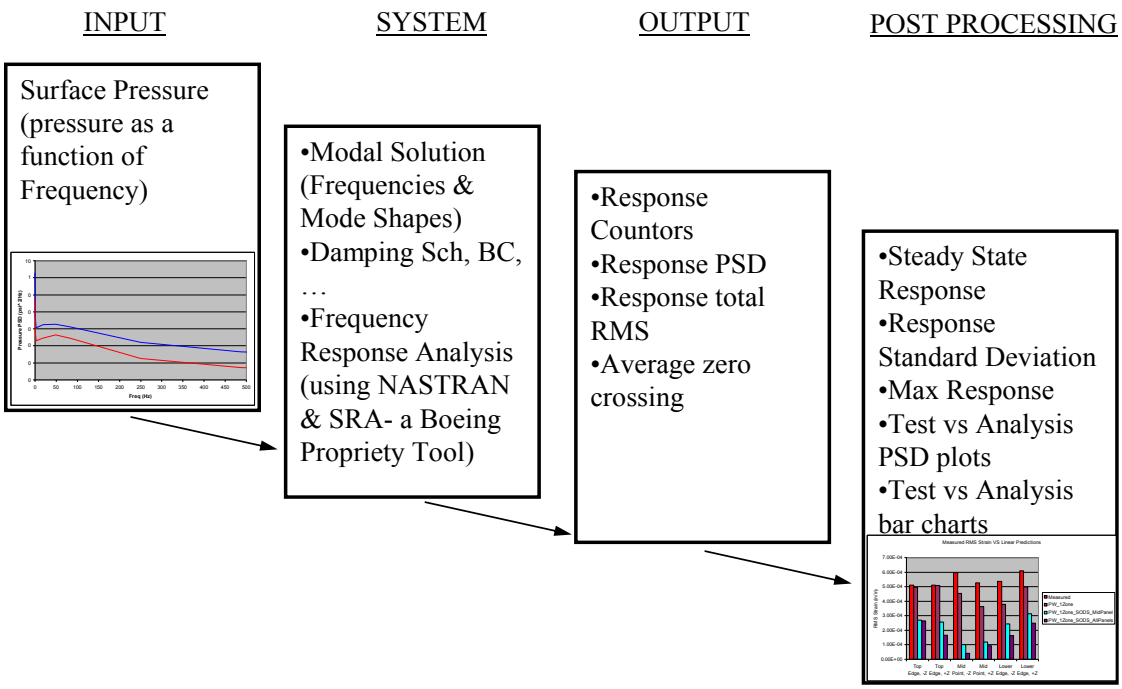

Figure 121. Analysis Process

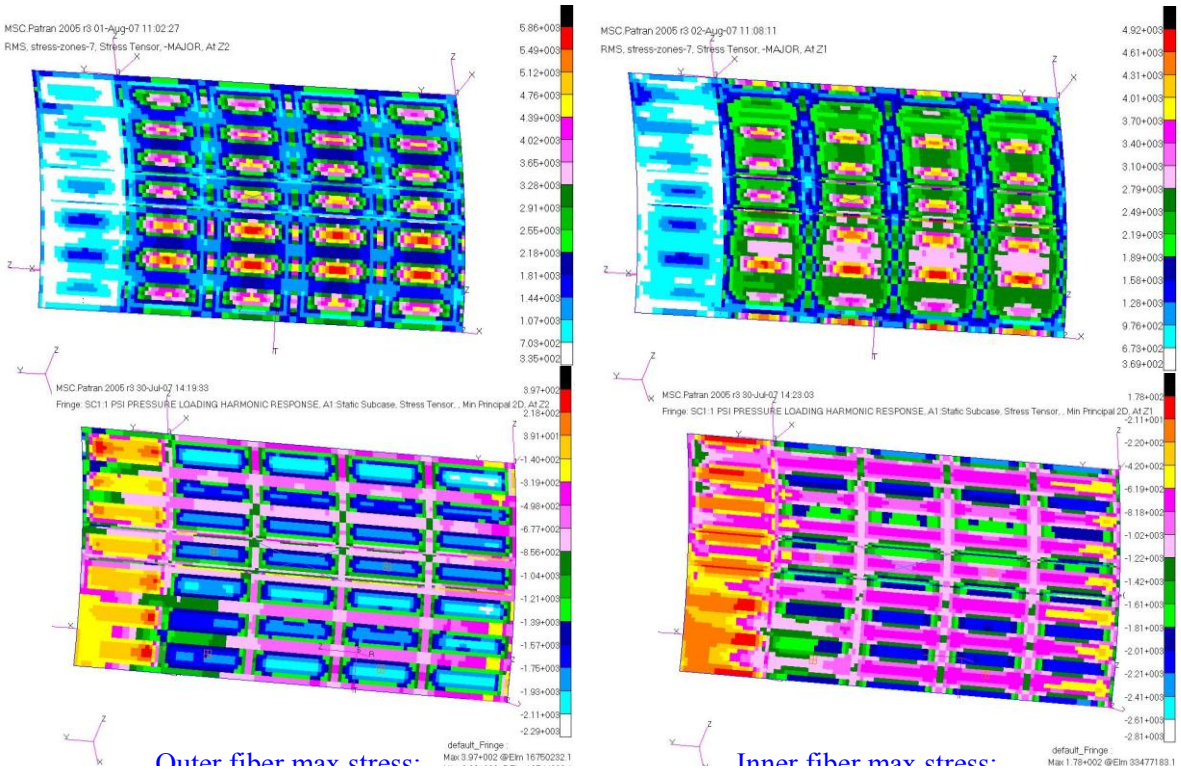

Figure 122. Typical Analysis Output

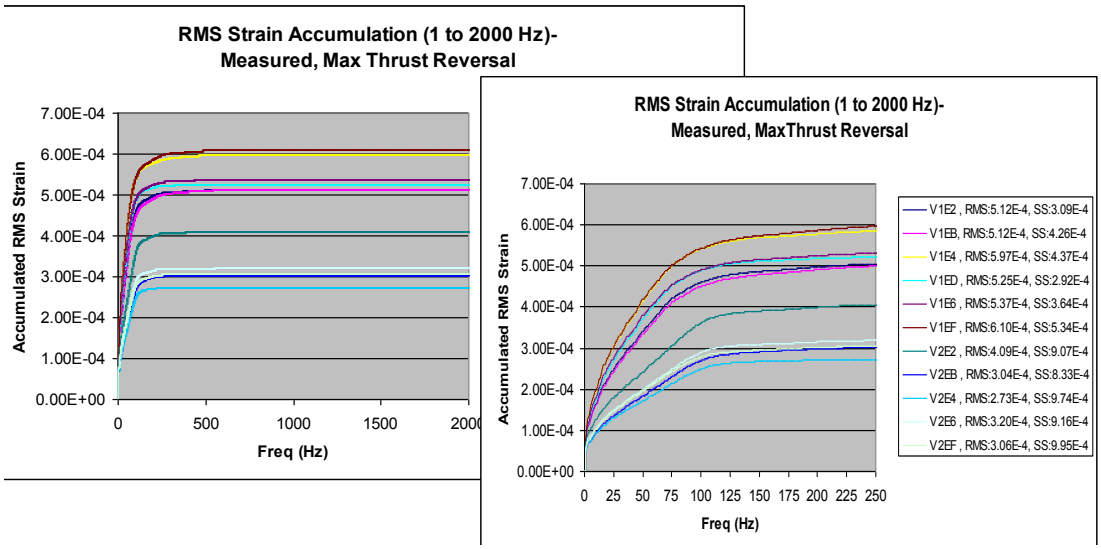

Figure 123. Based on Frequency Content of Measured Strains a Frequency Cutoff of 500 Hz Was Set for Analysis

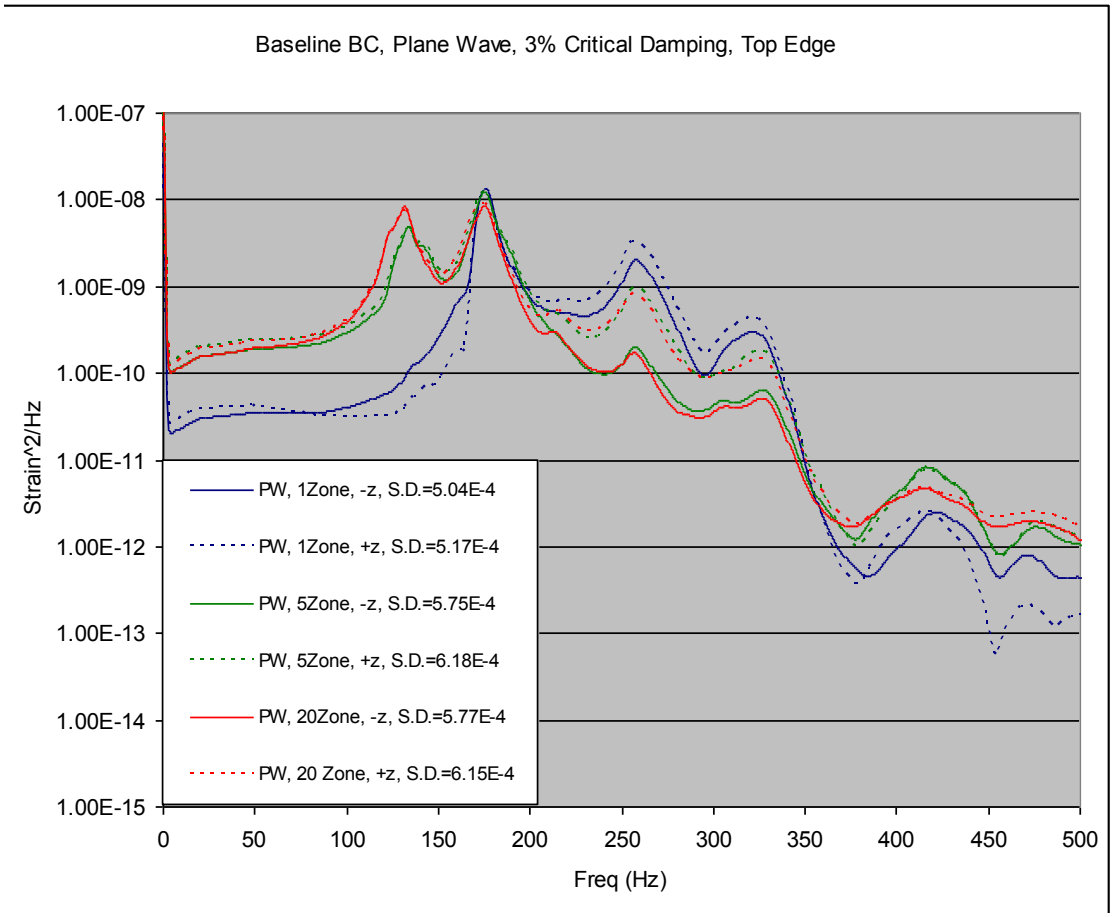

Figure 124. Effect of Input Zone Cross Correlation on Strain Predictions

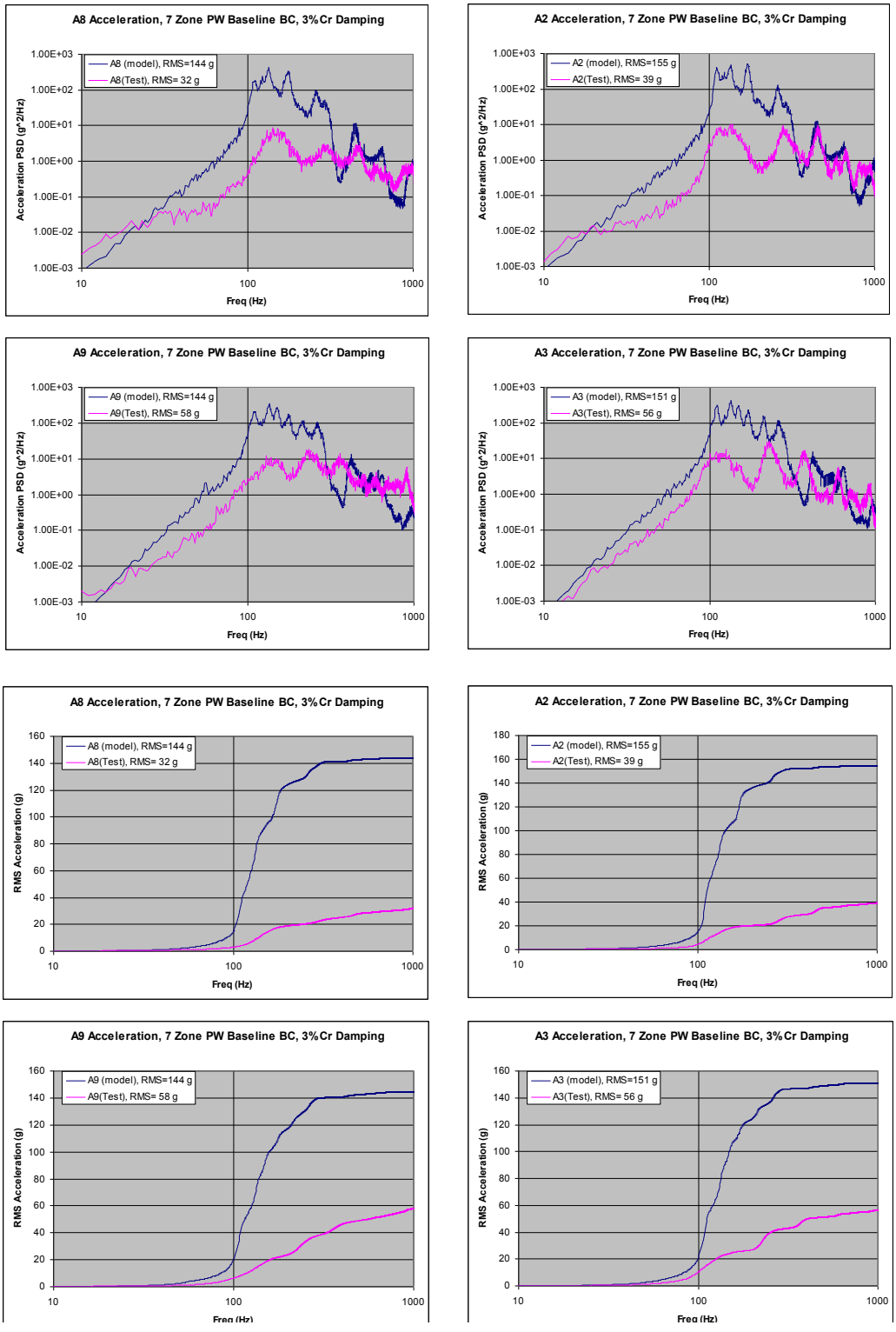

Figure 125. Comparison Between Measured and Predicted Responses

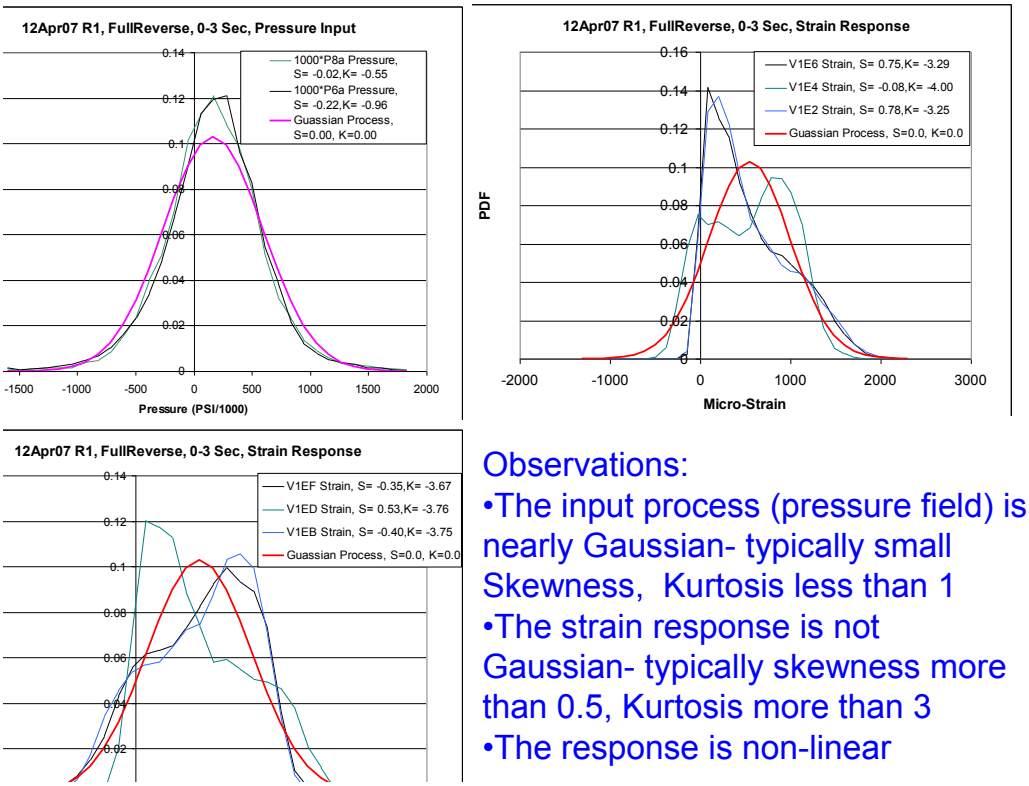

Figure 126. Probability Density Function of Measured Input (Pressure) and Output (Strain)

APPENDIX D – SCREENING METHODS FOR CRITICAL PANEL IDENTIFICATION FOR DETAILED ANALYSIS

Production Fighter/Attack Aircraft General Acoustic Fatigue Criteria

Aerodynamic flow noise and engine noise are the significant contributors to sonic fatigue for the high speed aircraft. To account for uncertainty, the absolute noise levels are increased by 3.5 dB during the analysis to comply with the factor of safety on sonic pressures of 1.5. All spectra are given relative to the OASPL in 1/3rd octave bands. Current sonic fatigue failure criteria are based on the fundamental resonant frequency response, and the acoustic loading is expressed in terms of the sound spectrum level at this frequency. The sound spectrum level (SSL) used in the sonic fatigue analysis is defined as the energy per unit (1 Hz) bandwidth. The spectrum level for equal energy distribution over a given 1/3rd octave band is calculated by the formula:

$$SL = OBSPL * 10 \text{ Log10} * \Delta f \qquad \text{(Eqn. D.1)}$$

Where OBSPL is the 1/3rd octave band sound pressure level in dB and Δf is the width of the 1/3rd octave band in Hz.

Aerodynamic flow can cause boundary layer noise, wake and vortex noise, cavity noise, base pressure fluctuation noise, protuberance noise (spoilers, stores, louvers, etc.), and oscillating shock noise. The aerodynamic flow acoustic loads are divided into three distinct categories: (1) boundary layer smooth flow, (2) average disturbed flow, and (3) maximum disturbed flow. Smooth flow is that which remains attached to the surface, (i.e. laminar flow). Average disturbed flow is separated flow that occurs behind protuberances or on the upper aft surfaces at moderate AOA. Maximum disturbed flow results from highly separated flow behind spoilers, large protuberances, or at high AOA. The aft control surfaces experience average to maximum disturbed flow when the angle of attack exceeds buffet onset, which is dependent on vehicle aerodynamics.

The general relation for definition of the overall sound pressure level (OASPL) for aerodynamic flow noise is

$$OASPL = 20 \text{ Log10 } Q + K. \qquad \text{(Eqn. D.2)}$$

This relation implies that for a given aerodynamic flow condition, the acoustic pressure is proportional to the free stream dynamic pressure. For flight dynamic pressures (Q) greater than 100 psf, OASPLs on the surface of the aircraft range from 132 dB up to as high as 171 dB. The highest levels are associated with maximum Q flight conditions and regions of disturbed flow (i.e. buffet and/or high AOA vortices, engine inlet duct flow spillage, etc.). Different regions of the aircraft experience different amounts of flow separation at increasing AOAs and therefore require the choice of various relations to define the aerodynamic flow noise. Typically, the aircraft will be divided into regions so that applicable aerodynamic flow noise loading for any location on the aircraft can be found by referring to a map of the aircraft surface. Aerodynamic flow regions and the maximum OASPL encountered in each region can be mapped to the aircraft surfaces based on CFD. Local regions are further divided into smaller distinct zones based on the magnitudes and trends in the measured data.

Production Fighter/Attack Aircraft Methodology Overview

The overall procedure used to evaluate structure for sonic fatigue consists of three operations. The first operation is to define the environment. Acoustic noise is not always the sole component of the fatigue environment. The structure may be subjected to a steady pressure from high-speed airflow. As well, for high speed aircraft, high temperature flight regimes can cause an elevated structural temperature resulting in thermal stresses/strains.

The second operation is to predict the response of the structure due to the environment. Various methods exist to predict the response of aircraft structure when subjected to acoustic excitation. Often, empirical methods utilizing simplified equations from test data for common structure are employed. Other times, analytic approximations are used. For simple skin/stiffener/substructure designs, the analytic and empirical algorithms are usually adequate and generally conservative. In addition to direct application for purposes of design, the simplified methods can identify areas of the structure where a more detailed analysis is warranted. The use of detailed finite element analysis has become more commonplace, especially in the sonic fatigue analysis of complex structure constructed with advanced materials such as composites. The use of finite element analysis can be costly and time consuming however.

The third operation is to predict the fatigue life of the structure. The life is a function of the structural response to the environment and the fatigue properties of the material. Aircraft structures generally experience sonic fatigue failure under one of two conditions. The first failure condition exists when the damage caused by the dynamic response of the structure exceeds the material fatigue allowable. That is, if the total number of exposure cycles (n) is greater than the cycles to failure (N) defined by the fatigue data (i.e. S-N curve) for the magnitude of structural response, failure occurs (i.e. n/N>1). This fatigue failure condition also exists when the accumulated damage from a series of exposures (n_i, i=1,m) at varying magnitudes exceeds the maximum allowed accumulated damage for failure (i.e. $\sum(n_i/N_i)>1$). The second type of failure is referred to as a quasi-static failure. This occurs when an instantaneous magnitude of response exceeds the static allowable for the material. The quasi-static failure is of more concern to composites rather than metallic structure. The general step-by-step approach to performing sonic fatigue analyses is outlined in this section. Some specific references are made to metallic panel sonic fatigue analysis in the general procedure.

Panel Structure

1. Establish the environment over the areas of interest

    a. Thermal-Acoustic-Usage (e.g. [^{o}F, OASPL, Time]=f(Q,AOA))

    b. Acoustic Spectra (i.e. OASPL, SSL=f(Hz))

    c. Apply 3.5dB factor of safety to acoustics.

    d. Steady pressure, if appropriate.

2. Establish the panel definition.

a. Dimensions (i.e. width (a), length (b), thickness (chem-mil pocket (skin) thickness (ts) and fastener land thickness (tl), as appropriate), radius of curvature (R), fastener details (fastener diameter (D) and fastener spacing (W)), etc.).

b. Material Properties (i.e. stiffness (Young's Modulus (E), poisson's ratio (ν), etc.), density (ρ), etc.

3. Specify damping (ζ, 0.016 is often assumed in absence of measured data).

4. Compute the fundamental natural frequency (fn) of the panel.

5. Correct the panel resonant frequency from previous step for panel curvature, as necessary

6. Calculate the acoustic sound spectrum level (i.e. SSL from step 1b above) at the panel frequency. Correct the spectrum level from previous step for panel curvature, as necessary. Note: Noise magnitude correction adjusts panel response to account for lower stress/strain due to panel curvature.

8. Compute the nominal root mean square structural response (σ_{rms}) of the panel at the location of interest (generally the center of the edge of the long side).

9. Compute the panel steady structural response (σ_{steady}).

10. Compute the panel thermal structural response ($\sigma_{thermal}$).

11. Apply the stress/strain concentration factor (K_t), as appropriate

12. Compute R ratio where; and,

$$R = \frac{\sigma_{min}}{\sigma_{max}} = \frac{\sigma_{static} - \sigma_{rms}}{\sigma_{static} + \sigma_{rms}} = \frac{\varepsilon_{min}}{\varepsilon_{max}} = \frac{\varepsilon_{static} - \varepsilon_{rms}}{\varepsilon_{static} + \varepsilon_{rms}}$$

and,

$$\sigma_{static} = \sigma_{steady} + \sigma_{thermal} \quad , \quad \varepsilon_{static} = \varepsilon_{steady} + \varepsilon_{thermal} \qquad \text{(Eqn. D.3)}$$

13. Consult the appropriate fatigue data and retrieve cycles to failure (N_i) for this loading condition. Note: In the absence of s-N data, the maximum structural response due to maximum acoustics is often compared to an Endurance and/or Design Limit. In the event that the maximum response is greater than the limit, finite life is indicated and redesign may be warranted.

14. Using resonant frequency (f_r) and exposure time (t_i), calculate exposure cycles (n_i) for this loading condition as,

$$n_i = f_r * t_i \qquad \text{(Eqn. D.4)}$$

15. Form damage fraction (D_i) for this loading as,

$$D_i = n_i/N_i \qquad \text{(Eqn. D.5)}$$

16. Repeat steps 5 through 14 for all loading conditions (i = 1 to m).

17. Perform cumulative damage calculation according to Miner's Rule as,

$$D = \Sigma D_i = \Sigma\,(n_i/N_i) \qquad \text{(Eqn. D.6)}$$

18. Calculate sonic fatigue life using total exposure time (i.e. $T = \Sigma\, t_i$) as,

$$\text{Life} = T/D \qquad \text{(Eqn. D.7)}$$

A sample analysis summary using the above method is shown below;

OVERALL SPL (dB)	EXPOSURE TEMPERATURE (deg F)	STATIC PRESSURE (psi)	EXPOSURE TIME (hr)	SPECTRUM LEVEL (dB)	THERMAL STRESS (psi)	STATIC STRESS (psi)	NOMINAL DYNAMIC STRESS (psi)	"R" FACTOR	EQUIVALENT DYNAMIC STRESS (psi)	CYCLES TO FAILURE	FATIGUE DAMAGE
** CHEM-MILL RADIUS **											
162.0	200.0	0.0	0.2	134.5	1340.0	0.0	12680.2	-0.81	0.141E+05	0.155E+06	0.662E+00
160.4	200.0	0.0	1.8	132.9	1340.0	0.0	10546.9	-0.77	0.117E+05	0.640E+06	0.144E+01
159.0	200.0	0.0	1.3	131.5	1340.0	0.0	8976.9	-0.74	0.996E+04	0.267E+07	0.249E+00
157.6	200.0	0.0	0.1	130.1	1340.0	0.0	7640.6	-0.70	0.848E+04	0.139E+08	0.370E-02
157.4	200.0	0.0	0.8	129.9	1340.0	0.0	7466.6	-0.70	0.829E+04	0.180E+08	0.229E-01
157.0	200.0	0.0	25.5	129.5	1340.0	0.0	7130.6	-0.68	0.791E+04	0.305E+08	0.429E+00
153.4	200.0	0.0	35.2	125.9	1340.0	0.0	4711.1	-0.56	0.523E+04	0.142E+11	0.127E-02
153.2	150.0	0.0	0.6	125.7	777.5	0.0	4603.9	-0.71	0.511E+04	0.216E+11	0.143E-04
152.0	200.0	0.0	8.5	124.5	1340.0	0.0	4009.8	-0.50	0.445E+04	0.194E+12	0.225E-04
151.8	150.0	0.0	82.1	124.3	777.5	0.0	3918.5	-0.67	0.435E+04	0.203E+12	0.207E-03
150.6	200.0	0.0	2.7	123.1	1340.0	0.0	3412.9	-0.44	0.379E+04	0.191E+13	0.724E-06
150.6	AMBIENT	0.0	0.1	123.1	0.0	0.0	3412.9	-1.00	0.379E+04	0.817E+12	0.628E-07
150.4	150.0	0.0	148.9	122.9	777.5	0.0	3335.2	-0.62	0.370E+04	0.143E+13	0.535E-04
150.2	AMBIENT	0.0	0.1	122.7	0.0	0.0	3259.3	-1.00	0.362E+04	0.127E+13	0.405E-07
150.0	150.0	0.0	0.1	122.5	777.5	0.0	3185.1	-0.61	0.354E+04	0.237E+13	0.216E-07
149.6	150.0	0.0	1.4	122.1	777.5	0.0	3041.8	-0.59	0.338E+04	0.387E+13	0.185E-06
149.0	150.0	0.0	0.1	121.5	777.5	0.0	2838.7	-0.57	0.315E+04	0.781E+13	0.657E-08
148.8	150.0	0.0	151.7	121.3	777.5	0.0	2774.1	-0.56	0.308E+04	0.978E+13	0.796E-05
148.6	150.0	0.0	0.2	121.1	777.5	0.0	2711.0	-0.55	0.301E+04	0.122E+14	0.841E-08
148.4	150.0	0.0	0.2	120.9	777.5	0.0	2649.3	-0.55	0.294E+04	0.151E+14	0.677E-08
148.4	AMBIENT	0.0	4.6	120.9	0.0	0.0	2649.3	-1.00	0.294E+04	0.725E+13	0.326E-06
148.2	AMBIENT	0.0	0.1	120.7	0.0	0.0	2589.0	-1.00	0.287E+04	0.861E+13	0.596E-08
148.0	150.0	0.0	0.1	120.5	777.5	0.0	2530.0	-0.53	0.281E+04	0.231E+14	0.222E-08
147.8	AMBIENT	0.0	0.2	120.3	0.0	0.0	2472.4	-1.00	0.274E+04	0.120E+14	0.854E-08
147.6	150.0	0.0	5533.6	120.1	777.5	0.0	2416.2	-0.51	0.268E+04	0.347E+14	0.817E-04
TOTALS	6000.2 HR										0.281E+01

When thermal loads are important, the analysis starts with a preliminary evaluation procedure for areas of concern using approximate methods. The followings are the equations used in the panel evaluation spreadsheet based on the classical plate theory for evaluating an equivalent structural panel. They are applicable to flat to slightly curve quasi-isotropic rectangular panels with clamped edges at elevated temperatures, which is assumed to be constant for the panel. There can be provisions for orthotropic, sandwich, and panels with other boundary conditions. Material degradation due to temperature and internal loads from the vehicle level analysis cannot be included in the equations.

1. Calculate skin buckling temperature above ambient, T_c,

$$T_c = \left(5.25\, h^2\, F_{11}\right)/\left[\alpha\, a\, b\,(1+\nu)\right] \qquad \text{(Eqn. D.8)}$$

In which h is the thickness of skin, F_{11} =(b/a) + (a/b), a and b are dimensions of rectangular panel, α is the coefficient of thermal expansion, and ν the Poisson ratio.

2. Compute skin buckle amplitude W_o with r = T_c/T; T the ambient temperature,

$$W_0 = \left(2.50hF_{11}^{1.75}\right)\left[(r-1)/R\right]^{1/2} \quad \text{(Eqn. D.9)}$$

where $R = 3\left[\left(5-\nu^2\right)F_{11}^2 - 2(5+\nu)(1-\nu)\right]$. (Eqn. D.10)

3. Compute thermal stresses at mid points of each side of the panel with $\Delta T = T_c - T$

$$\sigma_x = -\frac{E\alpha\Delta T}{1-\nu} + \frac{0.82E}{ab(1-\nu^2)}\left[\left(2-\nu^2\right)\frac{b}{a} + \nu\frac{a}{b}\right]W_0^2 \quad \text{(Eqn. D.11)}$$

$$\sigma_y = -\frac{E\alpha\Delta T}{1-\nu} + \frac{1.667E}{ab(1-\nu^2)}\left[\left(2-\nu^2\right)\frac{a}{b} + \nu\frac{b}{a}\right]W_0^2 \quad \text{(Eqn. D.12)}$$

4. Compute the room temperature fundamental frequency with $\gamma = \rho h$ (mass per unit area)

$$f_0 = \left(0.79\, F_{11}/ab\right)\quad \left\{Eh^3/\left[\gamma\left(1-\nu^2\right)\right]\right\}^{1/2} \quad \text{(Eqn. D.13)}$$

5. Compute the fundamental frequency ratio f(r) at the temperature of the structure being analyzed;

$$f(r) = f_0\left[0.60 + 0.40(1-r)^{1/2}\right], when(0 \le r \le 1) \quad \text{(Eqn. D.14)}$$

$$f(r) = f_0\left[0.60 + 0.44(r-1)^{1/2}\right], when(r \ge 1) \quad \text{(Eqn. D.15)}$$

In practice the measured frequency does not decrease to zero at buckling temperature. Hence the constant 0.60 appears in the equation. The trend of the frequency variation with temperature is shown below.

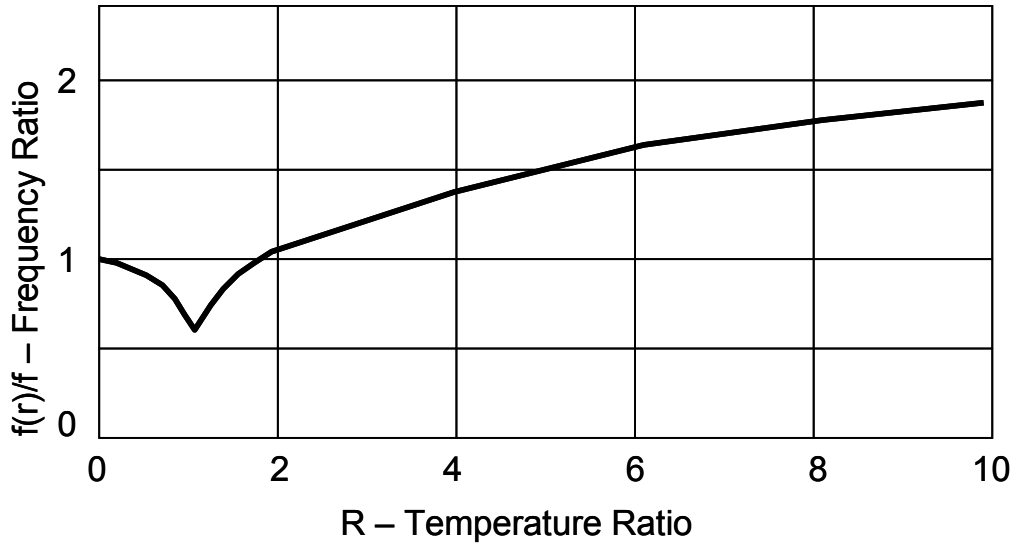

Figure 127. Frequency Variation

The frequency variation is significant, since large changes in the frequency may occur with only a slight change in ambient temperature. This can have a significant effect on the acoustic response and fatigue life.

6. Dynamic stresses are then calculated based on the clamped edge conditions. The preferred method to calculate the dynamic stresses is the Miles Method.

$$S_{rms} = (S_0)\left[\frac{\pi}{4}\frac{f_r}{\xi}G(f)\right]^{1/2} \qquad \text{(Eqn. D.16)}$$

where S_o is the static stress due to a unit 1-psi pressure load on the panel, f_r is the temperature adjusted frequency, ξ is the modal damping, and G(f) is the PSD (psi^2/hz) at the natural frequency. The term is the bracket is also called the Dynamic Load Factor, DLF.

7. Compute the fatigue life margin with respect to the endurance limit. The endurance limit is usually defined for room temperature, but it needs to be adjusted for elevated temperatures.

The adjustment for temperature is done with factors to "knockdown" the curves to account for deterioration of fatigue allowable at higher temperatures. One method of obtaining this factor is to observe trends found in constant amplitude fatigue data (Reference MIL-HDBK-5). A knockdown factor can be calculated either as an average stress ratio from various life values or just one critical value such as the fatigue endurance. In acoustic fatigue analysis the endurance limit ratio is used since panel frequencies are quite high (>250 Hz), and exposure to damaging levels for any significant length of time (>100 hours) results in high numbers of cycles (> 100e6).

Another method of adjusting for temperature is to use the material yield stress to determine the knockdown factor. This method is only used when material fatigue data at elevated temperature is not available. Mil-HDBK-5 is a good source of temperature effects on material yield stress.

These ratios of yield stresses can then be applied to the room temperature fatigue data to obtain fatigue curves at elevated temperatures.

The following values from Mil-HDBK-5 data were used to determine the endurance limit ratio and the tensile yield stress ratio:

TI 6AL-4V Sheet

	Temperature		
	80°F	**400°F**	**800°F**
Endurance Limit[1] (Ratio to 80°F)	25 ksi (—)	20 ksi (.80)	16 ksi (.64)
Tensile Yield Stress (Ratio to 80°F)	145 ksi (—)	104 ksi (.72)	87 ksi (.60)

[1] K_t=2.8 and R=-1

8. The s-N curve also needs to be adjusted for the mechanical mean stresses. The typical assumption is R=-1 (no mean stress). The R-ratio is defined as

$$R\text{ - mean stress factor} = \frac{S_{min}}{S_{max}} = \frac{-S_{dyn} + S_{mean}}{S_{dyn} + S_{mean}} \qquad \text{(Eqn. D.17)}$$

Most random high cycle fatigue data is generated from R=-1 tests. But, most applications have a mean stress component, Figure 128. Hence, it is necessary to adjust the random s-N curve for mean stress effects.

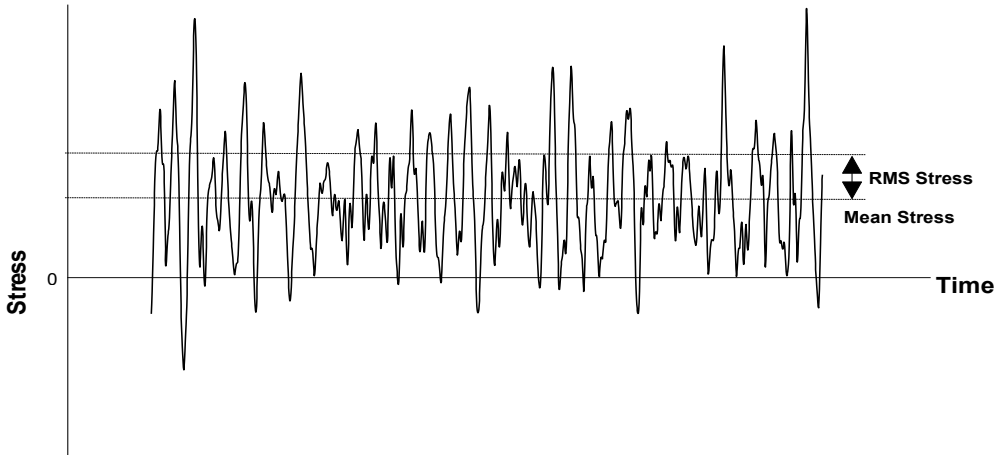

Figure 128. Random Time History

In order to account for the possibility of mean stress, which degrades fatigue properties, there needs to be a method to adjust this baseline curve. The method selected to adjust zero mean stress fatigue curves to curves of different mean stress. Using the Goodman equation:

$$S_g = S_{dyn}\left(1 - \frac{S_{mean}}{S_{ult}}\right) \qquad \text{(Eqn. D.18)}$$

S_g - Goodman's equivalent stress

S_{dyn} - alternating stress

S_{mean} - mean stress

S_{ult} - ultimate stress

These equations are normally used for constant amplitude sinusoidal fatigue curves, but here they are applied to random data using the following definitions and substitutions:

$$\sigma_g = \sigma_{rms}\left(1 - \frac{\sigma_{mean}}{S_{ult}}\right) \qquad \text{(Eqn. D.19)}$$

$$R = \frac{-\sigma_{rms} + \sigma_{mean}}{\sigma_{rms} + \sigma_{mean}} \qquad \text{(Eqn. D.20)}$$

Adjustments were made to the baseline fatigue curve for three different R ratios $(+\frac{1}{2}, 0, -\frac{1}{2})$ and the results are shown in Figure 129. For the high mean stress case $(R = +\frac{1}{2})$, the curve starts to heel over for high stress levels (low cycles to failure).

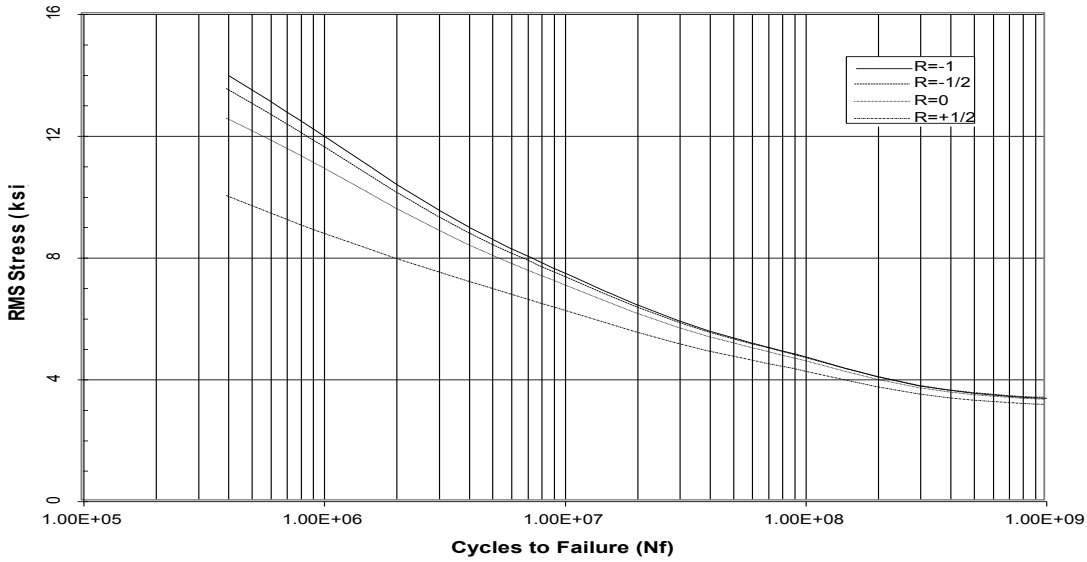

Figure 129. Adjustment for Mean Stress

The endurance limit method is a conservative approach to fatigue life assessment, but for a screening process it is only used to determine the critical panels. For fatigue life assessment, we use two basic methods:

Infinite Life Design

It is based on a fatigue limit, below which the stress will not induce fatigue. For Infinite Life Design, all RMS stresses are predicted to be below the endurance limit of the material, as defined by random S-N testing. The most common definition is;

$$S_e@N = 1 \times 10^9 \text{cycles}$$

where S_e is the strength endurance limit.

The Rules of thumb is to use the 95% confidence limit on the S-N curve. If no S-N data exists, use the relationship between ultimate strength (S_u) and S_e. For example, $S_e = 0.50\ S_u$ for high strength materials like steel and titanium.

The Infinite Life Design method is most common for a screening level analysis. The requirement of the number of cycles that define endurance limit may differ based on vehicle requirements.

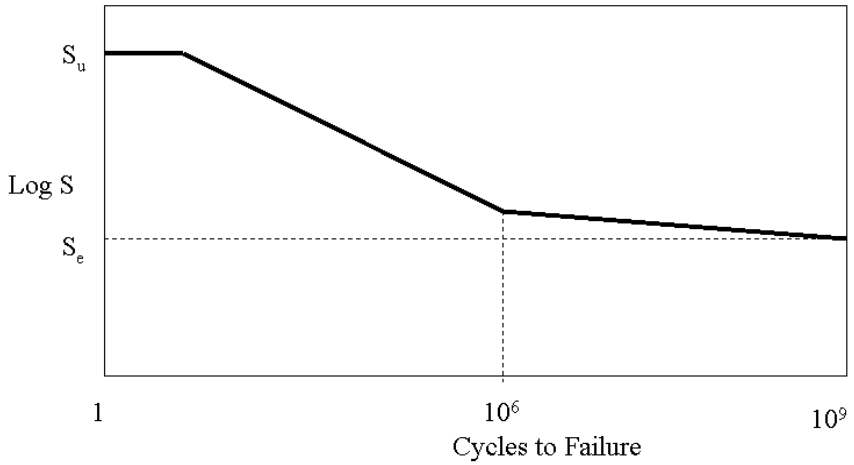

Figure 130. Cycles to Failure

Finite (Safe) Life Design

Instead of designing a component that never fails, parts are designed for a specified life deemed —safe" or the fatigue that is unlikely to occur during the rated life of the system except in cases of abusive loading.

For Finite Life Design, the most common practice is to use

- Scatter factor on acoustic load of 1.5 times (or add 3.5 dB for acoustic loads);
- 95% Confidence limits on S-N data;
- 2 times of the Design Life (a factor of 4 may be required).

Calculate the RMS stress allowable, RMS $\sigma_{all,}$ based on the required number of cycles.

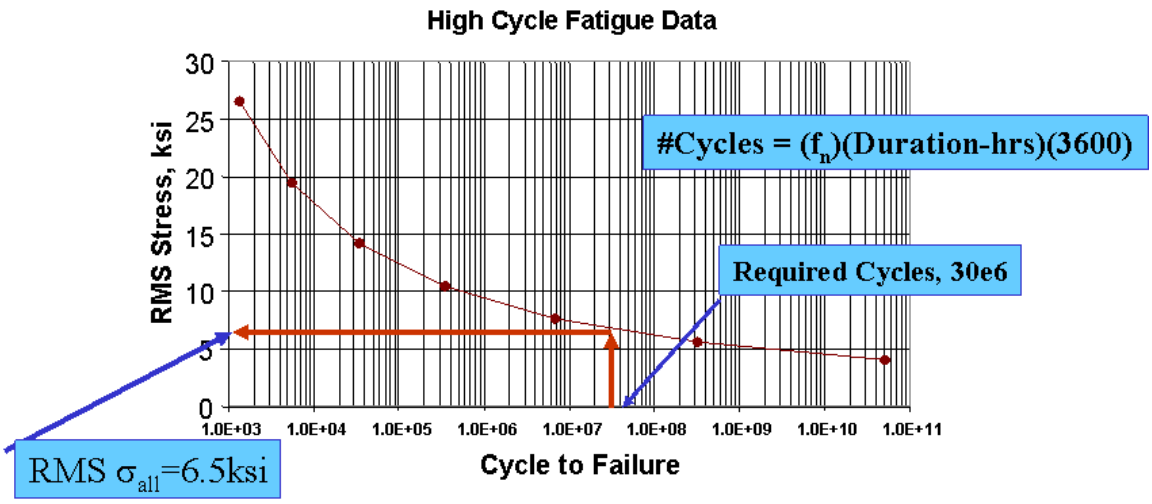

Figure 131. High Cycle Fatigue Data

where f_n is the center frequency of the PSD response, or the fundamental frequency based. Duration is a Time at condition in hours.

The center frequency of the response is going to be determined by either a PSD (analytical or experimental) or from a modal analysis (analytical or experimental). From a PSD, the center frequency of excitation can be determined from the expected number of zero crossing E[0].

$$fc = \left(\sqrt{\left(\sum_{i=1}^{n} \frac{\sigma_{rms_i}}{\sigma_{OArms}} f_i \right)^2} \right) \qquad \text{(Eqn. D.21)}$$

Where m_0 and m_2 are the 0th and 2nd moments of the PSD, this is also called the Center Frequency of the response. A simple hand calculation can be performed using,

$$E[0] = \sqrt{\frac{m_2}{m_0}} \qquad \text{(Eqn. D.22)}$$

The moments of the PSD response can be calculated from this equation:

$$m_n = \int_0^\infty f^n G(f) df = \sum f_k{}^n G_k(f) \delta f \qquad \text{(Eqn. D.23)}$$

where G(f) is the PSD, and f_n is the frequency, and n is the order of the moment.

Also, of interest is the expected number of peaks in the response. This can be thought of as an upper frequency bound. Note, m_4 and m_2 are the 4th and 2nd moments of the PSD.

$$E[P] = \sqrt{\frac{m_4}{m_2}} \qquad \text{(Eqn. D.24)}$$

The second part is determining the Duration (or Time at Condition) for fatigue. For acoustics, typically the highest noise levels cause the most damage. After sufficient flight testing, the highest noise level can be associated with a given flight condition or maneuver, which in turn can be associated with a Usage block. Hence, knowing the environment (Grms, OASPL) as a function of flight conditions (Q/alpha/Mach/Alt) and knowing the response at a Reference condition (i.e., S_{rms}=7ksi at OASPL=162 dB) can help determine damage or help perform a fatigue life time compression to the Max (or Ref.) environment (Grms or OASPL).

APPENDIX E – HYPERSIZER STRENGTH CHECKS

This appendix presents the detailed strength checks that HyperSizer performs during structural sizing for Honeycomb sandwich panels.

Material Strength, Isotropic (Metals) Failure Criteria

Analysis Methods:

110 = Isotropic Strength, Longitudinal Direction

111 = Isotropic Strength, Long Transverse Direction

Approach Summary

HyperSizer's failure criteria for isotropic, and in particular ductile metallic materials, are based on various well-accepted industry practices and recommendations from MIL-HDBK-5J [1], which is the industry standard for metallic material properties and failure prediction.

The material properties shown in Table 22, provided by MIL-HDBK-5J, are entered into the HyperSizer database for the isotropic failure mechanisms. For two of these properties, the material properties are not available from the handbook directly, but are calculated from other properties based MIL-HDBK-5J recommendations.

Table 22. Material properties available from MIL-HDBK-5J and entered into HyperSizer.

Limit/ Yield	Ultimate	Description
$\mathbf{F_{tyL}}$	F_{tuL}	Tensile strength in the longitudinal (parallel to grain) direction
$\mathbf{F_{tyLT}}$	F_{tuLT}	Tensile strength in the long transverse (perpendicular to grain) direction. "Long" refers to the longest dimension parallel to the grain, also called the "width" direction. There is a "short transverse" direction as well (e.g. FtyST), but it is not widely available for many materials in MIL-HDBK-5 and is not included in HyperSizer
$\mathbf{F_{cyL}}$	F_{cuL}*	Compressive strength in the longitudinal (parallel to grain) direction. *F_{cuL} and F_{cuLT} are not listed for materials in MIL-HDBK-5, and are not entered into HyperSizer directly. HyperSizer implements $F_{cuL}=F_{tuL}$ and $F_{cuLT}=F_{tuLT}$ as recommended by MIL-HDBK-5J.
$\mathbf{F_{cyLT}}$	F_{cuLT}*	Compressive strength in the long transverse direction.
$\mathbf{F_{sy}}$**	F_{su}	Shear strength. **F_{sy} is not given for most materials in MIL-HDBK-5 and is not entered into HyperSizer directly. The procedure implemented in HyperSizer for calculating this property was recommended by MIL-HDBK-5J and is discussed below.

Sandwich Panel Facesheet Wrinkling

Analysis Methods:

090 = Wrinkling, Eqn 1, Isotropic or Honeycomb Core, X, Y & Interaction

091 = Wrinkling, Eqn 2, Honeycomb Core, X, Y & Interacton

Approach Summary

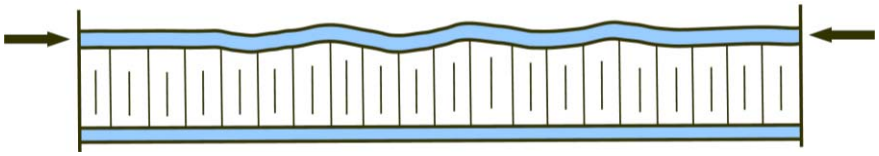

Sandwich structures with thin facesheets and lightweight cores are prone to a type of local failure known as facesheet wrinkling. The term wrinkling refers to local, short wavelength buckling phenomenon of the facesheet, with mode shapes having wavelengths up to the thickness of the core. The small buckling wavelength of the wrinkling mode results in the allowable load being insensitive to structural boundary conditions and curvature. Sandwich structures exhibit little or no post-wrinkling load carrying capability, therefore failure of these structures by wrinkling is typically catastrophic. As a consequence, accurate prediction of wrinkling is important to quantifying structural integrity of sandwich structures.

There are two distinct wrinkling modes: symmetrical and antisymmetrical.

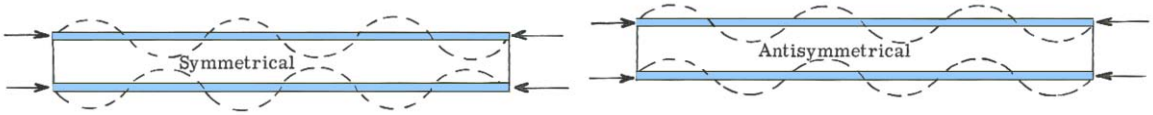

Sandwich Panel Facesheet Intracell Dimpling

Analysis Method:

094 = Intracell Dimpling, X, Y & Interaction

Summary Approach

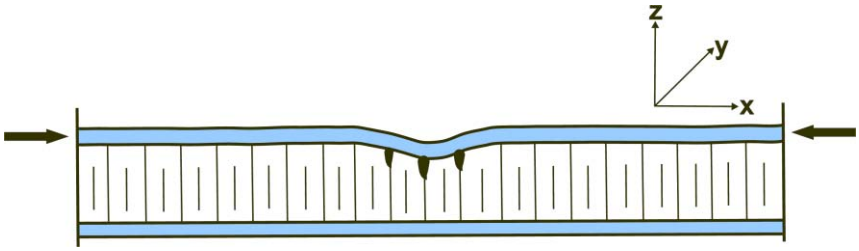

Intracell Dimpling, or Intracell buckling, is a failure specific to honeycomb sandwich concepts that is caused by local instability of the facesheets. If the face thickness of a honeycomb sandwich is reduced while cell size and material are held

constant, a thickness will eventually be reached at which the facesheet will buckle between the cell walls. A typical Intracell dimpling failure is shown in the figure below.

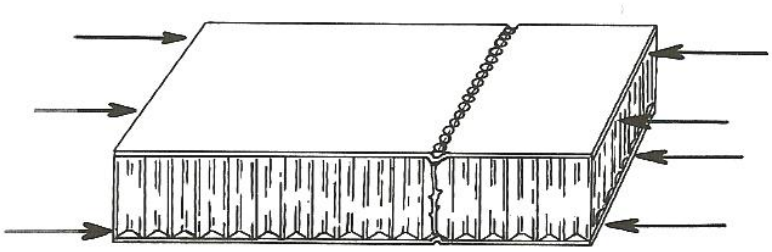

Allowable Equation

The Intracell dimpling allowable stress is primarily a function of facesheet material stiffness, thickness and honeycomb cell size. The equation used to determine this stress is from [1].

$$\sigma_{dp} = \frac{2E_f}{\left(1-\nu^2\right)}\left(\frac{t_f}{S}\right)^2 \qquad \text{(Eqn. E.1)}$$

Sandwich Panel Core Crushing

Analysis Methods:

100 = Core Crushing Concentrated Load (not yet implemented)

101 = Core Crushing Flexural Bending Load (not yet implemented)

102 = Core Crushing Joint Support Load

Approach Summary

There are three different types of loadings that can cause core crushing. The first is from a concentrated load. The second is caused by flexural bending moments. The third is caused by joint support loads.
For all three types of loadings, the choice will be available for the user to compare calculated core compressive stress to either: crush, bar, or stabilized material allowables.

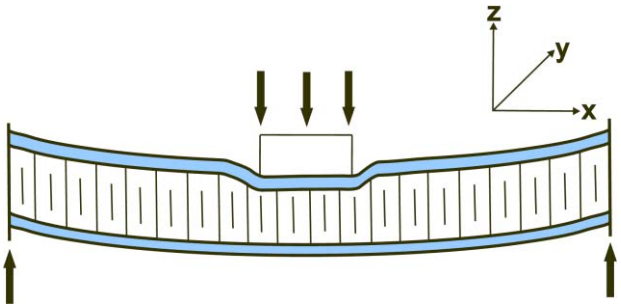

$$User\,Choice\ \ of\,(Fcu_{crush}, Fcu_{bare}, Fcu_{stablized})$$

The HyperSizer default is to take the lowest of these three core material allowables.

Analysis Methods:

105 = Shear Strength, X (longitudinal) direction (Hexcel)

106 = Shear Strength, Y (transverse) direction (Hexcel)

107 = Shear Strength, Interaction

Summary Approach

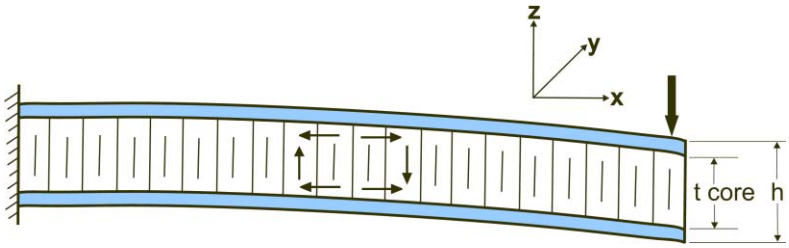

The shear strength failure calculation is a comparison of the shear strength in the core to the out-of-plane shear loads induced by cantilevered loads (as shown here) or pressure loads, which are common in aerospace applications. In the case of coupling of HyperSizer with FEA, the shear loads in the panels, Q_x and Q_y are extracted directly from the element forces of the FEA results.